High Affinity Iron Uptake Pathways are Indispensable for Virulence of the Maize Pathogen *Colletotrichum graminicola*

Dissertation

zur Erlangung des

Doktorgrades der Agrarwissenschaften (Dr. agr.)

der

Naturwissenschaftlichen Fakultät III

des Instituts für Agrar- und Ernährungswissenschaften (IAEW)

der Martin-Luther-Universität

Halle-Wittenberg

vorgelegt

von

Herrn M. Sc. Emad Albarouki

geb. am 05.10.1977 in Sweida, Syrien

Gutachter / in:

1. Prof. Dr. Holger B. Deising: Martin Luther University, Phytopathology and Plant Protection Institute, Betty-Heimann-Str. 3, D-06120 Halle (Saale), Germany

2. Prof. Dr. Nicolaus von Wirén: Molecular Plant Nutrition, Leibniz Institute of Plant Genetics and Crop Plant Research (IPK), Gatersleben, Correns-Str. 3, D-06466 Stadt Seeland, Germany

3. Prof. Dr. Uwe Conrath: Plant Biochemistry and Molecular Biology Group, Department of Plant Physiology, RWTH Aachen University, Aachen, 52056, Germany

Halle (Saale), 11.11.2013

Index

Acknowledgements

Curriculum vitae

List of scientific publications and abstracts

Eidesstattliche Erklärung / *Declaration under Oath*

Abbreviations

ACP	acyl carrier protein
ADH1	alcohol-dehydrogenase
ad.	add to desire volume
amp	ampicillin
ap	appressorium
approx.	approximately
ATP	adenosine-triphosphate
bidest	two times distilled
BLAST	basic local alignment search tool
bp	base pair
BPS	bathophenanthroline disulfonate sodium
°C	grade Celsius
cDNA	complementary DNA
CgM2	*Colletotrichum graminicola* isolate M2
CHSV	chitin synthase number 5 encodes the myosin motor domain
CM	complete medium
cm	centimeter
CAPS	N-cyclohexyl-3-aminopropanesulfonic acid
Co.	company
CoA	coenzyme A
COM	complementary strain
DIC	dichroic mirror/differential interference contrast
DIG	digoxigenin
DJ-PCR	double-joint PCR
DMSO	dimethyl sulfoxide
DNA	deoxyribonucleic acid
dNTP	deoxynucleotide triphosphate
dATP	deoxyadenosine triphosphate
dCTP	deoxycytidine triphosphate
dGTP	deoxyguanosine triphosphate
dTTP	deoxythymidine triphosphate

dUTP	deoxyuridine triphosphat		
DNaes	DNA nuclease		
E. coli	*Escherichia coli*		
e.g.	for example, from Latin "*exempli gratia*"		
eGFP	enhanced green fluorescence protein		
EDTA	ethylenediaminetetraacetic acid		
et al.	and others, from Latin "*et alii*"		
EtOH	ethanol		
µE	micro Einstein		
FAD	flavin adenine dinucleotide		
FET3	gene encode Ferroxidase		
Fig.	figure		
Fw.	forward primer		
g	gram		
µg	microgram	=	1×10^{-6} gram
ng	nanogram	=	1×10^{-9} gram
pg	picogram	=	1×10^{-12} gram
fg	femtogram	=	1×10^{-15} gram
g	Earth gravity		
G418	geneticin (aminoglycoside antibiotic)		
gDNA	genomic DNA		
h	hour		
HCl	chloride acid		
HEPES	N-2-Hydroxyethylpiperazine-N'-2-Ethanesulfonic acid		
HFC	hydroxyferricrocin		
hph	hygromycin phosphotransferase gene		
HPLC-MS	high performance liquid chromatography-mass spectrometry		
Hyg	hygromycin resistance cassette		
I	intron		
ITS	internal transcript spacer		
i.e.	that is to say, from Latin "*id est*"		
IPTG	Isopropyl thio galactoside		
Kan	kanamycinss		
Kb	kilo base pair		

Klx	kilolux
l	liter
Lac Z	ß-Galactosidase gene from *E. coli*
LB	lysogeny broth
LB^{amp}	LB medium supplemented with ampicillin
LB^{kan}	LB medium supplemented with kanamycin
Li	Lithium
LiAcO	Lithium acetate
M	molar
MES	2-(N-morpholino) ethanesulfonic acid
mg	milligram
µg	microgram
min	minute
ml	milliliter
µl	micro liter
mm	millimeter
mM	millimole
µmol	micromole
mol	mole
MOPS	3-Morpholinopropansulfonic acid
MPa	mega Pascal
NaAcO	sodium acetate
NaCl	sodium chloride
NAD	nicotineamid adenine dinucleotide
NaOH	sodium hydroxide
nat1	nourseothricin resistance cassette
NCBI	National Center for Biotechnology Information
NEB	New England Biolabs
nm	nanometer
NPSs	nonribosomal peptide synthases
NPS6	nonribosomal peptide synthase gene number 6
NRPSs	nonribosomal peptide synthetases
ORF	open reading frame
P	phosphate, Phospho-

PCP	peptidyl carrier protein
PCR	polymerase Chain Reaction
pH	potential of hydrogen,
PEG	poly ethylene glycol
PM	plasma membrane
Proteinase K	also called protease K: broad spectrum serine-protease from *Engyodontium album*
PPTase	4´-phosphopanteine transferases
qPCR	quantitative PCR
qRT-PCR	quantitative RT-PCR
RIA	reductive iron assimilation
Rel. unit	relative unit
Rv.	reverse primer
RNA	ribonucleic acid
RNase	ribonuclease
rpm	rotations per Minute
RT	room temperature
RT-PCR	reverse transcriptase PCR
s	second
SAP	selective anchor primer
SCM	synthetic complete medium
SCM-BPS	synthetic complete medium supplement with BPS
SD	standard deviation
SDS	sodium dodecyl sulfate
SIA	siderophore-mediated iron acquisition
SID1	gene encode siderophore synthase protein (ornithine-N^5-monooxygenase)
Sid1	siderophore synthase protein (ornithine-N^5-monooxygenase)
SidA	Sid1 ortholog (ornithine-N^5-monooxygenase)
SidC	nonribosomal peptide synthetase responsible for ferricrocin synthesis
SidD	nonribosomal peptide synthetase responsible for fusarinines C synthesis
SidF	acyl transferase
SidG	acyl transferase
SidL	acyl transferase
SSC	sodium chloride/sodium citrate

TAE	Tris/acetate/EDTA
TAFC	triacetylfusarinine C
Taq	thermus aquaticus
TdT	terminal deoxynucleotide transferase
TE	Tris/EDTA
TES	Tris/EDTA/SDS
T_m	melting temperature
Tris	Tris (hydroxymethyl) amino methane
TSS	transformation and storage solution
u	enzyme unit
UAP	universal amplification primer
URA	uracil
UV	ultra violet
V	volt
vol.	volume
v/v	volume percent
w/v	weight percent
WT	wild type
x	x-times
X-Gal	5-Brom-4-Chlor-3-Indolyl-β-D-Galactoside
YPAD	yeast extract peptone dextrose supplemented with adenine
YPD	yeast extract/peptone/dextrose
μ	micro-/micron
Ø	diameter

List of figures

List of tables

Explanatory notes

The present work was written in English. Latin terms, species and genus names are in italics. Gene designations are written with capital letters in italics (e.g. *SID1*). The name of the corresponding protein uses small letters with exception of the first letter is in capital (e.g. Sid1). Deletion mutants carry a Δ and the gene name with lower-case letters in italics (e.g. Δ*sid1*). Genes, proteins and mutants, which are described in the literature, are named according to the nomenclature in the appropriate publication.

I. Introduction

I.1 Biology of *Colletotrichum graminicola*

The genus *Colletotrichum* harbors several economically important species causing anthracnose in a wide range of host plants, including cereals, legumes, vegetables, fruit trees and ornamentals. Diseases caused by *Colletotrichum* species are known as bitter rot of apple, ripe rot of grape, pears, and peaches, anthracnose of tomato, cucurbits, ornamentals, strawberry, and maize (Bailey and Jeger, 1992; Agrios, 2005). Yield reduction, depending on the crop, may exceed 40% in some cases (Bergstrom and Nicholson, 1999; Tsror et al., 1999). *Colletotrichum graminicola* (Cesati) Wilson, Teleomorph *Glomerella graminicola* Politis, a representative of the filamentous ascomycetes (class: *Sordariomycetes,* subclass: *Hypocreomycetidae,* family *Glomerellaceae* (Lumbsch and Huhndorf, 2007)), is the cause of anthracnose and stem rot of maize plant (Fig. 1) (Wilson, 1914).

C. graminicola is a facultative pathogen. Therefore it is well adapted for survival in corn-based agroecosystem. It has short reproduction life cycle (3-4 days) during the growing season, where it produces a huge number of asexual spores (conidia) allowing the fungus to be spread in wide area of corn fields and can grow as a saprophyte on maize residues. Overwintering achieved via saprophytic growth on decaying plant debris that remains on soil surface and forms a reservoir for primary inoculum for the next season (Bergstrom and Nicholson, 1999).

Reproduction in nature takes place by producing sickle-shaped conidia, formed in acervuli (Fig. 1 G, c and ac). Conidia are imbedded in a water-soluble spore matrix, mucilage, of polysaccharides and proteins that allows conidial survival until a potential host is present (Nicholson and Moraes, 1980). The dissemination of the falcate-shaped conidia takes place via splashing water and blowing of raindrops, aerial dissemination has been reported by some resources but not verified experimentally (Nicholson and Moraes, 1980; Bergstrom and Nicholson, 1999).

After the dissemination of conidia from acervuli and deposition on a surface of potential host, (e.g. hydrophobic leaf surface), a signal transduction cascades process are readily turned on that activates different genes responsible for the establishment of pathogen-host interaction (i.e. glycoproteins secretion required for spore adhesion, signal for germination, etc.). Conidial adhesion is a crucial process needed for the establishment of penetration and

invading host cells (Epstein and Nicholson, 2006). Adhesion pads are formed within 30 min post inoculation, making their adhesion on a hydrophobic surface possible (Taira et al., 2002).
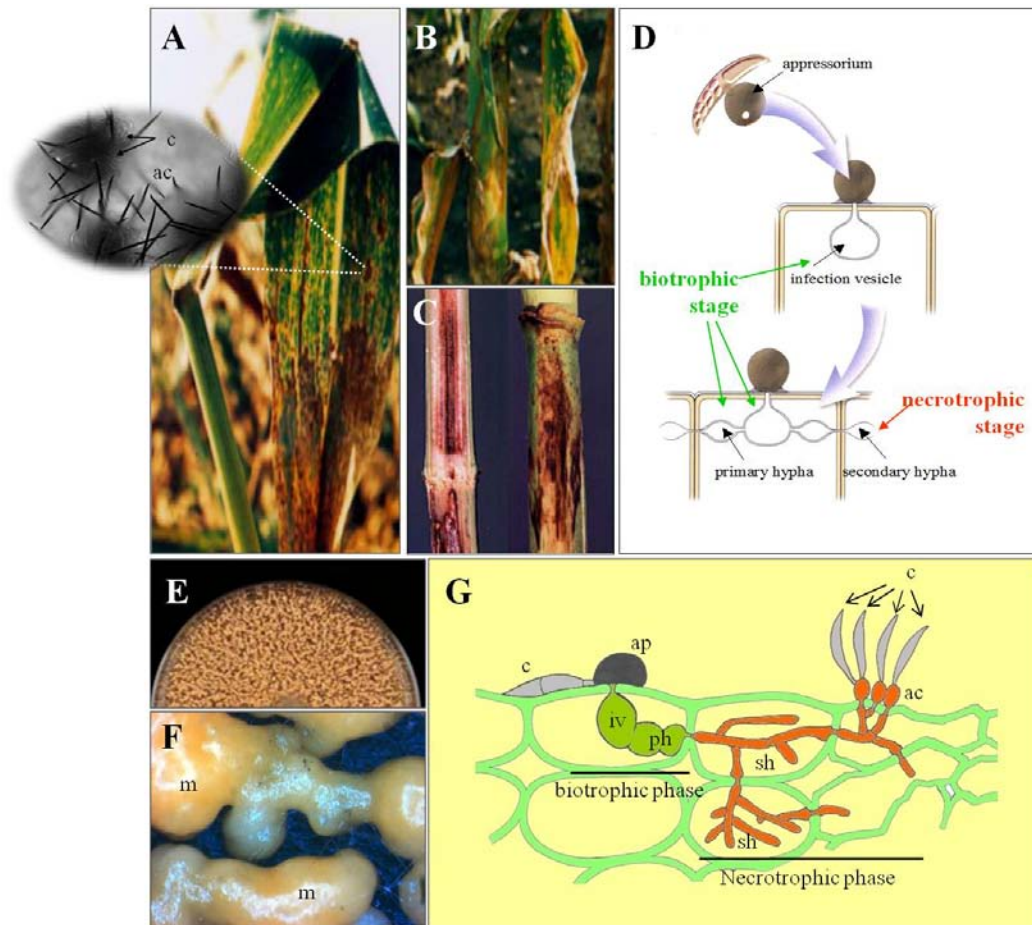
Fig. 1: *Colletotrichum graminicola* **infection of susceptible maize plants and the life cycle.**
A and B: Anthracnose leaf blight (ALB), the characteristic necroses lesion surrounded by yellow hallo on leaf and the sheath.
C: Different manifestations of anthracnose stalk rot (ASR) systemically or on the rind.
D: Life cycle of *C. graminicola* after the landing of conidium on the host plant, it germinates and forms an appressorium that facilitates the penetration of host cell and forms an infection vesicle and primary hypha (biotrophic stage); integrity of the host cell at this stage is still intact. Thereafter, the fungus transits to necrotrophy by developing out-breaking thin hyphae to the neighboring cells.
E and F: Typical growth and acervuli production *in-vitro* on oat meal agar (OMA) plate and 20 x magnification of formed acervuli, notice the conidia are imbedded in mucilage (m).
G: Cartoon shows the infection structures formed on maize plant. c, conidium; ap, appressorium; iv, infection vesicle; ph, primary hypha; sh, secondary hypha; ac, acervulus.
(A to D were adapted from Bergstrom and Nicholson (1999), G is an artwork by D. Deising).

Approximately five to six hours later, a germ tube develops from the two-celled septated conidia. In rare cases, both halves of the conidia form germ tube and appressoria. Frequently, differentiation of the infectious cell takes place directly beside the conidium, whereby an extremely short germ tube is only formed (Bergstrom and Nicholson, 1999). Appressoria allow for direct penetration of the host epidermis, which need approximately 15-20 hours

after the adhesion of conidia to be fully differentiated as a black spheric structure of approx. 7 µm diameter (Fig. 1 D and G, ap). A high turgid pressure is developed and maintained by the deposition of melanin into the cell wall of appressorium and synthesis of osmolytes (e.g. glycerol) within the appressorium that is directed through an infection pore at its basis to the epidermal cell wall of the host (Bechinger and Bastmeyer, 1999; Deising et al., 2000). In the rice blast pathogen *Magnaporthe oryzae*, a high turgor pressure generated by accumulation of glycerol in melanized appressoria may reach up to 8 MPa (Howard et al., 1991; De Jong et al., 1997), whereas it may reach in *C. graminicola* up to 5 MPa (Bechinger and Bastmeyer, 1999; Ludwig, 2012). The role of melanin synthesis in the stability of appressorium against its own generated turgor pressure is still under debate (Howard et al., 1991; De Jong et al., 1997; Horbach, 2010; Ludwig, 2012). Although the Δ*pks1* strain defective in polyketide synthase gene are not able to produce melanin, the turgor pressure measured for this strain was 3.7 MPa, in comparison, it was 2.8 MPa for WT (Horbach, 2010). Therefore, beside the turgor pressure apparently cell wall-degrading enzymes such as cellulase, xylanase, pectinase and polygalacturonase also play a role in the penetration of host epidermis (Nicholson et al., 1976; Wernitz, 2004). After penetration of epidermal host cell, infection vesicle (iv) and primary hyphae (ph) are formed (Fig. 1D and G). Up to this stage of development the fungus feeds on the living host cell and the mode of nutrition is therefore called biotrophic. Fungal hyphae and the host plasma membrane are in close contact without the integrity of the epidermis cell being hurt. At this stage, the fungus develops different strategies to avoid plant defense response such as masking invading hyphae (Perfect et al., 1998; El Gueddari et al., 2002; Oliveira Garcia, 2013) or active suppressing of plant defense (Stephenson et al., 2000). Transition to necrotrophic mode of nutrition takes place 24 to 36 hours after the beginning of penetration (Fig. 1 D and G, sh). It is still not fully understood which signals make the fungus decide to switch to the necrotrophic mode of nutrition. However, in a closely related fungus, *Colletotrichum lindemuthianum*, the causal agent of common bean anthracnose, a transcriptional activator *CLTA1* was found, which is essential for the biotrophy-necrotrophy-switch (Dufresne et al., 2000). In the necrotrophic phase the fungus forms secondary hyphae (sh), characteristic thin branched hyphae, which break through the host cell walls and membranes (Bergstrom and Nicholson, 1999). During this phase a vast array of genes encoding plant cell wall degrading enzymes are up-regulated, allowing the invading hyphae to feed on polymeric cell wall compounds. In *C. lindemuthianum*, several lysing enzymes (i.e. pectin lyases, α- and β-galactopyranosidase, endo-polygalacturonases, α-arabinofuranosidase and proteases) have been found as secreted

enzymes during this phase (Wijesundera et al., 1984; Wijesundera et al., 1989; Govrin et al., 2006). Moreover, the fungus may not only rely on averting plant defense but rather actively kill the host cells by secreting toxins or generating reactive oxygen species (ROS) (Perpetua et al., 1996; Howlett, 2006; Thines et al., 2006). Through the proliferation of the pathogens in plant tissue, first symptoms are to be recognized as chlorotic spots. In further development necrotic spots arise, in which the fungus forms acervuli and conidia for further spreading of the disease (Fig.1 A and G, ac) (Bergstrom and Nicholson, 1999).

I.2 The biological role of iron

Iron is an indispensable element for almost all organisms. The ubiquitous presence of cytochromes and non-heme iron in the respiratory chains of aerobic and facultative anaerobic species provides a central role for this element in the energy metabolism of organisms. With the dependency on O_2 as electron acceptor came the need to protect the cell against hydrogen peroxide, the side product of electron transport reaction, and once more iron is involved by the hydroperoxidases, catalase and peroxidase, and by certain forms of superoxide dismutases. Table 1 lists some important enzymes in biological process of microorganisms, which use iron as a cofactor or as a prosthetic group.

Table: 1 Iron enzymes from microorganisms (adapted from Neilands, 1981b)

Molecular function	Enzymes
Electron transfer proteins	Cytochromes Hydrogenase iron-sulfur proteins (ferredoxin) Succinate dehydrogenase
H_2O_2 and O_2 metabolism	Catalase (haem enzyme) Peroxidase Superoxide dismutase Oxygenases
Tricarboxylic acid cycle	Aconitase
N_2 fixation	Nitrogenase
DNA biosynthesis and repair system	Ribotide reductase B2 subunit DNA Primase p58 subunit Helicase-nuclease complex

Paradoxically, iron can be harmful for cells because it causes production of hydroxyl radicals by Fenton/Haber Weiss reaction (Halliwell and Gutteridge, 1984; Halliwell and Gutteridge, 1992). This may lead to protein denaturation, DNA breakage and lipid oxidation (Schaible and Kaufmann, 2004). Generation and disarming of radicals involving iron in biological niches are listed in Table 2. In order to avoid generation of ROS, iron is bound to various proteins/chelators during storage and transport within all organisms' cells. In other words, iron homeostasis must be fine-tuned by complex regulatory pathways.

Table 2: Redox reactions involving iron and oxygen (adapted from Pierre and Fontecave, 1999)

Oxidizing agent	Reaction	Example
O_2	$LFe^{(II)} + O_2 \rightarrow Fe^{(III)} + O_2^{\bullet-}$	Autoxidation
$O_2^{\bullet-}$	$L\,Fe^{(II)} + O_2^{\bullet-} \xrightarrow{2H^+} L\,Fe^{(III)} + H_2O_2$	FeSOD
H_2O_2	$L\,Fe^{(II)} + H_2O_2 \rightarrow L\,Fe^{(III)} + OH^- + OH^{\bullet}$	Fenton reaction
$Fe^{(III)}$	$L\,Fe^{(III)} + O_2^{\bullet-} \rightarrow L\,Fe^{(II)} + O_2$	Haber-Weiss reaction
$LFe^{(IV)}=O$	$L^+Fe^{(IV)}=O + D^{n+} \xrightarrow{2H^+} LFe^{(III)} + D^{(n+1)+} + H_2O$	Peroxidase
$LFe^{(V)}=O$	$LFe^{(V)}=O + D^{n+} \rightarrow LFe^{(III)} + DO$	mono oxygenases

L: ligand, D: electron donor, FeSOD: iron type superoxide dismutase

In animal cells, iron is bound to ferritin, transferrin and lactoferrin or forms a complex into haem within hemoproteins or iron-sulfur cluster (Kaplan, 2002; Hentze et al., 2004; Schaible and Kaufmann, 2004). Ferritin is the main iron reservoir in animal cells, it was found ubiquitously from lower invertebrates (worm and flies), amphibians and fish, to higher mammalians including humans (Harrison et al., 1987). The mammalian ferritin is able to store up to 4500 Fe^{3+} ions in its core and contains around 30% of iron pool (Matzanke, 1994; Miethke and Marahiel, 2007). Bacterioferritins have been found in various gram-negative bacteria, in filament-forming gram-positive *streptomyces* and *mycoplasms* (Bauminger and Rottem, 1980; Matzanke, 1994; Crichton, 2001). Mycoferritin was also detected in Zygomycetes and recently in some ascomycetes under special conditions (Seckback, 1982; Shashidhar et al., 2005; Vakdevi and Deshpande, 2009; Validandi and Deshpande, 2009). The major iron reservoir in filamentous fungi is siderophore (Haas et al., 2008). In plant, phytoferritin is found in plastids (David and Easterbrook, 1971; Briat et al., 2010). That clearly gives a strong evidence of the tightly bound-form of iron in different type of living cells.

I.3 Iron uptake pathways in fungal pathogens

Although iron is one of the most common elements of earth's crust, its availability stands in sharp contrast to its abundance. Both Fe^{2+} and Fe^{3+} exhibit an extremely high affinity for hydroxy ions, with which they form insoluble complexes. In the case of $Fe^{(III)}$, the predominant oxidation state existing in an aerobic environment, the solubility product may be less than 10^{-18} M (Neilands et al., 1987). The labile iron in animal and plant tissues is much lower than what exists in nature, where the majority of iron is delivered to various proteinous (iron-sulfur-, haem-, or iron-proteins) and non-proteinous iron binding molecules (citrates, mugineic acid (MA), phytosiderophores (PS), etc.). The concentration of free iron in human serum around 10^{-24} M (Miethke and Marahiel, 2007), whereas it is supposed to be ten times less in plant (Expert, 1999). Pathogenic fungi have evolved at least two major high affinity iron uptake pathways to acquire iron from their host cells, the reductive iron assimilation (RIA) and the siderophore-mediated iron acquisition (SIA) systems (Fig. 2).
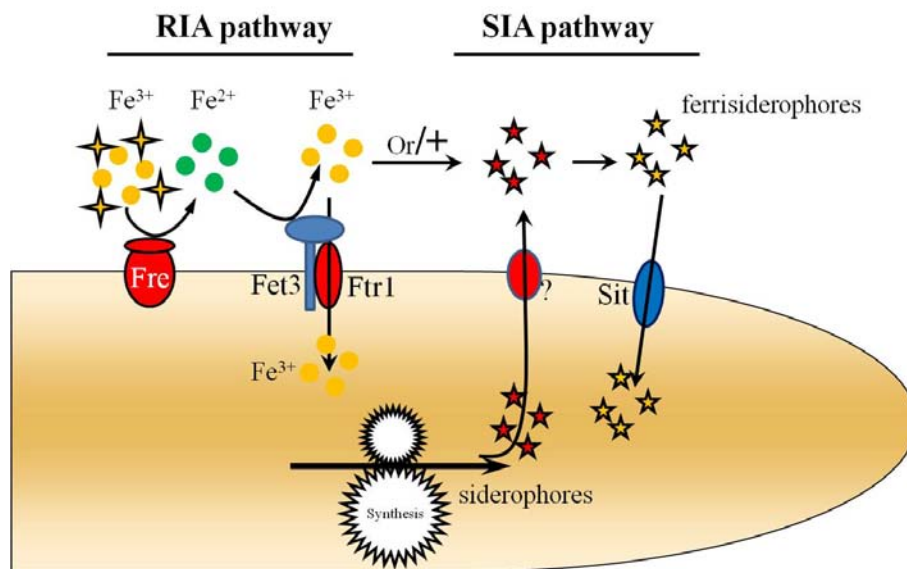
Fig. 2: High affinity iron uptake system in fungal pathogens
RIA pathway represented by the three components; ferric reductase (Fre), ferroxidase (Fet3) and permease (Ftr1). The SIA pathway represented by siderophore synthetic machinery (synthesis), secretion and uptake transporters (Sit). ●, Fe^{2+}; ●, Fe^{3+}; ★, desferrisiderophore; ★, ferrrisiderophore; ⭒, pseudosiderophore.

I.3.1 The reductive iron assimilation (RIA) pathway

RIA pathway is well characterized in the eukaryotic model yeast *Saccharomyces cerevisiae* (Askwith et al., 1994; Lesuisse and Labbe, 1994; Stearman et al., 1996; Askwith and Kaplan, 1998; Bonaccorsi di Patti et al., 2000; Bonaccorsi di Patti et al., 2001; Wang et al., 2003;

Kwok et al., 2006). It is a two-step process. First, plasma membrane-localized iron reductases catalyze extracellular reduction of insoluble and/or chelator-complexed ferric (Fe^{3+}) to soluble ferrous (Fe^{2+}) iron, and subsequently Fe^{2+} is bound by a bipartite high affinity iron transport complex, consisting of a multicopper ferroxidase (Fet3), and an iron permease (Ftr1), transferred across the plasma membrane, and delivered into the cytoplasm as Fe^{3+} (Eide, 1997; Shi et al., 2003; Haas et al., 2008) (Fig. 2). Thus, high affinity translocation requires Fet3-mediated oxidation of iron. The advantage gained by this indirect mechanism of iron uptake is unknown, but one may speculate that it confers specificity for iron, as other divalent ions are not prone to changes in their redox status and are therefore excluded from the RIA-mediated uptake system (Eide, 1997; Kosman, 2003; Haas et al., 2008).

In the biotrophic corn smut fungus *U. maydis*, two components of the high affinity RIA system, i.e. the high affinity iron permease Fer2, and the iron multicopper oxidase Fer1 were studied. Both, Δ*fer2* as well as Δ*fer1* deletion mutants were severely affected in virulence, demonstrating the importance of this iron uptake pathway for biotrophic development of *U. maydis* on maize (Eichhorn et al., 2006). Likewise, mutants of the dimorphic human pathogen *Candida albicans* lacking Ftr1 exhibited severe growth defects in iron-deficient medium and were unable to establish systemic infection in mice, indicating that iron uptake via RIA is essential for full virulence also in this pathogen (Ramanan and Wang, 2000). In the mammalian pathogen *Cryptococcus neoformans*, which is also a dimorphic pathogen of mammals, one of the two ferroxidases, Cfo1, is required for utilization of transferrin, an important iron source during infection, and virulence of a *cfo1* mutant was clearly attenuated in mice (Jung et al., 2009).

I.3.2 The siderophore-mediated iron acquisition (SIA) pathway

Siderophores (from ancient Greek; *sídēros,* iron; and *phoros,* carrier), are small molecules with high affinity to ferric iron. Their molecular weight ranges from 100-500 daltons (Hider, 1984). They are secreted by many microorganisms such as bacteria and fungi, and also graminaceous plants (Hider, 1984; Neilands, 1995; Howard, 1999; Haas, 2003; Schmidt, 2003; Miethke and Marahiel, 2007; Haas et al., 2008). Siderophores are among the strongest soluble Fe^{3+}-binding agents known, with iron binding constants over 10^{30} M, depending on pH. The largest ferric binding constant found was for enterobactin with $K_f = 10^{52}$ (Raymond and Carrano, 1979; Neilands, 1981a). There are around 500 compounds identified as siderophores (Boukhalfa and Crumbliss, 2002), and they may be classified into three different

types, depending on their iron binding moieties: i) Catecholates, ii) hydroxamate and iii) carboxylate types (Fig. 3). Moreover, some bacteria can produce miscellaneous types. Almost all fungal siderophores characterized so far are of the hydroxamate type (with the exception of some zygomycetes, which produce the carboxylate type) (Van der Helm and Winkelmann, 1994; Haas et al., 2008). Noticeably, many fungi produce transporters with specificities for xenosiderophores, secreted by other species of fungi and bacteria. The budding and fission yeast do not produce its own siderophores, but it can take up different types of siderophores either by expressing specific transporter or by using RIA (Neilands, 1995; Chen et al., 1999; Yun et al., 2000b; Yun et al., 2000a; Yun et al., 2001; Haas, 2003; Severance et al., 2004; Philpott, 2006; Haas et al., 2008). An explanation for this observation may be due to the evolution of *S. cerevisiae* in an environment that was populated by many other microorganisms and was rich in siderophores. Obviously, these uptake systems enable fungi to efficiently compete with other microorganism for the limiting amount of iron, in addition to allowing fungi to compete for host iron.
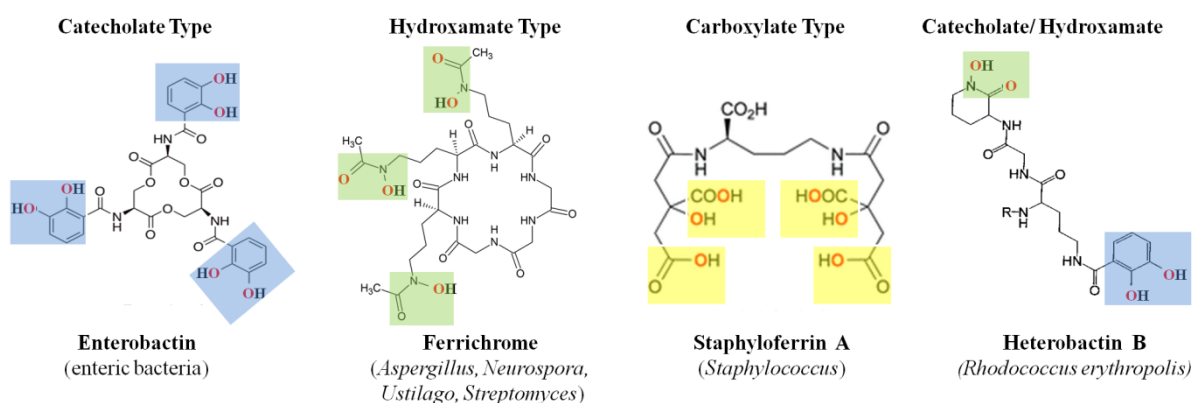
Fig. 3: Molecular structure of some representative examples of different siderophore types and their natural producer. Moieties involved in iron coordination are highlighted as following: catecholates are in pale blue, hydroxamates are in pale green, hydroxy-carboxylates are in light yellow. The oxygen atoms that are ligands to the iron are red colored. The chatecolate/hydroxamate type is an example of the miscellaneous type. (adapted from Miethke and Marahiel, 2007).

Fungal siderophores are derived from the amino acid L-ornithine and different acyl groups and can be grouped into four structural families, namely the rhodotorulic acid, the fusarinine, the coprogen, and the ferrichrome family (Haas et al., 2008). Figure 4 shows a representative of each family. The simplest hydroxamate siderophore, rhodotorulic acid, comprises two N^5-acetyl-N^5-hydroxyorninthine units linked by peptide bond and forms (siderophore)$_3$-(Fe^{3+})$_2$ complexes, whereas all the other types form (siderophore)-(Fe^{3+}) complexes (Haas et al.,

2008, and reference therein). The most frequently occurring fusarinine and fusarinine C consists of three N^5-*cis*-anhydromevalonyl-N^5-hydroxyornithine units linked by ester bonds (Fig. 4, triacetylfusarinine C). Triacetylfusarinine C is formed by N^2-acetylation of fusarinine C that leads to increased chemical stability and hydrophobicity (Haas et al., 2008). Coprogens are linear hydroxamates. Coprogen B contains two *trans*-fusarinine molecules connected head-to-head by a peptide bond to form a diketopiperazine unit (dimerumic acid) and a third *trans*-fusarinine molecule by an ester bond (Fig. 4; coprogen). N^{α}-acetylation and N^{α}-methylation of the latter fusarinine molecule are responsible for the diversity of the coprogen family (Supplementary Fig. S1). Ferrichromes such as ferrichrome, ferrichrome A, and ferricrocin are cyclic hexapeptides, comprising three N^5-acyl-N^5-hydroxyornithines and three amino acids (i.e. alanine, glycine, or serine). Ferrichromes are typically used as intracellular siderophores in ascomycetes, whereas in basidiomycetes they may be used extracellularly (Haas et al., 2008; Winterberg et al., 2010).

The biosynthetic pathway of hydroxamate siderophores is presented in Figure 5. The first committed step is hydroxylation of L-ornithine. This step is carried out by L-ornithine-N^5-monooxygenase, which was first characterized as the product of the *SID1* gene in *U. maydis* (Mei et al., 1993). This enzyme was thereafter identified as SidA in *A. nidulans* and *A. fumigatus* and DffA in *A. oryzae* (Eisendle et al., 2003; Yamada et al., 2003; Schrettl et al., 2004b). Genes with homology to *U. maydis Sid1* and *A. nidulans SidA* have been identified in many fungal species (Greenshields et al., 2007; Hwang et al., 2008). However, orthologs to these genes were found neither in *S. cerevisiae* nor in *C. albicans* (http://www.yeastgenome.org/ and http://www.candidagenome.org/). Surprisingly, the fission yeast *Schizosaccharomyces pombe* contains an ortholog of *Sid1*, and although this species was assumed not to produce siderophores (Neilands et al., 1987), *S. pombe* was recently shown to produce both intra- and extracellular siderophores (Schrettl et al., 2004a). Deletion of the gene encoding L-ornithine-N^5-monooxygenase blocks the synthesis of all siderophores in all *Ustilago, Aspergillus* and *Fusarium* species investigated (Haas et al., 2008, and reference therein).
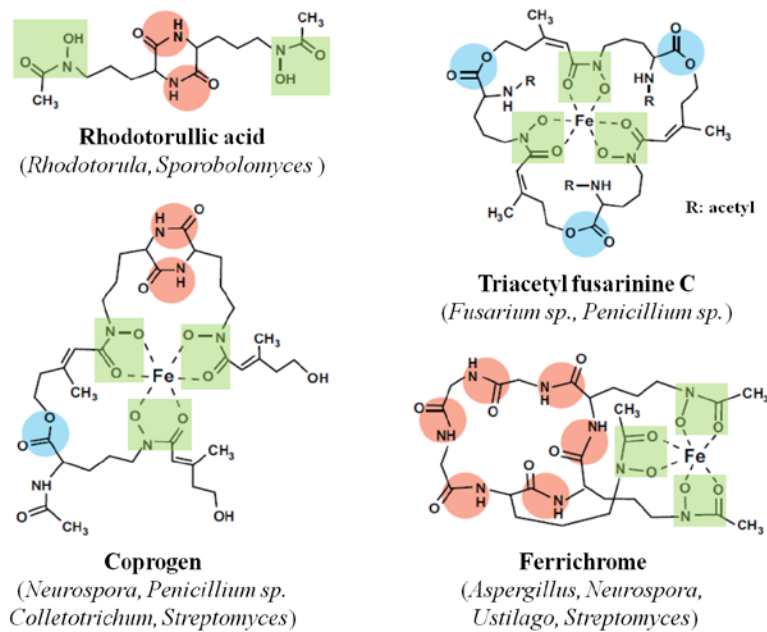
Fig. 4: Representative fungal siderophores of the hydroxamate type and their natural producers. Peptide and ester bonds separating N^5-acyl-N^5-hydroxyornithine groups are indicated in *red* and *blue* spheres, respectively. The hydroxamate group is indicated as in figure 3 (adapted from Haas et al., (2008)).

Interestingly, the $\Delta sidA$ mutant of *A. nidulans* was unable to grow unless it was supplemented with siderophores or high amounts of Fe^{2+}, due to the lack of another high affinity iron uptake system (Eisendle et al., 2003). In contrast, strains of *U. maydis, A. fumigates, A. oryzae* and *F. graminearum* unable to synthesis siderophores showed some reduction of growth rate under iron-depleted conditions and was comparable to wild type under iron replete conditions, as these fungi comprise RIA (Yamada et al., 2003; Schrettl et al., 2004b; Greenshields et al., 2007; Haas et al., 2008). The second biosynthetic step results in the formation of the hydroxamate group, and is accomplished by acylation of the N^5-hydroxyornithine (Fig. 5). The hydroxamate group is formed by transferring an acyl group from acyl-coenzyme A derivatives (acyl-CoA) to N^5-hydroxyornithine. Here the pathway splits according to the choice of the acyl group of different siderophores. The simplest is acetyl (e.g. for ferrichrome, ferricrocin and rhodotorulic acid) or more complex ones such as methylglutaconyl (e.g. for ferrichrome A) or anhydromevalonyl (e.g. for fusarinines and coprogens). In *A. fumigatus,* SidF is the corresponding acyl transferase for the extracellular siderophores fusarinine C and triacetylfusarinine C (Budde and Leong, 1989; Schrettl et al., 2007). A SidF homolog (SidL) was also found in *A. fumigatus* that is involved in biosynthesis of the intracellular siderophores ferricrocin and hydroxyferricrocin (Yasmin et al., 2012). SidF and SidL homologs can also be found among hydroxamate-producing fungi. For example, Fer5 is involved in the transfer of a methylglutaconyl residue to N^5-hydroxyornithine in ferrichrome

A biosynthesis in *U. maydis* (Fig. 5) (Winterberg et al., 2010), and Ato1 from *Omphalotus olearius* (Welzel et al., 2005).

In the third siderophore biosynthetic step, the hydroxamates are linked by peptide (e.g. rhodotorulic acid, ferrichromes and coprogens) or ester bonds (e.g. fusarinines and coprogens) (see Fig. 4) established by nonribosomal peptide synthetases (NRPS) (Fig. 5). NRPSs are large multifunctional enzymes that synthesize peptides from proteinogenic and nonproteinogenic precursors, independently of the ribosomal machinery (Mootz et al., 2001; Finking and Marahiel, 2004; Marahiel and Essen, 2009). NRPSs have a modular structure. One full module harbors all catalytic units for incorporation of one amino acid or amino acid-like residue. It typically consists of: i) adenylation domain for substrate specificity and activation, ii) a peptidyl carrier protein (PCP; also called thiolation domain) for attachment of the activated substrate, and iii) a condensation domain for bond formation (Marahiel and Essen, 2009). The activation of the NRPSs, as well as the acyl carrier protein (ACP) of fatty acid and polyketide synthetases, requires a covalent attachment of the 4´-phosphopanteine prosthetic group into the ACPs and PCPs domains; this is accomplished by the 4´-phosphopanteine transferases (PPTases). A posttranslational modification of the ACPs and PCPs domains is needed to be converted from their inactive apo to active holo form (Mootz et al., 2002). A genetic and biochemical studies showed that PPTase defective (Δ*npgA*) strains of *A. nidulans* (Marquez-Fernandez et al., 2007) and Δ*ppt1* strains of *Colletotrichum graminicola* and *Magnaporthe oryzae* (Horbach et al., 2009), lack the ability to produce polyketides and nonribosomal peptides including siderophores

Strains of *Cochliobolus heterostrophus, C. miyabeanus, Alternaria brassicicola, F. graminearum* (Oide et al., 2006) and *A. fumigatus* (Schrettl et al., 2007) defective in the respective NRPSs responsible for assembling extracellular siderophore show a large decrease in growth rate in iron depleted media. These strains have also shown an elaborated sensitivity to ROS stress and consequently virulence attenuation. However, these strains were absolutely dependant on the reductive iron uptake pathway (see I.3.1), which cannot fully compensate for the loss of siderophore-mediated iron uptake and consequently iron storage. The increased sensitivity to ROS can be explained by the dependence of several oxidative stress-detoxifying enzymes on iron, e.g. Fe-SOD, catalases and peroxidases that require heme as a cofactor. Deletion of NRPSs responsible for assembling intracellular siderophore results in increased sensitivity to ROS stress, reduction of germination rate and self sterility in both homothallic (Eisendle et al., 2006) and heterothallic strains (Oide et al., 2007).
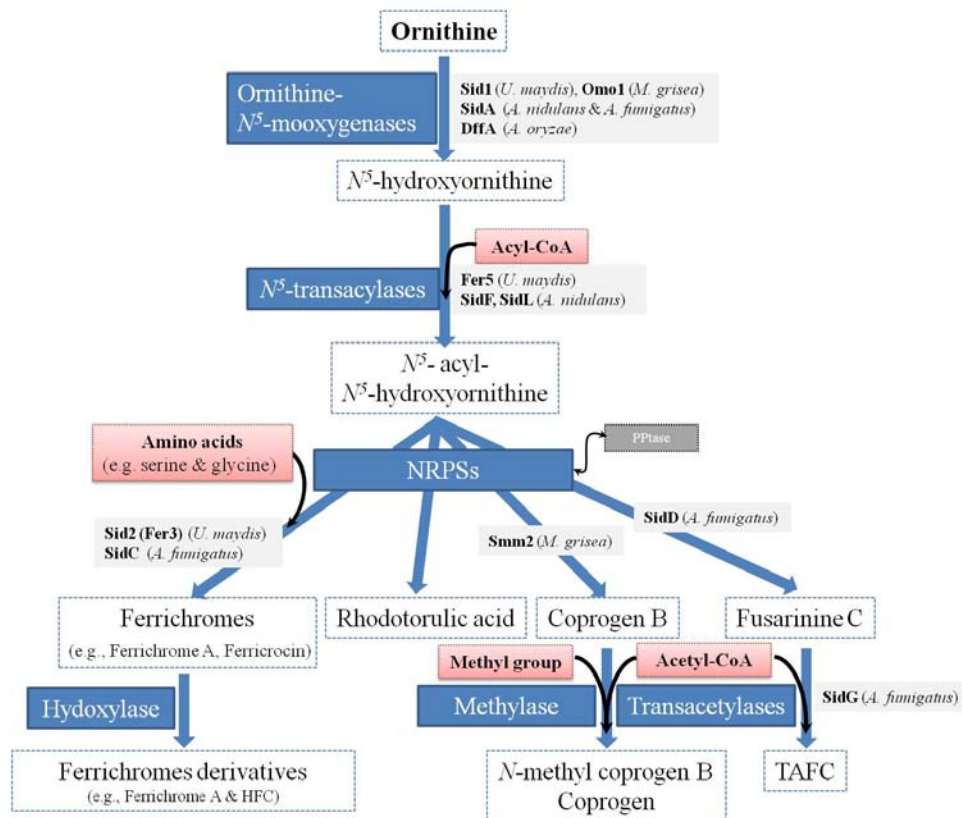
Fig.5: Hydroxamate siderophore biosynthetic pathway in fungi. The core product of all hydroxamate siderophores known so far is the L-ornithine amino acid. Steps are in blue boxes, characterized enzymes in different fungi are in light blue boxes. Acyl groups, amino acids and methyl groups (red box) are linked via acyl transferases, NRPSs and methylases, respectively. TAFC, Triacetylfusarinine C; HFC, hydroxyferricrocin. For description see text. Adapted after Haas et al., (2008).

The last step in siderophore biosynthesis is an additional modification to the NRPSs products, which leads to a further siderophores variants (see Fig. 5). For example, modification of coprogens, the hydroxylation of ferricrocin to form hydroxyferricrocin and the acetylation of fusarinine C to form triacetylfusarinine C (Schrettl et al., 2007; Haas et al., 2008). Apparently, these modifications may play a role in siderophore stability and specificity.

So far, there are no published researches have already described iron uptake mechanism in the hemibiotrophic maize pathogen *C. graminicola.* The only available study on the hemibiotrophic rice pathogen *M. oryzae* on siderophore-mediated iron acquisition had shown the indispensable role of siderophores for vegetative growth, conidiation and full virulence {Hof, 2008 #138; Hof, 2007 #184}. There is no published research on the RIA pathway on hemibiotrophic pathogen.

I.4 Aims of the work

The overall aim of this work was to characterize iron uptake mechanisms in the fungal pathogen *C. graminicola* during vegetative development and plant infection. In fact, iron is not only a limiting factor in the environment and probably inside the plant tissue. It is also extremely low on the plant surface and in the bifacial matrix formed during biotrophic interactions. Therefore, the evaluation of the high affinity iron uptake pathways RIA and SIA during vegetative, under iron limited condition, and during pathogenic development is of significant interest. Moreover, as iron homeostasis is essential for ROS generation and tolerance, the roles of RIA and SIA in ROS generation and tolerance were investigated.

In hemibiotrophs, biotrophic and necrotrophic hyphae are sequentially formed. Therefore, *C. graminicola* allows studying the role of RIA and SIA pathways during pathogenesis, and, moreover, to discriminate between the importance of each high affinity iron uptake pathway in different pathogenic lifestyles. Thus, studying the role of both pathways in the hemibiotroph *C. graminicola* was performed to better understand the differential roles of RIA and SIA in biotrophy and necrotrophy.

In biotrophic development, the maize anthracnose and stem rot fungus avoids recognition by plant receptors. Thus, siderophore secretion during this phase may trigger or prime plant defense. Therefore, another goal was to investigate whether siderophores are involved in activation of defense responses, and, if so, how siderophore-primed immunity can be avoided.

To achieve these aims, the *FET3-1* and *FET3-2* genes as components of the RIA, and the *SID1* and *NPS6* genes as components of the SIA were deleted by targeted mutagenesis. Moreover, eGFP tagging of selected RIA- and SIA-related genes was made in order to analyze their cell-specific expression during *in-vitro* and *in-vivo* growth, and infection.

II. Materials and Methods

II.1 Biological Material

II.1.1 Fungal Material

II.1.1.1 *Colletotrichum graminicola*

The reference wild type strain CgM2 of *Colletotrichum graminicola* (Ces.) G. W. Wilson (teleomorph *Glomereella graminicola* D. J. Politis) (Anderson and Nicholson, 1996; Bergstrom and Nicholson, 1999) was provided by R. L. Nicholson, Purdue University, IN. The WT CgM2 strain and generated $\Delta fet3$-1 and $\Delta fet3$-2 strains were grown on oat meal agar (OMA) in 5 cm Petri dishes in an incubator (Binder, Tuttlingen, Germany) at 23°C and constant UV-light (TLD36W/08; Philips, Hamburg, Germany) to stimulate formation of conidia. Alternatively, strains were grown in complete medium (CM, see VIII.1.1 in the appendix), in an incubation shaker (Unitron, Infors AG, Bottmingen, Switzerland) at 23°C and 100 rpm. The double deletion mutant $\Delta fet3$-$1/2$ and the $\Delta nps6$ and $\Delta sid1$ mutants were kept on OMA medium supplemented with 100 µM Fe^{III}-EDTA.

Conidia from CgM2 WT and all other generated strains were washed with sterile H_2O_{bidest} from OMA plate and stored in 40% (v/v) glycerol at -80°C. Because the $\Delta sid1$ cannot make spores on OMA plates, it was grown on a sterile filter paper and stored in 40% (v/v) glycerol at -80°C.

II.1.1.2 *Saccharomyces cerevisiae*

The yeast strains used in this study were wild-type DY1457 (MATα, *ade6*, *can1*, *his3*, *leu2*, *trp1, ura3*) and $\Delta Scfet3fet4$ DEY1433 (MATα, *ade2, can1, his3, leu2, trp1, ura3, fet3*::*HIS3*, *fet4*::*LEU2*). The yeast strains were a kind gift from Prof. Dr. N. von Wirén (Leibniz Institute of Plant Genetics and Crop Plant Research; IPK, Gatersleben). The yeast strains were grown in Petri dishes on YPD-agar or SC-agar medium supplemented with their auxotrophic amino acid (VIII.1.3 in the appendix) at 30°C for 3-4 days in an incubator (Function LINE series, Kendro Laboratory Products, Langenselbold, Germany). To cultivate the yeast strains in

liquid media, a single colony was selected and grown in 2x YPAD or SCM media at 30°C and 200 rpm shaking (Classic C25, New Brunswick Scientific Co., New Jersey, USA).

Yeast strains were stored in 30% (v/v) glycerol at -80°C.

II.1.2 Bacterial Material

II.1.2.1 *Escherichia coli*

Escherichia coli XL1-Blue (Bullock et al., 1987), DH10B (Grant et al., 1990; Durfee et al., 2008) and *dam⁻/dcm⁻* (NEB, Ipswich, England) were grown on LB-agar plates at 37°C (Function LINE series, Kendro Laboratory Products, Langenselbold, Germany). Liquid cultures were initiated by inoculation of a single colony into LB medium. Incubation was at 37°C and 200 rpm in a culture shaker (Classic C25, New Brunswick Scientific Co., New Jersey, USA). The addition of antibiotics to media was according to the selection marker used in this study (VIII.1.1 in the appendix). Petri dishes and liquid cultures were stored, if necessary, at 4°C for up to one month. A stock culture was set up in LB-medium with 7% (v/v) DMSO and stored at - 80°C.

XL1-Blue	(*recA1 endA1 gyrA96 thi-1 hsdR17 supE44 relA1 lac* [F´ *proAB lacI*qZΔM15 Tn*10* (Tetr)])
DH10B	(*araD139* Δ (*ara,leu*) *7697 fhuA lacX74 galK16 galE15 mcrA f80d* (*lacZ*ΔM15) *recA1 relA1 endA1 nupG rpsL rph* spoT1 (*mrr-hsdRMS-mcrBC*)
dam⁻/dmc⁻	*ara-14 leuB6 fhuA31 lacY1 tsx78 glnV44 galK2 galT22 mcrA dcm-6 hisG4 rfbD1 R* (*zgb210::Tn10*) Tet^S *endA1 rspL136* (Str^R) *dam13::Tn9* (Cam^R) *xylA-5 mtl-1 thi-1 mcrB1 hsdR2*

II.1.3 Plant Material

II.1.3.1 *Zea mays*

The maize variety Nathan (KWS SAAT AG**,** Einbeck, Germany), was grown in steamed compost in 12 cm diameter pots, with three plants per pot in a controlled greenhouse at 22°C, 60% relative humidity and additional light at maximal 15 Klx, using OSRAM Plantastar 600W (OSRAM, Munich, Germany).

Alternatively, maize plants were grown in a climate chamber (AR-75L, Percival Scientific, Perry, USA) under the following condition:

16 h day
- 70% light intensity of the fluorescent tubes, light bulbs is on.
- 50% relative humidity
- 25°C

8 h night
- Darkness
- 70% relative humidity
- 20°C

II.1.3.2 *Allium cepa*

For infection assays on the alternate host onion, biologically grown onions of the variety Grano were used.

II.2 Chemicals

Chemicals, if not otherwise mentioned, were from Carl Roth (Karlsruhe, Germany). Primers were from MWG-Biotech (Ebersberg, Germany) and biomere.net (Ulm, Germany). Restriction enzymes and other reagents for molecular biology were from Fermentas (St. Leon-Rot, Germany) and New England Biolabs (NEB) (Ipswich, England). Bathophenanthroline disulfonate (BPS) was from GFS Chemicals (Powell OH, USA).

II.2.1 Media, buffers and solutions

Media, buffers and solutions used in this study are listed in the appendix (section VIII.1).

II.2.2 Vectors

Vectors used in this study are listed in the appendix (section VIII.2).

II.2.3 Primers

Primers used in this study are listed in the appendix (section VIII.3).

II.3 Infection and growth assays

II.3.1 Plant infection

II.3.1.1 Production of conidia

C. graminicola strains were grown as described on OMA plates (II.1.1.1). Conidia were collected from 2 weeks old OMA plates under sterile conditions by rinsing ca. 1 cm^2 of the plate with 1 ml sterile H_2O_{bidest}. The conidial suspension was centrifuged (Eppendorf 5417R, Hamburg, Germany) at 5000 *g* for 1 min. The conidial pellet was resuspended in 1 ml sterile H_2O_{bidest}, the washing step was repeated 3 times to remove traces of germination inhibitors in the mucilage (Bergstrom and Nicholson, 1999), and reference therein). Thereafter the conidial concentration was determined by counting an aliquot in a hemocytometer (Thoma, LO-Laboroptik, Friedrichsdorf, Germany).

II.3.1.2 Maize inoculation

Fourteen days old maize plants were inoculated with conidial suspension (10^6 conidia/ml) in 0.02% (v/v) Tween 20, whereas 20 ml of the conidial suspension was sprayed evenly on 3 plants/pot, using a sprayer (Carl Roth, Karlsruhe, Germany). A mock inoculation was done using 20 ml of 0.02% (v/v) Tween 20. Subsequently the inoculated plants were transferred to a climate chamber and covered with plastic tubes to keep the relative humidity at 100% for 24 h. The climate chamber parameters were set during the first day of inoculation as following: 16 h day light, with 70% light intensity of the fluorescent tubes, 99% relative humidity and 28°C; 8 h darkness with 99% relative humidity and 25°C. The following days, the parameters were set back to growth conditions as in II.1.3.1.

Symptom development was assessed and photographed from 1 to 6 days after inoculation.

Alternatively, conidia formed in liquid CM or 0.5 M sucrose medium (VIII.1.1 in the appendix) were harvested by filtration using Miracloth (EMD Chemical, Darmstadt, Germany) and collected in 15 ml Falcon tube (Greiner bio-one, Frickenhausen, Germany), washed three times with sterile H_2O_{bidest} and counted as previously described (II.3.1.1). The inoculum was as previous, but using 10^7 conidia/ml instead of 10^6 conidia/ml.

Leaf segments (8-10 cm) were cut from second and third leaves of fourteen days old maize plants. The leaf segments were placed in Petri dishes (14 cm Ø) on 2 layers of moist filter paper (Carl Roth, Karlsruhe, Germany). Leaf segments were inoculated with 10 µl droplets containing $2x\ 10^3$ or $1x\ 10^4$ conidia according to the aim of the experiment. The inoculated leaf segments were incubated in the climate chamber at 28°C and darkness for the first 24 hours then at 25°C in darkness the following days. Artificial wounding was made immediately before inoculation using a sterile needle (B. Braun Sterican hypodermic needle 0.4 x 20 mm, Melsungen, Germany).

Defence responses were analysed after infiltrating the leaf segments with 0.05-0.1 µg/µl desferricoprogen or H_2O 1 h before inoculation with *C. graminicola* WT.

The number of newly formed conidia was counted 6 days after inoculation through rigid washing of the inoculated leaf segments in 2 ml of 0.02% (v/v) Tween 20 using a hemocytometer (II.3.1.1).

II.3.1.3 Inoculation of onion epidermis

Onion epidermis was carefully removed, cut (ca. 2×1 cm) and washed three times in H_2O_{bidest} to remove traces of nutrients. Thereafter the onion epidermis was placed into Petri dishes containing 1.5% (w/v) agarose-water and inoculated with 10 µl droplets containing $2x\ 10^3$ conidia. The inoculated epidermic layers were incubated as previously indicated (II.3.1.2).

II.3.2 Growth assays

II.3.2.1 Plate growth assays

To quantify the vegetative growth of the *C. graminicola* WT strain and the corresponding deletion mutants, growth assays were performed on PDA medium. Iron depleted medium was made by adding different concentration of the iron scavenger BPS (0, 20, 50, 100, 250 µM) (VIII.1.3 in the appendix). Sensitivity assays to ROS was performed on PDA supplemented with either H_2O_2 or rose bengal. Mycelial blocks were taken from the growing front of the investigated strains grown on PDA using a cork borer (0.4 cm Ø). All growth assays, with the exception of those on rose bengal medium, were done at 23°C and darkness in an incubator

(Binder, Tuttlingen, Germany). The rose bengal experiment was done at 23°C and constant light ($10\,\mu E\,m^{-2}\,S^{-1}$). The growth was measured daily and colonies were photographed after 4-13 days, according to the experiment.

II.3.2.2 pH sensitivity assays in liquid media

To quantify vegetative growth of *C. graminicola* WT and the corresponding deletion mutants under different pH conditions, liquid PD medium was adjusted to pH 4.5; 7.0 and 10.0. The buffers used 100 mM MES, pH 4.5; 100 mM HEPES, pH 7.0; and 100 mM CAPS (AppliChem, Darmstadt, Germany), pH 10.0. Fungal inocula were cut using 0.4 cm Ø cork borer from the front edge of a colony growing on PDA plates. One disk was used to inoculate 100 ml PD medium in 250 ml Erlenmeyer flasks. Three independent mutants were used for each strain. The inoculated flasks were placed in an incubation shaker (Unitron, Infors AG, Bottmingen, Switzerland) at 23°C and 100 rpm for 10 days. At the end of experiment, pH value of the medium was measured using a glass electrode pH meter (Sentix81 WTW, Weilheim, Germany) and the grown mycelia were collected by filtration (601A Carl Roth, Karlsruhe, Germany). The collected mycelia were transferred to pre-weighed pieces of aluminum foil and oven-dried at 100°C for 24 h (Linn High Therm, Eschenfelden, Germany). The dried mycelia were then measured using a precision balance (SBC21 SCALTEC, Gottingen, Germany).

II.3.2.3 Yeast complementation assay

To confirm the function of both Fet3-1 and Fet3-2 as functional ferroxidases, cDNAs of both genes were expressed in the yeast Δ*Scfet3fet4* mutant that lacks the ability to assimilate iron via the reductive pathway (Askwith et al., 1994; Dix et al., 2004). The Δ*Scfet3fet4* mutant has a severe growth defect under iron-limited conditions. Wild-type *S. cerevisiae* and Δ*Scfet3fet4* strains harboring either the complementation vectors pAG300-FET3-1 or pAG300-FET3-2, or the empty vector pAG300 (II.4.7.1) were grown overnight on synthetic complete medium lacking uracil and supplement with 50 µM BPS (SCM-BPS) at 30°C and 200 rpm in a culture shaker (Classic C25, New Brunswick Scientific Co., New Jersey, USA). A 10-fold dilution series (10^6-10^2) was spotted onto SCM-BPS plates lacking uracil, and the plates were incubated at 30°C in an incubator (Heraeus, Hanau, Germany) and were photographed after 4 days.

II.3.2.4 Conidial formation assays

The *Colletotrichum graminicola* wild-type strain produces conidia when grown on OMA at 23°C and constant UV-light (TLD36W/08; Philips, Hamburg, Germany). The ability of the WT strain and the corresponding mutants to form conidia was assayed on OMA plates supplemented with different concentration of $FeSO_4$, $FeCl_3$, Fe^{III}-EDTA, siderophores (i.e. ferricrocin, coprogen, ferrichrome, rhizoferrin or enterobactin) or the iron scavenger BPS. 50 mm plates were filled with 10 ml OMA and inoculated with a 0.4 cm Ø mycelial block using a cork borer from the front edge of the growing *C. graminicola* strains.

The plates were incubated at 23°C and constant UV light for two weeks. Thereafter, the conidia formed were washed from the plate with 2 ml distilled water, the washing process was repeated three times until the conidia were completely removed from the plate. The washed conidia were collected in 15 ml Falcon tube (Greiner bio-one, Frickenhausen, Germany), and counted in a hemocytometer (Thoma, LO-Laboroptik, Friedrichsdorf) as described. Four plates have been used per strain and growth assays were repeated four times.

II.3.2.5 Protoplasting of oval conidia

Conidia from 10-14 days old colonies grown on OMA plates were washed under sterile conditions, using 1 ml of H_2O_{bidest} and inoculated into 100 ml of CM medium to get a final concentration of 10^6 conidia/ml. The culture was incubated without shaking at RT for 6-8 days.

The culture was filtered through two layers of Miracloth (EMD Chemical, Darmstadt, Germany), and the filtrate was centrifuged at 4260 g and 4°C for 10 min. to collect the oval and falcate conidia. The conidia were resuspended in a protoplasting solution (solutions in the appendix). The suspension was incubated at 30°C and 80 rpm (Unitron, Infors AG, Bottmingen, Switzerland). The protoplasting efficiency was microscopically assessed every hour.

II.4. Molecular Biology

II.4.1 Preparation of nucleic acid

II.4.1.1 Genomic DNA isolation from Fungi (maxi prep)

Isolation of genomic DNA (gDNA) was done according to (Döbbeling et al., 1997). 500 mg of fungal mycelium (6 to 8 days old in liquid culture) were briefly dried on absorbent paper towel and ground using mortar and pestle in liquid nitrogen to a homogeneous powder. To the frozen powder 800 µl of extraction buffer I (VIII.1.2 in the appendix) and 800 µl of phenol: chloroform (1:1) was added and mixed carefully. Phases were separated by centrifugation in Eppendorf centrifuge 5417R (Eppendorf, Hamburg, Germany) for 10 min at 14500 g and 4°C. The upper aqueous phase was transferred into a new DNase/RNaes-free micro centrifuge tube, re-extracted with the same volume of chloroform and centrifuged as described above. Subsequently, for precipitation of DNA the same volume isopropanol was added and incubated for 60 min at -20°C. The DNA was precipitated by centrifugation (15 min, 6800 g, 4°C) and the pellet was re-suspended in 700 µl extraction buffers II (VIII.1.2 in the appendix). RNA and remaining proteins were removed by a 30 min treatment with 3.5 µl (10 mg/ml) RNase-A (Roche diagnostics, Mannheim, Germany) at 37°C, followed by proteases treatment using 10 µl (20 mg/ml) Proteinase K (Roche diagnostics, Mannheim, Germany) for 60 min at 60°C. A phenol: chloroform and chloroform extraction, followed by isopropanol precipitation (see above) was repeated. The precipitated DNA was centrifuged (20 min, 14500 g, 4°C), washed with 70% (v/v) EtOH and centrifuged for extra 20 min (14500 g, 4°C). The supernatant was aspirated and the pellet was dried under the sterile bench or by vacuum centrifuge (UNIVAPO 100 H, Uni Equip, Dresden, Germany). The pellet was suspended in H_2O_{bidest} or TE buffer (VIII.1.2 in the appendix).

Alternatively, DNA isolation was performed using the PeqLab DNA extraction kit (PEQLAB Biotechnology, Erlangen, Germany) following the manufacturer's instruction.

The DNA concentration was measured using NanoDrop 1000 (Thermo Scientific, Braunschweig, Germany).

II.4.1.2 Genomic DNA isolation from fungi (mini prep)

For fast screening of positive fungal transformants, a quick DNA isolation method was applied. First, single spore isolates were grown on OMA plates 5 to 7 days until the colony covered the plate. Thereafter 4 to 6 pieces of fungal mycelium of a size 5 x 5 mm^2 were sliced and put into 2 ml microcentrifuge tubes. Then 500 µl lyses buffer (VIII.1.2 in the appendix) was added to the mycelial pieces and vigorously vortexed for 30 s followed by 10 min incubation at room temperature (RT). Afterward the mycelial pieces were vigorously vortexed for 1 min and centrifuged at 18000 g for 10 min and 4°C. The supernatant was then carefully removed and transferred to a new 1.5 ml microcentrifuge tube and mixed gently by inverting with 750 µl 100% EtOH to facilitate DNA precipitation. The microcentrifuge tubes were then centrifuged at 18000 g for 10 min at 4°C and the pellets were washed with 500 µl 70% EtOH and centrifuged at 18000 g for additional 10 min at 4°C. Thereafter the DNA pellet was thereafter dried under a sterile bench for 10 min and then suspended with 50 µl sterile H$_2$O$_{bidest}$ or TE buffer.

The quality of the DNA obtained is sufficient for fast screening of candidate transformants using PCR (II.4.4.1).

II.4.1.3 Plasmid isolation from bacteria

Plasmids were isolated using Fermentas Plasmid Miniprep (Fermentas, St. Leon-Rot, Germany) or the Qiagen Plasmid midiprep (Qiagen, Hilden, Germany) kits following the manufacturer's instruction.

II.4.1.4 Total RNA isolation

RNA isolation was done according to (Chirgwin et al., 1979). *Colletotrichum graminicola* was grown in a liquid complete medium (CM) for 4-5 days followed by two days in iron limited medium (ILM; VIII.1.1 in the appendix), to induce the expression of iron-related genes (II.4.4.8).

Alternatively, RNA was isolated using the PeqGold plant and fungal RNA isolation kit (PEQLAB, Erlangen, Germany), following the manufacturer's instruction. The resulting RNA was stored at -20 for short or -80°C for long term.

To determine the quantity of the RNA, a 50-fold dilution of 100 µl aliquots was measured by a spectrophotometer (Specord$^{®}$ 250 Double beam UV/VIS spectrophotometer; Analytik Jena AG, Jena, Germany) at 260 and 280 nm. To determine the quality of the RNA, 2 µl of total RNA was run on 0.8% agarose gel electrophoresis and visualized by ethidium-bromide under UV light (MultiImage^{TM} light Cabinet; Alpha Innotech Corporation, USA).

Alternatively, a 10 ng of RNA samples was analyzed on Agilent 2100 Bioanalyzer nano-plates (Agilent Biotechnology, Waldbronn, Germany)

II.4.2. Gel electrophoresis

DNA or RNA fragments were separated on 0.7-2% (w/v) agarose gels (Seakem$^{®}$ LE-Agarose, Biozym Diagnostik, Oldendorf, Germany). Agarose was dissolved in 1x TAE or 1x $Na_2B_4O_7$ buffer (VIII.1.2 in the appendix). The DNA/RNA samples were mixed with 0.2 vol. of 6x loading buffer and loaded into the gel wells and separated with constant current (70-110 V; TAE gel) and (200-250 V; $Na_2B_4O_7$ gel) in an electrophoresis chamber. Subsequently, the gel was stained by ethidium bromide solution (0.5-1 µg/ml H_2O) for 20-60 min and visualized by UV light with a wavelength of 320 nm and photographed (MultiImage^{TM} light Cabinet; Alpha Innotech Corporation, USA). As a standard with defined sizes of DNA fragments (GeneRuler DNA Ladder-Mix, GeneRuler 50 bp DNA Ladder; Fermentas, St. Leon-Rot, Germany) was used for size estimation.

II.4.3 Southern-hybridization

II.4.3.1 Generation of DIG-labeled probes

Hybridization probes were generated by standard PCR (II.4.4.1), except that the regular dNTP mix was replaced by a digoxigenin (DIG)-dNTPs-mix, consistsing of 2 mM of dATP, dCTP, and dGTP, 1.9 mM dTTP each and 0.1 mM DIG-dUTP (PCR DIG Labelling Mix Alkali-labil; Roche Diagnostics, Mannheim, Germany). Successful labeling was verified by agarose gel electrophoresis (II.4.2). DIG-labeled fragments appeared larger than non-labeled reference fragments, due to the incorporated digoxigenin.

II.4.3.2 Genomic DNA digestion and gel electrophoresis

DNA samples (5 μg) were digested overnight (ca. 16 h) with the appropriate restriction enzymes and buffers at 37°C (Function LINE series, Kendro Laboratory Products, Langenselbold, Germany). The digested DNA fragments were separated on a 0.8% agarose gel after addition of DNA-loading buffer (II.4.2). The complete digestion was confirmed by ethidium-bromide staining and digital documentation of the gel under UV light (320 nm).

II.4.3.3 Capillary transfer, hybridization and detection

After electrophoresis, the DNA was depurinated in 0.25 M HCl for 10 min. Then the gel was incubated for two times 20 min each in 0.4 M NaOH to denature the double stranded-DNA fragments. Blotting the fragmented DNA was accomplished by downward capillary transfer to a positively charged nitrocellulose membrane (Hybond-N+, Amersham Pharmacia Biotech, Freiburg, Germany) (Brown, 1999), using alkaline transfer buffer (VIII.1.2 in the appendix) for ca. 6-8 h.

After transfer, DNA fragments were cross-linked to the filter for 1 h at 80°C in a hybridization oven (Biozym Scientific, Hess, Oldendorf, Grmany). Subsequently, the membrane was pre-hybridized in 20 ml of hybridization buffer (VIII.1.2 in the appendix) at 65°C for 2 h. Thereafter, the denatured probe was (boiled at 99°C for 2 min and chilled in a salt-ice bath) added to the hybridization buffer and incubated overnight at 65°C. The filter was then washed stepwise for 5 min with 2x wash buffer I at RT twice, then 2x 15 min with 0.5x washing buffer I at 65°C, and finally equilibrated for 1 min with wash buffer II. Afterwards, the filter was incubated for 1 h in blocking buffer, followed by the addition of anti-DIG antibody (diluted to 1:10000; anti-DIG AP Fab-Fragment; Roche Diagnostics, Mannheim, Germany) to the blocking buffer. The unbound antibodies were removed by 2 washing steps for 15 min each, using washing buffer II at RT. The membrane was then shortly swung in detection buffer and placed between two plastic sheets after the addition of 1 ml of CSPD solution (0.25 mM CSPD ready-to-use; Roche Diagnostics, Mannheim, Germany) and incubated for 5 min in darkness. All buffers used are listed in the appendix.

The membrane was then sandwiched between two plastic sheets and exposed onto an X-ray film (Hyperfilm ECL; Amersham Pharmacia Biotech, Freiburg, Germany). Exposure time depended on the signal strength, ranging from 2 h to overnight (ca. 16 h). The film was then

developed in automatic developing machine (Optimax TR; MS Laborgeräte, Heidelberg, Germany).

II.4.4. Polymerase chain reaction (PCR)

II.4.4.1 Standard PCR

All PCR reactions were performed in Biometra personal or Biometra T-Professional thermocyclers (Biometra Analytika, Göttingen, Germany). The Enzymes used and related buffers were from New England Biolabs (Thermopol Taq polymerase; Ipswich, England), or Fermentas (Fermentas native Taq polymerase; St. Leon-Rot, Germany). Typically, a 50 µl reaction mix was set up as follows:

Ingredient	Volume
10x Thermopol buffer	5 µl
dNTPs (10mM)	1 µl
$MgCl_2$ (50mM)	1.5 µl
DNA template	50 -300 ng
Forward/Reverse primers (10 pmol)	1 µl
Taq polymerase (5 u/µl)	0.2- 0.5 µl
H_2O_{bidest}	*ad*. 50 µl

The standard PCR cycles were conducted as follows:

Time	Temperature	Step	Cycles
2 min	95°C	Initial denaturation	1
30 s	94°C	Denaturation	
30 s	T_m+3-5°C	Annealing	30-40
1 min/Kb	72°C	Extension	
10 min	72°C	Final extension	1
	4°C	Hold	

The number of cycles was depending on the PCR product required and DNA template. The annealing temperature depends on the melting temperature (T_m) of the chosen primers and was set 3 to 5 degrees above the melting temperature (a gradient PCR was sometimes needed to find the suitable annealing temperature for primers combination). The duration of extension step depends on the size of amplified fragment and the used Taq polymerase (~1 kb/min).

II.4.4.2 PCR with degenerate primers

Degenerate primers of the ferroxidase gene *FET3-1* was constructed based on conserved sequences of putative ferroxidase genes from closely related filamentous fungi (i.e. *A. fumigatus*; AAT84595.1, *Claviceps purpurea*; CAD21518.1, *Candida albicans;* P78591.1, *Fusarium graminearum*; EAA74443.1, *M. oryzae;* XP_365454.1, *Neurospora crassa*; XP_955835.1). These sequences were used to construct the degenerate primers FET3-deg-Fw.1, FET3-deg-Fw.2, FET3-deg-Rv.1 and FET3-deg-Rv.2 (VIII.3.1 in the appendix). Degeneracy of the chosen primers was less than 512.

Similar to the standard PCR, a 50 µl PCR set were used containing 100-300 ng DNA template, 0.5 µl Taq polymerase and 6 µl of each degenerate primer (10 pmol). The PCR program was as in II.4.4.1with 40-50 cycles.

Control PCR set was performed with single primers. PCR products were separated on agarose gel electrophoresis (II.4.2) and the PCR product of the expected size was extracted, cloned into pGEM®-T easy (Promega; Manheim, Germany) and used as a template for sequencing (II.4.6).

II.4.4.3 Genome walking

The unknown 5´and 3´regions adjacent to the sequence obtained by degenerated PCR were identified by tail PCR (Liu and Baird, 2001). First, 10 µg of gDNA was partially digested (60 min at 37°C for 1 h) with 0.5 u *Nla*III (NEB, Ipswich, England). The digested DNA was separated on a 0.7% (w/v) agarose gel and the fragments >2 kb were eluted from the gel. Subsequently, these fragments were tailed in a tailing reaction consisting of the following compounds: 3-5 µg DNA elutions; 50 u TdT; 0.25 mM $CoCl_2$; 1 mM dCTP and 1x reaction buffer (NEBuffer 4, Ipswich, England) in a 50 µl reaction at 37°C for one hour. The inactivation of TdT enzyme was accomplished by incubation at 80°C for 20 min.

The amplification process of unknown regions was achieved using two rounds of PCR, The primary PCR round was in a 50 µl reaction as following:

Ingredient	Volume
10x Thermopol buffer	5 µl
dNTPs (10 mM)	1.25 µl
MgCl$_2$ (50 mM)	1.5 µl
SAP (10 pmol)	2.5 µl
FET3-GSP1 (10 pmol)	1 µl
Taq polymerase 5 u/µl	0.5 µl
Oligo dC-DNA	0.5 µg
H$_2$O$_{bidest}$	*ad*. 50 µl

The PCR program used was as following

Time	Temperature	Step	Cycles
2 min	95°C	Initial denaturation	1
30 s	95°C	Denaturation	5
2 min	72°C	Extension	
30 s	95°C	Denaturation	
30 s	70°C	Annealing	5
2 min	72°C	Extension	
30 s	95°C	Denaturation	
30 s	68°C	Annealing	20
2 min	72°C	Extension	
5 min	72°C	Final extension	1
	4°C	Hold	

One microliter from the first PCR reaction was used as a template to perform the second PCR reaction, using combination of UAP and FET3-GSP2 nested primers (VIII.3.1). Standard PCR programs were performed (II.4.4.1), with 2 min extension and 68°C annealing temperature. The PCR products were analyzed on a 1% agarose gel (II.4.2) and bands > 500 bp were extracted and eluted from the gel, cloned into pGEM®-T easy and sequenced (II.4.6).

II.4.4.4 PCR with high fidelity polymerase (fusion PCR)

All PCRs for amplifying deletion and fusion constructs were performed using Phusion High-Fidelity DNA Polymerase (Finnzymes Oy, Espoo, Finland). All ingredients were from New England Biolabs (NEB, Ipswich, England). 20 or 50 µl PCR set was performed according to manufacturer's instructions (Finnzymes Oy, Espoo, Finland).

The annealing temperature depends on the T$_m$ of the chosen primers and was calculated using the Finnzymes Tm calculator web site (http://www.finnzymes.fi/tm_determination.html). The duration of extension step depends on the size of amplified fragment (20 s/kb).

II.4.4.5 DJ-PCR (Double-Joint PCR)

The construction of deletion cassettes (KO) of target genes was performed using double joint PCR (DJ-PCR) method (Yu et al., 2004). The first 50 µl-PCR reactions were to generate the 3´- and 5´- flanks in addition to the selection marker. 25-30-bp overhangs were introduced to 5´- and 3´-flanks complementary to the selection marker by primers listed in the appendix (VIII.3). Products from the first PCR reaction were checked on agarose gel and purified using Qiagen Mini Elute kit (Qiagen, Hilden, Germany). Then, those products were used as mega primers to be combined in a second PCR reaction. The second PCR set was as following:

Ingredient	50 µl reaction
5x Phusion HB buffer	10 µl
dNTPs (10 mM)	1 µl
5´-Flank	
Resistance cassette	Stoichiometric relation (1:3:1)
3´-Flank	
Phusion DNA Polymerase	0.5 µl
H_2O_{bidest}	*ad*. 50 µl

And the PCR program was as following:

Time	Temperature	Step	Cycles	Note
30 s	98°C	Initial denaturation	1	
20 s	98°C	Denaturation		
30 s	60°C	Annealing	10	1[rst] reaction
1 min	72°C	Extension		
20 s	98°C	Denaturation	25	2nd reaction
1:30 min	72°C	Annealing/Extension		
5 min	72°C	Final extension	1	
	4°C	Hold		

The second PCR product was used as a template to generate the final fusion construct using nested primers and Phusion DNA polymerase according to manufacturer's instructions (Finnzymes Oy, Espoo, Finland). The amplified cassettes were purified with QIAquik PCR purification kit according to the manufacturer's instructions (Qiagen, Hilden, Germany) and used for either cloning (II.4.5) or directly for *C. graminicola* transforming (II.4.8).

II.4.4.6 RT-PCR

RT-PCR assay was used to analyze the transcript abundance of the *FET3-1, FET3-2, NPS6,* and *SID1* genes in deletion mutants and the wild-type strains, or strains harboring KO cassettes ectopically. Target gene was amplified using OneStep RT-PCR kit (Qiagen, Hilden, Germany) according to manufacturer's instruction. 50 ng RNA were used for 20 µl RT-PCR set.

Control reactions were performed in parallel, using specific primers (H3-qRT.Fw.2/H3-qRT.Rv.2) to amplify an 85-bp fragment of the Histon 3 from *C. graminicola*.

II.4.4.7 Verification of the ORFs of iron uptake-related genes

In order to predict the open reading frame (ORF) of the studied genes, they were first directed to the gene prediction server (Augustus; University of Gottingen, http://bioinf.uni-greifswald.de/augustus/ and FGENESH; http://www.softberry.com/) against *F. graminearum* and *M. oryzae* databases. cDNA synthesis and PCR amplification was performed using OneStep RT-PCR Kit (Qiagen, Hilden, Germany) using specific primer combination as follows:

Gene	Primers combination		cDNA/gDNA (bp)
FET3-1	FET3-1-ORF-Fw.	× FET3-1-ORF-Rv.	1756/2024
FET3-2	FET3-2-ORF-Fw.	× FET3-2-ORF-Rv.	1866/1987
FTR1-1	FTR1-1-ORF-Fw.	× FTR1-1-ORF-Rv.	1177/1339
FER2	FRE2-ORF-Fw.	× FRE2-ORF-Rv.	2332/2647
SID1	SID1-ORF-Fw.1	× SID1-ORF-Rv.2	1774/1885
NPS6	NPS6-1.int.-Fw.1	× NPS6-1.int.-Rv.1	432/354
	NPS6-2.int.-Fw.2	× NPS6-2.int.-Rv.2	320/320
SIT1	SIT1-ORF-Fw.1	× SIT1-ORF-Rv.1	1791/1914
SRE1	SRE1-ORF-Fw.1	× SRE1-ORF-Rv.1	1798/1919

The ORFs were verified by sequencing the PCR products and comparing with gDNA sequences, using the SeqMan 5.00© program (DNASTAR, Inc.; Madison, USA).

II.4.4.8 Quantitative analyses of gene transcripts using qRT-PCR

In order to induce iron starvation, mycelium of *C. graminicola* was grown in CM medium for 4 days, filtered through Miracloth (EMD Chemical, Darmstadt, Germany), washed three

times with sterile deionized water (Milli-Q, TKA, Thermo Electron LED GmbH, Niederelbert, Germany) and transferred to ILM medium for two days. Subsequently, the mycelium was transferred to fresh CM medium containing 0.01 mM or 1 mM $FeCl_3$, or $FeSO_4$, or 200 µM BPS for additional two days.

To analyze the transcript abundance of the maize defense markers *PR1* and *PR3*, RNA (II.3.1.2) from *C. graminicola* WT-inoculated maize leaves was used.

Total RNA was isolated using the PeqGOLD plant and fungal RNA kit (PEQLAB, Erlangen, Germany). Genomic DNA was removed using the peqGOLD DNase I Digest Kit (PEQLAB, Erlangen, Germany). Quantitative RT-PCR (qRT-PCR) was performed using the Power SYBR Green RNA- to- C_T *1*-step Kit (Applied Biosystems, Foster City, CA, USA), according to the instructions of the manufacturer, using 50 ng total RNA, 10 µl Power SYBR Green RT-PCR mix (2x), 2 pmol of each primers and 0.16 µl of RT enzyme-mix (125x).was. RT-PCR reactions were performed in an iQ5 real time PCR (Bio-Rad, Munich, Germany), using standard RT-PCR programs (Applied Biosystems, Foster City, CA, USA). The number of cycles was 40-60 depends on the transcript abundance of target gene. PCR products were verified on 2- 2.5% sodium borate ($Na_2B_4O_7$) agarose (II.4.2).

Gene-specific primers are listed in the primer table (VIII.3.6). To confirm the absence of genomic DNA, RT-PCR and qRT-PCR assays were performed without reverse transcriptase as a negative control. A sigmoidal curve-fitting has been performed for all qRT-PCR analyses (Rutledge, 2004), and relative transcript abundance has been quantified as described (Livak and Schmittgen, 2001). The relative transcript abundance has been normalized using the two constitutive housekeeping genes actin *ACT1* and histone *H3* (Horbach et al., 2009; Behr et al., 2010).

II.4.4.9 Quantification of fungal DNA

Quantitative PCR (qPCR) was employed for quantifying fungal mass of infection sites (F. Weihmann and S.G.R. Wirsel, personal communication), briefly as the following:

II.4.4.9 1 Infection process and genomic DNA isolation

Leaf samples were collected four days post inoculation (4 DPI) from 8 independent leaf segments using a cork borer (1 cm Ø) and pooled (8 pieces) in 2 ml Eppendorf tubes

containing two metal balls, flashed frozen in liquid nitrogen and kept at -80°C. Inoculated reference samples were collected at 0 HPI.

Samples were homogenized using a Tissue-Lyser II (Qiagen, Hilden, Germany) for 30 seconds at 30 Hz in buffer P1 of the PeqLab DNA extraction kit (PEQLAB Biotechnology, Erlangen, Germany) containing 50 pg of plasmid pUC18 (Fermentas, St. Leon-Rot, Germany) as an external reference standard. The DNA extraction followed the manufacturer's protocol (PeqGold plant DNA extraction Kit).

II.4.4.9 2 Quantification of fungal mass using qPCR

The resulting DNA was measured and the fungal DNA mass was analyzed using real time PCR (iQTM5, Bio-Rad, Munich, Germany) using primers ITS2-qPCR-Fw. and ITS2-qPCR-Rv. The concentration of plasmid pUC18 was analyzed using the primers M13-qPCR-Fw. and M13-qPCR-Rv.

II.4.5 Cloning and transformation of *E. coli*

Cloning of DNA Fragments into plasmids pGEM®-T easy, pJET1.2/blunt (Fermentas St. Leon-Rot, Germany) and others (VIII.2) was performed according to manufacturer's protocols and (Sambrook and Russel, 2001). Competent *E. coli* (XL1-Blue strain) was prepared and transformed according to (Chung et al., 1989). Electrocompetent *E. coli* cells were obtained from NEB (Ipswich, England) and transformed according standard protocol.

II.4.6 Sequencing and sequence analysis

For DNA sequencing, templates were either PCR products or plasmids. 10 µl of the sequence reaction mix was prepared according to the instructions of the manufacturer (BigDye Terminator v3.1, Applied Biosystems, Foster City, CA, USA). Sequence evaluation and manual correction of the sequence data were done by the Lasergene program package of DNASTAR (DNASTAR, Inc.; Madison, USA). Homology comparison and BLAST searches (Altschul et al., 1997) were made using the web sites of the NCBI (www.ncbi.nlm.nih.gov).

II.4.7 Yeast complementation

C. graminicola FET3-1 and *FET3-2* cDNA was amplified from mRNA isolated from the WT strain grown on CM medium containing 50 µM BPS, using the Phusion® RT-PCR Kit (New England Biolabs, County Road, Ipswich, England) and primer combinations FET3-1-SfiIA-Fw.1 and FET3-1-SfiIB-Rv.1; and FET3-2-SfiIA-Fw.1 and FET3-2-SfiIB-Rv.1, respectively. The resulting cDNAs were cloned into pJET1.2/blunt. After confirming the sequences, the plasmids containing the cDNAs were digested with *Sfi*I and subcloned into the *Sfi*I-digested yeast expression plasmid pAG300 (Horbach et al., 2009), yielding pAG300-FET3-1 and pAG300-FET3-2. Both cDNAs were thus expressed under the control of the constitutive ADH1 promoter (Vernet et al., 1987). Yeast WT and Δ*fet3fet4* strains were transformed with pAG300, pAG300-FET3-1 or pAG300-FET3-2, using a standard protocol (Gietz and Woods, 2002).

To visualize the localization of the Fet3-1 and Fet3-2 proteins, enhanced green fluorescent protein (*eGFP*) fusions of *FET3-1* and *FET3-2* were generated, using double-joined PCR (Yu et al., 2004). cDNA of *FET3-1* was amplified with primers FET3-1-SfiIA-Fw.1 and FET3-1-eGFP-Rv.1, using pAG300 containing cDNA of *FET3-1* as template. The cDNA of *FET3-2* was amplified using primers FET3-2-SfiIA-Fw.1 and FET3-2-eGFP-Rv.1, and pAG300 containing cDNA of *FET3-2* as template. The eGFP cassette was amplified with primers EGFP-Fw.1 and EGFP-SfiB-Rv.1 from plasmid pSH1.6EGFP. In a second PCR, the products of the first PCR were used to fuse the *FET3-1* and the *FET3-2* cDNAs with *eGFP*. These cassettes were digested with *Sfi*I, ligated into *Sfi*I-digested pAG300 and transformed into yeast mutant Δ*fet3fet4*.

II.4.8 Transformation of *C. graminicola*

C. graminicola transformation was done using standard protocols established in our lab as described by (Werner, 2002).

II.4.9 Deletion Strategy

II.4.9.1 Deletion of *FET3-1* and *FET3-2*

Deletion cassettes (knock-out cassettes: KO) were generated by double-joint PCR (Yu et al., 2004). The 5'- and 3'-flanking regions of the *FET3-1* gene were amplified with the primer combinations FET3-1-KO-5'-Fw.1 and FET3-1-KO-5'-Rv.1, and FET3-1-KO-3'-Fw.1 and FET3-1-KO-3'-Rv.1, and 100 ng of genomic DNA as template. The nourseothricin acetyl transferase (*nat1*) cassette was amplified from plasmid pNR1 (Malonek et al., 2004), using primers Nat1-Fw.1 and Nat1-Rv.1. In a second PCR, the 5'- and 3'-flanks were fused with the *nat1* cassette, and the complete product was amplified using nested primers FET3-1-KO-nest-Fw.1 and FET3-1-KO-nest-Rv.1. The 4167-bp product was cloned into pJET1.2/blunt, yielding plasmid pFET3-1KO.

To generate the *FET3-2* deletion construct, the 5'- and 3'-flanks were amplified with the primer pairs FET3-2-KO-5´-Fw.1 and FET3-2-KO-5´-Rv.1, and FET3-2-KO-3´-Fw.1 and FET3-2-KO-3´-Rv.1. The hygromycin phosphotransferase (*hph*) cassette was amplified from plasmid pAN7-1 (Punt et al., 1987), using primers Hyg-Fw.1 and Hyg-Rv.1. In a second PCR, the 5'- and 3'-flanks were fused with the *hph* cassette, and the complete product was amplified using nested primers FET3-2-KO-nest-Fw.1 and FET3-2-KO-nest-Rv.1. The 4971-bp product was cloned into pJET1.2/blunt, yielding plasmid pFET3-2KO.

The FET3-1 and FET3-2 deletion constructs were amplified by PCR, using pJET1.2-Fw. and pJET1.2-Rv. primers and transformed into conidial protoplasts as described (Werner, 2002).

To facilitate screening of positive candidate strains harboring the KO cassette homologically, genomic DNA was isolated using mini prep method, and the KO cassettes were amplified using primers FET3-1-KO-nest-Fw.2 and FET3-1-KO-nest-Rv.2, and FET3-2-KO-nest-Fw.2 and FET3-2-KO-nest.Rv.2. To prove the correct integration site of the KO cassette, Southern assays were performed using *Psc*I (*FET3-1*) and *Nco*I (*FET3-2*) enzymes, and hybridized

with specific probes as following: 1.6-kb-FET3-1-probe was amplified using primers Nat1-prob-Fw.1 and FET3-1-KO-nest-Rv.2, 1.5-kb-FET3-2-probe was amplified using primers Hyg-Prob-Fw.1 and FET3-2-KO-nest-Rv.3).

II.4.9.2 Deletion of *SID1*

To generate the *SID1* deletion construct, the 5´ and 3´ flanking regions were amplified using primers (SID1-KO-5´-Fw.1/SID1-KO-5´-Rv.1) and primers (SID1-KO-3´-Fw.1/SID1-KO-3´-Rv.1), respectively. The hygromycin resistance cassette was amplified from vector pAN7-1 as in II.4.9.1. In a second PCR, the 5'- and 3'-flanks were fused with the *hph* cassette, and the complete product was amplified using nested primers SID1-KO-nest-Fw.1 and SID1-KO-nest-Rv.1. The 4519-bp product was cloned into pJET1.2/blunt, yielding pSID1KO. This vector was used as a template to amplify the KO construct using primers SID1-KO-nest-Fw.2 and SID1-KO-nest-Rv.2 for fungal transformation. Genomic DNA was isolated from candidate strains using mini prep method, and the KO cassette was amplified by standard PCR, using primers SID1-KO-nest-Fw.3 and SID1-KO-nest-Rv.3.

To confirm the correct integration site of the KO cassette, a Southern assay was performed (II.4.4). The genomic DNA of positive candidate strains was isolated using maxi prep and digested with *Mun*I endonuclease, and analyzed by Southern hybridization using a specific 1512-bp probe (Hyg-Prob-Fw.1/SID1-KO-nest.Rv.2).

II.4.9.3 Inactivation of *NPS6*

The inactivation of the *NPS6* gene was achieved by a partial deletion of the ORF and substitution by hygromycin resistance cassette. First, a 5912-bp fragment of the *NPS6* was amplified by PCR using primer pairs NPS6-Fw.1 and NPS6-Rv.1, and cloned into pJET1.2/blunt. The resulting plasmid pNPS6 was digested with the *Age*I endonuclease, resulting removal of 3229 bp of the ORF. The linearized plasmid was then dephosphorylated. The 2692-bp hygromycin resistance cassette was cut from pAN7-1 using (*Age*I/*Ngo*MIV) double digestion and subcloned into the *Age*I digested pNPS6, resulting pNPS6KO. The entire 5.6-Kb KO cassette was amplified form pNPS6KO by PCR using primer pairs NPS6-KO-nest-Fw.1 and NPS6-KO-nest-Rv.1, and used to transform *C. graminicola* protoplast.

Genomic DNA was isolated from candidate strains using mini prep method, and the KO cassette was amplified by standard PCR, using primers NPS6-KO-nest-Fw.2 and NPS6-KO-nest-Rv.2. The genomic DNA of positive candidate strains was isolated using maxi prep and digested with *EcoR*V endonuclease, and analyzed by Southern hybridization using a specific 1523-bp probe amplified with primers Hyg-Prob-Fw.1 and NPS6-KO-nest-Rv.1.

II.4.9.4 Deletion of *NPS2*

To generate the *NPS2* deletion construct, the 5´ and 3´ flanking regions were amplified using primers (NPS2-KO-5´-Fw.1/NPS2-KO-5´-Rv.1) and primers (NPS2-KO-3´-Fw.1/NPS2-KO-3´-Rv.1), respectively. The 1251-bp geneticin resistant cassettes (G418), containing the neomycine phosphotransferase II gene (*nptII*) from transposon Tn5 (Beck et al., 1982), controlled by the *A. nidulans TRPC* promoter and terminator, was amplified from the plasmid pII99 (Namiki et al., 2001), using the primer pair UNI-G418-Fw.1 and UNI-G418-Rv.1. In a second PCR, the 5'- and 3'-flanks were fused with the G418 cassette, and the complete product was amplified using nested primers NPS2-KO-nest-Fw.1 and NPS2-KO-nest-Rv.1. The 3036-bp product was cloned into pJET1.2/blunt, yielding pNPS2KO. This vector was used as a template to amplify the KO construct using primers pJET1.2-Fw. and pJET1.2-Rv. for fungal transformation. Genomic DNA was isolated from candidate strains using mini prep method, and the KO cassette was amplified by standard PCR, using primers NPS2-KO-nest-Fw.2 and SID1-KO-nest-Rv.2, and primers NPS2-KO-nest-Fw.3 and SID1-KO-nest-Rv.2 for confirming the deletion of the *NPS2* ORF (Supplementary Fig. S16).

II.4.10 eGFP tagging

II.4.10.1 Generation of the *FET3-1:eGFP* and *FET3-2:eGFP* constructs

FET1:eGFP fusions were produced by double-joined PCR (Yu et al., 2004). A PCR with the primer combination FET3-1-Fw.1 and FET3-1-eGFP-Rv.1 yielded a 2992-bp fragment, containing the *FET3-1* ORFand 1103-bp of the 5'-flanking region. The promoterless *eGFP* gene and the *hph* cassette were amplified from the eGFP plasmid pSH1.6EGFP, using primers EGFP-Fw.1 and EGFP-Rv.1, yielded a 3621-bp fragment containing the *eGFP* gene, the *GPDA* promoter from *A. nidulans*, the *hph* gene of *E. coli*, and the *TRPC* terminator of *A. nidulans*. The *FET3-1:eGFP* construct and the *hph* , and the complete product was amplified using nested primers FET3-1-eGFP-nest-Fw.1 and EGFP-nest-Rv.1, and cloned into plasmid pJET1.2/blunt, yielding the pFET3-1-eGFP-hyg plasmid.

To fuse the promoter region of *FET3-1* (P$_{FET3-1}$) directly to *eGFP*, primers FET3-1-Fw.1 and FET3-1-eGFP-Rv.2 and genomic DNA of *C. graminicola* were used to amplify a 1103-bp fragment (bp -1100 to +3) of the 5'-region of *FET3-1*. The *eGFP* gene and the *hph* cassette were amplified from plasmid pSH1.6EGFP as described above, and the fragments were fused by joint PCR. Nested primers FET3-1-eGFP-nest-Fw.1 and EGFP-nest-Rv.1 were used to amplify a 4693-bp fragment, which was cloned into plasmid pJET1.2/blunt, resulting in plasmid pP$_{FET3-1}$-eGFP-hyg.

The *FET3-2:eGFP* fusion cassette was generated as follows: The *eGFP* cassette, containing the *eGFP* gene and the *TRPC* terminator from *A. nidulans*, was amplified from plasmid pSM1 (Pöggeler et al., 2003), using primers EGFP-Fw.2 and EGFP-Rv.2. The 1645-bp G418 cassette was amplified from the plasmid pII99, using the primer pair Gen-Fw.1 and Gen-eGFP-Rv.1. Both fragments were used as mega primers and fused to produce a 3791-bp PCR fragment, which was cloned into plasmid pJET1.2/blunt, yielding plasmid pJET-eGFP-G418. This plasmid was double-digested with *Nco*I and *Age*I, yielding a 5821-bp fragment. The 1984-bp *FET3-2* gene, including its 950-bp promoter region was amplified using primers FET3-2-AgeI-Fw.1 and FET3-2-PciI-Rv.1, containing *Age*I and *Pci*I restriction sites. After purification the resulting 2955-pb *FET3-2* PCR fragment, it was double-digested, using *Age*I and *Pci*I, and the 2941-bp *Age*I/*Pci*I fragment was ligated into plasmid pJET-eGFP-G418, which was double-digested with the same enzymes, in the frame with *eGFP*. The resulting plasmid pFET3-2-eGPF-G418 was sequenced and used as a template for PCR.

The *FET3-1:eGFP*, *FET3-2:eGFP* and the P*~FET3-1~*:*eGFP* constructs were amplified by PCR, using primers pJET1.2-Fw. and pJET1.2-Rv. and transformed into conidial protoplasts as described previously.

II.4.10.2 Construction of universal pEB14-eGFP vector

The construction of the universal *eGFP* vector, was constructed as following: The *eGFP* fragment was amplified by primer pairs EGFP-Fw.3 and EGFP-Rv.2 from the pFET3-2-eGPF-G418 plasmid (II.4.10.2, (Albarouki and Deising, 2013)), resulting in a1300-bp fragment. The *SID1* promoter (P*~SID1~*) was amplified by primer pairs SID1-Kpn2I-SfiIA-Fw.1 and SID1-DraIII-SfiIB-Rv.1 resulting 904-bp fragment. Both PCR fragments were purified and digested using *Dra*III. The two pieces were then ligated for 15 min and amplified by PCR using primer pairs SID1-Kpn2I-SfiIA-Fw.1 and EGFP-Rv.2. The resulting fused P*~SID1~*:*eGFP* construct was then ligated into *Oli*I-digested pNR1 plasmid. The resulting plasmid pEB14-eGFP, which has the *eGFP* reporter gene under the control of *SID1* promoter and conferring resistance to nourseothricin, was sequenced. The introduced *Sfi*I A and *Sfi*I B sites before the *eGFP* gene allow the oriented fusion of target gene in the frame of the *eGFP* gene. This plasmid was used as a general cloning plasmid for eGFP tagging of target genes (Supplementary Fig. S2).

The P*~SID1~*:*eGFP* fusion construct conferring nourseothricin resistance was amplified with universal primers (pEB-uni-Fw.1 and pEB-uni-Rv.1) for protoplast transformation.

II.4.10.3 Generation of the *SID1:eGFP* construct

The construction of the *SID1:eGFP* fusion cassette was mediated by the cloning of *SID1* gene into pEB14-eGFP vector (II.4.10.3). The *SID1* gene was amplified with primer pairs SID1-Kpn2I-SfiIA-Fw.1 and SID1-SfiIB-Rv.1, and 100 ng of gDNA, yielding a 2654-bp fragment. The PCR fragment was purified using MinElute PCR Purification kit and digested with *Sfi*I at 50 °C for 2 h. Enzymatic reaction termination and removal was achieved by 10 min precipitation with SureClean reagent (Bioline, Luckenwalde, Germany), according to the manufacturer's instruction. The 5´- *Sfi*I A and 3´- *Sfi*I B overhangs (Supplementary Fig. S2) allow the oriented ligation of the PCR product into the pEB14-eGFP plasmid in the frame of *eGFP* gene. The resulting plasmid pEB14-SID1-eGFP was afterwards sequenced and the

ORF of the chimeric *SID1*:*eGFP* gene was confirmed. The *SID1*:*eGFP* construct was then amplified with the primer pair pEB.uni.Fw.1 and pEB.uni.Rv.1 for fungal protoplast transformation.

II.4.10.4 Generation of the *SIT1*:*eGFP* and *SIT2*:*eGFP* constructs

SIT1 and *SIT2* genes were amplified using primers combination SIT1-SfiIA-Fw and SIT1-SfiIB-Rv, and SIT2-SfiIA-Fw and SIT2-SfiIB-Rv, resulting in 2.9-kb and 3.3-kb fragments, respectively. Both PCR fragments were treated as explained in II.4.10.4 to yield pEB14-SIT1-eGFP and pEB14-SIT2-eGFP. These vectors were used as a template to amplify the *SIT1*:*eGFP* and *SIT2*:*eGFP* cassettes for fungal transformation.

II.4.11 Siderophore Analysis

II.4.11.1 Samples preparation

C. graminicola strains were grown in CM medium in an incubation shaker (Unitron, Infors AG, Bottmingen, Switzerland) at 25°C and 100 rpm for 7-10 days. Then the fungal mycelia were filtrated under sterile conditions through Miracloth filter (EMD Chemical, Darmstadt, Germany) and washed three times with H_2O_{bidest}. The fungal mycelia were then dried gently with sterile filter paper (601A Carl Roth, Karlsruhe, Germany) and weighed.

II.4.11.2 Inoculation of the Sundström minimal medium (SMM)

One gram fresh weight of fungal mycelium was used to inoculate 150 ml of Sundström minimal medium (VIII.1.1 in the appendix) in 500 ml Erlenmeyer flasks. The inocula were grown at 25°C for additional 10 days. The mycelia and the growth broth were separated by filtration (601A Carl Roth, Karlsruhe, Germany) and send to Innsbruck medical University, Division of Molecular Biology, Innsbruck, Austria.

II.4.12 Microscopy

Bright-field and differential interference contrast microscopy were performed using a Nikon Eclipse 90i microscope (Nikon, Düsseldorf, Germany), equipped with a DS-5M camera. Aniline blue, calcofluor-white and 3,3'-Diaminobenzidine (DAB) staining was performed as described (De Neergaard, 1997).

Fluorescence microscopy was performed, using a Nikon Eclipse 90i confocal laser scanning microscope (Nikon, Düsseldorf, Germany), equipped with a D-Eclipse C1-SHV camera and a pinhole diameter of 30 µm. For detection of eGFP fluorescence, an excitation wavelength of 488-nm and a 535/550-nm detection channel were employed.

For FM4-64 staining (SynaptoRed; Sigma Aldrich, Munich, Germany), fungal mycelia were incubated in 5 µg/ml SynaptoRed in CM for 30 min at 28°C. Mycelia were then washed with distilled water and incubated in CM medium containing 100 µM BPS for 0; 0.5; 2; 4 and 8 h. FM4-64 fluorescence was detected using an excitation wavelength of 633-nm and the 650 LP detection channel.

Fluorescence intensity was measured using the EZ-C1 software (Nikon, Düsseldorf, Germany), mounted on a Nikon Eclipse 90i confocal laser scanning microscope (Nikon, Düsseldorf, Germany). To study mycelial growth, sterile microscopy slides were covered with a thin layer of 1% agarose (Biozym Diagnostik, Oldendorf, Germany), inoculated with 50 µl of a suspension containing 10,000 conidia of the eGFP strains in potato dextrose (PD) medium and incubated overnight at 23°C. The slides were then washed three times with sterile H_2O_{bidest} and growing mycelia were further incubated for 24 hours in PD supplemented with either 100 µM $FeSO_4$, or 100 µM BPS.

II.4.13 Photography and image processing

All images were taken by a Nikon D50 Digital camera (Nikon, Düsseldorf, Germany). Image processing was done with Adobe Photoshop CS8.8 (Adobe Systems Inc., San Jose, CA, USA) or the LSM imaging software (Carl Zeiss, Jena, Germany).

II.4.14 Bioinformatics and prediction tools

In silico sequence analyses, gene deletion, gene fusion and primer constructions, were made using Clone Manager 9 professional (Sci-Ed., Cary, NC, USA).

Synteny map of iron uptake-related genes in *C. graminicola* were searched in the broad institute database (http://www.broadinstitute.org/annotation/genome/colletotrichum_group/).

Phylogenic analyses were conducted using MEGA4 software (Tamura et al., 2007). The evolutionary relationship was analyzed using the Minimum Evolution method (Rzhetsky and Nei, 1992), and bootstrap consensus trees were inferred from 1000 replicates (Felsenstein, 1985).

To predict transmembrane domains, different prediction programs (i.e. SOSUI, TMHMM Server v. 2.0, PRED-TMR and DAS-TMfilter) were used.

Calculation and statistical analyses of differences between groups were made using the One Way ANOVA test, followed by the Holm-Sidak test at a freedom degree of $p < 0.001$ (Sigma Plot v.11, Systat Software, Erkrath, Germany).

III. Results

III.1 Identification of iron uptake-related genes of *C. graminicola*

III.1.1 Identification and cloning of iron responsive genes of *C. graminicola*

To identify iron uptake-related genes in *C. graminicola*, I searched the relevant literature and found characterized iron uptake-related genes in other fungal species. Putative iron uptake-related genes were used to query *C. graminicola* trace sequences. Trace sequences were assembled using SeqMan 5.00$^{©}$ program (DNASTAR, Inc.; Madison, USA). If the assembly coverage met the coverage threshold, and the deduced amino acids of these genes matched a known characterized iron uptake-related gene from another species (i.e. low E-value $\leq$ e^{-50}, and identity $\geq$ 50% at the amino acid level), it was investigated further.

Table 3: Iron uptake-related genes of *Colletotrichum graminicola*

Gene	GenBank	Putative function	Intron$^{\pm}$	Best BLAST hit	E-value */ identity%*	Reference
FET3-1	EFQ33392.1	ferroxidase	4	*F. graminearum*	0.0/68 %	(Greenshields et al., 2007)
FET3-2	EFQ26799.1	ferroxidase	2	*A. fumigatus*	0.0/60 %	(Schrettl et al., 2004)
FTR1-1	EFQ33393.1	iron permease	3	*F. graminearum*	3e^{-163}/66 %	(Park et al., 2006)
FTR1-2	EFQ26800.1	iron permease	4	*A. fumigatus*	4e^{-133}/59 %	(Schrettl et al., 2004)
NPS6	EFQ32921.1	nonribosomal peptide synthetase (NRPS)	1	*Ajellomyces capsulatus*	0.0/56 %	(Hwang et al., 2008)
NPS2	EFQ31398.1	NRPS	5	*F. graminearum*	0.0/47 %	Tobias et al. 2007
SID1	EFQ31396.1	L-ornithine-N^5-monooxygenase	1	*F. graminearum*	5e^{-175}/59%	(Greenshields et al., 2007)
SIT1	EFQ33577.1	siderophore transporter	2	*Ajellomyces capsulatus*	4e^{-179}/59 %	(Hwang et al., 2008)
FRE2	EFQ30907.1	ferric reductase	6	*Verticillium dahliae*	0.0/52%	(Ma et al., 2008)
SRE1	EFQ27712.1	GATA transcription factor	2	*Neurospora crassa*	3e^{-90}/55%	(Haas et al., 1999)

$\pm$ Intron numbers where deduced from comparisons between cDNA and gDNA sequences**.**
* E-value and percentage of identity of the deduced amino acid sequences and the best-characterized BLAST hit (best BLAST hit).

Ten genes matched these parameters, with the exception of the nonribosomal peptide synthetase 2 (NPS2, with identity value 47%), due to its big size (4895 aa) (Table 3). Intron's

numbers were confirmed by cDNA sequencing and comparison with the corresponding gDNA (see II.4.4.7 and Table 3).

Interestingly, genes encoding components of the siderophore system are not organized in gene clusters as it was reported in other filamentous fungi (Fig. 6A) (Eichhorn et al., 2006; Haas et al., 2008, and reference therein). In contrast, genes encoding the RIA components, i.e. the ferroxidases *FET3-1* and *FET3-2*, and the permeases *FTR1-1* and *FTR1-2*, are organized in clusters (Fig. 6B).
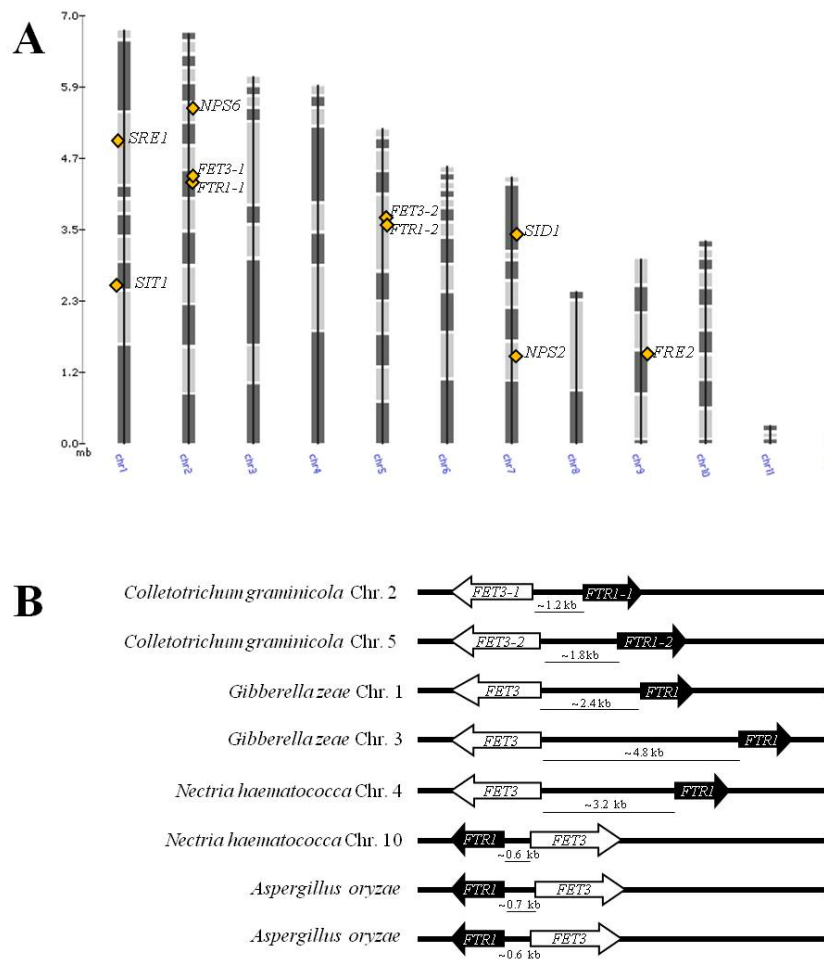
Fig. 6: Synteny map of iron uptake-related genes of *C. graminicola* and chromosomal linkage between ferroxidase and iron permease genes.
A: Iron uptake-related genes of *C. graminicola* distribute on different chromosomes, whereas the ferroxidases (*FET3-1* and *FET3-2*) and permeases (*FTR1-1* and *FTR1-2*) genes localized in close vicinity.
B: Chromosomal localization of the ferroxidase and iron permease genes in different pathogenic filamentous ascomycetes. Arrows show orientations of genes.

Like *C. graminicola*, the genomes of *Aspergillus oryzae, Gibberella zeae* (anamorph *Fusarium graminearum*) and *Nectria haematococca*, contain two ferroxidases genes located

in direct vicinity of *FTR1* genes encoding iron permeases (Fig. 6B). That strongly suggests that both genes are bidirectionally transcribed from one promoter region.

III.1.2 Transcript abundance of iron uptake-related genes in response to the iron status

Using quantitative RT-PCR (qRT-PCR), the transcriptional response to iron availability of genes involved in iron uptake in *C. graminicola* was analyzed. Iron-starvation was induced by adjusting the liquid growth medium to contain 200 µM BPS. The ferroxidase gene *FET3-1*, the ferric transporter gene *FTR1-1* and the ferric reductase gene *FRE2* from the RIA pathway showed significant transcript abundances under these conditions (Fig. 7). In contrast, even when using total RNA amounts as high as 100 ng in qRT-PRC assays, *FET3-2* and *FTR1-2* showed C_t values of 53 and 50 cycles, respectively, and their transcript abundance was therefore too low for reliable quantification. However, RT-PCR experiments showed a very low level of *FET3-2* transcripts in Δ*fet3-1*, but not in the WT strain (Supplementary Fig. S3). The L-ornithine-N^5-monooxygenase gene *SID1*, the nonribosomal peptide synthetases *NPS2* and *NPS6* and the siderophore transporter gene *SIT1* from the SIA pathway also showed significant transcript abundance under these conditions (Fig. 7). Under iron-limiting conditions, as expected, transcripts of the GATA transcription factor *SRE1*, a putative repressor of genes involved in iron uptake (Chao et al., 2008; Haas, 2012, and references therein), were present at low concentration. Increasing concentrations of Fe^{2+} or Fe^{3+} to 0.01 or 1 mM decreased the transcript concentrations of *FET3-1*, *FTR1-1*, *FRE2*, *SID1*, *NPS6*, and *SIT1*, but increased the transcript abundance of *SRE1*. Transcript abundance of *NPS2*, which is responsible for assembling intracellular siderophores (Haas, 2003; Eisendle et al., 2006, and reference therein), was decreased at concentration of 0.01 mM of both redox forms of iron, but re-increased at concentration of 1 mM, which is in a full agreement with the data obtained by Eisendle et al., (2006). At low concentrations of $FeSO_4$, the transcript concentration of *FRE2* was only reduced by approx. 50%, possibly because Fe^{2+} is not a substrate of ferric reductase. This may also be true for the *SID1* and *SIT1* genes (Hider, 1984; Neilands, 1995). Transcript abundance of the *SRE1* gene increased with increasing concentrations of available iron. Like *FRE2*, *SRE1* responded stronger to Fe^{3+} than to Fe^{2+} (Fig. 7).
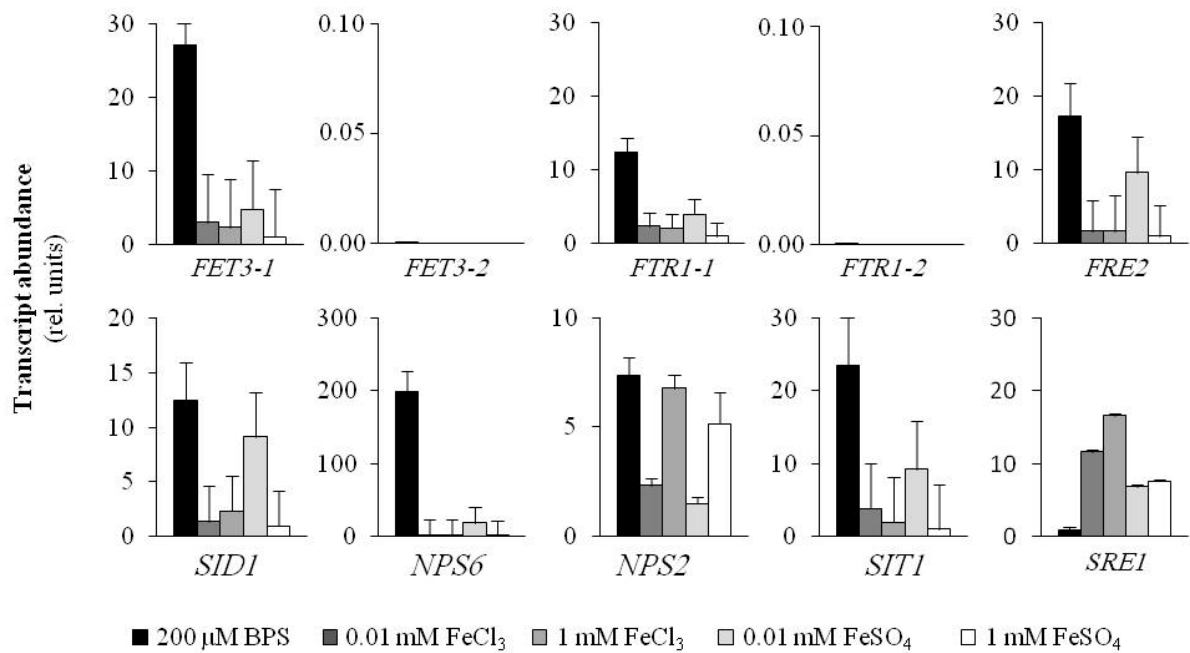
Fig. 7: Relative transcript abundance of iron uptake-related genes of *C. graminicola*. Relative transcript abundance has been normalized using the constitutive housekeeping genes actin *ACT1* and histone *H3*. Bars represent + standard errors.

These data indicate that the availability of extracellular iron regulates genes involved in both RIA and SIA pathways in *C. graminicola*.

III.2 Characterization of ferroxidases as components of the RIA pathway in *C. graminicola*

III.2.1 Identification and cloning of the ferroxidase genes of *C. graminicola*

The ferroxidase gene *FET3-1* (GenBank: EFQ33392.1) of *Colletotrichum graminicola* was originally amplified using degenerate PCR. A 950-bp fragment was obtained using primer combination FET3-deg-Fw.1 and FET3-deg-Rv.2 (Fig. 8, dPCR). Thereafter, the sequence was extended in both directions using the tail PCR (Liu and Baird, 2001). Approximately 2.1 and 3.6 kb of the 5'- and 3'- ends respectively, were successively amplified (Fig. 8A). The resulting *FET3-1* gene (2128 bp), in addition to 1.7 kb and 2.7 kb of the promoter and terminator regions, were successfully amplified and sequenced. *In silico* characterization of the *FET3-1* gene revealed five exons and four introns (Fig. 8B). The deduced amino acid sequence revealed significant identity with ferroxidases of other filamentous ascomycetes such as *Fusarium graminearum* (69%), *Botryotinia fuckeliana* (67%), and *Aspergillus fumigatus* (64%).
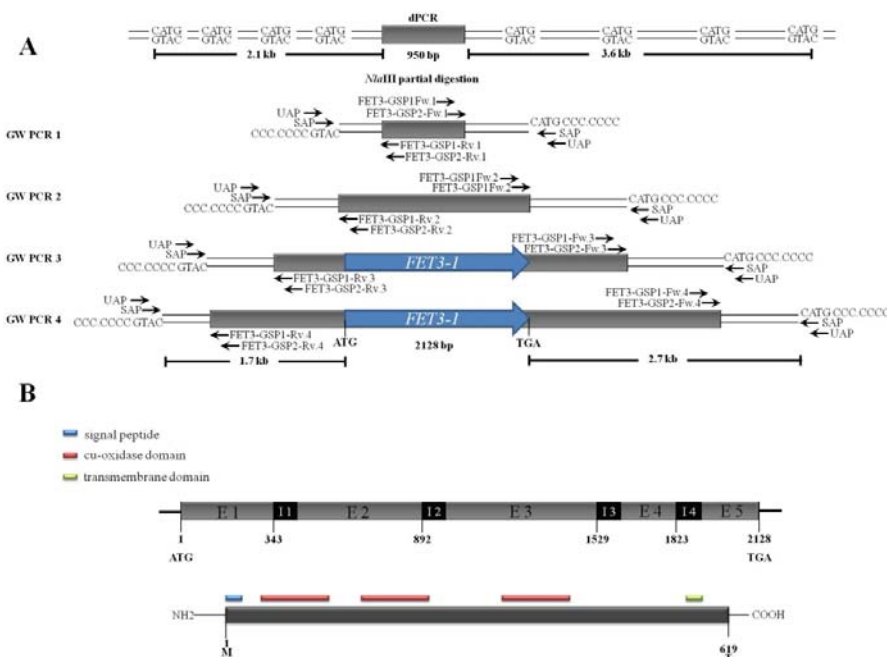
Fig. 8: Scheme depicting cloning of the full length *FET3-1* gene with promoter and terminator regions, using genome walking, and the deduced structure of *FET3-1*.
A: The PCR product of degenerate primers (dPCR) was extended using tailing PCR using consecutive primer combinations (GW PCR 1 to GW PCR 4). CATG: *Nla*III sites, primer sequences are listed in the table of primers in the appendix.
B: The coding region comprises five exons (E 1-5) and four introns (I 1-4). The deduced Fet3-1 protein is a type 1 plasma membrane protein with all functional ferroxidase domains, i.e. cu-oxidases domains (red bar), transmembrane domain (green bar) and the N-terminus oriented to the outside, signal peptide (blue bar).

Searching the genome sequence database of *C. graminicola* ([http://www.broadinstitute.org/](http://www.broadinstitute.org/annotation/genome/colletotrichum_group/Blast.html) [annotation/genome/colletotrichum_group/Blast.html](http://www.broadinstitute.org/annotation/genome/colletotrichum_group/Blast.html)), an additional ferroxidase copy was found with 60% identity to the Fet3-1 of *C. graminicola* and 60% identity with the ferroxidase *FET5* of *Magnaporthe oryzea*. This ferroxidase designated as Fet3-2 is a type 1 plasma membrane protein with all functional ferroxidase domains (Fig. 9). Fet3-2 also shows high similarity with the corresponding ferroxidases of other filamentous ascomycetes (Fig. 10A).
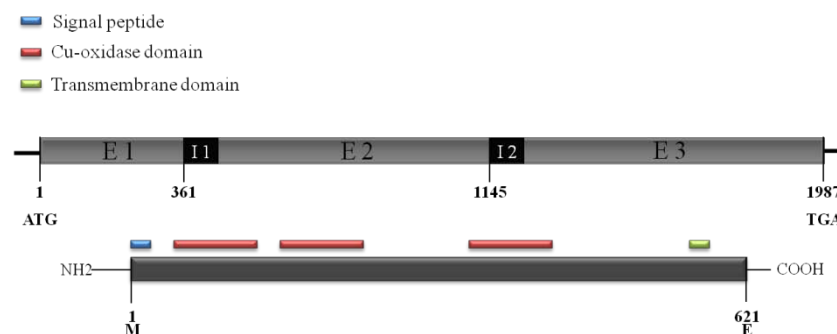
Fig. 9: Structure of the *FET3-2* gene of *C. graminicola* and the deduced protein structure. The coding region comprises three exons (E 1-3) and two introns (I 1-2). The Fet3-2 protein comprises all standard ferroxidases domains (colored bars).

As expected, both ferroxidases of *C. graminicola* cluster with ferroxidases of other filamentous ascomycetes (Fig. 10A), clearly revealing that ferroxidases are conserved in filamentous ascomycetes. However, *C. graminicola* ferroxidases Fet3-1 and Fet3-2 show 45% and 43% identity with the well characterized ferroxidase of *Saccharomyces cerevisiae* (Fet3) (Fig. 10B).

The ferroxidases of *C. graminicola* show the elements common to all fungal ferroxidases, i.e. four highly conserved boxes (Fig. 10B, boxes 1-4), a transmembrane domain (Fig. 10B, dotted box), four copper-binding motifs (Fig. 10B, solid circles), and a putative Fe^{2+} ligand-binding motif (Fig. 10B, solid triangles). This protein organization is in full agreement with that of ferroxidases of other fungi (Bonaccorsi di Patti et al., 2001; Kosman, 2002; Wang et al., 2003).
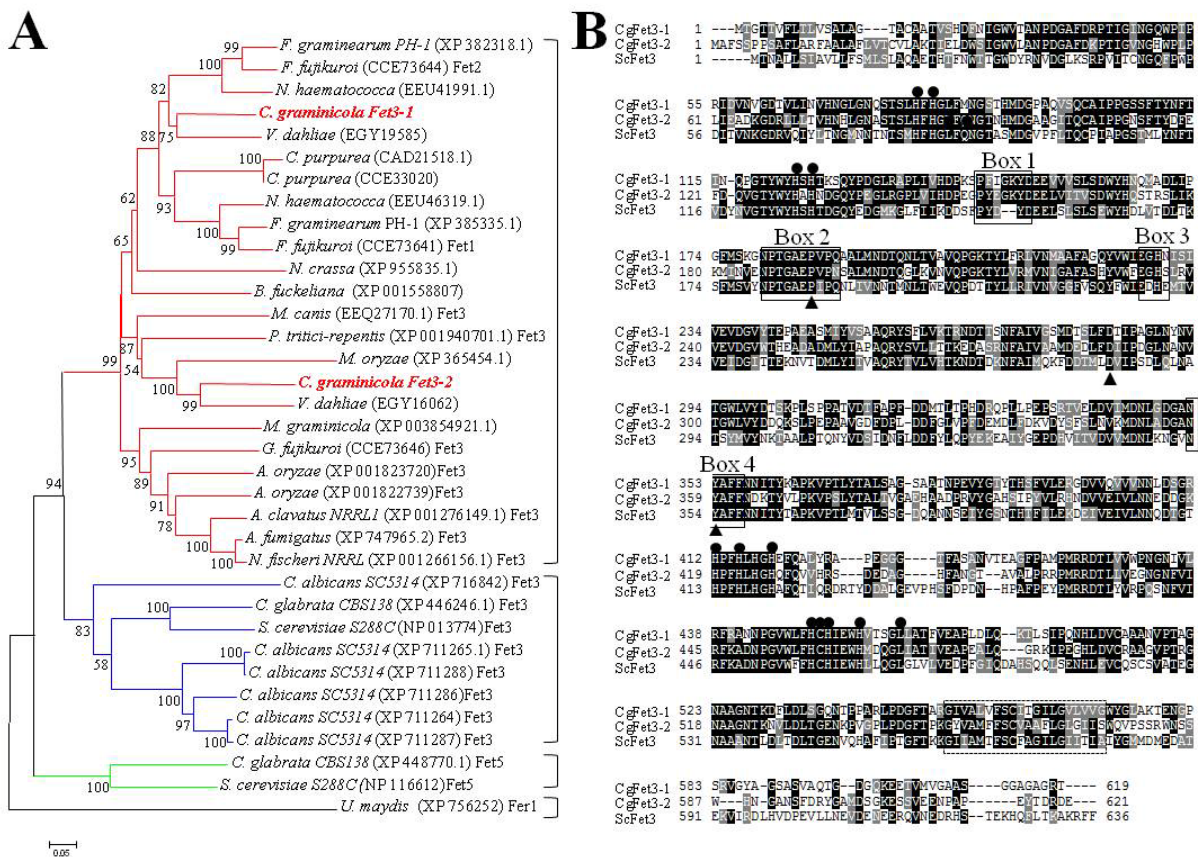
Fig. 10: Phylogeny and conserved regions of fungal ferroxidases.
A: Phylogenetic tree of putative ferroxidases of different fungi. The ferroxidases of *C. graminicola* show high similarity with those of other filamentous ascomycetes, whereas the dimorphic fungi *Candida albicans* and *C. glabrata* ferroxidases show high similarity to the yeast *S. cerevisiae* ferroxidases. *U. maydis* ferroxidase Fer1 was used as out-group. For accession number see VIII.5 in the appendix.
B: Amino acid sequence alignment of the two putative ferroxidases CgFet3-1 and CgFet3-2 of *C. graminicola* with that of the *S. cerevisiae* ferroxidase ScFet3.

III.2.2 Functional characterization of *C. graminicola* ferroxidases by complementing the *S. cerevisiae* strain Δ*Scfet3fet4*

To confirm that both, Fet3-1 and Fet3-2 of *C. graminicola* represent functional ferroxidases, I performed complementation assays with the *S. cerevisiae* Δ*fet3fet4* double mutant that is unable to grow under iron-limiting conditions (Askwith et al., 1994; Dix et al., 2004) (Fig. 11). The Δ*fet3fet4* mutant is auxotroph for uracil and therefore unable to grow on synthetic complete medium lacking uracil and containing 50 µM of the iron scavenger bathophenanthroline disulfonate (SC + BPS). The Δ*fet3fet4* strain transformed with the empty transformation vector pAG300 (Fig. 11A, T_{pAG300}), conferring uracil prototrophy, showed reduced growth on SC + BPS. However, growth of Δ*fet3fet4* strains transformed with the expression vector pAG300 either harboring the *FET3-1* or the *FET3-2* gene of

C. graminicola, was not distinct from that of the wild type yeast strain (Fig. 11A, compare WT with T*$_{FET3-1}$* and T*$_{FET3-2}$*).

Different programs predicting sub-cellular protein localization (TMHMM Server v. 2.0, SOSUI, PRED-TMR and DAS-TMfilter) identified a transmembrane domain of Fet3-1 (aa 553 to 575) and Fet3-2 (aa 556 to 578) and suggested that these ferroxidases are plasma membrane-localized. To confirm the predicted plasma membrane localization of Fet3-1 and Fet3-2, eGFP-fusions of *FET3-1* or *FET3-2* were expressed in *S. cerevisiae* Δ*fet3fet4* cells. As expected, in transformants T*$_{FET3-1:eGFP}$* and T*$_{FET3-2:eGFP}$*, eGFP-tagged proteins localized to the plasma membrane (Fig. 11B; T*$_{FET3-1:eGFP}$* and T*$_{FET3-2:eGFP}$*).

Taken together, these results show that *FET3-1* and *FET3-2* encode functional ferroxidases.
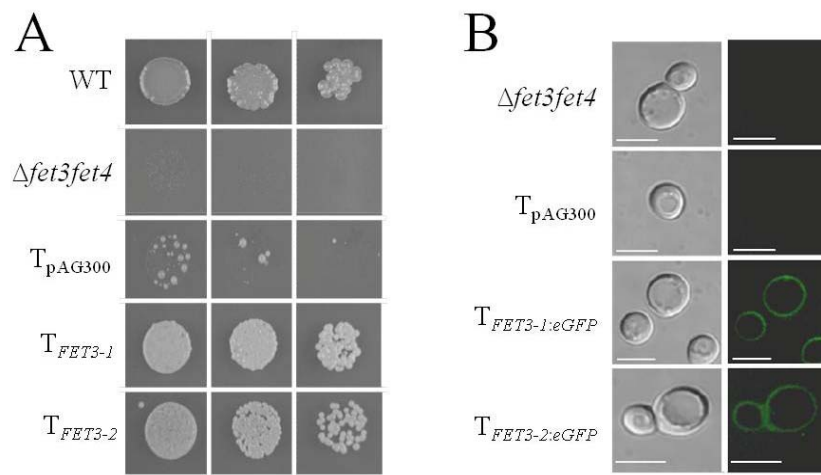
Fig. 11: Complementation of the *S. cerevisiae* ferroxidase mutant *fet3fet4* by the *C. graminicola* ferroxidase genes *FET3-1* and *FET3-2*.
A: *S. cerevisiae* (WT) and yeast mutant Δ*fet3fet4* harboring the plasmids pAG300-FET3-1 (T*$_{FET3-1}$*), pAG300-FET3-2 (T*$_{FET3-2}$*), or the empty vector pAG300 (T*$_{pAG300}$*) were grown overnight in SC medium (ura⁻) containing 50µM BPS. A 10-fold dilution series was dotted onto solidified SC medium containing 50µM BPS, and incubated for 4 days. The Δ*fet3fet4* was grown in SC medium and served as a control.
B: To visualize the localization of Fet3-1 and Fet3-2 of *C. graminicola*, the yeast expression vector pAG300 harboring *eGFP* fusions of *FET3-1* (T*$_{FET31:eGFP}$*) or *FET3-2* (T*$_{FET3-2:eGFP}$*) were transformed into yeast mutant Δ*fet3fet4*. eGFP fluorescence can be seen in the plasma membrane of transformants T*$_{FET3-1:eGFP}$* and T*$_{FET3-2:eGFP}$*. Bars = 5µM.

III.2.3 Deletion of the *FET3-1* and *FET3-2* genes

III.2.3.1 Targeted mutagenesis of *FET3-1* and *FET3-2* genes

To characterize the *FET3-1* and *FET3-2* genes of *C. graminicola* functionally, targeted mutageneses were performed (Fig. 12). The *FET3-1* and *FET3-2* genes were replaced by the nourseothricin acetyl transferase (*nat1*) and by the hygromycin phosphotransferase (*hph)* genes, respectively (Figs. 12A, B). These two different resistance cassettes also allowed conducting double deletion mutants in a Δ*fet3-1* background. The deletion of the *FET3-1* and *FET3-2* genes and the insertion of a single copy of the *nat1*/*hph* genes into the coding region of *FET3-1*/*FET3-2* were confirmed using Southern assay (Fig. 12C to E). Three individual deletion mutants (KOs) were obtained for the *FET3-1* gene (Fig. 12C) and four individual deletion mutants were obtained for the *FET3-2* gene, as shown by Southern blot analysis (Fig. 12D). Additionally, the *FET3-2* gene was deleted in the background of Δ*fet3-1* strain, resulting four individual double deletion mutants (Fig. 12E). To confirm the loss of *FET3-1* and *FET3-2* genes at the transcriptional level, RT-PCR analyses were performed with *FET3-1* and *FET3-2* specific primers (see table of primer in the appendix). The 145-bp and 147-bp fragments of the *FET3-1* and *FET3-2* were amplified only when the WT gene existed, but not in the corresponding KO strains. Primers corresponding to transcripts of the constitutively expressed *H3* gene were used as a control and allowed amplifying the 85-bp H3 fragment from RNA of WT and KO strains.
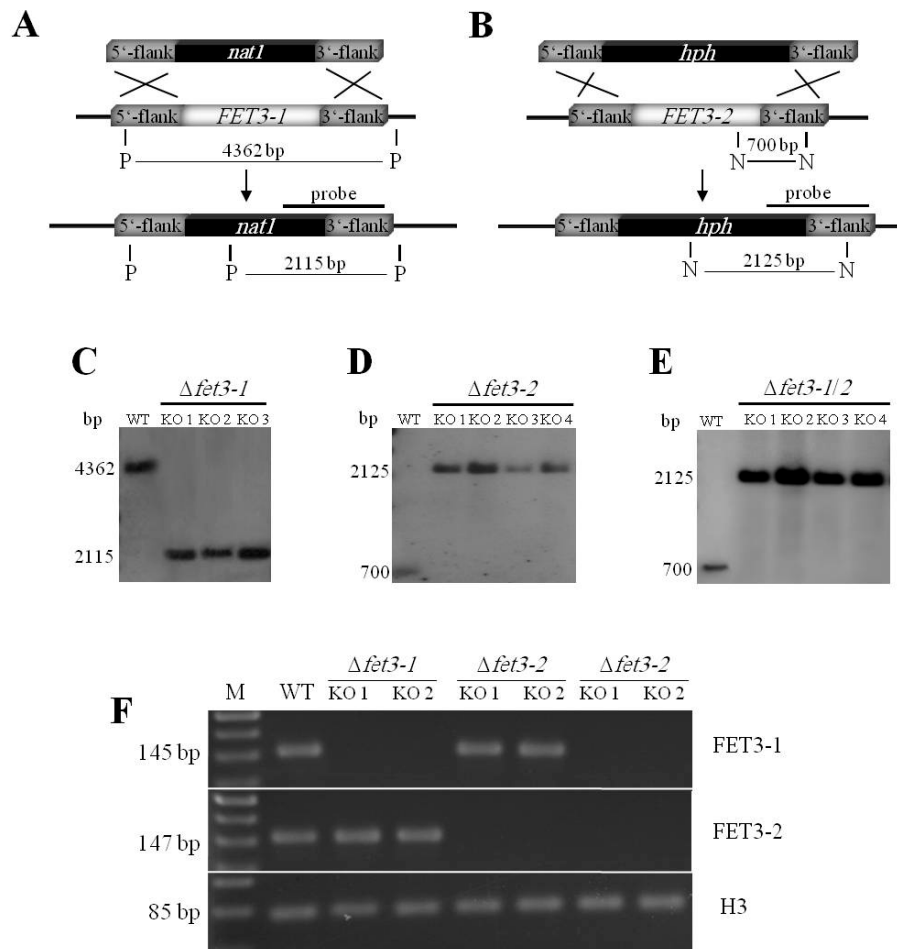
Fig. 12: Deletion of the *FET3-1* and *FET3-2* genes of *C. graminicola*.
A and B: Scheme of the deletion strategy of the *FET3-1* and *FET3-2* genes, showing native (middle) and recombinant (bottom) genomic regions of the respective genes. Deletion of the *FET3-2* gene has been done either in the CgM2 WT or in the Δ*fet3-1* deletion mutant. Restriction sites for Southern assay are shown: P, *Psc*I and N, *Nco*I. Bar above the disrupted gene represent the region used to probe the Southern blots.
C to E: Southern blot analyses performed with *Psc*I- (C) and *Nco*I- (D and E) digested genomic DNA from WT, Δ*fet3-1*, Δ*fet3-2* and Δ*fet3-1/2* deletion strains.
F: RT-PCR analyses performed with *FET3-1* and *FET3-2* specific primers to confirm gene inactivation at the transcript level. The *H3* transcript was used as a control.

III.2.3.2 Plant infection and *in-vivo* conidiation

Ferroxidases represent pathogenicity factors in the biotrophic maize smut fungus *U. maydis* (Eichhorn et al., 2006), but not in necrotrophic fungi (Schrettl et al., 2004; Oide et al., 2006; Greenshields et al., 2007). However, the importance of RIA for virulence of hemibiotrophs is unknown. In order to investigate whether the two ferroxidases identified in *C. graminicola* are required for virulence in this hemibiotroph, and if so, whether they are required during biotrophic and/or necrotrophic development, deletion mutants were employed in pathogenicity assays (Fig. 13).

The WT, the single deletion strains Δfet3-1 and Δ fet3-2, and the double deletion strain Δfet3-1/2 were inoculated onto intact and wounded maize leaves. On non-wounded leaves, the Δfet3-1 and the Δfet3-1/2 strains showed strongly retarded anthracnose disease symptom development, as compared to the wild-type strain (Fig. 13A). PCR-based quantification of the fungal mass in infected leaves at 4 days post inoculation (DPI) confirmed that the Δfet3-1 strain was significantly less virulent than the WT strain (Fig. 13B). On wounded leaves C. graminicola does not differentiate biotrophic, but only necrotrophic infection hyphae. On wounded leaves, Δfet3-1 strains showed virulence comparable to the WT strain, suggesting that FET3-1 is required for appressorial penetration and/or biotrophic development. On wounded leaves, the differences in virulence between the Δfet3-1 the Δfet3-1/2 strain became more obvious. The Δfet3-1/2 strain caused significantly reduced disease symptom severity on wounded leaves (Fig. 13A and B). Virulence defects of Δfet3-1 and Δfet3-1/2 strains were visible not only on leaf segments but also on whole plants (Fig. 13A).
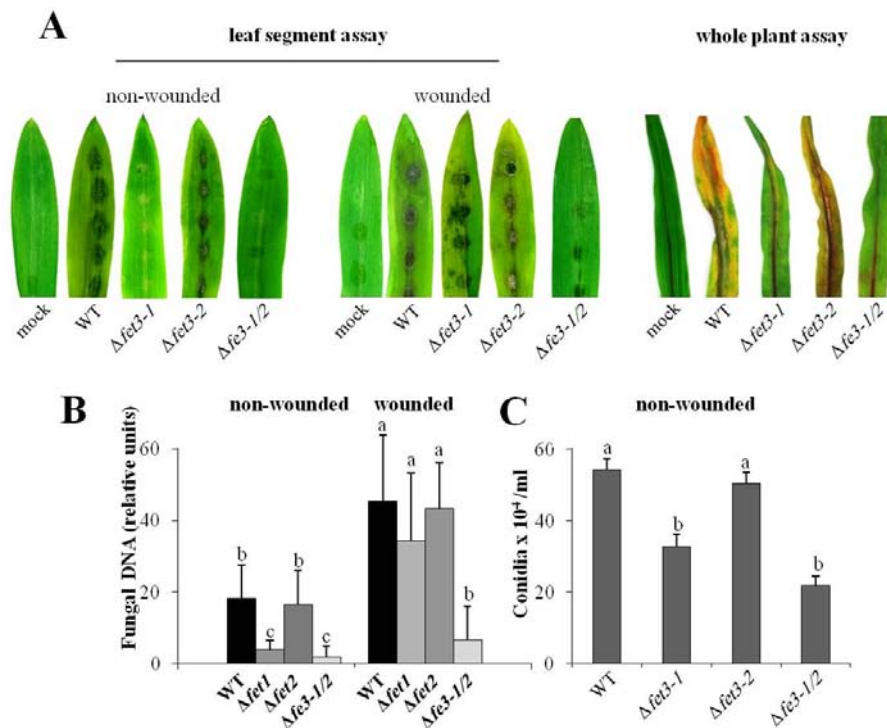
Fig. 13: Virulence assay of the ferroxidase mutants Δfet3-1, Δfet3-2 and Δfet3-1/2 in comparison to the C. graminicola WT strain on non-wounded and wounded maize leaves.
A: On non-wounded leaves, the WT and the Δfet3-2 strains caused severe anthracnose disease symptoms. Δfet3-1 and Δfet3-1/2 strains cause minor disease symptoms only. Mock-inoculated leaves (Mock) did not show symptoms. Photos were taken at 4 DPI, using the maize variety Nathan inoculated with 10^4 conidia per spot.
B: qPCR-based quantification of genomic DNA of C. graminicola in non-wounded and wounded maize leaves inoculated with the WT strain and Δfet3-1, Δfet3-2 and Δfet3-1/2 strains. Samples were taken at 4 DPI.
C: Formation of conidia in-vivo on infected leaves at 6 DPI.
Different letters represent significance groups at $p \leq 0.001$, and bars = + SD; n = 3.

Formation of conidia on infected leaves 6 DPI (Fig. 13C) were significantly different between the WT and each of Δ*fet3-1* and Δ*fet3-1/2*, but not between WT and Δ*fet3-2* strain.

Microscopical inspection of infection sites revealed that conidia of the WT and Δ*fet3-2* strains had formed appressoria on the maize leaf surface at 24 HPI (Fig. 14A, 24 HPI; WT and Δ*fet3-2*, co and ap). While 75% and 79% of the conidia of the WT and the Δ*fet3-2* strain had germinated at 24 HPI, germination rates of Δ*fet3-1* (ca. 25%) and Δ*fet3-1/2* strains (ca. 35%) were clearly reduced (Fig. 14B). Interestingly, in contrast to conidia of the WT and the Δ*fet3-2* strain, which formed single or, rarely, two germ tubes, conidia of Δ*fet3-1* and Δ*fet3-1/2* strains often formed multiple germ tubes (Fig. 14A, 24 HPI; Δ*fet3-1* and Δ*fet3-1/2*, inserts, arrowheads). At 24 HPI, 63% and 65% of the conidia of the WT and Δ*fet3-2* strains had formed appressoria, 98.5% and 98% of which had melanized. In comparison, at that time only 12% and 27% of the conidia of Δ*fet3-1* and Δ*fet3-1/2* strains had differentiated appressoria, and 50% and 75% of the appressoria of these strains were non-melanized (Fig. 14A, 24 HPI; ap). Thus, in comparison to the WT and Δ*fet3-2* strains, appressorium formation and melanization were severely delayed in Δ*fet3-1* and Δ*fet3-1/2* strains (Fig. 14B). Intriguingly, *on planta* growing hyphae of Δ*fet3-1* and Δ*fet3-1/2* strains showed cell wall defects, as indicated by formation of hyphal protrusions (Fig. 14A, 24 HPI; Δ*fet3-1* and Δ*fet3-1/2*, arrows).

At 48 HPI, the WT and Δ*fet3-2* strains had invaded the host leaf and formed biotrophic primary, and necrotrophic secondary hyphae (Fig. 14A, 48 HPI; WT and Δ*fet3-2*, sh). At this time point, many appressoria of Δ*fet3-1* and Δ*fet3-1/2* strains had also melanized (Fig. 14A, 48 HPI; Δ*fet3-1*, ap), but melanization appeared to be weaker than in the WT and Δ*fet3-2* strains. Appressoria of these strains often failed penetrating the host and formed lateral germ tubes on the cuticle (Fig. 14A, 48 HPI; Δ*fet3-1*, lgt). At 48 HPI, only ca. 13% and ca. 1% of the appressoria of Δ*fet3-1* and Δ*fet3-1/2* strains had formed secondary necrotrophic hyphae, as compared to ca. 55% of the WT and ca. 60% of the Δ*fet3-2* strain (Fig. 14C).

These data suggest that the ferroxidase *FET3-1* represents a virulence factor in *C. graminicola,* whereas the *FET3-2* does not play a major role during infection.
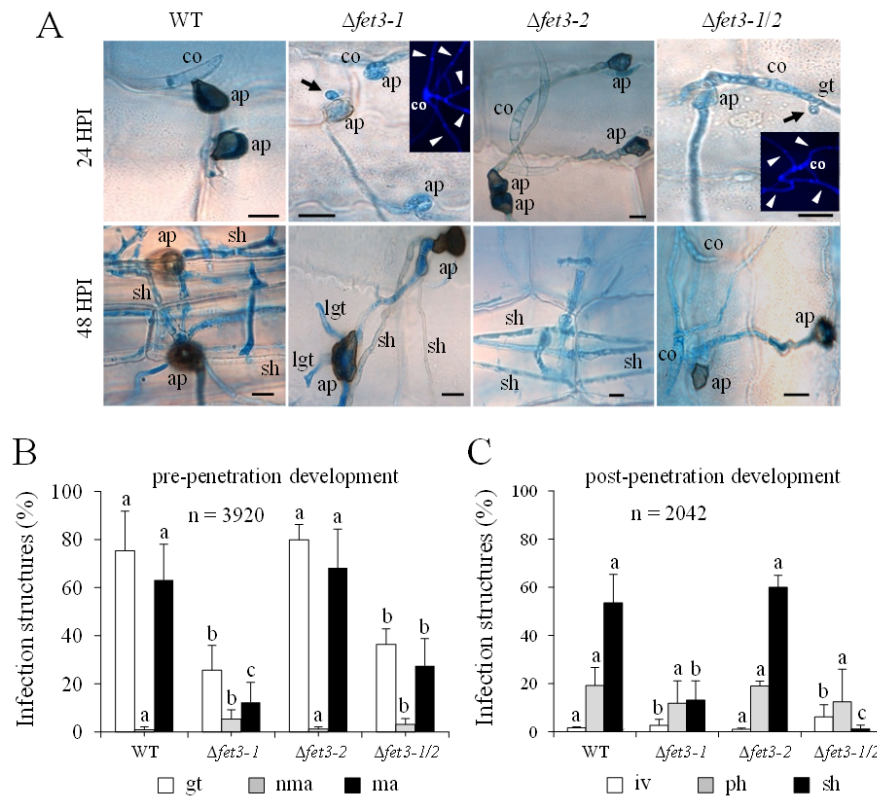
Fig. 14: Microscopical analysis of the infection process of the *C. graminicola* WT and ferroxidase-deficient deletion strains.
A: At 24 HPI, conidia (co) of the WT and Δ*fet3-2* strains had germinated and differentiated melanized appressoria (ap). Δ*fet3-1* and Δ*fet3-1/2* strains had formed non-melanized appressoria (ap), and germ tubes (gt) showed protrusions indicative of cell wall defects (arrow). Remarkably, conidia of these strains formed several germ tubes (insert, white arrowheads). At 48 HPI, the WT and Δ*fet3-2* strains had massively colonized the host tissue and formed necrotrophic secondary hyphae (sh). At this time, Δ*fet3-1* strains had also formed some secondary hyphae derived from melanized appressoria. Appressoria also formed lateral germ tubes (lgt) on the plant surface. Double deletion strain Δ*fet3-1/2* had also formed hyphopodia, but secondary hyphae were rarely observed. Infection structures were stained by aniline blue or calcofluor (inserts). Bars = 10 µm.
B: Quantification of pre-penetration infection structures at 24 HPI. gt, germ tube; nma, non-melanized appressoria; ma, melanized appressoria.
C: Quantification of post-penetration infection structures at 48 HPI revealed.
Different letters in B and C represent significance groups between strains for each infection structure at significance level p ≤ 0.001. Bars represent + SD. n = 3920 in B and 2042 in C.

III.2.4 Expression of ferroxidases during pathogenesis and *in-vitro* culture

III.2.4.1 *FET3-1* is differentially expressed during pathogenesis and *in-vitro*

Reduced rates of germination, appressorium formation, penetration of the host plant, and formation of primary hyphae in Δ*fet3-1* and Δ*fet3-1/2* strains suggested that *FET3-1* is required for iron uptake during the early stage of infection, i.e. during pre-penetration and biotrophic development (Fig. 14). The role of *FET3-1* in appressorial penetration and/or biotrophy was confirmed by comparative infection assays on non-wounded and wounded maize leaves (Fig. 13). As infection structure differentiation and leaf infection do not occur perfectly synchronously, qRT-PCR does not provide information of *FET3-1* expression in individual infection structures. Therefore, I analyzed the expression of this gene during the infection process on maize leaves, using *C. graminicola* transformants carrying the eGFP reporter under the control of the *FET3-1* promoter (P$_{FET3-1}$). Preliminary studies have shown that virulence was not affected in this transformant (Supplementary Fig. S5). Significant eGFP fluorescence was observed in dormant and germinating conidia, in appressoria (Fig. 15A, 24 HPI; co and ap), and in infection vesicles and primary hyphae, i.e. in biotrophic infection structures (Fig. 15A, 36 HPI; iv and ph). At 48 HPI, in late primary hyphae (Fig. 15A, 48 HPI; ph), the intensity of eGFP fluorescence was reduced, had disappeared completely at 72 HPI in necrotrophic secondary hyphae (Fig. 15A, 72 HPI; sh), and stayed undetectable until the fungus had formed acervuli with new conidia at 120 HPI (Fig. 15A, 120 HPI; co).

To demonstrate that eGFP fluorescence is detectable in necrotrophic secondary hyphae, the *eGFP* reporter gene was also fused to the constitutive *TOXB* promoter of the wheat pathogen *Pyrenophora tritici-repentis* (Andrie et al., 2005). As expected, strains expressing the P$_{TOXB}$:*eGFP* fusion showed fluorescence in conidia and in all infection structures, including necrotrophic secondary hyphae, clearly demonstrating that down-regulation of eGFP fluorescence in strains harboring the P$_{FET3-1}$:*eGFP* construct is due to infection structure-specificity of the P$_{FET3-1}$ (Fig. 15B).
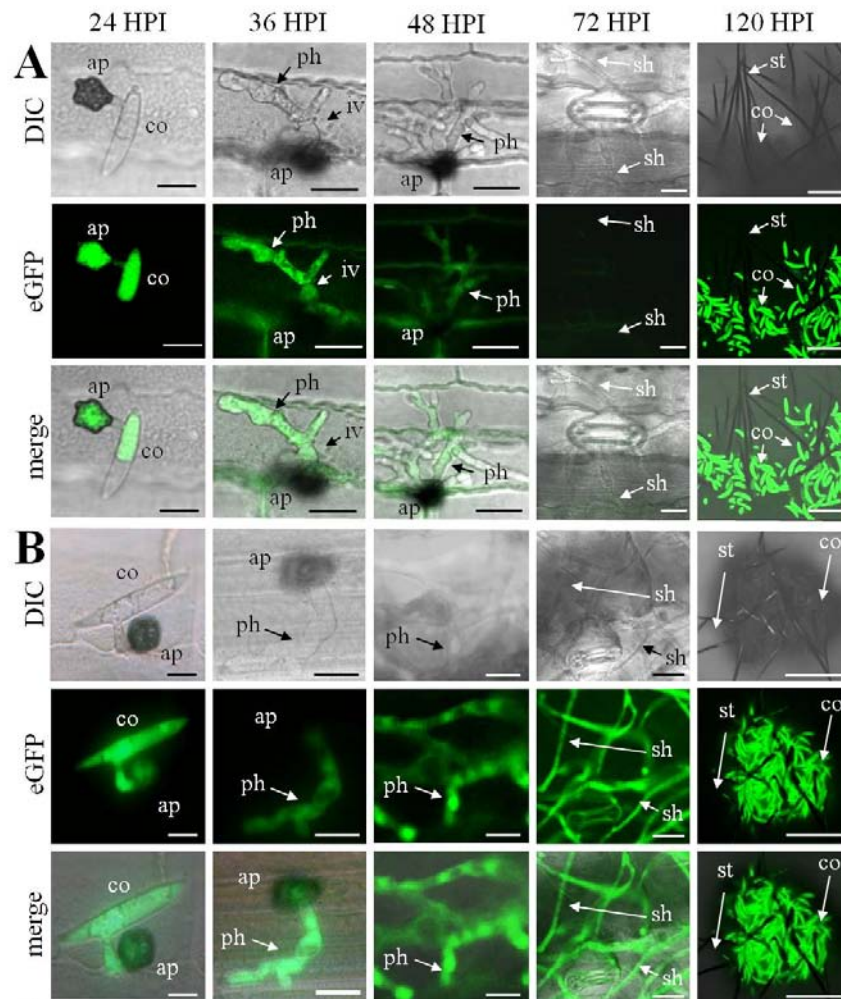
Fig. 15: Infection-structure-specific expression of *FET3-1*.
A: Expression of *FET3-1* was assessed in a *C. graminicola* replacement strain harboring a P*FET3-1*:*eGFP* fusion construct. eGFP fluorescence was clearly visible in conidia (co) and appressoria (ap), as well as in biotrophic infection vesicles (iv) and primary hyphae (ph). In necrotrophic secondary hyphae (sh) representing the vast majority of infection structures at 72 HPI, eGFP fluorescence was absent, but re-appeared in novel conidia formed at 120 HPI.
B: In a strain expressing the *eGFP* gene under the control of the constitutive *TOXB* promoter of *P. tritici-repentis,* eGFP fluorescence was seen in all infection structures.
DIC, differential interference contrast; st, sterigma; bars (24 and 36 HPI) = 10 µm; (48 and 72 HPI) = 20 µm; 120 HPI = 50 µm.

The expression of *FET3-1* was also analyzed during *in-vitro* growth. The fluorescence was very low during vegetative growth, but it increased dramatically in matured acervuli formed on OMA plates (Supplementary Fig. S5D).

The expression of *FET3-1* gene was also analyzed in response to iron status, therefore I used the P*FET3-1*:*eGFP* construct to measure the eGFP fluorescence under iron deplete or replete conditions (Supplementary Fig. S5G). There is an extreme response to iron status, where the fluorescence intensity is about 1200-fold in mycelia grown under iron limitation (100 µM BPS) in comparison to mycelia grown in iron replete condition (100 µM FeSO$_4$). These data fully agree with the result obtained from the qRT-PCR assay (Fig. 7).

III.2.4.2 FET3-1 is a an integral plasma membrane protein

In order to visualize the localization of *FET3-1*, a *FET3-1:eGFP* fusion construct (Supplementary Fig. S5A) was transformed into a Δ*fet3-1* deletion strain. The transformants harboring the *FET3-1:eGFP* construct did not differ from the WT strain with respect to colony phenotype, pigmentation, sporulation (Supplementary Fig. S5C and D), and growth rates on PDA (Supplementary Fig. S5E). Importantly, the *FET3-1:eGFP* construct fully complemented the virulence defect of the Δ*fet3-1* deletion strain (Supplementary Fig. S5F), indicating that function and localization of the Fet3-1:eGFP fusion protein resembled that of the Fet3-1 protein. Microscopic analyses of a strain expressing the *FET3-1:eGFP* fusion construct under control of the native P_{FET3-1} promoter showed that Fet3-1 localized to hyphal plasma membranes (Fig. 16A, arrowheads), with major fluorescence visible at hyphal tips and the septa of vegetative hyphae (Fig. 16A, solid arrow and sep). The strong fluorescence signal in septa may be due to two membranes of neighboring cells sandwiching the septum.

Plasma membrane localization of FET3-1 was further confirmed by protoplasting of vegetative hyphae of *FET3-1:eGFP* strains grown under iron-limiting conditions. In agreement with the yeast complementation experiments described above (Fig. 11), eGFP fluorescence was visible in the plasma membrane of the protoplasts of *C. graminicola* (Fig. 16C, arrowhead). Staining of vacuolar membranes with the red fluorescing styryl dye FM4-64 clearly indicated that Fet3-1 does not localize to the vacuole or vacuolar membrane (Fig. 16A and B, arrows).

The eGFP fluorescence is highly expressed in hyphal tips (Fig. 16A and B, solid arrow) and localized to the appressorial membrane (Fig. 16B, arrowhead). The strong fluorescence of the appressorial membrane may be due to the increased need of this protein for delivering the appropriate amount of iron for enzymes involved in cell wall and melanin biogenesis (i.e. reductases and laccases, Langfelder et al., 2003; Jung et al., 2006; Jung et al., 2009). These data were also supported by results obtained in the Δ*fet3-1* strain, which showed a significant delay in appressorial melanization (Figs. 14A and 33A; Δ*fet3-1*).
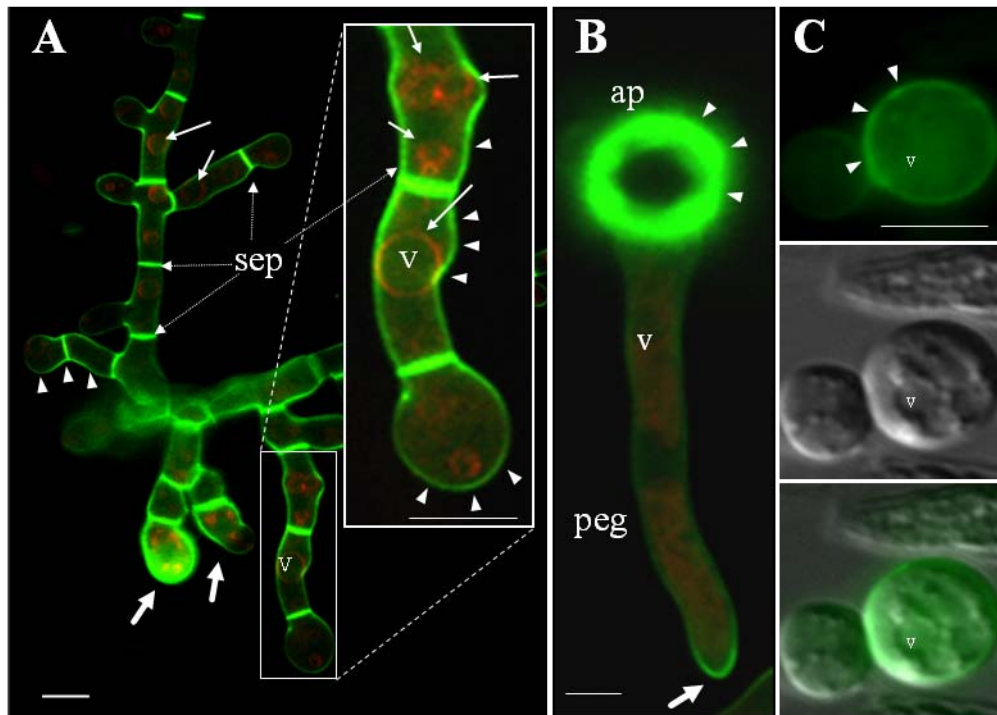
Fig. 16: Localization of the Fet3-1 protein to the plasma membrane of *C. graminicola*.
A: The eGFP fluorescence is mainly localized in plasma membranes (arrowhead) and septa (sep), whereas the styryl FM4-64 localized on the vacuole membrane (arrow; inset). Insert is a magnification of the rectangle-framed mycelia. The FM4-64 styryl staining was accomplished using 15 min/4 hours (pulse/chase) method.
B: *FET3-1:eGFP* is highly expressed in appressoria (ap) and localized to appressorial membrane (arrowhead), and hyphal tip (solid arrow).
C: Plasma membrane localization of Fet3-1 protein after protoplasting (arrowhead).
ap, appressorium; peg, penetration peg; star, appressorial pore; v, vacuole; Bars = 5µm

An attempt to localize the Fet3-2 protein by constructing a *FET3-2:eGFP* cassette (II.4.10.1 and Supplementary Fig. S4) has failed, likely due to low expression of this gene. That also agrees with results obtained by qRT-PCR (Fig.7).

III.3 Characterization of the SIA pathway in *C. graminicola*

III.3.1 Identification and cloning of *SID1* of *C. graminicola*

The *SID1* gene (EFQ31396.1) encodes the L-ornithine-N^5-monooxygenase, which catalyzes the first step in fungal hydroxamate-type siderophore biosynthesis (Fig. 5). This gene is essential for iron uptake, ROS tolerance, and consequently virulence of different animal and plant pathogens like *A. fumigatus, F. graminearum* and *M. oryzae* (Schrettl et al., 2004; Greenshields et al., 2007; Hof et al., 2008).
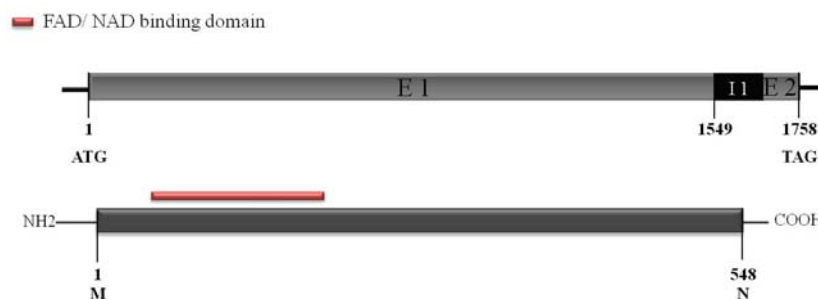
Fig. 17: Structure of the *SID1* gene and the deduced protein of *C. graminicola*. The coding region comprises two exons (E1: 1549 bp and E2: 99 bp) interrupted by 111-bp intron (I1). The FAD/NAD-binding domain is marked with red bar.

The complete sequence of the *SID1* gene was assembled from trace sequences. The predicted 111-bp intron was confirmed by cDNA sequencing. The deduce protein contains 548 amino acids having the FAD/NAD-binding domain that is essential for binding of flavin adenine dinucleotide (FAD) and/or nicotinamide adenine dinucleotide (NAD), cofactors essential for catalyzing activity (Fig. 17).

III.3.1.1 Deletion of *SID1*

III.3.1.1.1 Target mutagenesis of *SID1*

In analogy to the work performed with the ferroxidase genes, the *SID1* gene was deleted by homologous recombination (Fig. 18). The full length ORF of the *SID1* gene was replaced by a 1798-bp fragment carrying the *hph* gene (Fig. 18A). The deletion of the *SID1* gene and the insertion of a single copy of the *hph* gene into the coding region were confirmed by Southern

blot analyses, in which five individual deletion mutants (KO1-KO5) were identified (Fig. 18B).
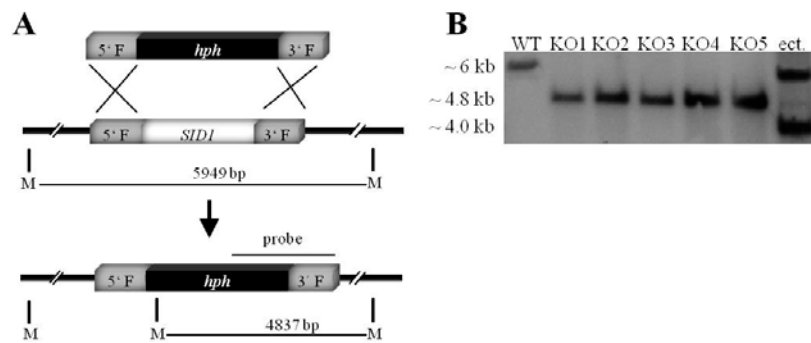
Fig. 18: Generation of Δ*sid1* strains of *C. graminicola* by homologous recombination.
A: Scheme of targeted mutagenesis of *SID1* by homologous recombination. The full ORF of the *SID1* gene was replaced by a 1798-pb fragment carrying *hph* gene. 3´F and 5´F, left and right flanks; M, *Mun*I restriction site used for Southern blot analysis.
B: Southern blot analysis performed with *Mun*I-digested genomic DNA from WT, ectopic (ect.), and KO strains showed that the 4837-bp fragment in all independent KOs replaced the 5949-bp WT band. Transformant with ectopically integrated KO vector showed an extra band in addition to the 4837-bp WT band.

III.3.1.1.2 Siderophore synthesis is essential for *in-vitro* conidiation of *C. graminicola*

The loss of the ability to produce siderophores of *C. graminicola* has led to the reduction in growth rate and loss of the ability to form conidia under standard condition (Fig. 19A). The Δ*sid1* strains were therefore grown on OMA plates supplemented with different concentrations of different iron sources (FeSO$_4$, FeCl$_3$, Fe^{III}-EDTA or siderophore) (Fig. 19). Obviously, the addition of iron as a salt (FeSO$_4$ or FeCl$_3$) or chelated (Fe^{III}-EDTA) cannot fully restore the fungal ability to produce conidia (Fig. 19A and B). By using a concentration of 100 µM (FeSO$_4$ or FeCl$_3$) or 50 µM (Fe^{III}-EDTA), approximately 5 to 10% of the conidia produced by the WT were observed, respectively (Fig. 19B; arrow). Supplying iron as an EDTA complex (500 µM Fe^{III}-EDTA) improved the formation of conidia (approx. 50% of the WT). In comparison, addition of 500 µM of either FeSO$_4$ or FeCl$_3$ led to approximately 20 and 11% of the conidiation rate of the WT (Fig. 19B). This may be due to the relatively long time (2 weeks) required to form conidia, whereas Fe^{+2} and Fe^{+3} readily form insoluble hydroxide complexes. Thus, increasing the iron concentration improved conidiation until Fe concentrations reached a toxic level (Fig. 19A and B, 1000 µM).

Interestingly, the increase of iron concentration of any type did not significantly improve conidiation of the WT strain. That may be due to reaching the WT strain to its saturation state

of conidiation and/or due to the limitation of other nutrition in the growth medium. In contrast, once the iron concentration increased over 500 µM, toxic effects became visible and the number of conidia dropped dramatically until almost no conidia were formed at a concentration of 1000 µM (Fig. 19A and B, WT). Noticeably, the Δ*sid1* strain is prone to deleterious effect of high iron concentration more than the WT strain (Fig. 19A, 1000 µM). The addition of siderophore-bound iron (ferrisiderophore) fully restored conidiation. Applying two µM of ferricoprogen restored approx. 50% of the wild-type conidiation rate, while five µM restored conidiation completely (Fig. 19A and B, coprogen).
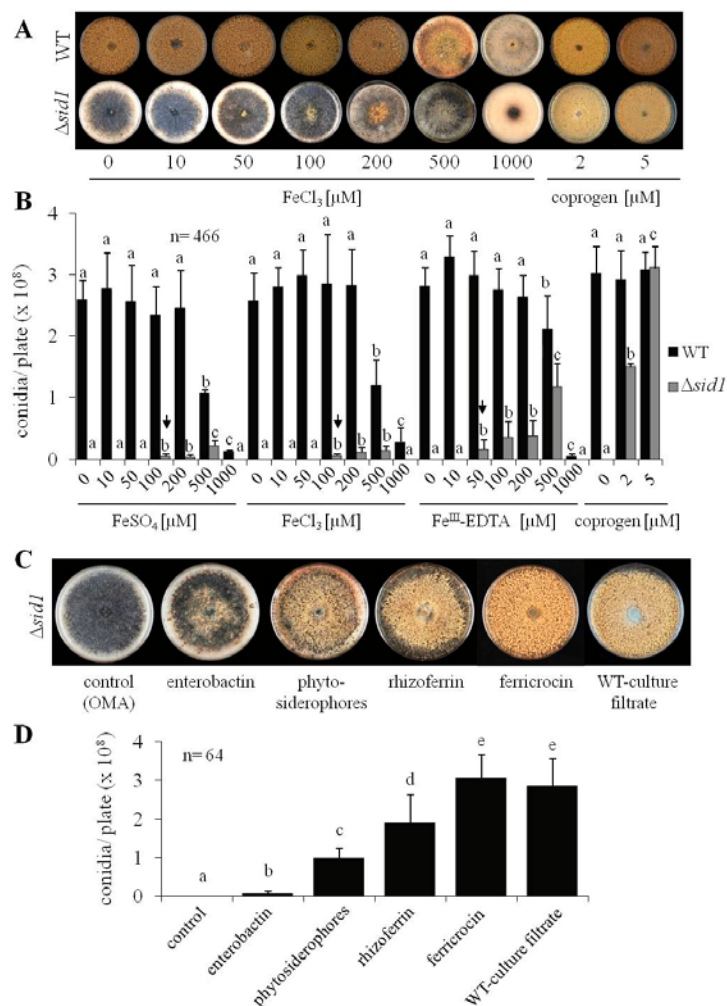
Fig. 19: Conidiation of the *C. graminicola* WT and Δ*sid1* strains in the presence of different iron sources and concentrations.
A and B: The Δ*sid1* strain does not produce conidia under standard condition (OMA; 0, control), whereas increased amount of ferric (FeCl$_3$), ferrous (FeSO$_4$) or complexed (Fe^{III}-EDTA) iron partially restored conidiation (arrows). The addition of high amounts of iron i.e. ≥ 500 µM reaches a toxic level and hence reduces growth and conidiation rates of the WT. The addition of iron as a siderophore complex fully restored the wild-phenotype of Δ*sid1* (2 and 5 µM). Different letters represent statistically significant differences between different concentrations within each treatment and strain at p < 0.001.
C and D: Supplementing the growth medium with different siderophores partially or fully restored conidiation of the Δ*sid1* strain. Different letters represent significant difference groups (p < 0.001, n = 64).

By adding different siderophores such as enterobactin (a catecholate-type siderophore), phytosiderophores, plant-source siderophores derived from 2´Deoxymugeneic acid (Tsednee et al., 2012), rhizoferrin (a polycarboxylate-type siderophore) and ferricrocin/ferrichrome (hydroxamate-type siderophores), (for molecular structures see Supplementary Fig. S6), conidiation of the $\Delta sid1$ strain was partially or fully restored (Fig. 19C and D).

The catecholate-type siderophore, which is produced by a wide range of bacteria, showed a very low complementation effect. That may be due to the absence of a transporter for this type of siderophores, or to the high affinity of this type of siderophores to iron ($K_f = 10^{52}$; Raymond and Carrano, 1979), which is much higher than that of fungal hydroxamate-type siderophores ($K_f \approx 10^{30}$). Interestingly, the plant siderophores (phytosiderophores) led to a partial complementation effect, which clearly shows the ability of the $\Delta sid1$ strain to take up this form of iron-complex. This is also true for the carboxylate siderophore (rhizoferrin), which was originally isolated from the soil porn fungus *Cunninghamella elegans*. The hydroxamate-type siderophores ferrichrome, coprogen, and ferricrocin fully complemented conidiation of the $\Delta sid1$ mutant (Fig. 19A-D). The addition of WT-culture filtrate to the $\Delta sid1$ strain also restored its ability to form conidia (Fig. 19C and D). Moreover, the culture filtrates of $\Delta fet3-1$ and $\Delta fet3-2$ strains, but not those of the $\Delta sid1$ and $\Delta nps6$ strains complemented conidiation (Supplementary Fig. S7, for strategy of gene deletion see III.3.2.1).

To prove that the failure of forming conidia in $\Delta sid1$ strains is due to iron shortage, the *C. graminicola* WT strain was grown on OMA plates supplemented with different concentration of the iron chelator BPS (Fig. 20). Obviously, increasing the concentration of the chelator BPS led to a significant decrease in growth rates and conidiation. Although the WT strain is able to produce siderophores, and all genes of the SIA pathway are over expressed under iron limitations (Fig. 7), WT was unable to produce conidia at concentrations higher than 500 µM and showed a $\Delta sid1$-like phenotype. These results clearly indicate that the inability of the $\Delta sid1$ strain to produce conidia is due to iron limitation rather than to the inability of producing siderophores.
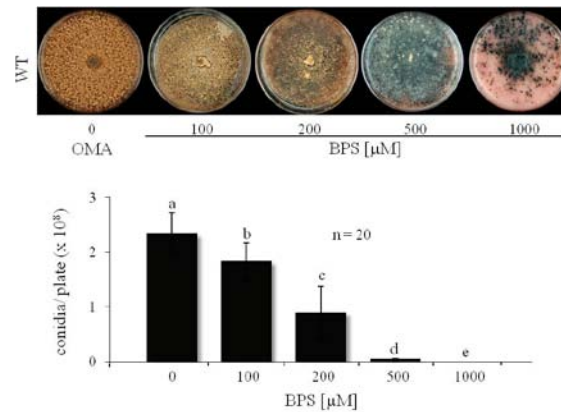
Fig. 20: The effect of iron limitation on conidiation of *C. graminicola*. The WT strain CgM2 showed decreased growth and conidiation rates by increasing the concentration of BPS. Different letters represent different significant groups. $p < 0.001$, $n = 20$.

Taken together, these results clearly show that vegetative hyphae of the Δ*sid1* mutant are unable to acquire sufficient iron for production of conidia. Ferrous or ferric iron only partially restored the ability of Δ*sid1* to form conidia, whereas the chelated iron (EDTA or siderophore complexes) restored largely or fully. *C. graminicola* can sufficiently take up and utilize xenosiderophores originated from fungi and plants, but not those from bacteria.

III.3.1.2 eGFP tagging of the Sid1 protein

III.3.1.2.1 The *SID1*:*eGFP* construct does fully complement the Δ*sid1* strains.

In analogy to the work done with *FET3-1* gene, the *eGFP* reporter gene was fused either to the *SID1* promoter (P_{SID1}) or to the 3´-end of the complete *SID1* gene under the control of its native promoter (Supplementary Fig. S8). The Δ*sid1* strain was transformed with the *SID1*:*eGFP* construct and eight out of twelve independent nourseothricin resistant transformants harbored the full *eGFP* construct, as confirmed by PCR (Supplementary Fig. S8A). The P_{SID1}:*eGFP* construct was transformed into either WT or Δ*sid1* strains, and eight and six transformants with the full length P_{SID1}:*eGFP* construct were obtained, respectively (Supplementary Fig. S8B). The *SID1*:*eGFP* construct fully complemented the Δ*sid1* strain, whereas growth and conidiation rates were completely restored (Fig. 21A, Δ*sid1*+*SID1*:*eGFP*). In contrast, the Δ*sid1* strain transformed with the P_{SID1}:*eGFP* construct did not differ from the Δ*sid1* strains (Fig. 21A, Δ*sid1*+P_{SID1}:*eGFP*). The Δ*sid1*+*SID1*:*eGFP* strains showed germination and appressorial formation rates comparable to the WT (Fig. 21B

and C). The germination and appressorial formation rates of Δ*sid1* strains were 22 and 15%, respectively, whereas those of the WT were 89 and 82.7%, and those of the Δ*sid1*+*SID1*:*eGFP* strains were 93 and 87% (Fig. 21C). Noticeably, the Δ*sid1* strains often showed cell wall defects in conidia and appressoria (Fig. 21B, 24 HPI; Δ*sid1*, white and black arrowhead, respectively). This was confirmed by protoplasting assays testing for cell wall integrity (see III.6). Furthermore, *C. graminicola* WT and the Δ*sid1*+*SID1*:*eGFP* strains formed acervuli four days after inoculation (Fig. 21B, 4 DPI; WT and Δ*sid1*+*SID1*:*eGFP*). Δ*sid1* strains failed to form acervuli or formed not fully developed acervuli (Fig. 21B, 4 DPI; Δ*sid1,* ac), indicating the insufficient iron supply to form conidia as found in *in-vitro* growth (III.3.1.1.2).
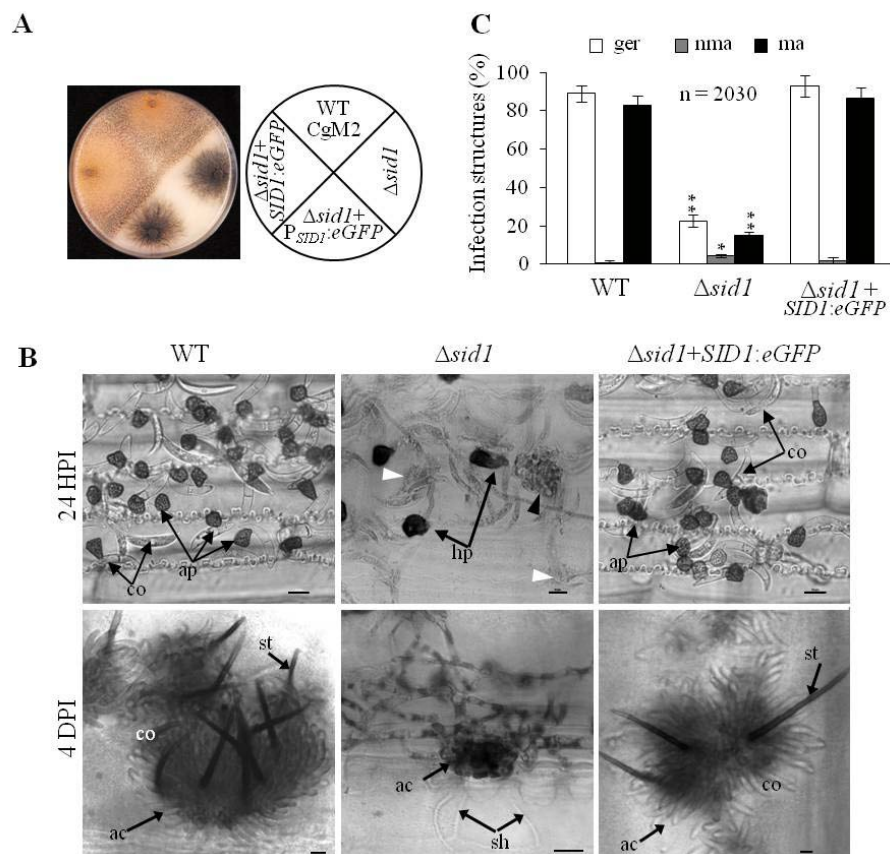
Fig. 21: Complementation of Δ*sid1* strain by the *SID1*:*eGFP* construct.
A: The *SID1*:*eGFP* construct complemented the Δ*sid1* strain and fully restored wild-type growth and formation of conidia.
B: Microscopical inspection of *C. graminicola* WT, the Δ*sid1*+*SID1*:*eGFP* and Δ*sid1* strains 24 HPI and 4 DPI, hp: hyphopodia, white and black arrowhead represent ruptured conidium and appressorium, respectively; co, conidia; st, sterigma; ac, acervuli; sh, secondary hyphae. Bar = 10 µm.
C: Germination and appressoria formation rates of the WT, Δ*sid1*+*SID1*:*eGFP* and Δ*sid1* strains at 24 HPI. Asterisks represent significance groups (p < 0.001, n =2030).

III.3.1.2.2 Expression of *SID1*:*eGFP* constructs *in-vitro*

The *SID1*:*eGFP* construct fully complemented the Δ*sid1* strain. These strains display colony phenotype, pigmentation, sporulation and growth rates, and virulence comparable to the WT strain (Fig. 21). This indicates that the function and localization of the Sid1:eGFP fusion protein resembled that of the Sid1 protein.

Different programs predicting sub-cellular protein localization (SOSUI, PRED-TMR and DAS-TMfilter) identified the Sid1 protein as a cytoplasmic soluble protein. To confirm the sub-cellular localization of this protein, Δ*sid1*+*SID1*:*eGFP* strains were used. As expected, the eGFP-tagged protein localized mainly in the cytoplasm, but not in the vacuolar lumen (Fig. 22A, arrow).
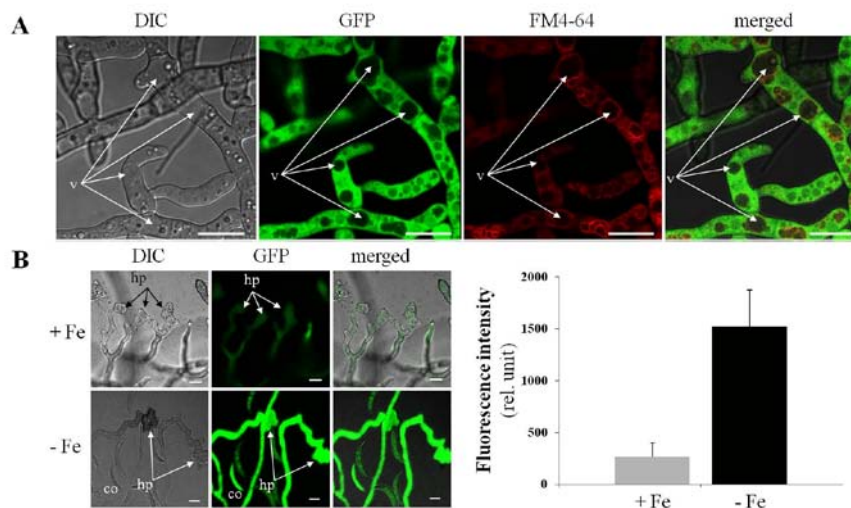
Fig. 22: Sub-cellular localization and iron response of Sid1 of *C. graminicola*.
A: Cellular localization of the Sid1 protein in the Δ*sid1*+*SID1*:*eGFP* strain. The localization of the red fluorescence styryl FM4-64 was accomplished by a 30-min pulse and 4-h chase prior to microscopy.
B: *eGFP* expression under the control of *SID1* promoter in mycelium cultured overnight in PDA media containing either 100 µM FeSO$_4$ (+ Fe), or 100 µM BPS (- Fe). Bars = + SD.

Moreover, the expression of the *SID1* gene in response to iron status was further studied by analyzing the eGFP fluorescence under the control of the *SID1* promoter. Indeed, eGFP fluorescence increased drastically under iron-limited condition (100 µM BPS), whereas it decreased in the presence of 100 µM FeSO$_4$ (Fig. 22B).

III.3.1.2.3 Biotrophy-specific down-regulation of *SID1*

To study the expression of *SID1* gene in individual infection structures during infection of maize leaves, the Δ*sid1*+*SID1*:*eGFP* strain was used. Slight eGFP fluorescence was observed in dormant and germinated conidia, and in appressoria. Surprisingly, after penetration of the plant cell wall eGFP fluorescence disappeared completely in biotrophic primary hyphae (Fig. 23, 36 HPI). At later stage of pathogenesis, i.e. when the fungus had switched to the destructive necrotrophic development, intensive eGFP fluorescence re-established in secondary hyphae (Fig. 23, 72 HPI; sh). Strong fluorescence intensity was also observed in secondary hyphae at 96 HPI and in acervuli initials (Fig. 23, 96 HPI; sh and arrowhead). Noticeably, the eGFP fluorescence had decline in fully developed acervuli and matured conidia (Fig. 23, 120 HPI; ac).
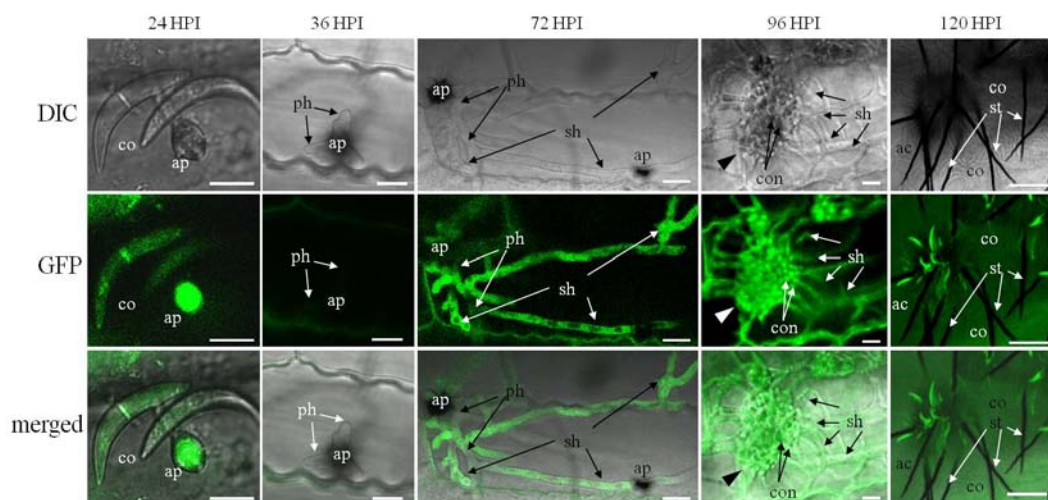
Fig. 23: Infection-structure-specific expression of *SID1*
Infection-structure-specific expression of *SID1* during *C. graminicola* infection of maize leaves.
ac, acervulus; ap, appressoria; co, conidia; con, conidiogenous initials; hp, hyphopodia; ph, primary hyphae; sh, secondary hyphae; arrowhead, acervulus initials; v, vacuole.
Bars: A: and B: (10 µm), C: (24-96 HPI = 10 µm, 120 HPI = 50 µm).

III.3.2 Identification and cloning of *NPS6* of *C. graminicola*

The *NPS6* gene (EFQ32921.1) encodes a nonribosomal peptide synthetase, which is responsible for the third step in hydroxamate-type siderophore biosynthesis (Fig. 5). Blast search and sequence similarity revealed the putative function for synthesis of extracellular siderophore. *NPS6* has a conserved function among filamentous ascomycetes. Deletion of this gene in the maize pathogen *Cochliobolus heterostrophus*, the rice pathogen *Cochliobolus miyabeanus*, the wheat pathogen *F. graminearum* and the *Arabidopsis thaliana* pathogen *Alternaria brassicicola* led to loss of extracellular siderophore production and reduction of virulence (Oide et al., 2006).

The predicted single intron (78 bp) was confirmed by cDNA sequencing. The deduce protein (1942 amino acids) contains all characteristic domains of NRPSs (adenylation, thiolation, and condensation domains) (Fig. 24).
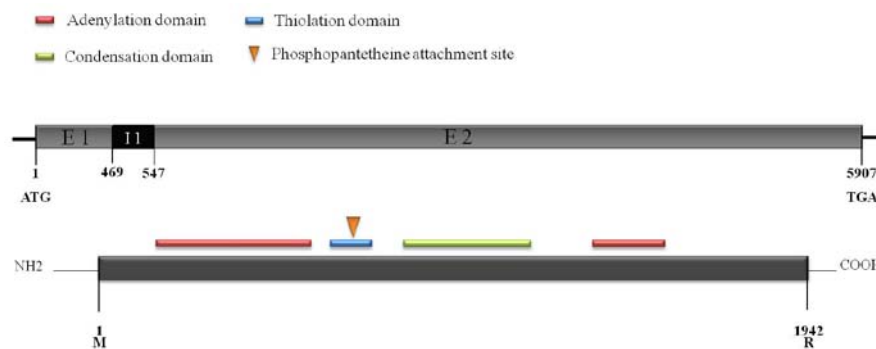
Fig. 24: Structure of the *NPS6* gene and the deduce protein in *C. graminicola*. The coding region comprises of two exons (E1: 469 bp and E2: 5361 bp) interrupted by a 78-bp intron (I1). The encoded protein is 1942 amino acids. The adenylation, thiolation, and condensation domains are marked with red, blue, and green bars, respectively. The phosphopantetheine attachment site is indicated by an orange triangle.

III.3.2.1 Inactivation of *NPS6*

To characterize the *NPS6* gene and to differentiate the Δ*nps6* phenotype from the Δ*sid1* phenotype, the *NPS6* gene was inactivated by homologous recombination (Fig. 24A). Approximately 60% of the ORF of the *NPS6* gene (containing its three main components) was replaced with 2692-bp fragment carrying the *hph* gene. The inactivation of the *NPS6* gene and the insertion of single copy of the *hph* into the coding region were confirmed by Southern blot analyses, in which seven individual mutants (KO1-KO7) were obtained (Fig. 24B).

To confirm gene inactivation at the transcriptional level, RT-PCR experiments were performed using RNA isolated from WT, deletion mutants, and an ectopic transformant (Fig.

24C). A 354-bp NPS6-fragment from the 5´-end of the ORF of the *NPS6* gene (Fig. 24A, arrows) was amplified just from RNA isolated from the WT and the ectopic, but not from the Δ*nps6* strains (KO1-KO7). Primers corresponding to transcripts of the constitutively expressed *H3* gene (Behr et al, 2010) were used as a control and allowed amplifying the 85-bp H3 fragment from RNA of WT, ectopic, and KO strains.
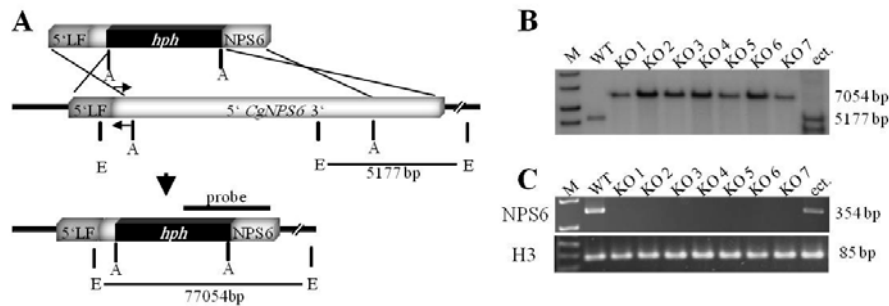
Fig. 25: Generation of Δ*nps6* strains of *C. graminicola* by homologous recombination.
A: Scheme of targeted mutagenesis of *NPS6* by homologous recombination. A 2692-bp fragment carrying the *hph* gene (not to scale) replaced a 3229-bp fragment of the *NPS6* gene. A, *Age*I restriction site; E, *EcoR*V site; 5´LF, left flank; arrows depicting the RT-PCR primers used for RT-PCR assay, probe, probe used for the Southern blot analyses.
B: Southern blot analyses performed with *EcoR*V-digested genomic DNA of WT, ectopic (ect.), and Δ*nps6* (KO) strains showed that the 7054-bp fragment in all independent KO strains replaced the 5177-bp WT band. Transformants with an ectopically integrated KO construct showed an extra band in addition to the 5177-bp WT band.
C: RT-PCR analysis performed with *NPS6*-specific primers confirmed gene inactivation at the transcript level. Primers corresponding to transcripts of the constitutively expressed gene histone (*H3*) were used as a control.

III.3.2.2 Phenotypic characterization of Δ*nps6* strain

Interestingly, on OMA the phenotype of Δ*nps6* mutants was variable. Δ*nps6* mutants exhibited two phenotypes differing from the WT phenotype, which were designated as phenotypes Δ*nps6*A and Δ*nps6*B (Fig. 26A). While phenotype Δ*nps6*A showed sparse conidiation even after three weeks of incubation, phenotype Δ*nps6*B formed neither acervuli nor conidia. For comparison, the WT strain and ectopic transformants had formed acervuli with salmon-colored conidia covering the entire plates already after two weeks of cultivation (Fig. 26B, arrowhead). Supplementing OMA with coprogen restored conidiation in phenotype Δ*nps6*A, but not in phenotype Δ*nps6*B, which showed massive formation of aerial mycelium.

This abnormal Δ*nps6*B phenotype was excluded from this study. However, these strains were not pathogenic when they were applied to inoculate maize plant.

Surprisingly, some strains of the Δ*nps6*A phenotype converted during sub-culturing on OMA plates to the phenotype Δ*nps6*B, and when sectorial colonies from phenotype Δ*nps6*A were sup-cultured on new growth media supplemented with siderophores, the sectored cultures showed Δ*nps6*B phenotype (Supplementary Fig. S9).
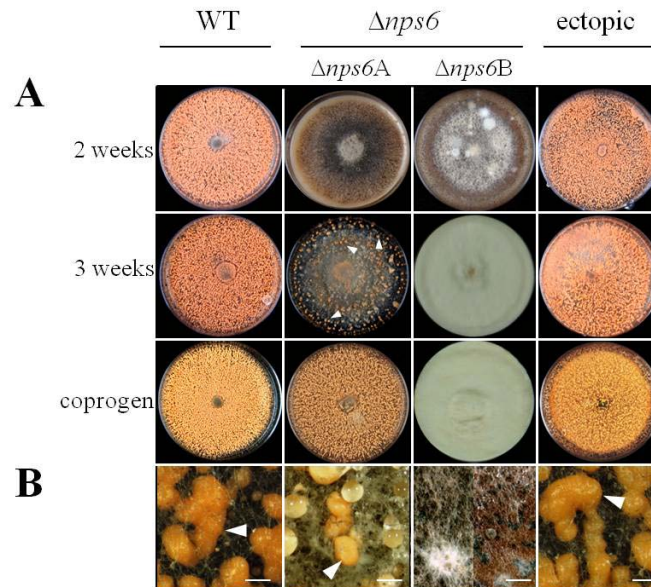
Fig. 26: Phenotypes of the Δ*nps6* strains in *C. graminicola*.
A: The *C. graminicola* Δ*nps6* strain showed two phenotypes (Δ*nps6*A and Δ*nps6*B on OMA plates. The Δ*nps6*A showed delayed growth and reduced conidiation in comparison to the WT and ectopic strains. Wild-phenotype was restored by adding siderophores. Phenotype Δ*nps6*B formed fluffy mycelium and was not complemented by siderophores.
B: Images at 5× magnification. In comparison to WT and ectopic strains, Δ*nps6*A strains form some small acervuli (arrowhead), but Δ*nps6*B strains were not able to form acervuli. (Δ*nps6*B right image, after removing the fluffy mycelium). Bar 200 µm.

On PDA, the variability of the phenotype of Δ*nps6* strains was even more pronounced (Fig. 27A). The WT strain was strongly melanized and did neither show sectoring nor formation of slowly growing mycelium. In contrast, 43% of the plates of the Δ*nps6* mutants showed uniform melanization, 42% showed sectoring and 8% exhibited slow growth. To investigate the phenotypic variability and sensitivity to ROS of Δ*nps6* mutants in more detail, both WT and mutant strains were challenged by H_2O_2. Under these conditions, slow growth was observed in approx. 9% of the plates inoculated with the WT strain. For comparison, melanized and sectored mycelia decreased to approx. 15% each on H_2O_2 plates inoculated with the Δ*nps6* mutants, whereas plates with slowly growing mycelium drastically increased to 70% (Fig. 27A and B).
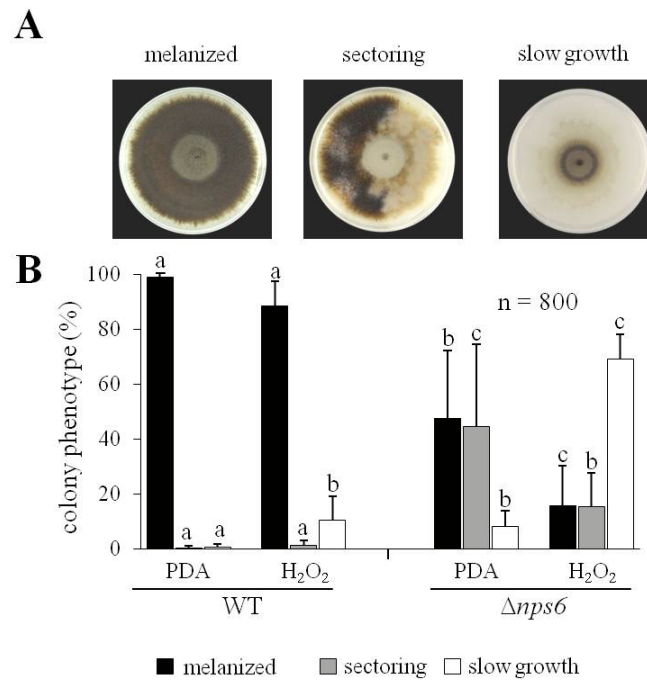
Fig. 27: Characterization of *C. graminicola* WT and Δ*nps6* strains growing on PDA with or without H₂O₂.
A: The three characteristic phenotypes obtained in this study.
B: *C. graminicola* WT and Δ*nps6* strains were grown on PDA and PDA amended with 0.01% H_2O_2 and cultivated at 23°C in darkness. In comparison to the WT, the Δ*nps6* strains showed increased sectoring, slow growth, and H_2O_2 sensitivity. Different letters represent significance groups ($p \leq 0.001$, n =800).

These data demonstrate that siderophore-mediated iron uptake is required for uniform colony development.

III.3.3 Plant infection and *in-vivo* conidiation

When the WT and the ectopic strains were used to inoculate maize leaves, a typical anthracnose symptom has been formed on both intact and wounded leaves at 4 DPI. No significant difference between these two strains was observed (Fig. 28A and B). When the Δ*nps6* strain was used to inoculate non-wounded leaves, it showed fluctuation and mainly attenuation of symptoms establishment, but it showed comparable anthracnose symptoms when it was used to inoculate wounded leaves (Fig. 28A). Analysis of the fungal mass by qPCR showed that Δ*nps6* strains were less than 20% of WT strain on non-wounded leaves, whereas it was approx. 60 % of the WT strain on wounded leaves (Fig. 27B).

The Δ *sid1* strains showed more pronounced pathogenicity defects than the Δ *nps6* strains. When Δ*sid1* strains were used to inoculate non-wounded leaves, approximately 3% of the WT and 18% of Δ*nps6* strains. On wounded leaves, the Δ*sid1* strain was 38.5% of the WT strain and ca. 60 % of the Δ*nps6* strain (Fig. 28B).

Noticeably, the virulence of different independent strains of Δ*sid1* ranged from 0 to ~ 10% in comparison to the WT, whereas the virulence of different Δ*nps6* strains ranged from 4 to 48% (Supplementary Fig. S10).

Formation of conidia on non-wounded leaves 6 DPI showed significant differences between the WT and each of Δ*sid1* and Δ*nps6*. On wounded leaves Δ*sid1*, but not Δ*nps6* differed significantly from WT (Fig. 28C).

Virulence of WT, Δ*nps6*, and Δ*sid1* strains were also compared on whole plants using 1x 10^7 conidia/ml of oval conidia formed in liquid culture as an inoculum. Obviously, the WT and ectopic strains formed typical anthracnose symptoms at 6 DPI (Fig. 28D, WT and ect.), whereas the Δ*nps6* strains showed drastically reduced symptoms (local and very small lesions) (Fig. 28D, Δ*nps6;* arrows). Noticeably, the Δ*sid1* strain showed no obvious symptoms at this time point (Fig. 28D, Δ*sid1*).
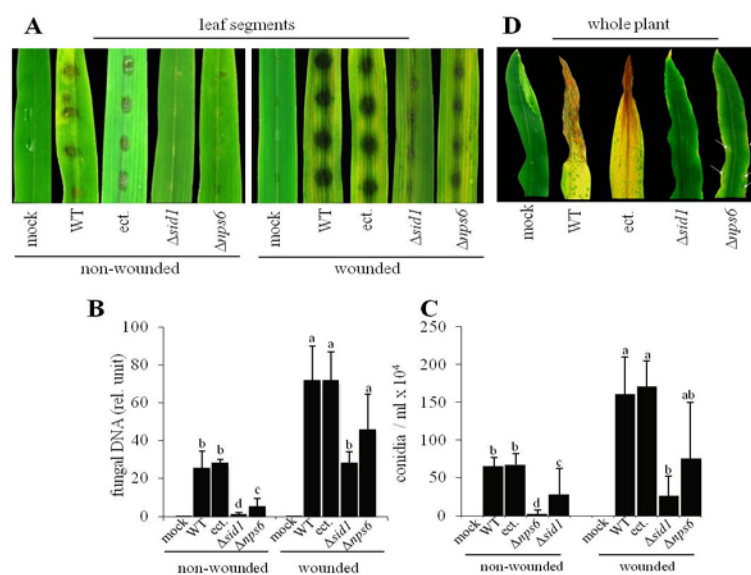
Fig. 28: Virulence assay of the representative Δ*sid1* and Δ*nps6* strains.
A: Detached leaf assays showed that WT and ectopic (ect.) strains, but not the representative Δ*sid1* and Δ*nps6* strains, cause the anthracnose symptoms on non-wounded leaves, whereas both Δ*nps6* and Δ*sid1* could colonize the wounded leaves.
B: Quantification of fungal mass in infected leaves by qPCR at 4 DPI. Different letters represent significance groups (p ≤ 0.001, n = 3).
C: Asexual sporulation *in-vivo* 6 DPI of WT, ect., Δ*sid1* and Δ*nps6* strains.
D: Tow week old maize plants were sprayed with 10 ml of a suspension containing 1x 10^7 conidia/ml suspension. Images were taken at 6 DPI. Some local lesions were observed in Δ*nps6*-infected leaves (arrow).

Microscopical inspection of the infection sites revealed reduced germination rates, and increased rates of spontaneous lysis of *on planta*-developed structures (Fig. 29A). The Δ*nps6* strain was comparable with the Δ*sid1* strain, whereby reduction of conidial germination, increased rate of conidial-, and appressorial-lyses were observed (Fig. 29A, black arrowhead). These characters are similar to some extent to the Δ*fet3-1* strain (Fig. 14A). Additionally, protrusions were also observed in germination tubes and hyphopodia (Fig. 29A, Δ*sid1*; 48 HPI, left; hp, arrowhead). Noticeably, lesions and cell wall leaking was not observed in conidia germinated on onion epidermis (Supplementary Fig. S11, Δ*sid1*). This may indicate a secretion of different lysing enzymes and/or generation of ROS as a part of the plant defense system. This defense system is usually suppressed or circumvented by the WT strain. Moreover, conidia of Δ*sid1* and Δ*nps6* usually form several germ tubes before forming appressoria or hyphopodia and these germ tubes of these strains branched, and hyphopodia showed lateral germination (Fig. 29A, 48 HPI; Δ*sid1* and Δ*nps6*, 48 HPI). This was also observed on onion epidermis (Supplementary Fig. S11, Δ*sid1*, 24 HPI; arrows and lg). In some cases, the Δ*nps6* strains formed spherical and oval cells on the leaf cuticle reminiscent of oval and spherical conidia formed in liquid culture (Fig. 29A, Δ*nps6*; 6 DPI, oco). In addition, Δ*nps6* strains formed small acervuli with small numbers of conidia (Fig. 29A, Δ*nps6*; 6 DPI, ac) (see Fig. 28C). Oval conidia were also observed in Δ*sid1* strains growing on onion epidermis (Supplementary Fig. S11, 48 HPI; arrowhead), and maize leaves (Fig. 29A, Δ*sid1*; 6 DPI, oco). Intriguingly, the Δ*sid1* strains formed in many cases empty acervuli (Fig. 29A, Δ*sid1*; 6 DPI, ac). These data fully agree with the data obtained for vegetative growth and *in-vitro* formation of conidia (III.3.1.1.2).

Germination and appressorium formation rates on maize leaves were significantly reduced at 24 HPI in both Δ*sid1* and Δ*nps6* strains, as compared to the WT strain (Fig. 29B). Germination rates ranged between 13 to 22% in Δ*sid1* strains, and 13 to 38% in Δ*nps6* strains, whereas it was 89% in the WT. Appressorial formation rate ranged from 10 to 15% and 10 to 26% in Δ*sid1* and Δ*nps6* strains, respectively, in comparison to 82% in the WT strain.
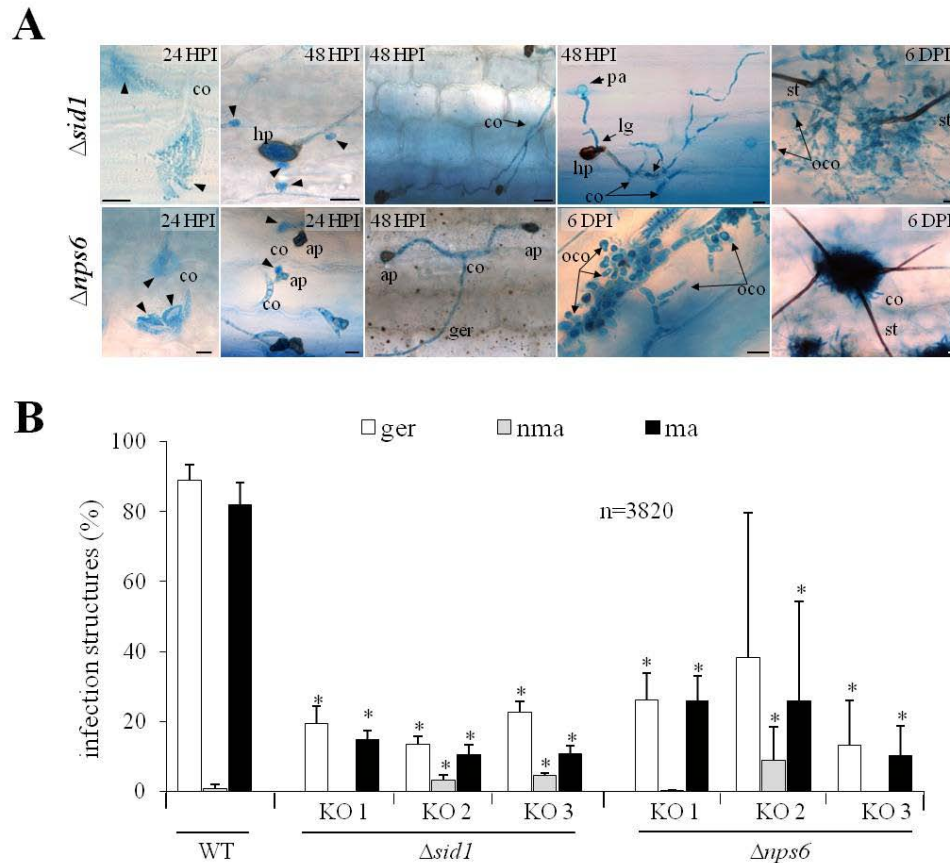
Fig. 29: Microscopical inspection of the Δ*sid1* and Δ*nps6* strains.
A: Micrographs show abnormality in germination and growth of *on-planta* structures of the Δ*sid1* and the Δ*nps6* strains developed at different time points (24 HPI to 6 DPI).
Bar = 10 µm; ap, appressoria; co, conidium; con, conidiogenous initials; ger, germination tube; oco: oval conidia; st, sterigma; hp, hyphopodia; asters, acervulus initials.
B: Germination and appressorium formation rates of the WT, three independent strains of Δ*sid1*, and Δ*nps6* strains at 24 HPI. ger, germination rate; nma, non-melanized appressoria; ma, melanized appressoria. Asterisk represents significance groups between the WT and individual strain of the studied structure ($p \leq 0.001$, n= 3820).

Taken together these results show that the SIA pathway represents a pathogenicity factor in *C. graminicola,* which is in agreement with the result obtained with necrotrophs such as *C. heterostrophus* and *F. graminearum* (Oide et al., 2006; Greenshields et al., 2007).

III.4 Siderophore production

HPLC (Fig. 30), in combination with mass spectrometry analyses (Supplementary Fig. S12) revealed that *C. graminicola* produces three extracellular siderophores, coprogen, coprogen B, and N^{α}-methylcoprogen B, as well as the intracellular storage siderophore ferricrocin, confirming and extend previous data (Horbach et al. 2009). In addition, dimerumic acid was identified, likely representing a siderophore precursor or a degradation product (Fig. 30, Supplementary Fig. S12). As expected, $\Delta sid1$ mutants are unable to synthesize any siderophore, whereas $\Delta nps6$ mutants are specifically devoid of secreted siderophores. On other hand, the ferroxidase mutants, $\Delta fet3-1$ and $\Delta fet3-1/2$ strains, were comparable to the WT strain.

These results clearly confirmed that the Sid1 protein responsible for siderophore biosynthesis, and the Nps6 protein for assembling the extracellular siderophores. The siderophore biosynthetic pathway is not affected in ferroxidase mutants ($\Delta fet3-1$ and $\Delta fet3-1/2$).
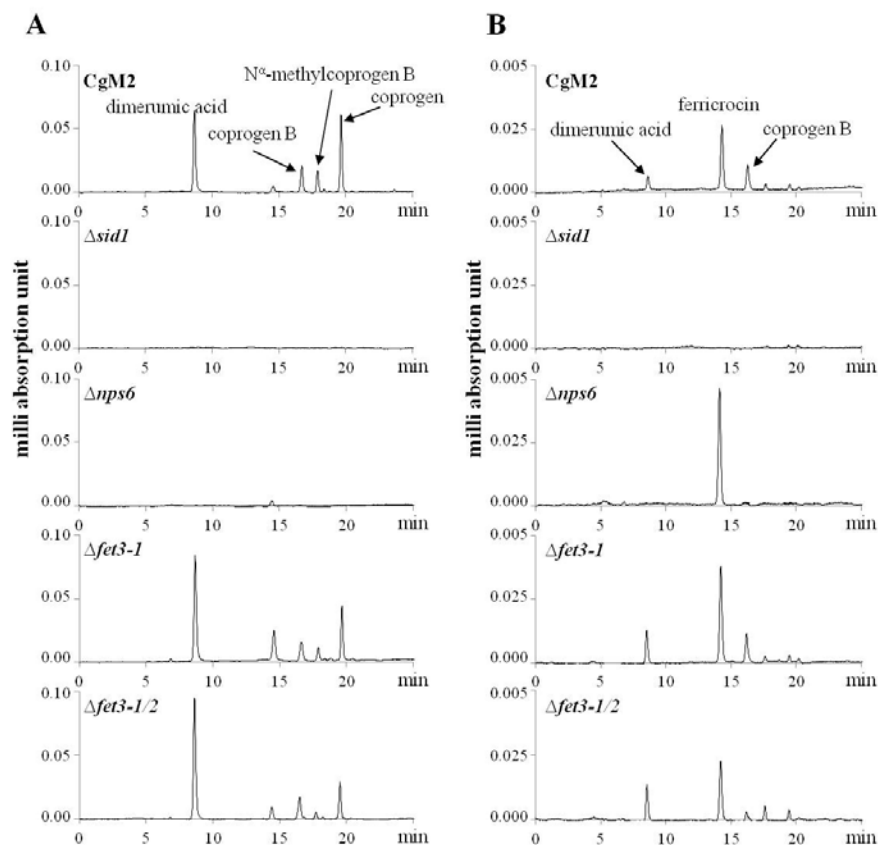
Fig. 30: HPLC-MS analysis of extracellular and intracellular siderophores of *C. graminicola* strains.
A: Extracellular siderophores analyzed in culture media of the WT, the $\Delta sid1$, the $\Delta nps6$, the $\Delta fet3-1$ and the $\Delta fet3-1/2$ strains.
B: Intracellular siderophore isolated from fungal mycelia of the strains referred in A.

III.5 Growth assays

III.5.1 Growth under iron limited condition

Growth assays of the ferroxidase mutants (Δ*fet3-1*, Δ*fet3-2*, and Δ*fet3-1/2* strain) as part of the RIA pathway, and Δ*sid1* and Δ*nps6* strains as part of the SIA pathway, was done on PDA amended with different concentration of BPS (0-250 µM). It is clearly shown that increasing amount of BPS led to decreased growth rates of the *C. graminicola* WT strain. There were no differences between WT and either of ectopic and ferroxidases mutants (Fig. 31). In sharp contrast, the Δ*nps6* and Δ*sid1* mutants showed dramatically decreased growth rates in the presence of BPS (Fig. 31).

Noticeably, the minimal inhibitory concentration is 50 µM and 100 µM BPS for the Δ*sid1* and Δ*nps6* strains, respectively (Fig. 31B; downward arrow). For comparison, the minimal inhibitory concentration of WT strain, ectopic strains, Δ*fet3-1*, Δ*fet3-2*, and Δ*fet3-1/2* strains were approx. 250 µM (Fig. 31B; upward arrow).
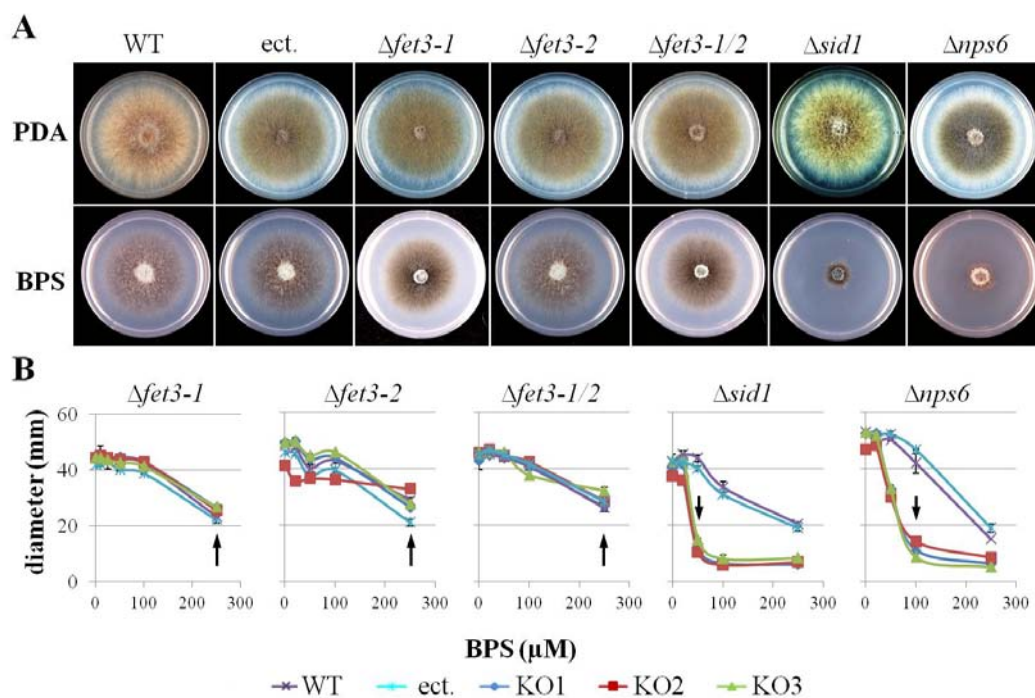
Fig. 31: Vegetative hyphae of the *C. graminicola* SIA mutants (Δ*sid1* and Δ*nps6*), but not the RIA mutants (Δ*fet3-1*, Δ*fet3-2*, and Δ*fet3-1/2*) are hypersensitive to iron depletion.
A: Five days old culture of WT, an ectopic strain (ect.), Δ*fet3-1*, Δ*fet3-2*, Δ*fet3-1/2*, Δ*nps6* and Δ*sid1* strains were grown in either PDA or PDA amended with 100 µM BPS.
B: Growth kinetics of the RIA and SIA strains on different concentration (0-250 µM) of BPS. RIA deletion strains showed no difference to the WT and the ectopic strains under different BPS concentrations, whereas the SIA strains showed significant differences in the presence of 50 µM (Δ*sid1*; arrow), or 100 µM (Δ*nps6*; arrow) BPS. Notice that the growth of RIA strains (upward arrow) in the presence of 250 µM BPS are higher than the growth of Δ*sid1* and Δ*nps6* strains in the presence of 50 and 100 µM BPS, respectively (downward arrow).

These data indicate that the SIA pathway, but not the RIA pathway, is required for iron uptake during vegetative growth. Nevertheless, the Δ*sid1* and Δ*nps6* strains were still viable and able to grow under very low iron concentrations.

III.5.2 Growth in the presence of reactive oxygen species (ROS)

As generation of ROS contributes to the prime defense responses of plants, and as iron plays an important role in quenching of ROS, I analyzed the role of the RIA and the SIA pathway in tolerance to ROS in *C. graminicola*. Both, singlet oxygen formed on illuminated plates amended with rose bengal (RB) and H_2O_2 strongly reduced growth rates of *C. graminicola*. With the exception of Δ*fet3-2* strains, the ferroxidase strains, Δ*fet3-1* and Δ*fet3-1/2*, and the Δ*sid1* and Δ*nps6* strains showed drastically increased susceptibility to both RB and H_2O_2 (Fig. 32).
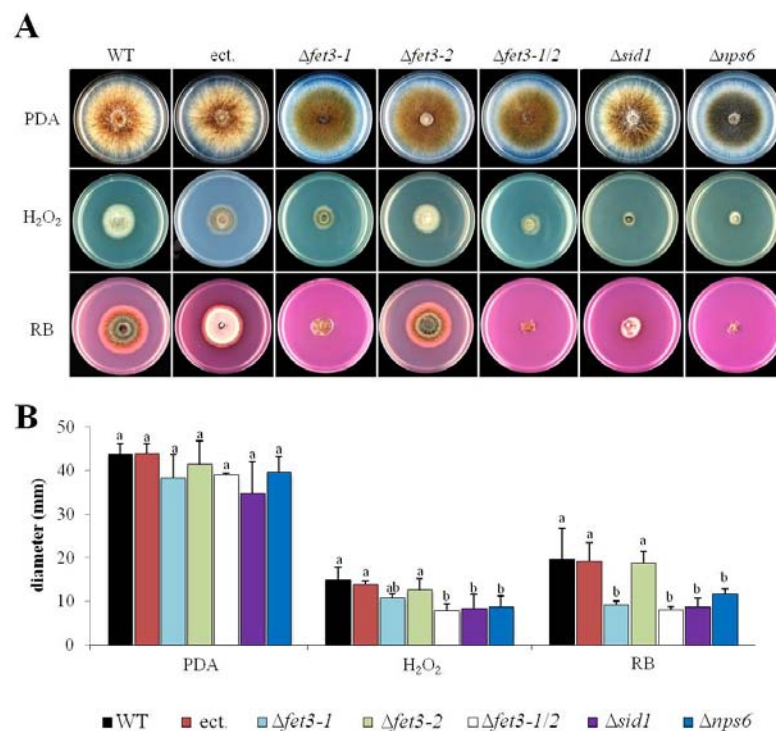
Fig. 32: *C. graminicola* **RIA and SIA strains are hypersensitive to ROS.**
A: Hypersensitivity of RIA and SIA strains to ROS (0.01% H_2O_2 and 100 µg/ml RB). With the exception of Δ*fet3-2* strain, all RIA and SIA strains showed significantly reduced growth rates in comparison to WT and ectopic strains.
B: Colony diameters were measured at 4 DPI (PDA and H_2O_2) and 13 DPI (RB). Bars represented + SD of three independent mutants. Different letters represent different significant groups (p ≤ 0.001).

Intriguingly, the addition of iron (FeCl$_3$ or FeSO$_4$) to plates amended with 0.0075% H_2O_2 improved the tolerance of *C. graminicola* toward H_2O_2 (Supplementary Fig. S13, 1 mM

$FeSO_4 + H_2O_2$). On the other hand, increased concentrations of iron (5 mM of either $FeCl_3$ or $FeSO_4$) caused increased susceptibility of *C. graminicola* to 0.0075% H_2O_2 (Supplementary Fig. S13, 5 mM + H_2O_2). These results strongly indicate the indispensable role of iron for tolerance and/or generation of ROS.

III.5.3 Growth at different pH values

As iron form and solubility are highly affected by the pH value of the growth medium, and as the pH value of the medium strongly influences the chelating efficiency of siderophores (Miethke and Marahiel, 2007, and reference therein), *C. graminicola* strains were grown at different pH values (Fig. 33). Obviously, the preferred pH value for *C. graminicola* strains was approx. pH 5.0, whereas the highest dry weight was produced at pH 4.5 and the pH value was increased to pH 5.0 (Fig. 33A and B). All strains attempted to bring the pH value between five and seven according to the buffering capacity of the used buffers (Fig. 33B). In general, there are clear reductions of growth rates under increased pH values (Fig. 33A). The Δ*fet3-1* and Δ*fet3-1/2* strains showed significant growth reduction at pH 4.5 in comparison to all other strains. This indicates that *C. graminicola* depends mainly on the RIA pathway of iron uptake under this condition (Fig. 33A, pH 4.5). This clearly indicates that ferroxidase is preferentially used at acidic conditions and agree with the result obtained by de Silva et al. (1997). At pH 7.0 there are no significant differences between WT and other strains tested, and the pH value was reduced to ca. 6.5 (Fig. 33B, pH 7). There is a significant retardation of growth rates under alkaline pH (pH 10.0) for all strains in comparison to acidic or neutral pHs. This may be due to the scarcity of soluble iron under this condition, or to toxicity of alkaline condition per se. Ferric iron, the predominant form at high pH value, forms hydroxylated complexes that condense very rapidly and the process is difficult to stop without using very strong chelating ligands or agents (Jolivet et al., 2004). Thus, *C. graminicola* strains that are able to produce siderophores are capable to circumvent with elevated pH value. In contrast, the Δ*sid1* strain was unable to grow under these conditions and showed a strong growth reduction (Fig. 33A, pH 10). The Δ*nps6* did not show significant difference to the WT and ferroxidase strains, which may be due to the production of additional ligands to ferric ion like citric acids or some volatiles that led to reduced pH value pH 6 (Fig. 33B, pH 10, Δ*nps6*).
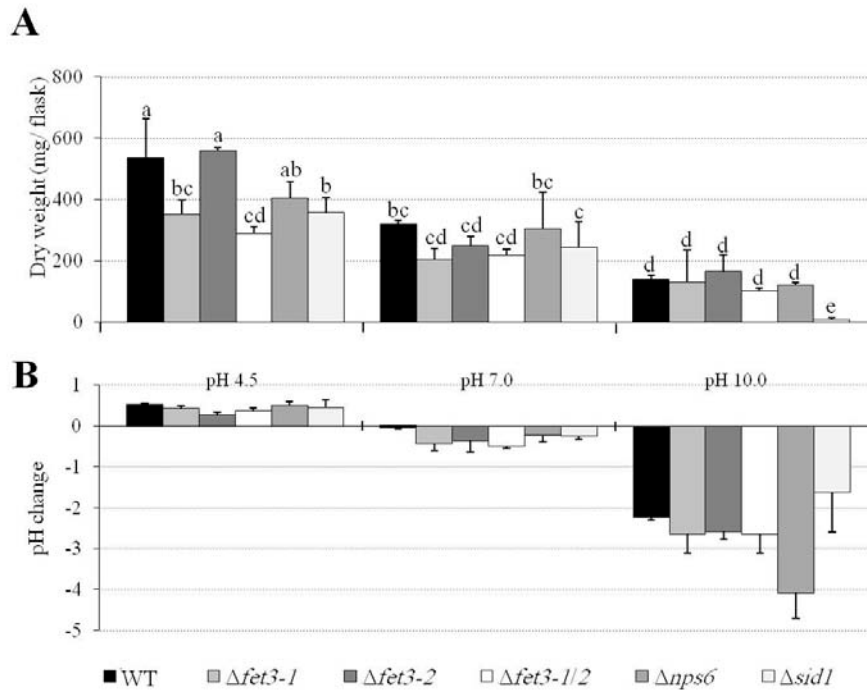
Fig. 33: Growth rates of *C. graminicola* strains at different pH values.

A: Dry weight of the WT, the RIA and SIA representative strains grown for 7 days in potato dextrose (PD) media buffered to three different pH values (4.5, 7.0 and 10). Bar represent standard deviation of the mean of four individual strains, different letters represent significance groups ($p < 0.05$, $n = 4$).
B: Changes occurred in the pH values of growth media after growing of *C. graminicola* strains.

Interestingly, the $\Delta nps6$ and $\Delta sid1$ strains grew as pseudo-hyphae and yeast-like oval conidia instead of hyphal growth like the WT. These oval conidia and pseudo hyphae restored their hyphal growth as soon as they transferred to normal PD medium (Supplementary Fig. S14). The $\Delta fet3$-*1*, $\Delta fet3$-*2,* and $\Delta fet3$-*1/2* strains grew like the WT strain (Supplementary Fig. S14).

III.6 Cell wall integrity

To analyze the cell wall defects of the Δ*fet3-1* and Δ*sid1* strains in more details, these strains were grown on OMA plates without additional iron supply for 14 d. Conidia of the WT strain, as well as those of Δ*fet3-1* formed appressoria on maize leaves (Fig. 34A). Interestingly, appressoria of Δ*fet3-1* strains had very thin cell walls, were non-melanized and several appressoria of these mutants ruptured spontaneously (Fig. 34A, Δ*fet3-1*). This phenotype clearly resembles appressorial cell wall defects of class V chitin synthase mutants of *C. graminicola* previously described (Werner et al., 2007). Δ*fet3-1* mutants also resembled Δ*chsV* mutants with respect to their strongly impaired ability to breach the intact host surface and to cause disease symptoms (Figs. 13 and 14). However, while Δ*fet3-1* mutants were unable to differentiate melanized appressoria on the surface of maize leaves, they were able to form alternative melanized infection cells called hyphopodia (Fig. 34A, Δ*fet3-1*; insert, hp), which is again in full agreement with Δ*chsV* mutants (Werner et al., 2007). As expected, the WT strain formed melanized appressoria and hyphopodia on the leaf surface (Fig. 34A, WT, ap; and insert, hp).

As the Δ*fet3-1* deletion strains represent a phenocopy of Δ*chsV* mutants, I analyzed the transcript abundance of *CHSV* and, for comparison, of the β-1,3-glucan synthase gene *GLS1* in *in-vitro*-differentiated appressoria of the WT strain and of the ferroxidase mutant Δ*fet3-1*. Indeed, qRT-PCR analyses showed that *CHSV* transcript abundance was reduced by approx. 80% in Δ*fet3-1* strains, as compared to the WT. Transcript abundance of *GLS1* was only reduced by approx. 20% (Fig. 34B).

The Δ*sid1* strain did not show a phenotype comparable to that of Δ*chsV* mutant. However, it showed a deleterious cell wall defect represented by spontaneously ruptured conidia and appressoria (Fig. 29), in addition to protrusions in germ tubes (gt) and hyphopodia (Fig. 34A, Δ*sid1*; hp, arrowhead). In some cases, the appressoria had a thin cell wall and were non-melanized (Fig. 34A, Δ*sid1*; insert, ap). Transcript abundance quantification of *CHSV* and *GLS1* in *in-vitro*-differentiated appressoria showed significant reductions by approx 95% for *CHSV* and 80% for *GLS1* in Δ*sid1* strains, as compared to WT (Fig. 34B).

Increased sensitivity to cell wall-degrading enzymes is a good indication for compromised cell wall integrity. However, as protoplasting efficiency cannot be quantified in vegetative hyphae, oval conidia were incubated with lyzing enzymes from *Trichoderma harzianum* (Werner et al., 2007). Indeed, oval conidia of Δ*fet3-1*, Δ*fet3-1/2*, Δ*sid1* and Δ*nps6* strains were significantly more sensitive to lysing enzymes than those of the WT and Δ*fet3-2* strains.

While 50% of the oval conidia of the WT and Δ*fet3-2* strains had protoplasted at ca. 4 and 3.8 hours, approx. 1.6 and 2.3 hours were sufficient for protoplasting 50% of the conidia of the Δ*fet3-1* and Δ*fet3-1/2* strains and 1.3 hours for protoplasting 50% of the conidia of Δ*nps6* and Δ*sid1* strains (Fig. 34C).

These results clearly show that Δ*fet3-1*, Δ*fet3-1/2*, Δ*nps6* and Δ*sid1* strains, but not Δ*fet3-2* strain, have significant cell wall defects.
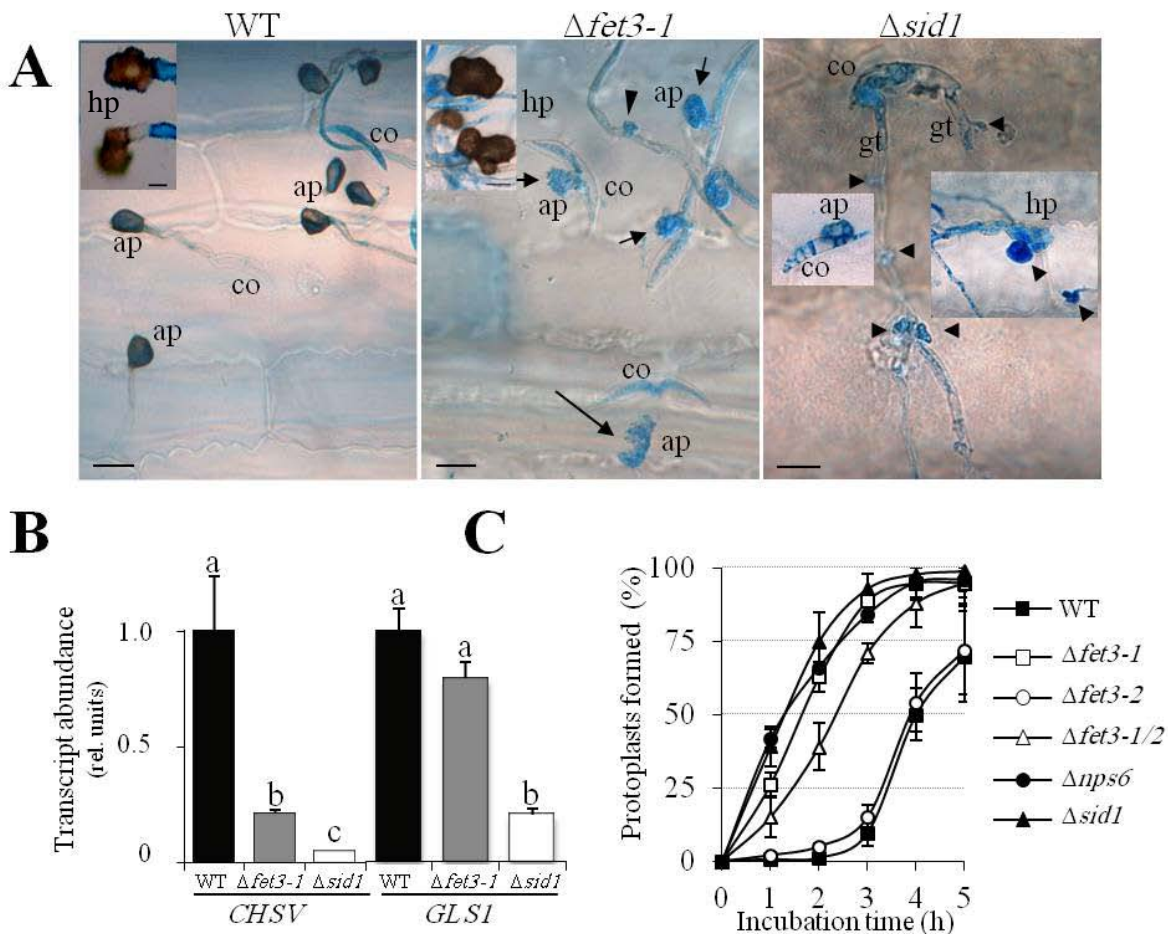
Fig. 34: Iron homeostasis affects the cell-wall integrity and resistance against cell-wall degrading enzymes.
A: Conidia (co) of the WT strain, but not of Δ*fet3-1* and Δ*sid1* strains, are able to differentiate melanized appressoria (ap) on the maize cuticle. Appressoria of Δ*fet3-1* strains have thin cell walls, are non-melanized (short arrows), and often rupture (long arrow). Appressoria of Δ*sid1* strains have thin cell walls and are non-melanized (ap). Different protrusion sites are obvious in germ tubes (gt) and hyphopodia (hp). Bars = 10 µm.
B: Transcript abundance of the chitin synthase gene *CHSV* and the β-1,3-glucan synthase gene *GLS1* in appressoria of WT, Δ*fet3-1*, and Δ*sid1* strains differentiated on polypropylene sheets. Different letters indicate significant difference (P ≤ 0.001). Bars represent + SD. Three replicates were analyzed for the tested strains.
C: Protoplasting efficiency assay show that oval conidia of Δ*sid1* (black triangles)*,* Δ*nps6* (black circles)*,* Δ*fet3-1* (white squares) and Δ*fet3-1/2* (white triangles) strains release protoplasts much faster than those of the Δ*fet3-2* (white circles) and the WT strain (black squares). Three individual replicates were counted of each strain, with 100 conidia each at each time point. Bars represent ± SD.

III.7 eGFP tagging of siderophore transporters (Sit1 and Sit2)

III.7.1. Localization of the Sit1:eGFP and Sit2:eGFP into the plasma membrane of *C. graminicola*.

Searching the *C. graminicola* database (http://www.broadinstitute.org/annotation/genome/ colletotrichum_group/Blast.html) (O'Connell et al., 2012) has revealed four putative siderophore transporters, which belong to the class of major facilitator superfamily transporters (MFS). Thirty-one MFSs exist in *C. graminicola*. Blast hits and phylogenic analysis have shown that other MFS transporters are closely related to different efflux transporters and multidrug resistance proteins (Supplementary Fig. S15A). These putative siderophore transporters have been assigned as Sit1 (GLRG 08506); 586 aas, Sit2 (GLRG 11550); 603 aas, Sit3 (GLRG 07668); 586 aas and Sit4 (GLRG 11169); 614 aas (Supplementary Fig. S15). Programs predicting the sub-cellular localization such as SOSUI software {Hirokawa, 1998 #419} suggested twelve (Sit2, Sit3 and Sit4) and thirteen (Sit1) transmembrane domains (Supplementary Fig. S15B). The putative transporters of *C. graminicola* Sit1 and Sit2 were tagged with eGFP for localization and expression analysis (II.4.10.4, Supplementary Fig. S4). As expected, both Sit1 and Sit2 proteins localized into the plasma membrane (Fig. 35A, arrowhead). Plasma membrane localization of Sit1 and Sit2 transporters was further confirmed by protoplasting vegetative hyphae of *SIT1*:*eGFP* and *SIT2*:*eGFP* strains grown under iron-limiting conditions. The eGFP fluorescence was visible on the plasma membrane of the protoplasts of *C. graminicola* (Fig. 35B, arrowheads). Remarkably, the eGFP fluorescence of the *SIT1*:*eGFP* and *SIT2*:*eGFP* strains were ca. 1500- and 200-fold higher in the presence of 100 µM BPS than in medium containing 100 µM $FeSO_4$, respectively (Fig. 35C). These results clearly show that the Sit1 has higher response to iron limiting condition than Sit2.
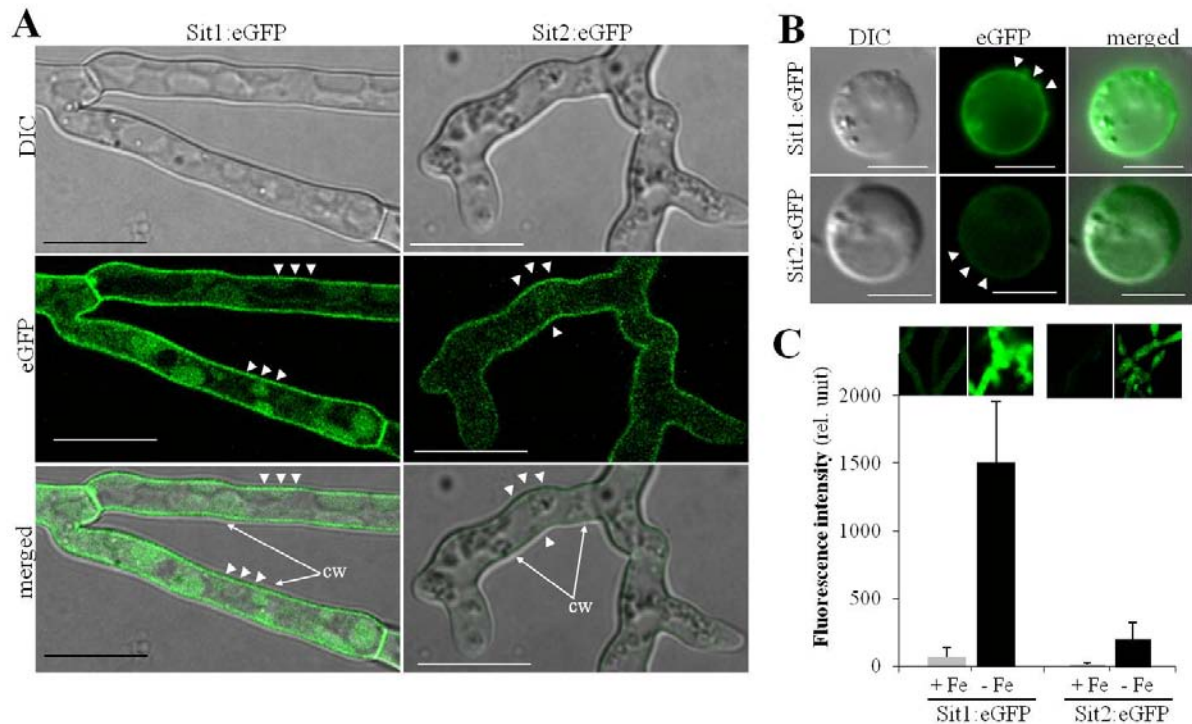
Fig. 35: Localization of the siderophore transporters Sit1 and Sit2 in plasma membranes of
C. graminicola*, and the expression of *SIT1* and *SIT2* genes *in-vitro
A: The eGFP fluorescence was localized in plasma membranes (arrowheads), but not in cell wall (cw).
B: Protoplast generated from a *SIT1:eGFP* and *SIT2:eGFP* strains showed eGFP fluorescence in
plasma membranes, confirming that eGFP fluorescence in A is not cell wall-associated.
C: Control of *SIT1* and *SIT2* expressions by the availability of iron, as measured by the eGFP
fluorescence of the WT strain harboring either the *SIT1:eGFP*, or the *SIT2:eGFP* fusion constructs.
Fluorescence intensity is given in relative units + SD. Bars = 10 µm in A and 5 µm in B.

These data strongly suggest that both Sit1 and Sit2 proteins are functional siderophore
transporters. They localized into the plasma membranes of *C. graminicola* and their
expression is highly linked to the availability of iron. Moreover, quantification of eGFP
fluorescence agrees with the data obtained by qRT-PCR (Fig. 7).

III.7.2. Biotrophy-specific down-regulation of *SIT1*

Taking advantage of transformants harboring the *SIT1:eGFP* construct, infection cell-specific
gene expression studies were performed. The *eGFP* expression of the *SIT1:eGFP* strain was
comparable to the expression of the *SID1:eGFP* strains (Fig. 22C), i.e. the eGFP fluorescence
appeared in conidia, disappeared in appressoria as well as in biotrophic infection vesicles and
primary hyphae (Fig. 36, 24 and 36 HPI). Subsequently, the fluorescence re-appeared clearly
in necrotrophic secondary hyphae after 72 HPI and the eGFP intensity increased remarkably
in the invading necrotrophic mycelia (Fig. 36D, 96 HPI; sh). The eGFP intensity remained

detectable until the fungus completed its life cycle and formed acervuli and novel conidia, in which the fluorescence declined slightly (Fig. 36, 120 HPI). Thus, the expression during plant infection is in full agreement with the expression of *SID1:eGFP* (III.3.1.2.2).
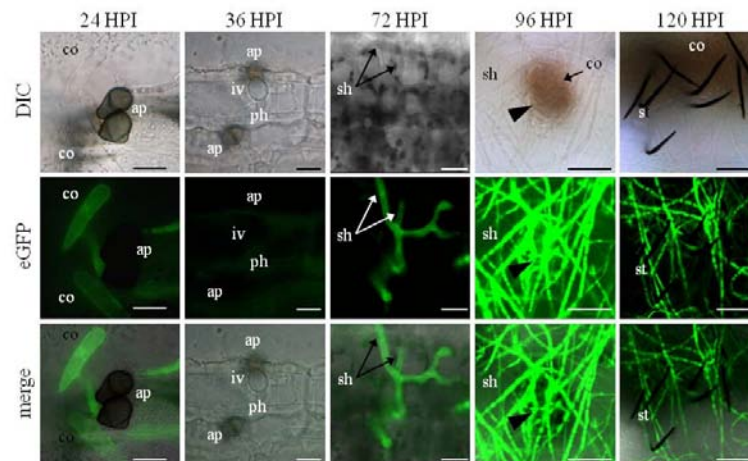
Fig. 36: Infection-structure-specific expression of *SIT1*
Expression of *SIT1* was assessed in *C. graminicola* replacement strain harboring a *SIT1:eGFP* fusion construct. co, conidia; ap, appressoria; iv, infection vesicles; ph, primary hyphae; sh, secondary hyphae; arrowhead, acervulus initials; st, sterigma; bars, 24-72 HPI = 10 µm, 96-120 HPI = 50 µm.

Infection cell-specific gene expression using the *SIT2*:*eGFP* strain was not possible, because the eGFP fluorescence of this strain was relatively low during maize infection.

III.8 Siderophores modulate plant defense

Comparison of high affinity iron acquisition pathways in pathogenic fungi differing in lifestyle suggested that biotrophs such as the maize smut fungus *Ustilago maydis* utilize reductive iron assimilation, whereas necrotrophs such as the Southern Corn Blight fungus, *C. heterostrophus*, or the head blight fungus of wheat, *F. graminearum*, use siderophore mediated iron uptake. Supporting the idea that iron uptake pathways are lifestyle-specifically employed, the hemibiotroph *C. graminicola* used in this study showed a stage specific iron uptake. It used the RIA pathway specifically during biotrophic development (Fig. 15) (Albarouki and Deising, 2013), while it used exclusively the SIA pathway during the necrotrophic development (Figs. 22 and 34).

These data suggested that siderophore secretion during biotrophic development imposes a disadvantage for the pathogen. Bacterial siderophores have been shown to modulate plant defense responses (Expert, 1999; Dellagi et al., 2009; Kieu et al., 2012), and Greenshields et al. (2007) speculated that this may also hold true for fungal siderophores. As forced expression of all genes contributing to the siderophore biosynthetic and secretory pathway in *C. graminicola* is hard to accomplish, one of the siderophores secreted by this fungus, coprogen, was infiltrated into the intercellular space of maize leaves and subsequently the infiltrated sites were inoculated with fungal conidia.

Generation of H_2O_2 is among the fast defense responses initiated after perception of pathogen ingress. Therefore, in order to investigate whether an H_2O_2 response was induced upon infiltration of the intercellular space of maize leaves with coprogen, H_2O_2 was visualized by dimaino benzidine staining (Thordal-Christensen et al., 1997). In order to discriminate between defense responses induced by coprogen and iron scavenging, leaves were also infiltrated with EDTA. To test for responses induced by infiltration stress, infiltration was also performed with sterile distilled water. In non-inoculated leaves, no H_2O_2 formation was detected, irrespective of whether leaves were non-infiltrated, water-, EDTA- or siderophore-infiltrated (Fig. 37A). However, at 48 HPI, i.e. when the fungus had established biotrophic hyphae in the apoplast, a dramatic H_2O_2 response was specifically observed in coprogen-pretreated leaves (Fig. 37A, coprogen, middle panel). Importantly, only the coprogen-infiltrated leaf area exhibiting dark appressoria (Fig. 37A coprogen, middle panel) showed a DAB-positive response, while DAB staining at the margins of the inoculation site was negligible. At larger magnification, cells decorated with fungal infection cells showed strong DAB staining (Fig. 37A, coprogen, lower panel, black asterisk) as well as intensive cell wall

staining (Fig. 37A, coprogen, lower panel, arrowheads). None of the other treatments tested elicited a comparable H_2O_2 response (Fig. 37A, lower panel). These observations suggest that coprogen, but not iron scavenging or mechanical stress exerted by the infiltration process, pre-conditions the leaf to respond to subsequent infection by *C. graminicola*.

Furthermore, also on the transcript level a strong modulation of defense responses by coprogen was identified. Infiltration of leaves with coprogen did not only significantly induce the transcript abundance of genes encoding classical PR proteins, e.g., PR1 and chitinase I (Figs. 36B and C), but also the transcript abundance of four cell wall-localized peroxidase genes was significantly up-regulated most prominently after infection of coprogen-infiltrated leaves by *C. graminicola* (Fig. 37D).

Taken together, these data show that the siderophore coprogen acts as an immuno-modulating compound, and that the hemibiotroph *C. graminicola* down-regulates siderophore biosynthesis and secretion in order to evade plant immune responses such as H_2O_2 formation, activation of PR gene expression and cell wall reinforcement.
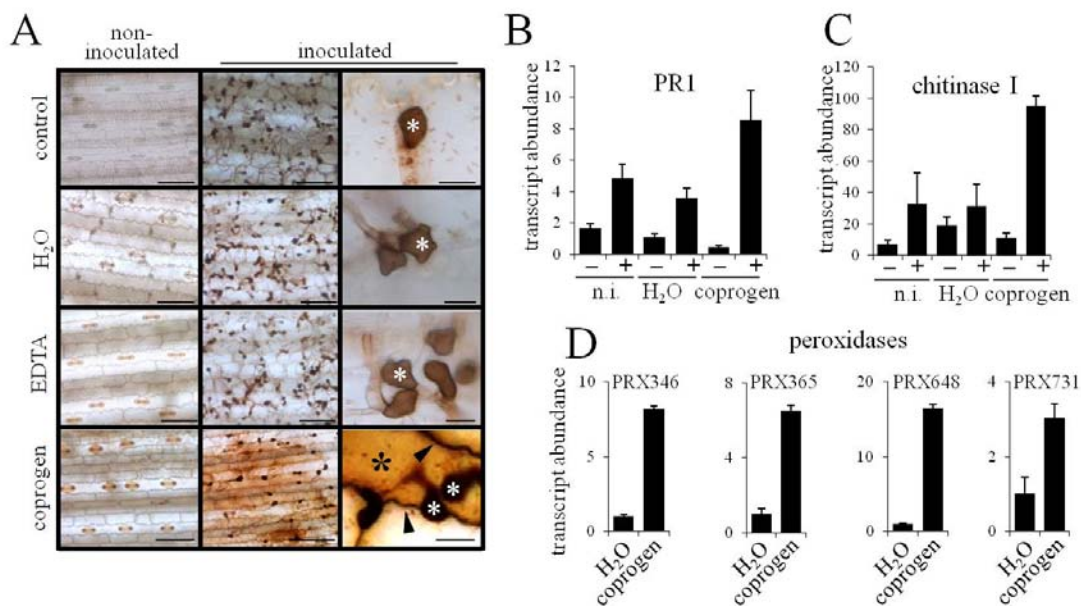
Fig. 37: Coprogen is a defense-priming factor.
A: DAB staining of the inoculation sites with the four different pre-treatments; non-infiltrated control, water-, EDTA-, or coprogen-infiltrated leaves. Bars = 100 µm (upper and middle panel) and 10 µm (lower panel).
B and C: Transcript abundance of the maize defense markers PR1 and chitinase I after 48 HPI of pre-treatments with; (n.i.), non-infiltrated; (H₂O), water infiltrated and coprogen infiltrated; (-), non-inoculated; (+), inoculated with the WT strain.
D: Transcript abundance of the maize peroxidases PRX346, PRX365, PRX648, and PRX731 (for accession number, see VIII.5.3 in the appendix) after 48 HPI of water and coprogen infiltrated leaves and inoculation with the WT strain. There is strong up-regulation of the transcript abundance of peroxidases specifically in the coprogen-infiltrated leaves.

IV. Discussion

IV.1 Regulation of iron uptake in *C. graminicola*

The conclusions which were drawn from the results of this thesis led to the current model for iron homeostasis in *C. graminicola* (Fig. 38). Two major high affinity iron uptake pathways exist in *C. graminicola*. The first one is the RIA pathway, which is an indirect uptake way. It comprises a two-step process; first, plasma membrane-localized iron reductases (Fre) catalyze extracellular reduction of insoluble and/or chelator-complexed ferric (Fe^{3+}) to soluble ferrous (Fe^{2+}) iron, and subsequently Fe^{2+} is bound by a bipartite high affinity iron transport complex, consisting of the multicopper ferroxidase (Fet3), and the iron permease (Ftr1). The resultant Fe^{3+} is then transferred across the plasma membrane, and delivered into the cytoplasm (Eide, 1997; Shi et al., 2003; Haas et al., 2008) (Fig. 38, RIA pathway). *C. graminicola* harbors 14 ferric reductase homolog genes in its genome (O'Connell et al., 2012), the identified *FRE2* gene showed a strong response to iron starvation, and specificity to Fe^{3+}. There are two copies of ferroxidase-and permease-encoding genes in *C. graminicola* (*FET3-1* and *FTR1-1*, *FET3-2* and *FTR1-2*), which are bidirectionally transcribed from one promoter region. GFP localization and qRT-PCR analyses have shown that the Fet3-1 is a plasma membrane-localized ferroxidase and is up-regulated under iron starvation. The iron permease gene *FTR1-1* was also up-regulated under iron limited conditions. The second ferroxidase Fet3-2 was not possible to be localized by GFP tagging, due to its low transcript abundance under the conditions tested. However, low concentrations of transcripts of FET3-2 were detected in Δ*fet3-1* strains (Supplementary Fig. S3).

The yeast complementation assay confirmed that Fet3-2 is a functional membrane transporter and complements the *S. cerevisiae* Δ*fet3fet4* strain when expressed under the constitutive *ADH1* promoter. Therefore, it was assumed that the Fet3-2 could be an ancillary transporter to Fet3-1. The RIA pathway appears to be desirable under slightly acidic conditions (Fig. 38, RIA pathway), as the Δ*fet3-1* and Δ*fet3-1/2* showed significant growth rates reduction at pH 4.5 (Fig. 33A). These data are in agreement with the data obtained by de Silva et al. (1997), which showed that the optimal pH value for the ferroxidase activity is 5.
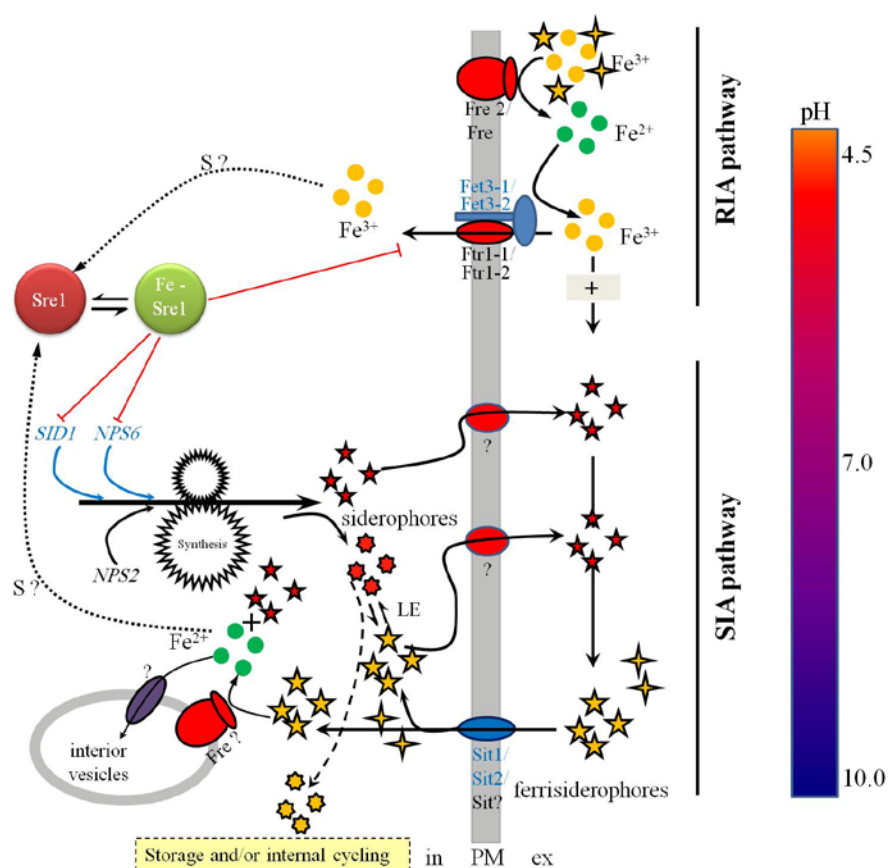
Fig. 38: Postulated model of iron homeostasis in *C. graminicola* including functional components of RIA and SIA uptake pathways. Depending on cytosolic iron, the transcriptional repressor Sre1 is up-regulated (green Fe-Sre1) when iron concentration increased and down-regulated (red Sre1) when its concentration is decreased. Genes and proteins further studied by target mutagenesis or GFP tagging are in blue; all others were studied *in silico* and *in-vitro* by qRT-PCR assay. The pH scale refers to preferred iron uptake pathway used by *C. graminicola* at the referred pH. The genes *SID1, NPS6* and *NPS2* contribute to siderophore biosynthesis (see Fig. 39), Sit1 and Sit2, siderophore transporters; Fet3-1 and Fet3-2, ferroxidases; Ftr1-1 and Ftr1-2, iron permeases; Fre2/Fre, ferric reductase; Iron sensing (S) is indicated with dotted arrow; PM, plasma membrane; in, intracellular; ex, extracellular; LE, ligand exchange; ⬤, ferric iron; ⬤, ferrous iron; ★, coprogen and its derivatives (see text); ★, ferricoprogen; ✦, desferricrocin; ✦, ferricrocin; ✛, xenosiderophore.

The second pathway is the SIA, including synthesis, secretion and uptake of siderophores. Two genes of the siderophore biosynthetic pathway of *C. graminicola*, i.e. *SID1* and *NPS6*, were characterized. There are two types of siderophores produced by *C. graminicola*; four extracellular siderophores (coprogen, coprogen B, N^α-methylcoprogen B and dimerumic acids) and one intracellular siderophore (ferricrocin). The extracellular siderophores facilitate capturing and solubilizing ferric iron from the surrounding environment. Two novel siderophores, coprogen and dimerumic acid, were found in this study. The putative model for siderophore biosynthetic pathway of *C. graminicola* is depicted in Figure 39. The gene *SID1* encodes L-ornithine-N^5-monooxygenase and catalyzes the hydroxylation of L-ornithine to N^5-hydoxylornithine, representing the first step in the hydroxamate siderophore biosynthetic

pathway. Deletion of this gene leads to the inability to produce siderophores (Fig. 30). The resulting N^5-hydroxyornithine is subsequently acetylated and the pathway splits at this point. The intracellular siderophore ferricrocin is formed by combining N^5-hydroxyornithines with glycine and serine, a reaction catalyzed by a non ribosomal peptide synthetase encoded by *NPS2*. An attempt to delete this gene has failed, as all transformants obtained showed ectopic integration of the deletion construct (Supplementary Fig. S16). Transcript abundance data have shown that *NPS2* gene is up-regulated under both iron limiting conditions and in the presence of high concentrations of iron (Fig. 7). This strongly suggests that the intracellular siderophore ferricrocin plays an indispensable role in coping with high iron concentrations. The extracellular siderophores are formed by building a peptide backbone between N^5-hydroxyornithine molecules. This reaction is catalyzed by a nonribosomal peptide synthetase encoded by the *NPS6* gene, leading to coprogen B or dimerumic acid. Further modifications like acetylation or methylation required to form coprogen and N^α-methylcoprogen B are introduced. Deletion of *NPS6* of *C. graminicola* led to the inability of synthesizing extracellular siderophores, whereas the intracellular siderophore ferricrocin was produced by Δ*nps6* strains (Fig. 30). Notably, the Δ*nps6* strains showed variable phenotypes and these variabilities were not observed in the Δ*sid1* strains. This variability may be due to the accumulation of the siderophore precursor N^5-acyl-N^5hydroxyornithine (Fig. 39), which has a toxic effect. This variability was also observed in the Δ*nps2nps6* strains of the *C. heterostrophus* and some other ascomycetes (Haas et al., 2008, and reference therein).
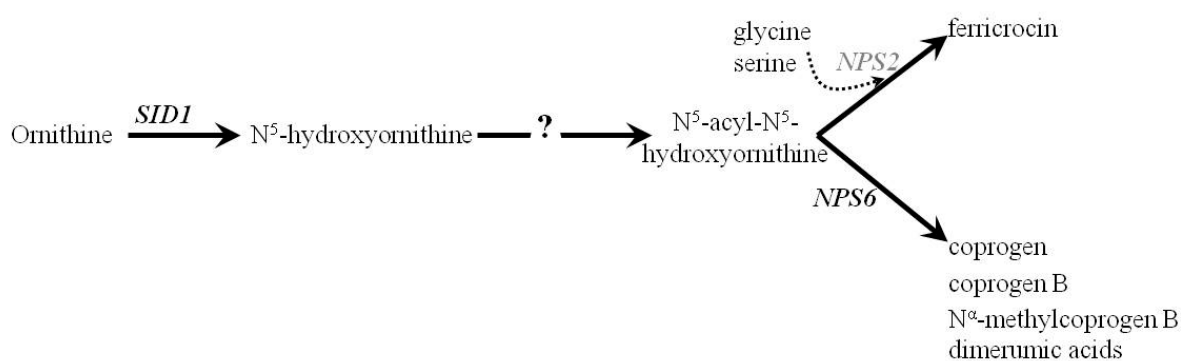
Fig. 39: Model of siderophore biosynthetic pathway in *C. graminicola*.
The *SID1* gene encodes L-ornithine-N^5-monooxygenase; *NPS2* and *NPS6* encode nonribosomal peptide synthetases (for description see text).

Secretion of siderophores may be facilitated by active transport, or via passive diffusion (Miethke and Marahiel, 2007, and reference therein). So far, no specific siderophore transporters recruited in secretion of siderophores in filamentous fungi have been characterized.

Next to secretion of extracellular siderophores, different scenarios may happen:

i)   Ferrisiderophores are taken up by siderophore transporters (Sit) (Fig. 38, SIA pathway); two out of four putative siderophore transporters (Sit1 and Sit2) have been characterized by eGFP tagging in which they show localization to the plasma membrane and a clear response to the availability of iron (Fig. 35). In the model eukaryotic yeast *S. cerevisiae*, different siderophore transporters (Arn1-Arn4) showed specificity for particular siderophores like ferrichrome, ferrichrome A, and triacetylfusarinine C (Yun et al., 2000). Therefore, further analysis of substrate-specificity of Sit1 and Sit2 transporters would be of great interest.

ii) A direct ligand exchange between extracellular and intracellular siderophores is also possible (Fig. 38, LE). The released ligand (extracellular desferrisiderophores) is reused to capture another iron molecule (Matzanke, 1994; Howard, 1999), and references therein). Thus, intracellular ferrisiderophores are used then for storage and/or internal cycling of iron (Haas et al., 2008; Wallner et al., 2009), and references therein).

iii) Another possibility is that siderophore-bound Fe^{3+} undergoes reduction to Fe^{2+}, which is catalyzed by free extracellular or membrane-localized ferric-chelate reductases (Fig. 38, Fre). This gives a common advantage for the organism to utilize xenosiderophores, which are not produced by it. It was found that *C. graminicola* is also able to utilize xenosiderophores originated from different organisms (Fig. 19). If iron is not released extracellularly from the siderophore, it has to be removed in the cytosol. This can be either achieved by intracellular reductases (Fre), or in a few cases by siderophore hydrolases (Miethke and Marahiel, 2007, and reference therein).

The SIA pathway appears to be more desirable under neutral and alkaline conditions, where Δ*sid1* strain had sever growth rate reduction (Fig. 33). These results are in full agreement with the results obtained in *A. nidulans* (Eisendle et al., 2004)*,* where siderophore synthesis and uptake are controlled by the pH regulatory system PacC. It was found that siderophore production of the WT strain increased approx. 35-fold by increasing the pH value in the culture media from 4.5 to 7.0. Moreover, the transcript abundance of genes involved in siderophore synthesis (*sidA*) and uptake (*mirA* and *mirB*) was higher in the alkaline-mimicking strain *pacC^c200* than in the WT strain. In comparison, it was lower in the acidity-mimicking strain *pacC^{+/c}20205* than in the WT strain (Eisendle et al., 2004). Thus this gives a clear clue of the close relation of the used iron uptake pathway and the pH of the surrounding environment. A *pacC* orthologs exist in *C. graminicola*, and it will be of interest to analyze its role on both, the RIA and the SIA pathway at different pH values.

When cytosolic iron concentration increases, transcript abundance of the GATA type transcription factor *SRE1* also increases and suppresses the expression of RIA and SIA related genes (Fig. 38). Previous studies had evidenced that in various fungi such as *A. nidulans*, *Pichia pastoris, U. maydis* and others, SIA and RIA genes were negatively regulated by a transcriptional repressor which binds to a 5´-(A/T)GATAA-3´ sequence (Haas et al., 1999; Miele et al., 2007; Chao et al., 2008; Hwang et al., 2008). Indeed, all the studied genes have GATA binding sites in their 5´-noncoding region, as in Table 4:

Table 4: Putative GATA binding sites exist in the immediate vicinity of the start codon of iron uptake genes.

Gene	Putative GATA binding sites
FET3-1	-53, -86, -229, -258, -359 and -831
FET3-2	-371 and -453
FTR1-1	-127 and -141
FTR1-2	-553 and -610
FRE2	-207, -289, -306, -318; -326, -544 and -575
SID1	-10 and -98
NPS6	-279, -360, -833 and 1014
NPS2	-214, -426 and -675
SIT1	-515 and -545
SIT2	-119 and -417

Quantitative RT-PCR analyses have confirmed this assumption, where the transcript abundance of the *SRE1* gene was up-regulated when iron was supplied regardless of its redox form (Fig.7).

IV.2 Iron acquisition determines virulence/pathogenicity and defense

Iron is an essential element for virtually all organisms, including fungi. For plant pathogenic fungi, iron likely represents a limiting factor not only on the leaf surface, but also inside of the host tissue. This latter aspect may be of particular importance in biotrophic hyphae and in haustoria, which are located in the apoplast and are encased by the plant plasma membrane. Inside of the plant cells, iron is tightly bound by proteins such as ferritin, and sequestration of iron by the plant may reduce the availability of this redox element and have a prominent role in weakening virulence of fungal pathogens that breach the plasma membrane and invade the host cell. Indeed, in *Arabidopsis thaliana* reduced iron availability correlated with reduced disease severity of the necrotrophic fungus *Botrytis cineria* (Kieu et al., 2012). In line with these observations, transgenic tobacco plants over-expressing the alfalfa *FER* gene, encoding an iron-binding ferritin, showed increased resistance to the necrotrophic fungal pathogens *Alternaria alternata* and *B. cinerea* (Deák et al., 1999). Not only in plants, but also in animals an iron withholding defense system exists. Here, processes activated in response to microbial attack include a rapid reduction of iron concentration in plasma, increased synthesis of macrophage ferritin, and release of apolactoferrin from neutrophil granules, leading to binding of iron in septic sites (Weinberg, 2009). Interestingly, a screen of mutants of the opportunistic dimorphic fungus *Candida albicans* deficient in components of three iron uptake systems showed that RIA is involved in acquisition of iron from ferritin by invasive hyphae (Almeida et al., 2008). Intriguingly, transgenic wheat (*Triticum aestivum*) plants expressing a bovine lactoferrin cDNA showed that increased contents of iron-binding protein significantly increased resistance against the head blight fungus *F. graminearum* (Han et al., 2012).

However, iron also plays an active role in plant defense. In wheat iron is a central mediator linking three defense responses, i.e., localized cell wall appositions known as papillae, generation of antimicrobial ROS, and ROS-mediated activation of defense genes expression, collectively leading to increased resistance to the powdery mildew fungus *Blumeria graminis*. After attack of wheat leaves by *B. graminis*, targeted iron re-distribution occurs, with reactive Fe^{3+}, but not Fe^{2+}, accumulating at cell wall appositions to mediate the oxidative burst (Liu et al., 2007). Thus, iron is not only required for growth and development of plants, but also for coordinating defense responses.

Therefore, utilization of high affinity iron uptake systems such as RIA and/or SIA pathways by fungal pathogens likely serves two functions, i) supply of iron to be used for fungal development, and ii) weakening of the redox-based pathogen defense systems of the host.

Studying RIA and SIA pathways in the hemibiotroph *C. graminicola* have revealed major discoveries, i) a central element of the RIA pathway, the ferroxidase-encoding gene *FET3-1* is expressed infection-structure-specifically during *on-planta* and biotrophic development, whereas the *SID1* and *SIT1* genes that are main components of the SIA pathway are strongly expressed during the destructive necrotrophic development; ii) a link between high affinity iron uptake pathways, transcriptional regulation of the class V chitin synthase gene *CHSV* and ß-1-3-glucan synthase gene *GLS1*, and cell wall integrity has been shown; iii) siderophores modulate plant defense in maize after *C. graminicola* infection; iv) asexual sporulation is highly dependent on production and storage of siderophores; v) *C. graminicola* uses mainly SIA pathway for iron uptake *in-vitro*.

IV.2.1 *C. graminicola* complementary uses RIA and SIA pathways during maize infection

In this work, it was shown for the first time that the hemibiotroph *C. graminicola* activates the high affinity RIA system at the early stage of fungal infection, i.e., during pre-penetration and biotrophic development, and the SIA system during late biotrophic and the shift to necrotrophic stage (Figs. 16, 23 and 35). Infection assays clearly indicated that the central component of RIA, the ferroxidase gene *FET3-1*, is required for full virulence. This role was fully abolished when wounded leaves were inoculated with the ferroxidase mutant Δ*fet3-1* (Fig. 13). In wound-inoculated leaves, *C. graminicola* does not differentiate biotrophic hyphae and directly forms necrotrophic secondary hyphae (Horbach et al., 2009). This is strongly suggesting that the high affinity RIA pathway is primarily required during biotrophic stages of pathogenesis. While these data are in agreement with the role of RIA in virulence of the biotroph *U. maydis* (Eichhorn et al., 2006), SIA rather than RIA, appears to be required for virulence in necrotrophs such as the maize pathogen *C. heterostrophus*, the rice pathogen *C. miyabeanus*, the cereal pathogen *F. graminearum*, and the Arabidopsis pathogen *Alternaria brassicicola* (Oide et al., 2006; Greenshields et al., 2007; Haas et al., 2008; Hwang et al., 2008). In *F. graminearum* the siderophore biosynthesis gene *SID1* encoding L-ornithine-N^5-monooxygenase, an early siderophore-synthesizing enzyme, but not the ferroxidase gene *FET3*, is required for full virulence (Greenshields et al., 2007). In line with the results obtained in necrotrophs, the SIA pathway appears to be more required than the

RIA pathway during the necrotrophic stage of the *C. graminicola* (Fig. 28, Δ*sid1*, wounded leaves).

So far, it is unclear why RIA is important primarily in biotrophic and hemibiotrophic pathogens, but not in necrotrophs; on the other hand, the SIA is important in necrotrophic, but not in biotrophic pathogens. Different hypotheses could be given here:

i)   The RIA pathway was more essential at acidic condition than the SIA pathway (Fig. 33), and as the biotrophic hyphae are encased by the plant plasma membrane, where the proton (H^+) potential in the bifacial matrix is high (acidic conditions) (Grignon and Sentenac, 1991; Hubert, 1998). Therefore, the RIA pathway is more beneficial than the SIA pathway during biotrophic development.

ii)   Growth assays under iron-limited medium showed that the SIA pathway is the major iron uptake pathway for *C. graminicola*. Elevated growth during the necrotrophic phase likely needs an increased amount of iron. There is evidence suggesting that these increased amounts cannot be provided by RIA.

iii) Obviously, secretion of siderophore during penetration and biotrophic development would trigger the defense system of the host plant (Fig. 37). Therefore, the fungus depends on the RIA pathway during biotrophic stage to acquire its need for iron.

Interestingly, BLAST searches using individual siderophore synthesizing enzymes, i.e. the Sid1 protein, or the adenylation domain of the Nps6 protein of *C. graminicola* as a query set against the genome database of the obligate biotrophic *Blumeria graminis* f. sp. *hordei* has identified no hits for siderophore synthesizing enzymes in this fungus. This further suggests that the SIA pathway is dispensable in biotrophic pathogens.

So far, the regulatory mechanism of iron uptake during fungal infection is poorly understood. In *A. nidulans*, iron homeostasis is controlled by a tight interplay of two major regulatory systems, the GATA transcription factor SreA and HapX, a part of the CCAAT-binding core complex (Hortschansky et al., 2007). Additionally, different SIA components of *A. nidulans* is under the control of the pH regulatory system mediated by the wide-domain zinc finger transcription factor PacC (Eisendle et al., 2004). In *C. graminicola*, the *SREA* and *HAPX* orthologs, *SRE1* and *HAPX* were slightly down-regulated during both biotrophic and necrotrophic development (O'Connell et al., 2012) (Fig. 40). That may be explained by the need to induce both high affinity iron uptake pathways during fungal infection, but the differential expression of both RIA and SIA pathways is still poorly understood. A feedback signal from the host plant may play here role of regulation. Noticeably, the expression of the

PACC ortholog in *C. graminicola* increased gradually but significantly during biotrophic- and the subsequent necrotrophic-phase (O'Connell et al., 2012). That may provide additional evidence for its regulatory role in inducing the SIA pathway and suppressing the RIA pathway, starting from the assumption that RIA is an acid-induced and SIA is an alkaline-induced pathway. Regulatory effects of *SRE1*, *HAPX* and *PACC* on both RIA and SIA pathways should be further investigated in *C. graminicola*, and deletion strains of the these regulatory factor should be generated and tested in pathogenicity assays.

In summary, Figure 40 illustrates the timing of iron uptake pathways and the postulated regulation during *C. graminicola* infection process (Fig. 40).
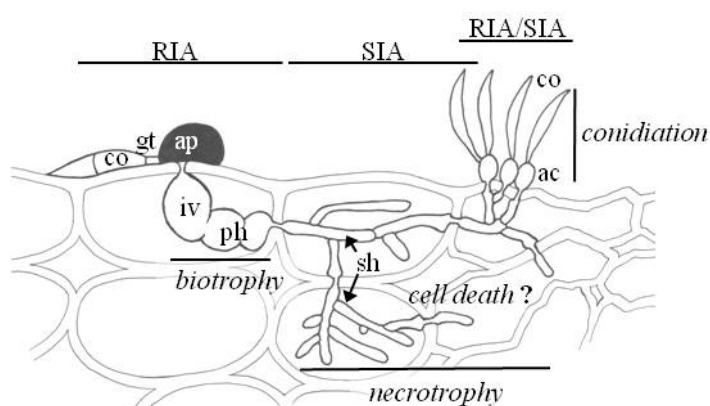
Fig. 40: Model of iron uptake and regulation during infection process.
The RIA pathway is activated during the early stage and biotrophic development, whereas SIA is active during necrotrophic development. Dashed arrows represent the activated pathway; up- and down-ward arrows represented up- and down-regulated genes.

IV.2.2 Cell-wall-biogenesis genes are transcriptionally regulated in both RIA and SIA defective strains

Surprisingly, our study revealed a link between high affinity iron uptake, transcriptional regulation of *CHSV*, and cell wall integrity in *C. graminicola*. Severe cell wall defects occurred in conidia, germination tubes, appressoria and hyphopodia of Δ*fet3-1*, Δ*sid1* and Δ*nps6* strains. The appressorial cell walls of Δ*fet3-1* strains disintegrated on the leaf surface and displayed a phenocopy of the Δ*chsV* mutants deficient in a class V chitin synthase (Werner et al., 2007). The Δ*sid1* and Δ*nps6* strains showed increased rates of abnormality of *on-plant* developed structures. Both Δ*chsV* and Δ*fet3-1* deletion strains formed appressoria, but the appressorial cell walls of the mutants were very thin and non-melanized. Interestingly, in *in-vitro* differentiated appressoria of Δ*fet3-1* and Δ*sid1* strains the transcript abundance of *CHSV*, and in Δ*sid1* strains the transcript concentration of *GLS1* decreased dramatically (Fig.

34B). Although a direct link between both RIA- or SIA-mediated iron uptake and cell wall defects has not been demonstrated so far, it is important to note that expression of the *RBT5* gene of the human pathogen *C. albicans*, encoding a glycosylphosphatidylinositol (GPI)-anchored protein, is required for cell wall integrity. This gene is regulated by the iron-responsive GATA-like factor Sfu1p (Mishra et al., 2011), and also in *C. graminicola* cell wall integrity genes such as *CHSV*, and others, might be under the control of an iron-responsive GATA-like factor. Indeed, GATA-binding sites are present at two positions (-163 and -434) of the 5'-noncoding region of *CHSV* and at two positions (-17 and -282) of the 5'-noncoding region of *GLS1*. Thus, control of cell wall biogenesis genes of *C. graminicola* by homologs of the GATA factor SreA, possibly in tight interplay with repressors like HapX as in *A. nidulans* (Hortschansky et al., 2007; Schrettl et al., 2008) might be required for cell wall integrity of *C. graminicola*. As a matter of fact, one (-231) and two (-490 and -997) HapX-like binding sites exist in the 5'-noncoding regions of the *CHSV* and the *GLS1* genes, supporting this assumption. One may further speculate that under iron limitation the cell wall defects in *C. graminicola* may be conferred by erroneous regulation of cell wall biogenesis genes. Recent studies have demonstrated that in *A. fumigatus* the MAP kinase MpkA controls cell wall integrity, iron adaptation and oxidative stress response (Valiante and Brakhage, 2009; Jain et al., 2011). Accordingly, in *C. graminicola* strict iron limitation in the studied strains (Δ*fet3-1*, Δ*fet31/2*, Δ*sid1* and Δ*nps6* strains) on the plant surface may lead to activation of MpkA, which, in turn, might activate a repressor of genes involved in cell wall biogenesis, eventually causing lysis of appressoria and infectious structures differentiated on the plant cuticle (Fig 35A, Δ*fet3-1* and Δ*sid1*) (Jain et al., 2011).

IV.2.3 Siderophores modulate plant defense response during *Colletotrichum*-maize interaction

In *C. graminicola*, two high affinity iron uptake systems are sequentially employed, with RIA used during biotrophy and SIA during necrotrophy. In *U. maydis*, in spite of the fact that this fungus is capable of producing siderophores, exclusively the reductive iron assimilation pathway is used during the infection process and required for full virulence (Mei et al., 1993; Eichhorn et al., 2006). Accordingly, in *C. graminicola* reductive iron assimilation is active during biotrophic development, and siderophore biosynthesis is rigorously down-regulated. The fact that siderophore biosynthesis genes are activated when the fungus shifts from biotrophic to necrotrophic development shows that *C. graminicola* is principally able to use

this iron uptake pathway during pathogenic development. Renunciation of utilization of the siderophores pathway in the biotroph *U. maydis* and during biotrophic development of the hemibiotroph *C. graminicola* suggests that secretion of siderophores into the narrow interfacial matrix surrounding biotrophic infection structures may lead to high concentrations of these molecules imposing a disadvantage for the pathogen. Bacterial siderophores have recently been shown to immuno-modulate plants. In these experiments, infiltration of *Arabidopsis thaliana* with the bacterial siderophores chrysobactin and desferrioxamine has strongly increased the transcript abundance of the ferritin gene *AtFer1*, part of an iron-withholding plant defense system against bacterial infection (Dellagi et al., 2005; Dellagi et al., 2009). Following this line of evidence Greenshields et al. (2007) suggested that fungal siderophores might act as pathogen associated molecular patterns (PAMPs). This idea is supported by the fact that evidence that siderophores are required for virulence comes only from work with necrotrophs, which interfere with defense responses by killing the plant (Horbach et al., 2011).

We tested this assumption by infiltration experiments (Fig. 37). Infiltration of siderophores into the intercellular space of maize leaves did not elicit defense responses such as rapid formation of H_2O_2, transcriptional activation of genes encoding PR proteins, or cell wall-localized peroxidases. Therefore, siderophores can clearly not be regarded as PAMPs. However, when *C. graminicola* developed biotrophic hyphae in leaves previously infiltrated with siderophores, dramatic H_2O_2 responses as well as transcriptional activation of genes encoding PR1, chitinase I and four peroxidases was detected. As this was not the case when *C. graminicola* invaded leaves infiltrated with the iron-scavenging agent EDTA, we conclude that the presence of the siderophore coprogen, and not iron scavenging in the apoplast was responsible for activation of defense responses by the fungus. Thus, coprogen acts as an immuno-modulator and, in combination with a plant defense-eliciting factor produced by *C. graminicola*, leads to dramatic defense responses. Similarly, lipopolysaccharides (LPSs) of gram-negative bacteria have multiple roles in microbe-plant interactions; they protect bacteria from plant-derived antimicrobial compounds by reducing their outer membrane permeability. In addition, LPSs can trigger or prime the plant defense system when they are applied prior the bacterial inoculation (Newman et al., 2007). Treatment of pepper leaves with LPSs prior inoculation with compatible or incompatible strains of *Xanthomans sp*. led to increased synthesis of different antimicrobial substances like hydroxycinnamoyl-tyramine conjugates, feruloyl-tyramine, coumaroyl-tyramine and ß1-3-glucanase, whereas LPSs alone did not induce their synthesis (Newman et al., 2002).

IV.2.4 The SIA system of *C. graminicola* is the major iron-uptake pathway during vegetative growth

The SIA deletion mutants Δ*sid1* and Δ*nps6* showed severe growth retardation under iron limited condition, while the RIA deletion mutants Δ*fet3-1*, Δ*fet3-2* and Δ*fet3-1/2* showed no significant differences of growth rates to that of the WT strain under those conditions (Fig. 31). These results indicate that the main iron uptake pathway of *C. graminicola* under the conditions studied is the SIA pathway, which is in full agreement with the results obtained in *A. fumigatus*, *C. heterostrophus* and *F. graminicola* (Schrettl et al., 2004; Oide et al., 2006; Greenshields et al., 2007).

However, both SIA and RIA (with the exception of Δ*fet3-2*) mutants showed hypersensitivity to ROS generators, which clearly indicates that insufficient iron concentration exist in these strains to cope with ROS stress (Fig. 32).

IV.2.5 Siderophore biosynthesis is indispensable for conidiation

The Δ*sid1* strains were unable to produce conidia under standard conditions, which reveals the extreme shortage of iron supply and storage facilitated by extracellular and intracellular siderophores. It is well documented so far, that intracellular siderophores account for approximately 47-74% of the iron pool in conidia of *A. nidulans, A. fumigatus, Aspergillus ochraceus*, and *N. crassa* (Matzanke, 1994; Eisendle et al., 2006; Schrettl et al., 2007). Loss of the intracellular siderophore production leads to reduction of conidiation of *A. nidulans* and *A. fumigatus* (Eisendle et al., 2006; Schrettl et al., 2007), but not in *M. oryzae* (Hof et al., 2008). Sexual sporulation was also impaired in ferricrocin deficient strains of *C. heterostrophus* and *F. graminearum* (Oide et al., 2007). The Δ*nps6* strains were unable to produce extracellular siderophores, but produced the intracellular siderophore ferricrocin (Fig. 30). The Δ*nps6* strains showed retardation in growth but were able to produce conidia on OMA plates (Fig. 26), which clearly indicates that the characteristic phenotype of Δ*sid1* strain (sporulation defect) is due to the lack of the intracellular siderophore ferricrocin.

Noticeably, the addition of siderophores to Δ*sid1* strain restored its ability to produce conidia. That may be due to two reasons, i) the existence of xenosiderophores in the growth media mediate a continuous supply of soluble iron essential for growth and conidiation, and ii) the assimilated siderophores can be hydrolyzed and their break-down products will be used as a building-blocks for producing ferricrocin by the Nps2 protein (Fig. 39). The latter idea was

supported in the triple mutant *arg5-ota-aga* of *N. crassa*. This mutant is neither able to produce extracellular (coprogen) nor intracellular (ferricrocin) siderophores (Matzanke, 1994). The *arg5-ota-aga* mutant was provided with ^{57}Fe-coprogen and the internal iron pool of mycelium was measured using Mössbauer spectroscopy (Matzanke, 1994, and reference therein). After 27 and 65 h of ^{57}Fe-coprogen uptake, 12% and 26% of the intracellular iron pool of *arg5-ota-aga* strain were ferricrocin, indicating that this strain was able to build ferricrocin from the degradation products of coprogen.

V. Perspective

Iron uptake and the regulatory network have recently gained increasing interest in the field of plant pathology, as iron-responsive genes have been shown to represent virulence factors (Dellagi et al., 2005; Eichhorn et al., 2006; Oide et al., 2006; Greenshields, 2007; Liu et al., 2007).

The field of siderophore biosynthesis and uptake, for instance, is gaining an increased interest for different reasons:

i) The siderophore-biosynthetic enzymes appear to be promising candidates as antimicrobial targets, since these enzymes do not exist in plants and mammals (Haas et al., 2008, and reference therein). The first antibiotic targeting siderophore biosynthesis of pathogenic bacteria has been reported recently by Ferreras et al (2005). This antibiotic inhibits the domain salicylation enzymes in a non-competitive fashion. Salycilation of an aroyl carrier protein domain is an indispensable step for the biosynthesis of salicylic acid-derived siderophores produced by *Mycobacterium tuberculosis* and *Yersinia pestis* (Ferreras et al., 2005). The Sid1 or the Nps6 protein can be a good candidate for developing a novel antifungal specific for filamentous ascomycetes.

ii) Siderophore-producing bacteria that were isolated from the plant rhizosphere have putative biocontrol capacity against fungal pathogens like *Alternaria* sp., *Fusarium oxysporum*, *Pyricularia oryzae*, *Sclerotium* sp., and *Colletotrichum gloeosporioides* (Chaiharn et al., 2009; de Los Santos-Villalobos et al., 2012). Bacteria isolated from the rhizosphere of rice in Thailand showed a strong but specific antagonistic effect against fungal pathogens. In particular, *Streptomyces* sp. and *Pseudomonas* sp. showed a significant strong antagonistic effect against *Alternaria* sp., while *Ochrobacterium anthropi* showed a good antagonistic effect against *F. oxysporum*. *Bacillus firmus* inhibited *P. oryzae* and *Kocuria rhizophila* inhibited *Sclerotium* sp. (Chaiharn et al., 2009). *Burkholderia cepacia*, isolated from the rhizosphere of mango caused more than 90% growth inhibition of *C. gloeosporioides,* the causal agent of anthracnose of mango. The inhibition was exclusively due to the production of hydroxamate-type siderophores (de Los Santos-Villalobos et al., 2012).

On the other hand, microbial siderophores enhance iron uptake by plants that are able to recognize bacterial siderophores. Bacteria belonging to the genera *Bacillus* and *Pseudomonas* that colonize plant roots and promote plant growth are referred to as plant growth-promoting rhizobacteria. These bacteria produce high amount of siderophores,

which have antagonistic effect against soil-borne pathogens and probably enhance the plant growth by supplying soluble iron (Beneduzi et al., 2012, and reference therein). Powell et al., (1980) suggested that hydroxamate siderophores present in soil at concentrations between 10^{-7} and 10^{-8} M are fully sufficient to improve plant growth. Therefore, these rhizobacteria can be used as putative bio-fertilizers with biocontrol potencies.

iii) The increased antimicrobial drug resistance forms a global challenge in both medical and agricultural fields. That forced pharmaceutical and agricultural industries to search for new effective antimicrobial drug. In medical field, siderophores have been efficiently used for specific delivery of those antimicrobial molecules into bacterial pathogens (the Trojan horse strategy). Here, the antimicrobial molecule is linked to a siderophore (sideromycin). The siderophore is then recognized by bacterial receptors and taken up by an active transport, together with the antimicrobial molecule attached. This increases the potency of antimicrobial uptake up to 100-fold in comparison to passive diffusion (Braun, 1999). The first natural sideromycin has been characterized was the antibiotic albomycin produced by *Actinomyces subtropicus* (Gause, 1955). This sideromycin is composed of ferrichrome and a nucleoside-analogous thioribosyl pyrimidine moiety linked by a serine spacer (Benz et al., 1982). Many other natural sideromycins exist, e.g. ferrimycins, produced by *Streptomyces griseoflavus* and salmycin, produced by *Streptomyces violaceus* (Möllmann et al., 2009, and reference therein). The first attempt to synthesize artificial sideromycins were done by Zähner et al. (1977). In the last three decades, increased siderophore-antimicrobial conjugates have been developed, in which different antimicrobial moieties were introduced such as *ß*-lactams, cephalosporins, carbacephalosporins, carbapenems or monobactams with one or two catecholates, or mixed catecholate and hydroxamate moieties (Möllmann et al., 2009, and reference therein).

So far, there are no reports of using siderophore as an antifungal carrier, and more investigations directed to designing siderophore-derived antifungal are therefore needed.

VI. Summary

Two main high affinity iron uptake pathways were analyzed in *C. graminicola*, i) the reductive iron assimilation (RIA), and ii) the siderophore-mediated iron acquisition (SIA). Therefore, the finding of this work can be split into two chapters:

i) **The RIA pathway**: An essential component of the RIA pathway in *C. graminicola* was investigated in this study, the ferroxidase. Two copies of the ferroxidase gene were identified, *FET3-1* and *FET3-2*. Complementation of growth defects of the ferroxidase-deficient *S. cerevisiae* strain Δ*fet3fet4* showed that both Fet3-1 and Fet3-2 represent functional ferroxidases (Fig. 11). Expression of eGFP fusions in *S. cerevisiae* and *C. graminicola* indicated that both ferroxidase proteins localize into the plasma membrane. Δ*fet3-1* and Δ*fet3-2* single as well as Δ*fet3-1/2* double deletion strains were generated by targeted mutagenesis (Fig. 12). Transcript abundance of *FET3-1* increased dramatically under iron-limiting conditions, but those of *FET3-2* were hardly detectable (Fig. 7). Under iron-sufficient or deficient conditions, vegetative growth rates of these strains did not significantly differ from that of the WT, but Δ*fet3-1* and Δ*fet3-1/2* strains showed increased sensitivity to reactive oxygen species. Furthermore, under iron-limiting conditions appressoria of Δ*fet3-1* and Δ*fet3-1/2* strains showed significantly reduced transcript abundance of a class V chitin synthase and exhibited severe cell wall defects. Infection assays on intact and wounded maize leaves, quantitative data of infection structure differentiation, and infection stage-specific expression of eGFP under control of the *FET3-1* promoter strongly suggest that reductive iron assimilation is required for appressorial penetration, biotrophic development and full virulence.

ii) **The SIA pathway:** The SIA pathway comprises syntheses, secretion and uptake (Fig. 2). *C. graminicola* synthesize three secreted siderophores, coprogen, coprogen B and N$^{\alpha}$-methylcoprogen B, and one intracellular siderophore, ferricrocin. The identified dimerumic acid can represent a standalone siderophore {Bertrand, 2009 #507}, or it represents a precursor or degradation product. Noticeably, dimerumic acid showed an antioxidant potent in the mold *Monascus anka* by donating one electron from the hydroxamic acid group of the dimerumic acid molecule toward the oxidant {Aniya, 2000 #509; Taira, 2002 #354}. Transcript abundance of *SID1*, *NPS2*, *NPS6* and *SIT1* genes belong to the SIA pathway increased dramatically under iron-limited conditions (Fig. 7). Notably, the *NPS2*-transcript

was also up-regulated under increased iron supply, confirming the putative role of intracellular siderophore for iron detoxification. The key siderophore biosynthesis gene, *SID1* encoding L-ornithine-N^5-monooxygenase, and the nonribosomal peptide synthetase gene *NPS6* required for assembling the extracellular siderophores were functionally analyzed by targeted mutageneses (Figs. 18 and 25). *eGFP* fusions with *SID1* and the main siderophore transporter gene, *SIT1*, suggested that siderophore biosynthesis and uptake is rigorously down-regulated specifically during biotrophic development. Analysis of Δ*sid1* and Δ*nps6* mutants revealed that siderophores are required for vegetative growth under iron-limiting conditions, conidiation, tolerance for reactive oxygen species, and cell wall integrity. On the maize leaf surface Δ*sid1* and Δ*nps6* mutants were hampered in formation of melanized appressoria and were impaired in virulence on non-wounded and wounded leaves. In agreement with biotrophy-specific down-regulation of siderophore biosynthesis and transport, Δ*sid1* and Δ*nps6* strains were not affected in formation of biotrophic infection structures, but spread of necrotrophic hyphae was reduced.

To address the question why siderophore biosynthesis is specifically down-regulated in biotrophic hyphae, maize leaves were infiltrated with siderophores. Siderophores infiltration alone did not induce defense responses, but invasion of and formation of biotrophic hyphae in siderophore-infiltrated leaves by *C. graminicola* caused dramatically increased ROS formation, as well as increased transcriptional activation of genes encoding cell wall-localized peroxidases and pathogenesis-related (PR) proteins (Fig. 37).

In Summary, It was also shown for the first time that both RIA and SIA pathways are infection structure-specifically regulated. Both pathways are differentially, but complementary regulated. It was also found that a link between iron homeostasis and biogenesis of the structural cell wall polymer chitin and β-1, 3-glucan. Apparently, *C. graminicola* use the iron-sparing strategy to reduce the expression of iron-using proteins. Both *CHSV* and *GLS1* genes have the CCAAT *cis*-acting sequences in their promoter region, which are presumably repressed by the Hap-like binding complex (Hortschansky et al., 2007).

VII. References

Agrios, G.N. 2005. Plant pathology fifth edition. Elsevier Academic Press, Oxford.

Albarouki, E., and Deising, H. 2013. Infection structure-specific reductive iron assimilation is required for cell wall integrity and full virulence of the maize pathogen *Colletotrichum graminicola*. Mol Plant Microbe Interact. 26:695-708.

Almeida, R.S., Brunke, S., Albrecht, A., Thewes, S., Laue, M., Edwards, J.E., Filler, S.J., and Hube, B. 2008. The hyphal-associated adhesin and invasin Als3 of *Candida albicans* mediates iron acquisition from host ferritin. PLoS Pathog. 4.

Altschul, S.F., Madden, T.L., Schäffer, A.A., Zhang, J., Zhang, Z., Miller, W., and Lipman, D.J. 1997. Gapped BLAST and PSI-BLAST: a new generation of protein database search programs. Nucleic Acids Res. 25:3389-3402.

Anderson, D.W., and Nicholson, R.L. 1996. Characterization of a laccase in the conidial mucilage of *Colletotrichum graminicola*. Mycologia 88:966-1002.

Andrie, R.M., Martinez, J.P., and Ciuffetti, L.M. 2005. Development of *ToxA* and *ToxB* promoter-driven fluorescent protein expression vectors for use in filamentous ascomycetes. Mycologia 97:1152-1161.

Askwith, C., and Kaplan, J. 1998. Site-directed mutagenesis of the yeast multicopper oxidase Fet3p. J Biol Chem. 273:22415-22419.

Askwith, C., Eide, D., Van Ho, A., Bernard, P.S., Li, L., Davis-Kaplan, S., Sipe, D.M., and Kaplan, J. 1994. The *FET3* gene of *S. cerevisiae* encodes a multicopper oxidase required for ferrous iron uptake. Cell 70:403-410.

Bailey, J.A., and Jeger, M.J. 1992. *Colletotrichum*: biology, pathology and control. British Society for Plant Pathology, Wallingford, UK.

Bauminger, E.R., Cohen, S.G., Labenski de Kanter, F., Levy, A., Ofer, S., Kessel, M., and Rottem, S. 1980. Iron storage in *Mycoplasma capricolum*. J Bacteriol. 141:378-381.

Bechinger, C., Giebel, K.F., Schnell, M., Leiderer, P., Deising, H.B., and Bastmeyer, M. 1999. Optical measurements of invasive forces exerted by appressoria of a plant pathogenic fungus. Science 285:1896-1899.

Beck, E., Ludwig, G., Auerswald, E.A., Reiss, B., and Schaller, H. 1982. Nucleotide sequence and exact localization of the neomycin phosphotransferase gene from transposon Tn5. Gene 19:327-336.

Behr, M., Humbeck, K., Hause, G., Deising, H.B., and Wirsel, S.G.R. 2010. The hemibiotroph *Colletotrichum graminicola* locally induces photosynthetically active green islands but globally accelerates senescence on aging maize leaves. Mol Plant Microbe Interact. 23:879–892.

Beneduzi, A., Ambrosini, A., and Passaglia, L.M.P. 2012. Plant growth-promoting rhizobacteria (PGPR): Their potential as antagonists and biocontrol agents. Genet Mol Biol. 23:1044–1051.

Benz, G., Schröder, T., Kurz, J., Wünsche, C., Karl, W., Steffen, G.J., Pfitzner, J., and Schmidt, D. 1982. Konstitution der Deferriform der Albomycine δ_1, δ_2 und ε Angewandete Chemie 94:552–553.

Bergstrom, G.C., and Nicholson, R.L. 1981. Invertase in the spore matrix of *Colletotrichum graminicola*. J Phytopathol. 102:139-147.

Bergstrom, G.C., and Nicholson, R.L. 1999. The biology of corn anthracnose. Plant Disease 83:596-608.

Bertani, B. 1951. Studies on lysogenesis. I. The mode of phage liberation by lysogenic *Escherichia coli*. Journal of Bacteriology 62:293-300.

Bonaccorsi di Patti, M.C., Felice, M.R., Camuti, A.P., Lania, A., and Musci, G. 2000. The essential role of Glu-185 and Tyr-354 residues in the ferroxidase activity of *Saccharomyces cerevisiae* Fet3. FEBS Lett. 472:283-286.

Bonaccorsi di Patti, M.C., Paronetto, M.P., Dolci, V., Felice, M.R., Lania, A., and Musci, G. 2001. Mutational analysis of the iron binding site of *Saccharomyces cerevisiae* ferroxidase Fet3. An in vivo study. FEBS Lett. 508:475-478

Boukhalfa, H., and Crumbliss, A.L. 2002. Chemical aspects of siderophore mediated iron transport. Biol Met. 15:325–339.

Braun, V. 1999. Active transport of siderophore-mimicking antibacterials across the outer membrane. Drug Resist Updat. 2:363-369.

Briat, J.F., Duc, C., Ravet, K., and Gaymard, F. 2010. Ferritins and iron storage in plants. Biochim Biophys Acta. 1800:806-814.

Brown, T. 1999. Southern blotting. Pages 2.9.1–2.9.15. in: Curr Protoc Mol Biol., F.M. Ausubel, R. Brent, R.E. Kingston, D.D. Moore, J.G. Seidman, J.A. Smith, and K. Struhl, eds. John Wiley & Sons, pp., New York.

Budde, A.D., and Leong, S.A. 1989. Characterization of siderophores from *Ustilago maydis*. Mycopathologia 108:125–133.

Bullock, W.O., Fernandez, J.M., and Short, J.M. 1987. Xl1-blue: A high efficiency plasmid transforming recA *Escherichia coli* strain with beta-galactosidase selection Biotechniques 5:376-378.

Chaiharn, M., Chunhaleuchanon, S., and Lumyong, S. 2009. Screening siderophore producing bacteria as potential biological control agent for fungal rice pathogens in Thailand. World J Microbiol Biotechnol. 25:1919-1928.

Chao, L.Y., Marletta, M.A., and Rine, J. 2008. Sre1, an iron-modulated GATA DNA-binding protein of iron-uptake genes in the fungal pathogen *Histoplasma capsulatum*. Biochemistry 47:7274-7283.

Chen, X.Z., Peng, J.B., Cohen, A., Nelson, H., Nelson, N., and Hediger, M.A. 1999. Yeast SMF1 mediates H^+-coupled iron uptake with concomitant uncoupled cation currents. J Biol Chem. 274:35089–35094.

Chirgwin, J.M., Przybyla, A.E., MacDonald, R.J., and W.J. Rutter. 1979. Isolation of biologically active ribonucleic acid from sources enriched in ribonuclease. Biochemistry 18:5294-5299.

Chung, C.T., Niemela, S.L., and Miller, R.H. 1989. One-step preparation of competent *Escherichia coli*: Transformation and storage of bacterial cells in the same solution. Proc Natl Acad Sci U S A. 86:2172-2175.

Crichton, R. 2001. Inorganic biochemistry of iron metabolism from molecular mechanisms to clinical consequences. John Wiley & Sons, Ltd, New York.

David, C.N., and Easterbrook, K. 1971. Ferritin in the fungus *phycomyces*. J Cell Biol. 48:15-28.

de Jong, J.C., McCormack, B.J., Smirnoff, N., and Talbot, N.J. 1997. Glycerol generates turgor in rice blast. Nature 389:244-245.

de Los Santos-Villalobos, S., Barrera-Galicia, G.C., Miranda-Salcedo, M.A., and Pena-Cabriales, J.J. 2012. *Burkholderia cepacia* XXVI siderophore with biocontrol capacity against *Colletotrichum gloeosporioides*. World J Microbiol Biotechnol. 28:2615-2623.

de Neergaard, E. 1997. Methods in botanical histopathology. Danish Government Institute of seed Pathology for Developing Countries (DGISP).

de Silva, D., Davis-Kaplan, S., Fergestad, J., and Kaplan, J. 1997. Purification and characterization of Fet3 protein, a yeast homologue of ceruloplasmin. J Biol Chem. 272:14208-14213.

Deák, M., Horváth, G.V., Davletova, S., Török, K., Sass, L., Vass, I., Barna, B., Király, Z., and Dudits, D. 1999. Plants ectopically expressing the ironbinding protein, ferritin, are tolerant to oxidative damage and pathogens. Nat Biotechnol. 17:192-196.

Deising, H.B., Werner, S., and Wernitz, M. 2000. The role of fungal appressoria in plant infection. Microbes Infect. 2:1631-1641.

Dellagi, A., Segond, D., Rigault, M., Fagard, M., Simon, C., Saindrenan, P., and Expert, D. 2009. Microbial siderophores exert a subtle role in Arabidopsis during infection by manipulating the immune response and the iron status. Plant Physiol. 150:1687-1696.

Dellagi, A., Rigault, M., Segond, D., Roux, C., Kraepiel, Y., Cellier, F., Briat, J.F., Gaymard, F., and Expert, D. 2005. Siderophore-mediated upregulation of Arabidopsis ferritin expression in response to *Erwinia chrysanthemi* infection. Plant J. 43 262–272.

Dix, D.R., Bridgham, J.T., Broderius, M.A., Byersdorfer, C.A., and Eide, D.J. 2004. The *FET4* gene encodes the low affinity Fe(II) transport protein of *Saccharomyces cerevisiae*. J Biol Chem. 269:26092-26099.

Döbbeling, U., Böni, R., Häffner, A., Dummer, R., and Burg, G. 1997. Method for simultaneous RNA and DNA isolation from biopsy material, culture cells, plants and bacteria. Biotechniques 22:88-90.

Dufresne, M., Perfect, S.E., Pellier, A.L., Bailey, J.A., and Langin, T. 2000. A GAL4-like protein is involved in the switch between biotrophic and necrotrophic phases of the infection process of *Colletotrichum lindemuthianum* on common bean. Plant Cell 12:1579-1589.

Durfee, T., Nelson, R., Baldwin, S., Plunkett, G., Burland, V., Mau, B., Petrosino, J.F., Qin, X., Muzny, D.M., Ayele, M., Gibbs, R.A., Csörgo, B., Pósfai, G., Weinstock, G.M., and Blattner, F.R. 2008. The complete genome sequence of *Escherichia coli* DH10B: insights into the biology of a laboratory workhorse. J Bacteriol. 190:2597-2606.

Eichhorn, H., Lessing, F., Winterberg, B., Schirawski, J., Kämper, J., Müller, P., and Kahmann, R. 2006. A ferroxidation/permeation iron uptake system is required for virulence in *Ustilago maydis*. Plant Cell 18:3332-3345.

Eide, D.J. 1997. Molecular biology of iron and zinc uptake in eukaryotes. Curr Opin Cell Biol. 9:573-577.

Eisendle, M., Oberegger, H., Zadra, I., and Haas, H. 2003. The siderophore system is essential for viability of *Aspergillus nidulans*: functional analysis of two genes encoding L-ornithine N^5 monooxygenase (*sidA*) and a non-ribosomal peptide synthetase (*sidC*). Mol Microbiol. 49:359–375.

Eisendle, M., Oberegger, H., Buttinger, R., Illmer, P., and Haas, H. 2004. Biosynthesis and uptake of siderophores is controlled by the PacC-mediated ambient-pH regulatory system in *Aspergillus nidulans*. Eukaryot Cell 3:561–563.

Eisendle, M., Schrettl, M., Kragl, C., Muller, D., Illmer, P., and Haas, H. 2006. The intracellular siderophore ferricrocin is involved in iron storage, oxidative-stress resistance, germination, and sexual development in *Aspergillus nidulans*. Eukaryot Cell 5:1596–1603.

El Gueddari, N.E., Rauchhaus, U., Moerschbacher, B.M., and Deising, H.B. 2002. Developmentally regulated conversion of surfaceexposed chitin to chitosan in cell walls of plant pathogenic fungi. New Phytol. 156:103–112.

Epstein, L., and Nicholson, R.L. 2006. Adhesion and adhesives of fungi and oomycetes. Pages 41-62 in: Biological Adhesives, A.M. Smith and J.A. Callow, eds. Springer-Verlag, Berlin Heidelberg.

Expert, D. 1999. Withholding and exchanging iron: interactions between *Erwinia* spp. and their plant hosts. Annu Rev Phytopathol. 37:307-334.

Felsenstein, J. 1985. Confidence limits on phylogenies: An approach using the bootstrap. Evolution 39:783-791.

Ferreras, J.A., Ryu, J.S., Di Lello, F., Tan, D.S., and Quadri, L.E.N. 2005. Small-molecule inhibition of siderophore biosynthesis in *Mycobacterium tuberculosis* and *Yersinia pestis*. Nat Chem Biol. 1:29-32.

Finking, R., and Marahiel, M. 2004. Biosynthesis of nonribosomal peptides Annu Rev Microbiol. 58:453-488.

Gause, G.F. 1955. Recent studies on albomycin, a new antibiotic. Br Med J. 12:1177–1179.

Gietz, R.D., and Woods, R.A. 2002. Transformation of yeast by lithium acetate/single-stranded carrier DNA/polyethylene glycol method. Methods Enzymol. 350:87-96.

Govrin, E.M., Rachmilevitch, S., Tiwari, B.S., Solomon, M., and Levine, A. 2006. An elicitor from *Botrytis cinerea* induces the hypersensitive response in *Arabidopsis thaliana* and other plants and promotes the gray mold disease. Phytopathology 96:299-307.

Grant, S.G., Jessee, J., Bloom, F.R., and Hanahan, D. 1990. Differential plasmid rescue from transgenic mouse DNAs into *Escherichia coli* methylation-restriction mutants. Proc Natl Acad Sci U S A. 87:4645-4649.

Greenshields, D.L. (2007). Iron and reactive oxygen in wheat-pathogen interaction. In The College of Graduate Studies and Research (Saskatoon: University of Saskatchewan), pp. 110.

Greenshields, D.L., Liu, G., Feng, J., Selvaraj, G., and Wei, Y. 2007. The siderophore biosynthetic gene *SID1*, but not the ferroxidase gene *FET3*, is required for full *Fusarium graminearum* virulence. Mol Plant Pathol. 8:411-421.

Grignon, C., and Sentenac, H. 1991. pH and ionic conditions in the apoplast. Annu Rev Plant Physiol Plant Mol Biol. 42:103-128.

Haas, H. 2003. Molecular genetics of fungal siderophore biosynthesis and uptake: the role of siderophores in iron uptake and storage. Appl Microbiol Biotechnol. 62:316-330.

Haas, H. 2012. Iron – a key nexus in the virulence of *Aspergillus fumigatus*. Front Microbiol. 3:1-10.

Haas, H., Eisendle, M., and Turgeon, B.G. 2008. Siderophores in fungal physiology and virulence. Annu Rev Phytopathol. 46:149-187.

Haas, H., Zadra, I., Stöffler, G., and Angermayr, K. 1999. The *Aspergillus nidulans* GATA factor SREA is involved in regulation of siderophore biosynthesis and control of iron uptake. J Biol Chem. 274:4613–4619.

Halliwell, B., and Gutteridge, J.M.C. 1984. Oxygen toxicity, oxygen radicals, transition metals and disease. Biochem J. 219:1-14.

Halliwell, B., and Gutteridge, J.M.C. 1992. Biologically relevant metal ion-dependent hydroxyl radical generation. FEBS Lett. 307:108–112.

Han, J., Lakshman, D.K., Galvez, L.C., Mitra, S., Baenziger, P.S., and Mitra, A. 2012. Transgenic expression of lactoferrin imparts enhanced resistance to head blight of wheat caused by *Fusarium graminearum*. BMC Plant Biol. 12:1-9.

Harrison, P.M., Andrews, S.C., Ford, G.C., Smith, J.M.A., Treffry, A., and White, J.L. 1987. Ferritin and bacterioferritin-iron sequestering molecules from man to microbe. Pages 445-475 in: Iron Transport in Microbes, Plants and Animals, G. Winkelmann, D. van der Helm, and J.B. Neilands, eds. VCH, Weinheim.

Hentze, M.W., Muckenthaler, M.U., and Andrews, N.C. 2004. Balancing acts: Molecular control of mammalian iron metabolism. Cell 117:285–297.

Hider, R.C. 1984. Siderophore mediated absorption of iron. Pages 25-87 in: Structure and Bonding, D.M.P. Mingos and J.B. Neilands, eds. Springer Verlag, Berlin.

Hirokawa, T., Boon-Chieng, S., and Mitaku, S. 1998. SOSUI: classification and secondary structure prediction system for membrane proteins. Bioinformatics 14 378-379.

Hof, C., Eisfeld, K., Antelo, L., Foster, A.J., and Anke, H. 2008. Siderophore synthesis in *Magnaporthe grisea* is essential for vegetative growth, conidiation and resistance to oxidative stress. Fungal Genet Biol. 46:321-332.

Horbach, R. (2010). Die Sfp-4'-phosphopantetheinyltransferase *CgPPT1* des maispathogens *Colletotrichum graminicola* (Ces.) Wilson aktiviert pathogenitätsfaktoren. In Naturwissenschaftlichen Fakultät I Biowissenschaften (Halle (Saale): Martin Luther University Halle-Wittenberg).

Horbach, R., Navarro-Quesada, A.R., Knogge, W., and Deising, H.B. 2011. When and how to kill a plant cell: Infection strategies of plant pathogenic fungi. J Plant Physiol. 168:51-62.

Horbach, R., Graf, A., Weihmann, F., Antelo, L., Mathea, S., Liermann, J., Opatz, T., Thines, E., Aguirre, J., and Deising, H.B. 2009. Sfp-Type 4'-phosphopantetheinyl transferase is indispensable for fungal pathogenicity. Plant Cell 21:3379–3396.

Hortschansky, P., Eisendle, M., Al-Abdallah, Q., Schmidt, A.D., Bergmann, S., Thon, M., Kniemeyer, O., Abt, B., Seeber, B., Werner, E.R., Kato, M., Brakhage, A.A., and Haas, H. 2007. Interaction of HapX with the CCAAT-binding complex--a novel mechanism of gene regulation by iron. EMBO J. 26:3157-3168.

Howard, D.H. 1999. Acquisition, transport, and storage of iron by pathogenic fungi. Clin Microbiol Rev. 12:394-404.

Howard, R.J., Ferrari, M.A., Roach, D.H., and Money, N.P. 1991. Penetration of hard substrates by a fungus employing enormous turgor pressures. Proc Natl Acad Sci U S A. 88:11281–11284

Howlett, B.J. 2006. Secondary metabolite toxins and nutrition of plant pathogenic fungi. Curr Opin Plant Biol. 9:371–375.

Hubert, H.F. 1998. The apoplastic pH of the *Zea mays* root cortex as measured with pH-sensitive microelectrodes: aspects of regulation. J Exp Bot. 49:987-995.

Hwang, L.H., Mayfield, J.A., Rine, J., and Sil, A. 2008. *Histoplasma* requires *SID1*, a member of an iron-regulated siderophore gene cluster, for host colonization. PLoS Pathog. 4:e1000044.

Jain, R., Valiante, V., Remme, N., Docimo, T., Heinekamp, T., Hertweck, C., Gershenzon, J., Haas, H., and Brakhage, A.A. 2011. The MAP kinase MpkA controls cell wall integrity, oxidative stress response, gliotoxin production and iron adaptation in *Aspergillus fumigatus*. Mol Microbiol. 82:39-53.

Jolivet, J.P., Chanéac, C., and Tronc, E. 2004. Iron oxide chemistry. From molecular clusters to extended solid networks. Chem Commun.:481-487.

Jung, W.H., Sham, A., White, R., and Kronstad, J.W. 2006. Iron regulation of the major virulence factors in the AIDS-associated pathogen *Cryptococcus neoformans*. PLoS Biol. 4:e410.

Jung, W.H., Hu, G., Kuo, W., and Kronstad, J.W. 2009. Role of ferroxidases in iron uptake and virulence of *Cryptococcus neoformans*. Eukaryot Cell. 8:1511–1520. .

Kaplan, J. 2002. Mechanisms of cellular iron acquisition: another iron in the fire. Cell 111:603-606.

Kieu, N.P., Aznar, A., Segond, D., Rigault, M., Simond-Cote, E., Kunz, C., Soulie, M.C., Expert, D., and Dellagi, A. 2012. Iron deficiency affects plant defence responses and confers resistance to *Dickeya dadantii* and *Botrytis cinerea*. Mol Plant Pathol. 10:1364-3703.

Koneman, E.W., Allen, S.D., Janda, W.M., Schreckenberger, P.C., and Winn, W. 1997. Color atlas and textbook of diagnostic microbiology. Lippincott-Raven Publishers, Philadelphia, PA, USA.

Kosman, D.J. 2002. FET3P, ceruloplasmin, and the role of copper in iron metabolism. Adv Protein Chem. 60:221-269.

Kosman, D.J. 2003. Molecular mechanisms of iron uptake in fungi. Mol Microbiol. 47:1185–1197.

Kwok, E.Y., Severance, S., and Kosman, D.J. 2006. Evidence for iron channeling in the Fet3p-Ftr1p high-affinity iron uptake complex in the yeast plasma membrane. Biochemistry 45:6317-6327.

Langfelder, K., Streibel, M., Jahn, B., Haase, G., and Brakhage, A.A. 2003. Biosynthesis of fungal melanins and their importance for human pathogenic fungi. Fungal Genet Biol. 38:143-158.

Leach, J., Lang, B.R., and Yoders, O.C. 1982. Methods for selection of mutants and in vitro culture of *Cochliobolus heterostrophus*. Journal of General Microbiology 128:1719-1729.

Lesuisse, E., and Labbe, P. 1994. Reductive iron assimilation in *Saccharomyces cerevisiae*. Pages 149–178 in: Metal Ions in Fungi, G. Winkelmann and D.R. Winge, eds. Marcel Dekker, Inc., N.Y., New York, N.Y.

Liu, G., Greenshields, D.L., Sammynaiken, R., Hirji, R.N., Selvaraj, G., and Wei, Y. 2007. Targeted alterations in iron homeostasis underlie plant defense responses. J Cell Sci.

Liu, X., and Baird, W.V. 2001. Rapid amplification of genomic DNA ends by *Nla*III partial digestion and polynucleotide tailing. Plant Mol Biol Reporter 19:261-267.

Livak, K.J., and Schmittgen, T.D. 2001. Analysis of relative gene expression data using real-time quantitative PCR and the 2^{-DDCT} Method. Methods 4:402-408.

Ludwig, N. (2012). Determinanten der Penetrationskompetenz Pflanzenpathogener Pilze. In Phytopathologie und Pflanzenschutz (Halle: Martin Luther University Halle-Wittenberg).

Lumbsch, H.T., and Huhndorf, S.M. 2007. Outline of *Ascomycota*- 2007. Myconet 13:1-58.

Ma, L.J.J., Klosterman, S.J., Subbarao, K., Dobinson, K., Veronese, P., Kang, S., Gold, S.E., Young, S., Jaffe, D., Gnerre, S., Berlin, A., Heiman, D., Hepburn, T., Sykes, S., Alvarado, L., Kodira, C.D., Lander, E., Galagan, J., Nusbaum, C., and Birren, B. (2008). The genome sequence of *Verticillium dahliae* VdLs.17. In Unpublished.

Malonek, S., Rojas, M.C., Hedden, P., Gaskin, P., Hopkins, P., and Tudzynski, B. 2004. The NADPH-cytochrome P450 reductase gene from *Gibberella fujikuroi* is essential for gibberellin biosynthesis. J Biol Chem. 279:25075-25084.

Marahiel, M.A., and Essen, L.O. 2009. Nonribosomal peptide synthetases: Mechanistic and structural aspects of essential domains. Pages 337-+ in: Complex Enzymes in Microbial Natural Product Biosynthesis, Part A: Overview Articles and Peptides, ELSEVIER ACADEMIC PRESS INC, SAN DIEGO.

Marquez-Fernandez, O., Trigos, A., Ramos-Balderas, J.L., Viniegra-Gonzalez, G., Deising, H.B., and Aguirre, J. 2007. Phosphopantetheinyl transferase CfwA/NpgA is required for *Aspergillus nidulans* secondary metabolism and asexual development. Eukaryot Cell 6:710-720.

Matzanke, B.F. 1994. Iron Storage in Fungi. Pages 179-214 in: Metal Ions in Fungi, G. winkelmann and D.R. Winge, eds. Marcel Dekker, Inc., New York.

Mei, B., Budde, A.D., and Leong, S.A. 1993. *sid1*, a gene initiating siderophore biosynthesis in *Ustilago maydis*: Molecular characterization, regulation by iron, and role in phytopathogenicity Proc Natl Acad Sci U S A. 90:903-907.

Miele, R., Barra, D., and Bonaccorsi di Patti, M.C. 2007. A GATA-type transcription factor regulates expression of the high-affinity iron uptake system in the methylotrophic yeast *Pichia pastoris*. Arch Biochem Biophys. 465:172–179.

Miethke, M., and Marahiel, M. 2007. Siderophore-based iron acquisition and pathogen control. Microbiol Mol Biol Rev. 71:413-451.

Mishra, P.K., Baum, M., and Carbon, J. 2011. DNA methylation regulates phenotype-dependent transcriptional activity in *Candida albicans*. Proc Natl Acad Sci U S A. 108:11965-11970.

Möllmann, U., Heinisch, L., Bauernfeind, A., Kohler, T., and Ankel-Fuchs, D. 2009. Siderophores as drug delivery agents: application of the "Trojan Horse" strategy. BioMetals 22:615-624.

Mootz, H.D., Finking, R., and Marahiel, M.A. 2001. 4´-phosphopantetheine transfer in primary and secondary metabolism of *Bacillus subtilis*. J Biol Chem. 276:37289–37298.

Mootz, H.D., Schwarzer, D., and Marahiel, M.A. 2002. Ways of assembling complex natural products on modular nonribosomal peptide synthetases 3:490–504.

Münch, S. (2012). Identifizierung von Virulenzgenen des Maispathogens *Colletotrichum graminicola* (Ces.) Wilson durch Agrobacterium tumefaciens-vermittelte Transformation. In Naturwissenschaftliche Fakultät (Halle: Martin-Luther University, Halle-Wittenberg).

Namiki, F., Matsunaga, M., Okuda, M., Inoue, I., Nishi, K., Fujita, Y., and Tsuge, T. 2001. Mutation of an arginine biosynthesis gene causes reduced pathogenicity in *Fusarium oxysporum* f. sp. *melonis*. Mol Plant Microbe Interact. 14:580-584.

Neilands, J.B. 1981a. Microbial iron compounds. Annu Rev Biochem. 50:715-731.

Neilands, J.B. 1981b. Iron absorbtion and transport in microorganisms. Annu Rev Nutr. 1:27-46.

Neilands, J.B. 1995. Siderophores: Structure and function of microbial iron transport compounds J Biol Chem. 270:26723–26726.

Neilands, J.B., Konopka, K., Schwyn, B., Coy, M., Francis, R., Paw, B.H., and Bagg, A. 1987. Comparative biochemistry of microbial iron assimilation. Pages 3–34 in: Iron Transport in Microbes, Plants and Animals., G. Winkelmann, Winge, D.R. and J.B. Neilands, eds. VCH, Weinheim.

Newman, M.A., Dow, J.M., Molinaro, A., and Parrilli, M. 2007. Priming, induction and modulation of plant defence responses by bacterial lipopolysaccharides. J Endotoxin Res. 13:69–84.

Newman, M.A., von Roepenack-Lahaye, E., Parr, A., Daniels, M.J., and Dow, J.M. 2002. Prior exposure to lipopolysaccharide potentiates expression of plant defenses in response to bacteria. Plant J. 29:487-495.

Nicholson, R.L., and Moraes, W.B.C. 1980. Survival of *Colletotrichum graminicola*: Importance of the spore matrix. Phytopathology 70:255-261.

Nicholson, R.L., Turpin, C.A., and Warren, H.L. 1976. Role of pectic enzymes in susceptibility of living maize pith to *Colletotrichum graminicola*. Phytopathologische Zeitschrift 87:324-336.

Niewerth, M., Kunze, D., Seibold, M., Schaller, M., Korting, H.C., and Hube, B. 2003. Ciclopirox olamine treatment affects the expression pattern of *Candida albicans* genes encoding virulence factors, iron metabolism proteins, and drug resistance factors. Antimicrob Agents Chemother. 47:1805-1817.

O'Connell, R.J., Thon, M.R., Hacquard, S., Amyotte, S.G., Kleemann, J., Torres, M.F., Damm, U., Buiate, E.A., Epstein, L., Alkan, N., Altmuller, J., Alvarado-Balderrama, L., Bauser, C.A., Becker, C., Birren, B.W., Chen, Z., Choi, J., Crouch, J.A., Duvick, J.P., Farman, M.A., Gan, P., Heiman, D., Henrissat, B., Howard, R.J., Kabbage, M., Koch, C., Kracher, B., Kubo, Y., Law, A.D., Lebrun, M.-H., Lee, Y.-H., Miyara, I., Moore, N., Neumann, U., Nordstrom, K., Panaccione, D.G., Panstruga, R., Place, M., Proctor, R.H., Prusky, D., Rech, G., Reinhardt, R., Rollins, J.A., Rounsley, S., Schardl, C.L., Schwartz, D.C., Shenoy, N., Shirasu, K., Sikhakolli, U.R., Stuber, K., Sukno, S.A., Sweigard, J.A., Takano, Y., Takahara, H., Trail, F., van der Does, H.C., Voll, L.M., Will, I., Young, S., Zeng, Q., Zhang, J., Zhou, S., Dickman, M.B., Schulze-Lefert, P., Ver Loren van Themaat, E., Ma, L.-J., and Vaillancourt, L.J. 2012. Lifestyle transitions in plant pathogenic *Colletotrichum* fungi deciphered by genome and transcriptome analyses. Nat Genet. 44,:1060–1065.

Oide, S., Krasnoff, S.B., Gibson, D.M., and Turgeon, B.G. 2007. Intracellular siderophores are essential for ascomycete sexual development in heterothallic *Cochliobolus heterostrophus* and homothallic *Gibberella zeae*. Eukaryot Cell 6:1339–1353.

Oide, S., Moeder, W., Krasnoff, S., Gibson, D., Haas, H., Yoshioka, K., and Turgeon, B.G. 2006. NPS6, encoding a nonribosomal peptide synthetase involved in siderophore-mediated iron metabolism, is a conserved virulence determinant of plant pathogenic ascomycetes. Plant Cell 18:2836–2853.

Oliveira Garcia, E. (2013). Infection structure-specificity of ß-1,3-glucan synthase is essential for pathogenicity of *Colletotrichum graminicola* and evasion of glucan-triggered immunity (Halle (Saale): Martin-Luther-Universität Halle-Wittenberg).

Park, Y.S., Choi, I.D., Kang, C.M., Ham, M.S., Kim, J.H., Kim, T.H., Yun, S.H., Lee, Y.W., Chang, H.I., Sung, H.S., and Yun, C.W. 2006. Functional identifcation of high-affnity iron permeases from *Fusarium graminearum*. Fungal Genet Biol. 43:273–282.

Perfect, S.E., O'Connell, R.J., Green, E.F., Doering-Saad, C., and Green, J.R. 1998. Expression cloning of a fungal proline-rich glycoprotein specific to the biotrophic interface formed in the *Colleotrichum*–bean interaction. Plant J. 15:273–279.

Perpetua, N.S., Kubo, Y., Yasuda, N., Takano, Y., and Furusawa, I. 1996. Cloning and characterisation of a melanin biosynthetic THR1 reductase gene essential for appressorial penetration of *Colletotrichum lagenarium*. Mol Plant Microbe Interact. 9:323-329.

Philpott, C.C. 2006. Iron uptake in fungi: A system for every source. Biochim Biophys Acta. 1763:636–645.

Pierre, J.L., and Fontecave, M. 1999. Iron and activated oxygen species in biology: The basic chemistry. Biol Met. 12:195-199.

Pöggeler, S., Masloff, S., Hoff, B., Mayrhofer, S., and Kuck, U. 2003. Versatile EGFP reporter plasmids for cellular localization of recombinant gene products in filamentous fungi. Curr Genet. 43:54-61.

Powell, P.E., Cline, G.R., Reid, C.P.P., and Szaniszlo, P.J. 1980. Occurrence of hydroxamate siderophore iron chelators in soils. Nature 287:833-834.

Punt, P.J., Oliver, R.P., Dingemanse, M.A., Pouwels, P.H., and Van den Hondel, C.A. 1987. Transformation of *Aspergillus* based on the hygromycin B resistance marker from *Escherichia coli*. Gene 56:117-124

Ramanan, N., and Wang, Y. 2000. A high-affinity iron permease essential for *Candida albicans* virulence. Science 288.

Raymond, K.N., and Carrano, C.J. 1979. Coordination chemistry and microbial iron transport. Acc Chem Res. 12:183-190.

Rutledge, R. 2004. Sigmoidal curve-fitting redefines quantitative real-time PCR with the prospective of developing automated high-throughput applications. Nucleic Acids Res. 32:e178.

Rzhetsky, A., and Nei, M. 1992. A simple method for estimating and testing minimum evolution trees. Mol Biol Evol. 9:945-967.

Sambrook, J., and Russel, D.W. 2001. Molecular cloning: A laboratory manual. Cold Spring Harbor Laboratory Press, New York.

Schaible, U.E., and Kaufmann, S.H.E. 2004. Iron and microbial infection. Nat Rev Microbiol. 2:946-953.

Schmidt, W. 2003. Iron solutions: Acquisition strategies and signaling pathways in plants. Trends Plant Sci. 8:188-193.

Schrettl, M., Winkelmann, G., and Haas, H. 2004a. Ferrichrome in *Schizosaccharomyces pombe* – an iron transport and iron storage compound. Biol Met. 17:647–654.

Schrettl, M., Bignell, E., Kragl, C., Joechl, C., Rogers, T., Arst, H.N.J., Haynes, K., and Haas, H. 2004b. Siderophore biosynthesis but not reductive iron assimilation is essential for *Aspergillus fumigatus* virulence. J Exp Med. 200:1213–1219.

Schrettl, M., Bignell, E., Kragl, C., Sabiha, Y., Loss, O., Eisendle, M., Wallner, A., Arst, H.N.J., Haynes, K., and Haas, H. 2007. Distinct roles for intra- and extracellular siderophores during *Aspergillus fumigatus* infection. PLoS Pathog. 3:1195-1207.

Schrettl, M., Kim, H.S., Eisendle, M., Kragl, C., Nierman, W.C., Heinekamp, T., Werner, E.R., Jacobsen, I., Illmer, P., Yi, H., Brakhage, A.A., and Haas, H. 2008. SreA-mediated iron regulation in *Aspergillus fumigatus*. Mol Microbiol. 70:27-43.

Seckback, J. 1982. Ferreting out the secrets of plant ferritin. J Plant Nutr. 5:369-394.

Severance, S., Chakraborty, S., and Kosman, D.J. 2004. The Ftr1p iron permease in the yeast plasma membrane: orientation, topology and structure–function relationships. Biochem J. 380:487–496.

Shashidhar, J., Sashidhar, R.B., and Deshpande, V. 2005. Purification and characterization of mycoferritin from *Aspergillus parasiticus* (255). FEMS Microbiol Lett. 245:285–294.

Shi, X., Stoj, C., Romeo, A., Kosman, D.J., and Zhu, Z. 2003. Fre1p Cu^{2+} reduction and Fet3p Cu^{1+} oxidation modulate copper toxicity in *Saccharomyces cerevisiae*. J Biol Chem. 278:50309-50315.

Stearman, R., Yuan, D.S., Yamaguchi-Iwai, Y., Klausner, R.D., and Dancis, A. 1996. A permease-oxidase complex involved in high-affinity iron uptake in yeast. Science 271:1552-1557.

Stephenson, S.A., Hatfield, J., Rusu, A.G., Maclean, D.J., and Manners, J.M. 2000. CgDN3: an essential pathogenicity gene of *Colletotrichum gloeosporioides* necessary to avert a hypersensitive-like response in the host *Stylosanthes guianensis*. Mol Plant Microbe Interact. 13:929–941.

Sundström, K.R. 1964. Studies on the physiology, morphology and serology of *Exobasidium*. Symbolae botanicae upsalienses 18:1-89.

Taira, J., Miyagi, C., and Aniya, Y. 2002. Dimerumic acid as an antioxidant from the mold, *Monascus anka*: The inhibition mechanisms against lipid peroxidation and hemeprotein-mediated oxidation. Biochem Pharmacol. 63:1019–1026.

Tamura, K., Dudley, J., Nei, M., and Kumar, S. 2007. MEGA4: molecular evolutionary genetics analysis (MEGA) software version 4.0. Mol Biol Evol. 24:1596-1599.

Thines, E., Aguirre, J., Foster, A.J., and Deising, H.B. 2006. Secondary metabolites as virulence determinants of fungal plant pathogens. Pages 132–159 in: Progress in Botany, K. Esser, Lüttge, U.E., Beyschlag, W. and J. Murata eds. Springer, Berlin, Heidelberg.

Thon, M.R., Nuckles, E.M., and Vaillancourt, L.J. 2000. Restriction enzyme-mediated integration used to produce pathogenicity mutants of *Colletotrichum graminicola*. Mol Plant Microbe Interact. 13:1356–1365.

Thordal-Christensen, H., Zhang, Z., Wei, Y.D., and Collinge, D.B. 1997. Subcellular localization of H_2O_2 in plants: H_2O_2 accumulation in papillae and hypersensitive response during the barley-powdery mildew interaction. Plant J. 11:1187-1194.

Tsednee, M., Mak, Y.W., Chen, Y.R., and Yeh, K.C. 2012. A sensitive LC-ESI-Q-TOF-MS method reveals novel phytosiderophores and phytosiderophore-iron complexes in barley. New Phytol. 195:951-961.

Tsror, L., Erlich, O., and Hazanovsky, M. 1999. Effect of *Colletotrichum coccodes* on potato yield, tuber quality, and stem colonization during spring and autumn. Plant disease. 83:561-565.

Vakdevi, V., Sashidhar, R.B., and Deshpande, V. 2009. Purification and characterization of mycoferritin from *Aspergillus flavus* MTCC 873. Indian J Biochem Biophys. 46:360-365.

Valiante, V., Jain, R., Heinekamp, T., and Brakhage, A.A. 2009. The MpkA MAP kinase module regulates cell wall integrity signaling and pyomelanin formation in *Aspergillus fumigatus*. Fungal Genet Biol. 46:909-918.

Validandi, V., Rupula, K., Beedu, S.R., and Deshpande, V. 2009. Purification and characterization of mycoferritin from *Fusarium verticillioides* MRC 826. Biol Met. 6:1063-1073.

Van der Helm, D., and Winkelmann, G. 1994. Hydroxamates and polycarbonates as iron transport agents (siderophores) in fungi. Pages 39–148 in: Metal Ions in Fungi, G. Winkelmann and D.R. Winge, eds. Marcel Dekker, Inc.

Vernet, T., Dignard, D., and Thomas, D.Y. 1987. A family of yeast expression vectors containing the phage fl intergenic region. Gene 52:255-233.

Wallner, A., Blatzer, M., Schrettl, M., Sarg, B., Lindner, H., and Haas, H. 2009. Ferricrocin, a siderophore involved in intra- and transcellular iron distribution in *Aspergillus fumigatus*. Appl Environ Microbiol. 75:4194-4196.

Wang, T.P., Quintanar, L., Severance, S., Solomon, E.I., and Kosman, D.J. 2003. Targeted suppression of the ferroxidase and iron trafficking activities of the multicopper oxidase Fet3p from *Saccharomyces cerevisiae*. J Biol Inorg Chem. 8:611-620.

Weinberg, E.D. 2009. Iron availability and infection. Biochim Biophys Acta. 1790:600-605.

Welzel, K., Eisfeld, K., Antelo, L., Anke, T., and H., A. 2005. Characterization of the ferrichrome A biosynthetic gene cluster in the homobasidiomycete *Omphalotus olearius*. FEMS Microbiology Letters 249:157–163.

Werner, S. (2002). Untersuchungen zur Regulation und Bedeutung der Chitin-Synthese beim Maispathogen *Colletotrichum graminicola* (CES.) WILS. (Teleomorph: *Glomerella graminicola* POLITIS). In Mathematische-Naturwissenschaftliche-Technische Fakultät (Halle (Saale): Martin-Luther-Universität Halle-Wittenberg), pp. 115.

Werner, S., Sugui, J.A., Steinberg, G., and Deising, H.B. 2007. A chitin synthase with a myosin-like motor domain is essential for hyphal growth, appressorium differentiation and pathogenicity of the maize anthracnose fungus *Colletotrichum graminicola*. Mol Plant Microbe Interact. in press.

Wernitz, M. (2004). Isolierung des Proteinkinasegenes snf1 aus *Colletotrichum graminicola* und ihre Bedeutung für die Pathogenese. In Fachbereich Biologie (Konstanz: Universität Konstanz), pp. 112.

Wijesundera, R.L.C., Bailey, J.A., and Byrde, R.J.W. 1984. Production of pectin lyase by *Colletotrichum lindemuthianum* in culture and infected bean (*Phaseolus vulgaris*) tissue. J Gen Microbiol. 130:285–290.

Wijesundera, R.L.C., Bailey, J.A., Byrde, R.J.W., and Fielding, A.H. 1989. Cell wall degrading enzymes of *Colletotrichum lindemuthianum*: Their role in the development of bean anthracnose. Physiol Mol Plant Pathol. 34:403–413.

Wilson, G.W. 1914. The identity of the anthracnose of grasses in the United States. Phytopathology 4:106-112.

Winterberg, B., Uhlmann, S., Linne, U., Lessing, F., Marahiel, M.A., Eichhorn, H., Kahmann, R., and Schirawski, J. 2010. Elucidation of the complete ferrichrome A biosynthetic pathway in *Ustilago maydis*. Mol Microbiol. 75:1260–1271.

Yamada, O., Nan, S.N., Akao, T., Tominaga, M., Watanabe, H., Satoh, T., Enei, H., and Akita, O. 2003. *dffA* gene from *Aspergillus oryzae* encodes L-Ornithine N^5-oxygenase and is indispensable for Deferriferrichrysin biosynthesis. J Biosci Bioeng. 95:82-88.

Yasmin, S., Alcazar-Fuoli, L., Gründlinger, M., Puempel, T., Cairns, T., Blatzer, M., Lopez, J.F., Grimalt, J.O., Bignell, E., and Haas, H. 2012. Mevalonate governs interdependency of ergosterol and siderophore biosyntheses in the fungal pathogen *Aspergillus fumigatus*. Proc Natl Acad Sci U S A. 109:E497-504.

Yu, J.H., Hamarib, Z., Hana, K.H., Seoa, J.A., Reyes-Domínguezb, Y., and Scazzocchio, C. 2004. Double-joint PCR: a PCR-based molecular tool for gene manipulations in filamentous fungi. Fungal Genet Biol. 41:973-981.

Yun, C.W., Tiedeman, J.S., Moore, R.E., and Philpott, C.C. 2000a. Siderophore-iron uptake in *Saccharomyces cerevisiae*: Identification of ferrichrome and fusarinine transporters. J Biol Chem. 275:16354–16359.

Yun, C.W., Bauler, M., Moore, R.E., Klebba, P.E., and Philpott, C.C. 2001. The role of the FRE family of plasma membrane reductases in the uptake of siderophore-iron in *Saccharomyces cerevisiae*. J Biol Chem. 267:10218-10223.

Yun, C.W., Ferea, T., Rashford, J., Ardon, O., Brown, P.O., Botstein, D., Kaplan, J., and Philpott, C.C. 2000b. Desferrioxamine-mediated iron uptake in *Saccharomyces cerevisiae*: Evidence for two pathways of iron uptake. J Biol Chem. 275:10709-10715.

Zähner, H., Diddens, H., Keller-Schierlein, W., and Nägeli, H.U. 1977. Some experiments with semisynthetic sideromycins. Jpn J Antibiot. 30:201-206.

VIII. Appendix

VIII.1 Media, buffers and solutions

VIII.1.1 Media

➢ **0.5 M sucrose medium**

171.2 g sucrose, and 0.1% yeast extract were dissolved in one liter of H_2O_{bidest}

➢ **Complete medium, CM** (modified after Leach et al., 1982)

To prepare 1 liter of CM medium, 10 ml of stock solution A and 10 ml stock solution B (see stock solutions) were added to 10 g glucose, 1 g yeast extract and 1 g casein hydrolysate (Difco Laboratories, Augsburg, Germany) dissolved in H_2O_{bidest} and the final volume was brought to 1000 ml and autoclaved for 20 minutes.

➢ **CM-agar**

CM medium supplemented with 1.5% agar-agar.

➢ **Iron limited medium, ILM**

Iron limited medium was made by adding 50 µM of the impermeable iron chelator bathophenanthroline disulfonate (BPS) to the CM medium.

➢ **LB-medium (Lysogeny Broth)** (Bertani, 1951)

One liter of LB medium contains 10 g bacto trypton, 5 g yeast extract and 5 g NaCl dissolved in H_2O_{bidest} and autoclaved. The addition of antibiotic, IPTG, and X-Gal were after cooling the media and according to the use in a 1:1000 dilution of the stock solution (see stock solutions).

➢ **LB-agar**

15 g of agar-agar was added to LB-medium and autoclaved. Antibiotic, IPTG and X-Gal were added after autoclaving and cooling the medium to ca 40°C as previous.

➢ **Oat meal agar, OMA** (Koneman et al., 1997)

For 1 liter OMA preparation, a 50 g oat flakes (Bio-Flakes meal) were mixed with 500 ml of H_2O_{bidest} and homogenized well by blender (Waring Blender BB 90 E; Waring, Torrington, USA), subsequently a 500 ml of 2.4% (w/v) water-agar, thawed in microwave, was added and autoclaved fro 45 min. heat sensitive additives like BPS, ferricrocin, coprogen, ferrichrome, etc. were added filter sterile after autoclaving.

➢ **Potato dextrose medium (PD)**

24 g of PD (BD, Heidelberg, Germany) was dissolved in 1000 ml H_2O_{bidest} and autoclaved. MES, HEPES, and CAPS buffers (see II.2.1.2) were added filter sterile after autoclaving.

➢ **Potato dextrose agar, PDA**

PD medium supplemented with 1.5% g agar-agar.
All antibiotics (i.e., hygromycin B, nourseothricin or geneticin) were added after cooling the medium to 40°C and at a final concentration 100 µg/ml.
The addition of either rose bengal or H_2O_2 was also after autoclaving and cooling the medium to 40- 45°C at a final concentration of 100 µg/ml and 0.01% (v/v) respectively.
Different concentration of BPS was added according to the experiment and purpose indicated after autoclaving and cooling the medium to ca. 45°C.

➢ **Sundström minimal medium SMM** (Sundström, 1964)

To prepare 1000 ml of SMM medium, a 20 g glucose, 0.35 g KH_2PO_4, 0.15 g $K_2HPO_4 3H_2O$, 0.5 g Na_2SO_4 $10H_2O$, 5 mg $CaCl_2$, 20 mg $MgCl_2$ $6H_2O$, 0.27 g sodium citrate, 0.26 g citric acid, 0.22 g $MnSO_4$ $4H_2O$ and 0.20 g $ZnSO_4$ $7H_2O$ was dissolved in 1000 ml H_2O_{bidest} and autoclaved.
1.4 g L-asparagine, and 0.1 mg thiamine were added filter sterile after cooling the autoclaved medium.

➢ **Synthetic complete medium, SCM**

20 g glucose; 1.7 g Yeast nitrogen base YNB without amino acids (BD, Heidelberg, Germany) and 5 g $(NH_4)2SO_4$ were dissolved in total volume of 950 ml H_2O_{bidest} and autoclaved. 50 ml 20 x amino acid mix were added after autoclaving and cooling the medium to ca. 45°C.

➢ **SCM-agar**

18 g Bacto agar (Difco) was added to SCM medium before autoclaving. Auxotrophic amino acids and additional supplements like BPS were added after autoclaving and cooling the medium to ca. 45°C.

➢ **Yeast peptone dextrose YPD**

To prepare 1 liter of YPD liquid medium, 10 g Bacto Tryptone/peptone , 5 g yeast extract and 10 g glucose were added and completed with H_2O_{bidest} to final 1000 ml and autoclaved for 15 min.

➢ **YPD-agar**

YPD media supplemented with 1.8% Bacto agar (Difco Laboratories, Augsburg, Germany). Autoclaved as previous.

➢ **Yeast peptone dextrose plus Adenine; 2x YPAD**

20 g Bacto Tryptone/peptone , 10 g yeast extract, 20 g glucose and 100 mg adenine hemisulphate were dissolved in 100 ml H_2O_{bidest} autoclaved for 15 min.
1.8% Bacto agar (Difco Laboratories, Augsburg, Germany) were added before autoclaving when needed.

All Media were, if not else mentioned, autoclaved for 20 min at 121°C and 2 bars. The addition of heat sensitive ingredients was after cooling the media to 45°C.

VIII.1.2 Buffers

- **2x/0.5x wash buffer I**

    2x or 0.5x SSC
    0.1% (w/v) SDS

- **20x SCC buffer**

    3 M NaCl
    0.3 M sodium citrate
    pH 7.5

- **50x TAE buffer**

    242g Tris base
    57.1 ml acetic acid
    50 mM EDTA
    pH 8.5

- **50x $Na_2B_4O_7$ buffer**

    95.3 g $Na_2B_4O_7.10\ H_2O$
    52 g H_3BO_3
    ad 1000 ml H_2O_{bidest}
    pH 6.7

- **6x Loading buffer**

    30% (v/v) glycerin
    60% 10x TAE-buffer
    0.25% (w/v) bromophenol blue

- **Blocking buffer**

    1% (w/v) blocking reagent (Roche Diagnostics, Mannheim, Germany) in wash buffer II
    Autoclaved

- **Detection buffer**

    100 mM NaCl
    100 mM Tris-HCl
    pH 9.5
    Autoclaved

- **CAPS buffer**

    0.5 M of CAPS buffer was prepared in 200 ml stock solution and pH was adjusted to
    10.00 by adding 1N NaOH.

- **DNA extraction buffer I**

    7 M Urea
    2% (w/v) SDS
    5 mM EDTA
    50 mM Tris-HCl
    pH 8.0

- **DNA extraction buffer II**

    150 mM NaCl
    5 mM EDTA
    50 mM Tris-HCl
    pH 8.0

- **HEPES buffer**

    0.5 M of HEPES buffer was prepared in 200 ml stock solution and pH was adjusted to 7.00 by adding 1N NaOH.

- **Hybridization buffer**

    5x SSC
    0.1% (w/v) N-Lauroylsarcosine
    0.02% (w/v) SDS
    1% (w/v) Blocking Reagent (Roche Diagnostics, Mannheim, Germany) dissolved in 0.1 M maleic acid
    Autoclaved

- **Lyses Buffer (DNA mini prep)**

    50 mM EDTA
    200 mM NaCl
    1% N-Lauroylsarcosine
    200 mM Tris-HCl
    pH 8.0

- **Maleic acid buffer**

    0.1 M maleic acid
    0.15 M NaCl
    pH 7.5

- **MES buffer**

    0.5 M of MES buffer was prepared in 200 ml stock solution and pH was adjusted to 4.50 by adding 1N NaOH.

- **Phosphate buffer 0.1 M**

    Solution I: 35.61 g of $Na_2HPO_4\,2H_2O$ is dissolved in 1 L of H_2O_{bidest}
    Solution II: 27.6 g of $NaH_2PO_4\,H_2O$ is dissolved in 1 L of H_2O_{bidest}
    The buffer is prepared by mixing I and II according to the ratios mentioned in the following table and added up to a total volume of 100 ml.

pH	Solution I (ml)	Solution II (ml)
5.8	4.0	46.0
6.4	13.25	36.75
7.0	30.5	19.5
7.6	43.5	6.5
8.0	47.35	2.65

> **PBS buffer**

  10 mM Na_2HPO_4
  1.75 mM KH_2PO_4
  13.7 mM NaCl
  2.65 mM KCl
  pH 7.0
  Autoclaved

> **TE buffer**

  10 mM Tris-HCl
  0.1 mM EDTA
  pH 8.0

> **TES buffer**

  10 mM Tris-HCl
  5 mM EDTA
  1% (w/v) SDS
  pH 7.4

> **Transfer buffer, Alkaline transfer buffer**

  0.4 M NaOH
  1 M NaCl

> **Wash buffer II**

  150 mM NaCl
  0.3% (v/v) Tween 20
  100 mM maleic acid-NaOH
  pH 7.5

VIII.1.3 Solutions

➢ **1x TSS (Transformation and storage solution)**
   10% (w/v) PEG (3350-8000) in LB pH 6.5
   5% DMSO
   50 mM MgCl2
   Filter sterile and stored at -20°C.

➢ **100x uracil stock solution**

   100 mg uracil in 100 ml $H_2O_{bidest,}$ filter sterile stored at 4°C.

➢ **20x Amino acid mix**

Amino acid	End concentration (µg/ ml)	Stock solution (mg/ 100ml)
Adenine hemisulfate	40	80
L-arginine (HCl)	20	40
L-aspartate	100	200
L-glutamate (mono-Na)	100	200
L-histidine	20	40
L-leucine	60	120
L-lysine (mono-HCl)	30	60
L-methionine	20	40
L-phenylalanine	50	100
L-serine	375	750
L-threonine	200	400
L-tryptophan	40	80
L-tyrosine	30	60
L-valine	150	300
Uracil	20	40

   100 ml H_2O_{bidest}, filter sterile and stored at 4°C.

➢ **Ampicillin stock solution**

   100 mg/ml in H_2O_{bidest}, filter sterile, -20°C.

➢ **Aniline Blue**
   1 % Aniline blue (CI42755) is dissolved in lacto-phenol solution.

➢ **Bathophenanthroline disulfonate (BPS) stock solution**

   100 mM BPS (GFS, Powell OH, USA) in H_2O_{bidest}, filter sterile, stored at 4°C.

➢ **Calcofluor White (Fluorescent brightener)**
   1 % Calcofluor White (CI 40622) is dissolved in 0.02 M phosphate buffer pH 8 (see buffers).

➢ **Coprogen stock solution**

   1 mg/ml desferri-Coprogen from *Neurospora crassa* (EMC microcollections, Tubingen, Germany) in H_2O_{bidest}, filter sterile, stored at -20°C

➢ **Denaturation solution (Southern blot)**

   1.5 M NaCl
   0.5 M NaOH

➢ **Enterobactin stock solution**

   1mg/ml desferri-Enterobactin from *Escherichia coli* (Sigma-Aldrich, Munich, Germany) in DMSO, filtered sterile stored at -20°C

➢ **Fe^{III}-EDTA stock solution**

   100 mM EDTA Ferric sodium (Duchefa, Haarlem, Netherland) in H_2O_{bidest}, filter sterile, stored at 4°C.

➢ **Ferrichrom stock solution**

   1 mg/ml desferri-Ferrichrom from *Ustilago maydis* (Sigma-Aldrich, Munich, Germany) in H_2O_{bidest}, filtered sterile stored at -20°C.

➢ **Ferricrocin stock solution**

   1 mg/ml desferri-Ferricrocin from *Aspergillus viridi-nutans* (Sigma-Aldrich, Munich, Germany) in H_2O_{bidest}, filtered sterile stored at -20°C.

➢ **Geneticin stock solution**

   100 mg/ml G418 Disulphate (ForMedium, Ltd, England) in DMSO, filter sterile, stored at -20°C.

➢ **Hygromycin stock solution**

   50 mg/ml Hygromycin B (InvivoGen, Toulouse, Frankreich) in PBS buffer (see buffer), filter sterile, -20°C.

➢ **IPTG stock solution**

   100 mM IPTG in H_2O_{bidest}, filter sterile, stored at -20°C.

➢ **Kanamycin A stock solution**

   50 mg/ml in H_2O_{bidest}, filter sterile -20°C.

➢ **Lacto-Phenol Stock solution**
   20 % (v/v) phenol
   20 % (v/v) lactic acid
   40 % (v/v) glycerol
   20 % H_2O_{bidest}

➢ **Neutralization solution**

   3 M sodium acetate
   0.5 M Tris-Cl
   pH 7.0

➢ **Nourseothricin stock solution**

   100 mg/ml nourseothricin (Werner Bio-Agents, Jena, Germany) in H_2O_{bidest}, filter sterile, stored at -20°C.

> **PEG solution (protoplast transformation)**
> 40 % (w/v) Polyethylene glycol 4000(3000-3700)
> 0.6 M KCl
> 50mM $CaCl_2$
> 50mM Tris-HCl
> pH 8.0

> **Protoplast solution**
> 20 mg/ml lyses enzymes from *Trichoderma harzianum* (Sigma, Deisenhofen, Germany)
> 0.1% Mercaptoethanol
> 0.7 M NaCl

> **Rhizoferrin stock solution**
> 1 mg/ml desferri-rhizoferrin from *Cunninghamella elegans* (EMC microcollections, Tubingen, Germany) in H_2O_{bidest}, filter sterile, stored at -20°C

> **Stock solution A**
> 50 g $Ca(NO_3)_2$
> 500 ml H_2O_{bidest}
> Autoclaved

> **Stock solution B**
> 10 g KH_2PO_3
> 12.5 g $MgSO_4$ x $7H_2O$
> 2.7 g NaCl
> *ad.* 500 ml H_2O_{bidest}
> Autoclaved

> **Tetracycline stock solution**
> 100 mg/ml in H_2O_{bidest}, filter sterile, -20°C.

> **X-Gal stock solution**
> 20 mg/ml X-Gal in DMSO, stored at -20°C.

All solutions, unless otherwise noted, were autoclaved 20 min at 121°C and 2 bar pressure. Heat sensitive solutions were filter sterilized using 0.2 µm pore CA membrane filter (Heinemann Labortechnik, Duderstadt, Germany)

VIII.2 Vectors

pJET1.2/blunt   (Fermentas, St. Leon-Rot, Germany)
High copy number plasmid is used for cloning of blunt-ended PCR products generated by proofreading polymerases (i.e., *Pfu* polymerase). pJET1.2/blunt mediates amplification in *E. coli* through resistance to ampicillin and facilitates the live-dead-selection of the transformants.

pGEM®-T easy   (Promega, Mannheim, Germany)
High copy number plasmid for T/A cloning of PCR products and amplification in *E. coli*. pGEM®-T easy vector facilitates the blue/weight selection of the transformants. It confers resistance against ampicillin.

pAN7-1   (Punt *et al*., 1987)
pUC18-derived plasmid with the hygromycin phosphotransferase *hph* gene from *E. coli* under the control of *Aspergillus nidulans GPDA* promoter and *TRPC* terminator. pAN7-1 confers resistance to ampicillin in *E. coli* Hygromycin B in fungi. Used as fungal transformation vector.

pNR1   (Malonek *et al*., 2004)
pBluescript II KS-derived plasmid with the *Streptomyces noursei nat1* gene (nourseothricin acetyltransferase) under the control of the *OLIC* promoter of *Aspergillus nidulans*, and the *TUB1*-terminator of *Botrytis cinerea*. pNR1 confers resistance to ampicillin in *E. coli* and nourseothricin in fungi. Used as fungal transformation vector.

pII99   (Namiki et al., 2001)
Plasmid vector carries the neomycin phosphotransferase II gene (*npt*II) that confers resistance to geneticin (G418) from transposon Tn5 (Beck et al., 1982), fused to the *A. nidulans TRPC* promoter and terminator (Mullaney et al. 1985). pII99 confers resistance to ampicillin in *E. coli*, used as fungal transformation vector.

pSH1.6EGFP

Plasmid vector with promoterless *eGFP* gene and the terminator *TrpC* from the *Aspergillus nidulans*. This vector mediates *E. coli* transformation through ampicillin resistance and fungal eGFP-tagging through Hygromycin B resistance.

pSM1   (Pöggeler et al., 2003)
Plasmid vector with *eGFP* gene under the control of *TrpC* promoter and terminator from the *Aspergillus nidulans*. This vector mediates *E. coli* transformation through ampicillin resistance and fungal eGFP-tagging through Hygromycin B resistance.

pAG300   (Graf A. 2004)

A binary yeast expression vector allows the expression of fungal genes in yeast under the control of the constitutive yeast *ADH1* promoter. This vector mediates *E. coli* transformation through ampicillin resistant. It mediates *S. cerevisiae* transformation through uracil autotrophy.

pFET3-1-cDNA   (this study)

pJET1.2/blunt plasmid with the full length cDNA of *FET3-1* gene

pFET3-2-cDNA   (this study)

pJET1.2/blunt plasmid with the full length cDNA of *FET3-2* gene

pAG300-FET3-1   (this study)

pAG300 plasmid with the full length cDNA of *FET3-1* gene.

pAG300-FET3-2   (this study)

pAG300 plasmid with the full length cDNA of *FET3-2* gene.

pFET3-1-cDNA-eGFP   (this study)

pJET1.2/blunt plasmid with the full length cDNA of *FET3-1* gene fussed to the *eGFP* gene.

pFET3-2-cDNA-eGFP   (this study)

pJET1.2/blunt plasmid with the full length cDNA of *FET3-2* gene fussed to the *eGFP* gene.

pAG300-FET3-1-eGFP   (this study)

pAG300 plasmid with the full length cDNA of *FET3-1* gene fused in frame to the *eGFP* gene from pSH1.6EGFP

pAG300-FET3-2-eGFP   (this study)

pAG300 plasmid with the full length cDNA of *FET3-2* gene fused in frame to the *eGFP* gene from pSH1.6EGFP.

pFET3-1   (this study)

pGEM-T easy plasmid with full length ORF of *FET3-1*, 1.1 kb of the promoter region and 1 kb of the terminator region.

pFET3-1KO   (this study)

pJET1.2/blunt plasmid with the whole FET3-1-KO construct.

pFET3-2KO   (this study)

pJET1.2/blunt plasmid with whole FET3-2-KO construct.

pSID1KO   (this study)

pJET1.2/blunt plasmid with whole SID1-KO construct

pNPS2KO   (this study)

pJET1.2/blunt plasmid with the entire NPS2-KO construct.

pNPS6   (this study)

pJET1.2/blunt plasmid with 5912 bp PCR fragment of the *NPS6* gene containing 4504 bp ORF and 1408 bp of the promoter region.

pNPS6KO   (this study)

pJET1.2/blunt plasmid with the entire NPS6-KO construct.

pFET3-1-eGFP-hyg   (this study)
                             pJET1.2/blunt plasmid containing *FET3-1* gene with its native 1.1 kb promoter fussed to the *eGFP* gene under the control of hygromycin resistance.

pP*FET3-1*-eGFP-hyg   (this study)
                             pJET1.2/blunt plasmid with 1.1 kb of the promoter region of *FET3-1* gene fussed to the *eGFP* gene.

pJET-eGFP-G418   (this study)
                             pJET1.2/blunt plasmid contains the promoterless *eGFP* gene and Geneticin resistance gene G418.

pFET3-2-eGFP-G418   (this study)
                             pJET1.2/blunt plasmid containing *FET3-2* gene with its native 950 bp promoter fussed to the *eGFP* gene and geneticin resistance cassette G418.

pEB14-eGFP   (this study)
                             pNR1 derived plasmid with *eGFP* gene under the control of *C. graminicola SID1* promoter and the *TRPC* terminator from *A. nidulans*. pEB14-eGFP plasmid mediates *E. coli* transformation through ampicillin resistant and fungal eGFP tagging through nourseothricin resistance.

pEB14-SID1-eGFP   (this study)
                             pEB14-eGFP plasmid with the full *SID1* ORF fused in the frame of the *eGFP* gene, under the control of its native 904-bp *SID1* promoter.

pEB14-SIT1-eGFP   (this study)
                             pEB14-eGFP plasmid with the full *SIT1* ORF fused with the frame of the *eGFP* gene, under the control of its native 1012-bp *SIT1* promoter.

pEB14-SIT2-eGFP   (this study)
                             pEB14-eGFP plasmid harboring 3264 bp fragment including the putative *SIT2* full ORF without stop codon and 1040-bp of the promoter sequence of *SIT2*, fussed in the frame of *eGFP* gene.

VIII.3 Primers

Primers used in this study are listed, sequence overlaps with the *eGFP*, the *hph*, and the *nat1* cassettes are underlined; restriction sites are given in bold.

VIII.3.1 *FET3-1* primers

Primer	sequence (5'→3')
FET3-deg-Fw.1	GGNCANTAYTGGTAYCAY
FET3-deg-Fw.2	AAYTAYGCNTTYTTYAAY
FET3-deg-Rv.1	TGCCAYTCDATRTGRCARTG
FET3-deg-Rv.2	CCRTGNAGRTGRAANGGRTG
FET3-GSP1-Fw.1	GAACCCCGAGGTCTACGGCACCTAC
FET3-GSP1-Fw.2	ATGGTACGGCCTGGCCAAGACAGAG
FET3-GSP1-Fw.3	GCCGGCTTGACGCYGTTGCCAGGTC
FET3-GSP1-Fw.4	AGTAGCTTCGTTGCCGTTTCCGTT
FET3-GSP1-Rv.1	GTTGTGGTACCAGTCGGACAGTGAC
FET3-GSP1-Rv.2	GTATCTGGAAGGACGGCACGGTCAC
FET3-GSP1-Rv.3	TCATGGGCCCGACACGCCACTCGTTC
FET3-GSP1-Rv.4	TCGCCCCGAGACCCCATTGGTCCG
FET3-GSP2-Fw.1	TCTACGGCACCTACACGCACAGCTTC
FET3-GSP2-Fw.2	TTGGGTACGCCGGCTCGGCGTC
FET3-GSP2-Fw.3	ACCGCTGCGTTGCACATTAC
FET3-GSP2-Fw.4	CTTGTCGGACAGGTTCATCGC
FET3-GSP2-Rv.1	CTTCGTCGTACTTGCCAATGAACGG
FET3-GSP2-Rv.2	GGATATTGTCCCACGAGACGAGAAG
FET3-GSP2-Rv.3	ATCAAGTCAGACCGCGTGCTG
FET3-GSP2-Rv.4	GTAGGCAGGTCAAGCTGGCGG
FET3-1-eGFP-nest-Fw.1	GCTCAGGTGCCATTAGACCTGT
FET3-1-eGFP-Rv.1	<u>CCGGTGAACAGCTCCTCGCCCTTGCTCACCAT</u>AGTTCGACCGGCTCCCGCTCCG (<u>*eGFP* cassette</u>)
FET3-1-eGFP-Rv.2	<u>GGTGAACAGCTCCTCGCCCTTGCTCACCAT</u>CATCGTTGCGCGGTCCCTGG (<u>*eGFP* cassette</u>)
FET3-1-Fw.1	CGAAGCCTGTAGATGGGCAAAGGAC
FET3-1-KO-3´-Fw.1	<u>ATGATTACTAACAGATATCAAGCTT</u>ATCGTGGCCCTCGTCTTCAG (<u>*nat1* cassette</u>)
FET3-1-KO-3´-Rv.1	CAAGCAGGGCATCAACGTCATCCAG
FET3-1-KO-5´-Fw.1	CGAAGCCTGTAGATGGGCAAAGGAC
FET3-1-KO-5´-Rv.1	<u>GCCCGAATCGGGAATGCGGCTCTAGAGCGG</u>CATCGTTGCGCGGTCCCTGG (<u>*nat1* cassette</u>)

FET3-1-KO-nest.Fw.1	TTGGCGCAGCTCTTGAAGGTTTAG
FET3-1-KO-nest.Fw.2	GCTCAGGTGCCATTAGACCTGT
FET3-1-KO-nest.Rv.1	GAAGGGCTTGCCTAGAAAGAAGAC
FET3-1-KO-nest.Rv.2	TTAGATGCGAGCGCATGCATAG
FET3-1-SfiIA-Fw.1	TACT**GGCCATTACGGCC**GCACGATGACAGGCACTAC *Sfi*I
FET3-1-SfiIB-Rv.1	AAT**GGCCGAGGCGGCC**ATACGTTTGACTGCACGTGGCTTC *Sfi*I

VIII.3.2 *FET3-2* primers

Primer	sequence (5'→3')
FET3-2-AgeI-Fw.1	CCGTG**ACCGGT**ATCAGAACCAGAGACGGCTAGGTG *Age*I
FET3-2-eGFP-Rv.1	<u>CCGGTGAACAGCTCCTCGCCCTTGCTCACCATT</u>TCGTCCCTGTCAGTGTATTCG (<u>eGFP</u> cassette)
FET3-2-KO-3´-Fw.1	<u>CTCGTGTACTGTGTAAGCGCCCGCTCTTCTATT</u>GGAGTCCAGTGTCGAAGAGAAC (*hph* cassette)
FET3-2-KO-3´-Rv.1	CTACTGCGAAACCGCTGAGTG
FET3-2-KO-5´-Fw.1	GAGTGACGGAATGGCCCAATC
FET3-2-KO-5´-Rv.1	<u>GACAGATTTGGGAGCTCGGTATCCCTGGGGAAT</u>GCGATGAGAAGGCCATGGTG (*hph* cassette)
FET3-2-KO-nest.Fw.1	GACGGAATGGCCCAATCAGAAC
FET3-2-KO-nest.Fw.2	CATGGCCTTCTCATCGCATTC
FET3-2-KO-nest.Rv.1	CGAAACCGCTGAGTGGACAGAG
FET3-2-KO-nest.Rv.2	GGTTCTCTTCGACACTGGACTC
FET3-2-KO-nest.Rv.3	CGCTTGGGCCTGGTACTTGATG
FET3-2-PciI-Rv.1	CGG**ACATGT**GTTCGTCCCTGTCAGTGTATTCG *Pci*I
FET3-2-Rv.3	CGCTTGGGCCTGGTACTTGATG
FET3-2-SfiIA-Fw.1	ATT**GGCCATTACGGCC**ATGCACCATGGCCTTCTCATCGC *Sfi*I
FET3-2-SfiIB-Rv.1	ATA**GGCCGAGGCGGCC**CTATTCGTCCCTGTCAGTGTATTC *Sfi*I

VIII.3.3 *SID1* primers

Primer	sequence (5'→3')
SID1-DraIII-SfiIB-Rv.1	TC**GAGCACCATGTGGCCGAGGCGGCC**GACATTATGATGATAGTGGTG *Dra*III and *Sfi*I
SID1-FW.1	CGTATAGTGTCTAGCCGCAGTAGC
SID1-KO-3´-Fw.1	<u>CTCGTGTACTGTGTAAGCGCCCGCTCTTCTATT</u>CGACGCCGGTGTTTATCTGC (<u>*hph*</u> cassette)
SID1-KO-3´-Rv.1	GAGCTCATGACGTGGATGGACAAC

SID1-KO-5´-Fw.1	CGTATAGTGTCTAGCCGCAGTAGC
SID1-KO-5´-Rv.1	<u>GACAGATTTGGGAGCTCGGTATCCCTGGGGAAT</u>GTGACTCGCAGTGAGGAGAC (<u>*hph* cassette</u>)
SID1-KO-nest-Fw.1	TAGTGTCTAGCCGCAGTAGC
SID1-KO-nest-Fw.2	CTTACCCATCTGCGTCGTTC
SID1-KO-nest-Fw.3	CCACCACCACCACTATCATC
SID1-KO-nest-Rv.1	CAGCGACATGCAACTGTATAG
SID1-KO-nest-Rv.2	CTTCAAGCTGCAAGCACAAG
SID1-KO-nest-Rv.3	GGGTCGTTAGTCAGAATGTC
SID1-Kpn2I-SfiIA-Fw.1	TCGAG**TCCGGAGGCCATTACGGCC**CGTATAGTGTCTAGCCGCAGTAGC ***Kpn*2I** and ***Sfi*I**
SID1-SfiIB-Rv.1	TGT**GGCCGAGGCGGCC**GTTGGAAACGGCCTTGGCCC ***Sfi*I**

VIII.3.4 *NPS6* and *NPS2* Primers

Primer	sequence (5'→3')
NPS6-Fw.1	CAGGCATTGACACGAACCATAC
NPS6-KO-nest-Fw.1	GCCACCCAATCACTCCACTCTC
NPS6-KO-nest-Fw.2	CTTGGAGGTCATCAAGGGCCTTAG
NPS6-KO-nest-Rv.1	GCCTCGGAGACGAGCTTCATAG
NPS6-KO-nest-Rv.2	AGGGCGTAGGTGTTGAACTTGAGG
NPS6-Rv.1	ATTCGTTGACGGTGAGCGTGAG
NPS2-KO-3´-Fw.1	<u>GTCTGGAGTCTCACTAGCTT</u>GGCAATTGTAACGGATAGGACTG (<u>*npt*II cassette</u>)
NPS2-KO-3´-Rv.1	GACGCAATGAAACCACGTTATC
NPS2-KO-5´-Fw.1	ACACCAGGTCCTTGCGTGTTAG
NPS2-KO-5´-Rv.1	<u>GTGCAACTGACAGTCGTACA</u>CGATGTCGTCGAACAGTCAAGC (<u>*npt*II cassette</u>)
NPS2-KO-nest-Fw.1	CCAGGTCCTTGCGTGTTAGTTG
NPS2-KO-nest-Fw.2	CTGCAATACCCGAAGCTAGCAG
NPS2-KO-nest-Fw.3	TGGGAGGTCAAGGACTGGACTG
NPS2-KO-nest-Rv.1	AATGAAACCACGTTATCGATCC
NPS2-KO-nest-Rv.2	AGTCGAGATGCGGCATGACAAG

VIII.3.5 *SIT1* and *SIT2* primers

Primer	sequence (5'→3')
SIT1-SfiIA-Fw.	TTA**GGCCATTACGGCC**CGACGATCCCTCAAGGAATAAAG *Sfi*I
SIT1-SfiIB-Rv.	TTA**GGCCGAGGCGGCC**AACAACATTTCCGCGCACCTG *Sfi*I
SIT2-SfiIA-Fw.	TTA**GGCCATTACGGCC**CAAGCACATGGTGGGACATCAG *Sfi*I
SIT2-SfiIB-Rv.	TTA**GGCCGAGGCGGCC**GAACACCGTTCCCTTCGTCTG *Sfi*I

VIII.3.6 RT-PCR and qRT-PCR primers

Primer	sequence (5'→3')
ACT1-qRT-Fw.1	TCCTACGAGCTTCCTGACGG
ACT1-qRT-Rw.1	CCGCTCTCAAGACCAAGGAC
CHSV-qRT-Fw.1	CGGAGACGTGCTGAAGATGGC
CHSV-qRT-Rv.1	AAGGGCTGGATGGCTTCTAAC
FET3-1-ORF-Fw.	GCCGTCTTCTCGAATTCC
FET3-1-ORF-Rv.	CCGAGGATGCCCGTTATG
FET3-1-qRT-Fw.5	TTCCGGGCGAATAACCCTGGC
FET3-1-qRT-Rv.4	CGCAGACGTCAAGGTGGTTC
FET3-2-ORF-Fw.	CCATGGCCTTCTCATCGC
FET3-2-ORF-Rv.	GTCCCTGTCAGTGTATTC
FET3-2-qRT-Fw.2	GTTCCAGAACGGCACCAACCAC
FET3-2-qRT-Rv.1	AGGTGCCGACTTGGTCAAACTC
FRE2-ORF-Fw.	TGAGAATGCGCGTCCTGTTG
FRE2-ORF-Rv.	CATCATGCCCGGTGTATGCC
FRE2-qRT-Fw.1	GCGAAGAGATTGCCGGTCTG
FRE2-qRT-Rv.3	GCCCGATAGCGATCACGATG
FTR1-1-ORF-Fw.	TCAGATCAAGCGGTTCTCCC
FTR1-1-ORF-Rv.	GACGTTCCGGACTGTTCCTC
FTR1-1-qRT-Fw.2	AGCGTCTGGCACGTCAACTG
FTR1-1-qRT-Rv.2	TCCCTTGGTCTCGCGGAATC
FTR1-2-qRT-Fw.1	CCGTCGTCGGCTACTTCATC
FTR1-2-qRT-Rv.1	CCTGGATGGGCGCTTTCTTG
GLS1-qRT-Fw.1	ACCCAACAGACCGATTCCTAC
GLS1-qRT-Rv.1	CTGGTGATAGGCACTGTTTGG
H3-qRT.Fw.2	ATCCGTCGCTACCAGAAGTC
H3-qRT.Rv.2	TGAAGTCCTGGGCAATCTCAC

NPS2 qRT-Fw.1	CGCCATTCGATTCTTGGAGTG
NPS2-qRT-Rv.1	GGTAGTAGCGGAATCGAGAAC
NPS6-1.int.-Fw.1	ACGCGCAAACAGTACCGGTG
NPS6-1.int.-Rv.1	CCTCGGCGATGATGTCTTGC
NPS6-2.int.-Fw.2	GGAGAGCAAGGAGGCTGTCAAG
NPS6-2.int.-Rv.2	ATTCGTTGACGGTGAGCGTGAG
NPS6-qRT-Fw.1	ACGCGCAAACAGTACCGGTG
NPS6-qRT-Rv.2	CTCGACCTGATATGTCCAGTC
SID1-ORF-Fw.1	CCACCACCACCACTATCATC
SID1-ORF-Rv.2	ATGACCGCCGTCAAACTTAG
SID1-qRT-Fw.2	ATCGACATGCTCCGCGACAG
SID1-qRT-Rv.3	GTCGCGGGAAAGATGGAGTC
SIT1-ORF-Fw.1	ACACCATGGGCGTCTTCTCC
SIT1-ORF-Rv.1	GGGTATTATCGCCAGCTTCC
SIT1-qRT-Fw.1	TGCTGCTTTGCTGGGTCCTC
SIT1-qRT-Rv.1	GCCTCCGCTGCTAAGAATGC
SRE1-ORF-Fw.1	ACTACGCTTCTCTTCGAATG
SRE1-ORF-Rv.1	GTTTATTCGTTTCCCAGTTC
SRE1-qRT-Fw.1	AACTGCGGCACCACCATCAC
SRE1-qRT-Rv.1	GCATCTCCTCGGTCCATTCG
ZmPR1-qRT-Fw.1	CAACAGCTGGACCCTCGAGATC
ZmPR1-qRT-Rv.1	AACTGCCTGACGCTGCCAAC
ZmPR3-qRT-Fw.1	ACCGCCTTATTCTTCGCTGTGC
ZmPR3-qRT-Rv.1	AAGCCCGCGTAGGTGTAGAAG
ZmPRX346-qRT-Fw.1	TTCCTGATGCCACCAAGGGTTC
ZmPRX346-qRT-Rv.1	GAGGGCAACGATGTCCTGATCAC
ZmPRX365-qRT-Fw.1	GAGATGACGACCGCTCCCATTG
ZmPRX365-qRT-Rv.1	AGCGGGCTTATGTTGCCCATC
ZmPRX648-qRT-Fw.1	TCCGCCTCCACTTCCATGACTG
ZmPRX648-qRT-Rv.1	ATCGCGTCGATCACCTCGTACC
ZmPRX731-qRT-Fw.1	CGGTGTTCGAGGTGATGGGCTAC
ZmPRX731-qRT-Rv.1	GCAGCAGTATGAGCGCCATGTTG

VIII.3.7 General Primers

Primer	sequence (5'→3')
EGFP-Fw.1	ATGGTGAGCAAGGGCGAGGAG
EGFP-Fw.2	GTGACCGGTGACTCTTTCTGG
EGFP-Fw.3	GGAGTCCAGTGTCGAAGAGAAC
EGFP-nest-Rv.1	CGGAAATGTTGAATACTCATACTC
EGFP-Rv.1	GGGCGACACGGAAATGTTGAATAC
EGFP-Rv.2	GCTGGTGACGGAATTTTCATAG
EGFP-Rv.3	GGAGTCCAGTGTCGAAGAGAAC
EGFP-SfiB-Rv.1	ATA**GGCCGAGGCGGCC**GACAAATGAACGTATCTTATC *SfiI*
Gene-eGFP-Rv.1	<u>GCCAGAAAGAGTCACCGGTCAC</u>GGCTGGTGACGGAATTTTCATAG (*eGFP* cassette)
Gene-Fw.1	CTTGGCTGGAGCTAGTGGAGGT
Hyg-Fw.1	ATTCCCCAGGGATACCGAGCTCCCAAATCTGTC
Hyg-prob-Fw.1	TCCGAGGGCAAAGGAATAGAGTAG
Hyg-Rv.1	AATAGAAGAGCGGGCGCTTACACAGTACACGAG
ITS2-qPCR-Fw.	CGTCGTAGGCCCTTAAAGGTAG
ITS2-qPCR-Rv.	TTACGGCAAGAGTCCCTC
M13-qPCR-Fw.	GTAAAACGACGGCCAGTGC
M13-qPCR-Rv.	CACAGGAAACAGCTATGACC
Nat1-Fw.1	CCGCTCTAGAGCCGCATTC
Nat1-prob-Fw.1	CCACGTTGATCTCGAAGGTTTG
Nat1-Rv.1	AAGCTTGATATCTGTTAGTAATCATCATTAAG
pEB-uni-Fw.1	GGAAACAGCTATGACCATGATTAC
pEB-uni-Rv1.	TACGACTCACTATAGGGCGAATTG
pJET1.2-Fw.	ATCCATCCGGCGTAATACGACTC
pJET1.2-Rv.	ACGGTTCCTGATGAGGTGGTTAG
SAP primer	GGAGACTGACATGGACTGAAGGAGTAAAGGGIIGGGIIGGGIIGGGCATG
UAP primer	GGAGACTGACATGGACTGAAGGAGT
UNI-G418-Fw.1	<u>TGTACGACTGTCAGTTGCAC</u>AGCGCGTTGTTGGATTAAG (<u>universal overhangs</u>)
UNI-G418-Rv.1	<u>AAGCTAGTGAGACTCCAGAC</u>CTCAGAAGAACTCGTCAAGAAG (<u>universal overhangs</u>)

VIII.4 Supplementary figures
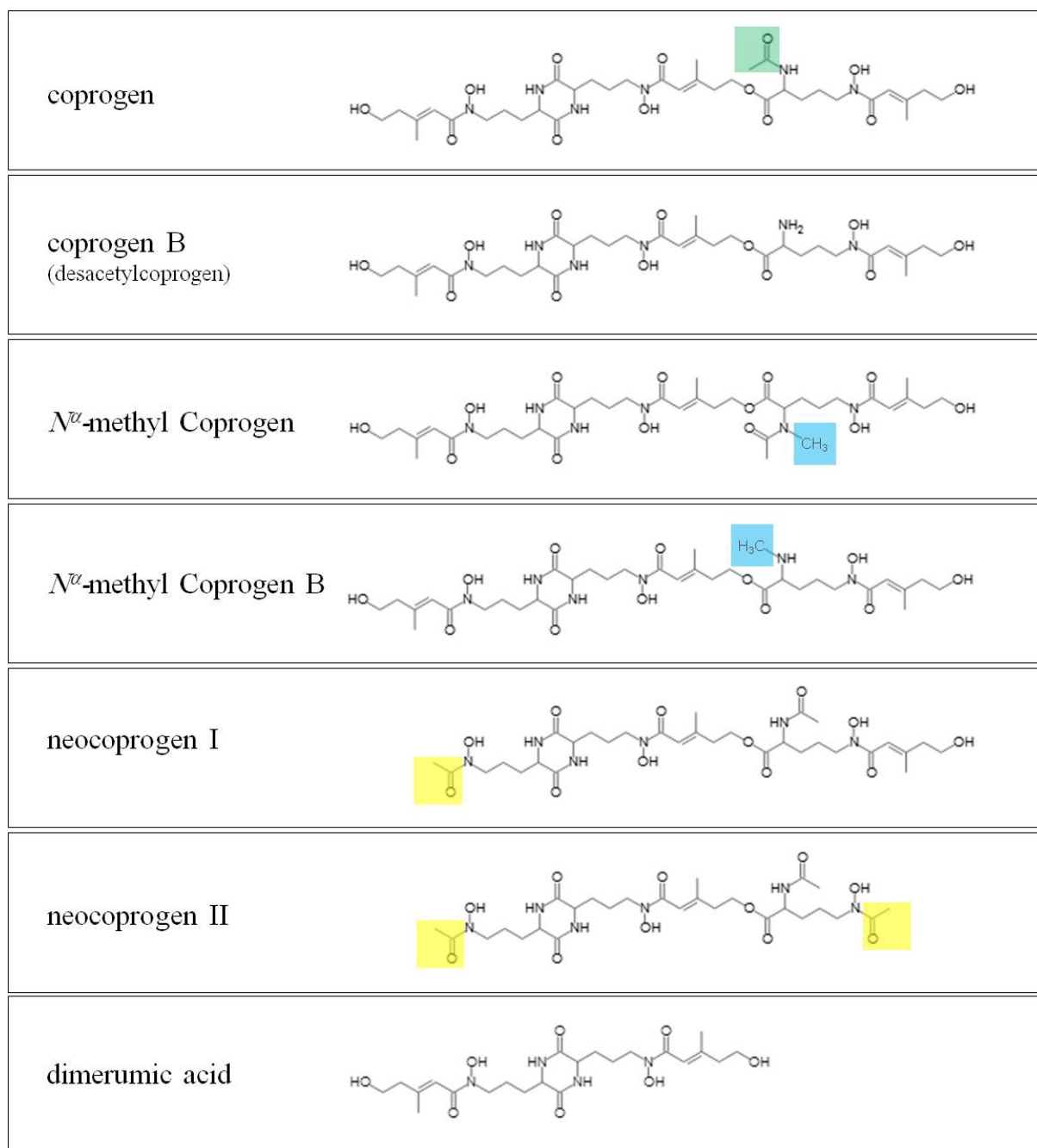
Supplementary Fig. 1: Molecular structure of coprogen derivatives produced by different fungi: The N^{α}- acetylation (green box) of the Coprogen B leads to formation of Coprogen, whereas the methylation (blue box) leads to formation of N^{α}-methyl-coprogen B and N^{α}-methyl-coprogen, respectively. In neocoprogen I, one of the terminal N^{δ}-acyl groups is an acetyl group, while in neocoprogen II both of the terminal N^{δ}-acyl groups are acetyls (yellow box, respectively). Dimerumic acid is the breakdown product of coprogen
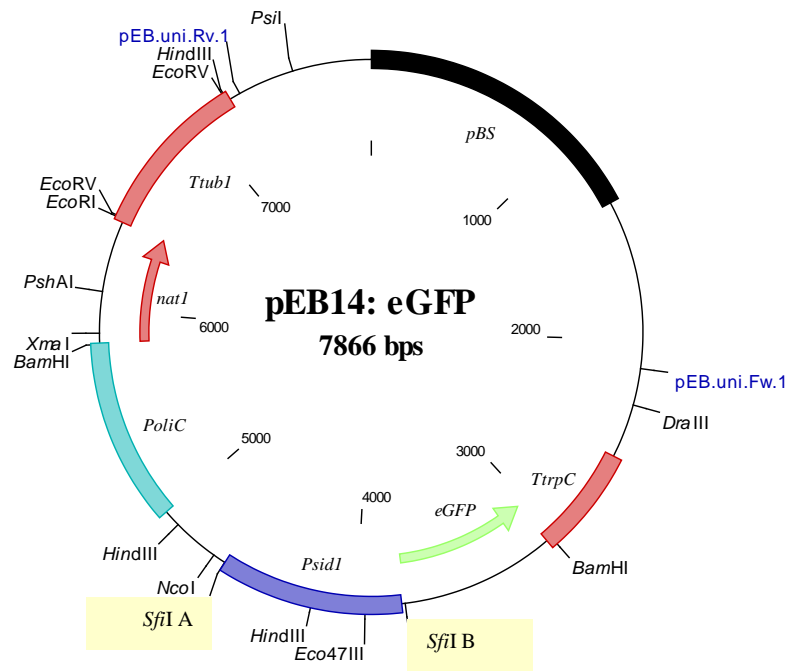
Supplementary Fig. 2: Map of the pEB14-eGFP vector: The plasmid origin is the pNR1 plasmid (Malonek et al., 2004), which has the backbone of pBluescriptII KS plasmid (pBS). The nourseothricin acetyltransferase gene (*nat1*) from *Streptomyces noursei* under the control of *oliC* promoter from *A. nidulans* and terminated by *Botrytis cinerea* terminator Tub 1. The *eGFP* gene under the control of the *SID1* promoter from *C. graminicola* and terminated by *TrpC* terminator from *A. nidulans*. The *Sfi*I A (GGCCATTACGGCC) and *Sfi*I B (GGCCGAGGCGGCC) restriction sites allow the oriented integration of the target gene for C-terminal GFP tagging. The universal unique primers (pEB.uni.Fw.1/pEB.uni.Rv.1) allowi the amplification of the target-eGFP cassette.
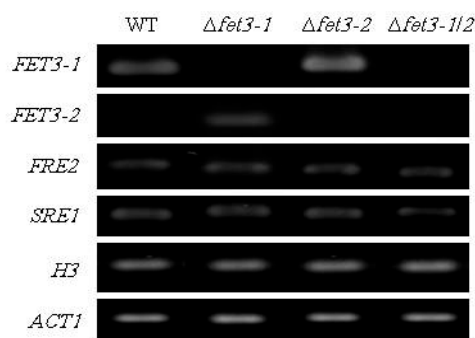
Supplementary Fig. 3: RT-PCR analysis of transcripts of genes involved in reductive iron assimilation in the WT and ferroxidase deletion strains. Transcripts of *FET3-1* are present in the WT and Δ*fet3-2* under iron-limiting conditions, but not in Δ*fet3-1* and Δ*fet3-1/2* strains. In contrast, transcripts of *FET3-2* are only detectable under iron-limiting conditions in the Δ*fet3-1* deletion background. Transcripts of *FRE2* were present under iron-deficient, and transcripts of the GATA transcription factor gene *SRE1* were present under iron-deficient conditions in all strains tested. Actin *ACT1* and histone *H3* transcripts were used as reference.
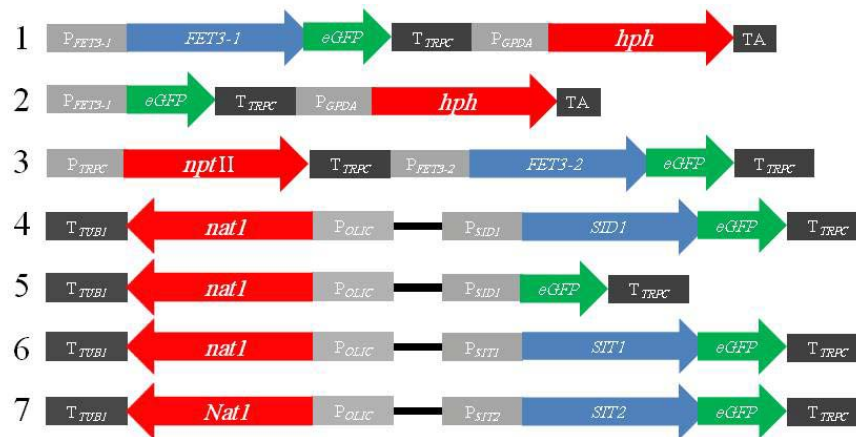
Supplementary Fig. 4: Schematic illustration of the enhanced green fluorescence reporter (*eGFP*) tagged to different genes in this study. The *eGFP* gene was fussed to different genes of iron uptake pathways in *C. graminicola*. (**1**), *FET3-1*:*eGFP* cassette, (**2**), P$_{FET3-1}$:*eGFP* cassette, (**3**), *FET3-2*:*eGFP* cassette, (**4**), *SID1*:*eGFP* cassette, (**5**), P$_{SID1}$:*eGFP* cassette, (**6**), *SIT1*:*eGFP* cassette, (**7**), *SIT2*:*eGFP* cassette.

P$_{FET3-1}$: native promoter region of the *C. graminicola* Ferroxidase (*FET3-1*)

FET3-1: coding region of the Ferroxidase from *C. graminicola*

eGFP: the enhanced green fluorescent protein gene originated from the jellyfish *Aequorea victoria*

T$_{TRPC}$: terminator region from *A. nidulans TRPC* gene

P$_{GPDA}$: glyceraldehyde-3-phosphate dehydrogenase (*GPDA*) promoter from *A. nidulans*

hph: hygromycin B phosphotransferase from *E. coli*

TA: terminator sequences from pSH1.6 EGFP plasmid

P$_{TRPC}$: *TRPC* promoter from *A. nidulans.*

*npt*II: neomycin phosphotransferase II that confers resistance to geneticin (G418) from transposon Tn5 (Beck et al., 1982)

FET3-2: coding region of the ferroxidase *FET3-2* gene from *C. graminicola*

P$_{SID1}$: native promoter region of the *SID1* gene from *C. graminicola*

SID1: coding region of the L-Ornithine-N^5-monooxygenase from *C. graminicola*

SIT1: coding region of the siderophore transporter with its native promoter region (P$_{SIT1}$)

SIT2: coding region of the siderophore transporter with its native promoter region (P$_{SIT2}$)

P$_{OLIC}$: *OlIC* promoter from *A. nidulans*

Nat1: nourseothricin acetyltransferase gene from *Streptomyces noursei*

T$_{TUB1}$: terminator region of *TUB1* gene from *Botrytis cinerea.*

■■■: non coding sequences (plasmid backbone)
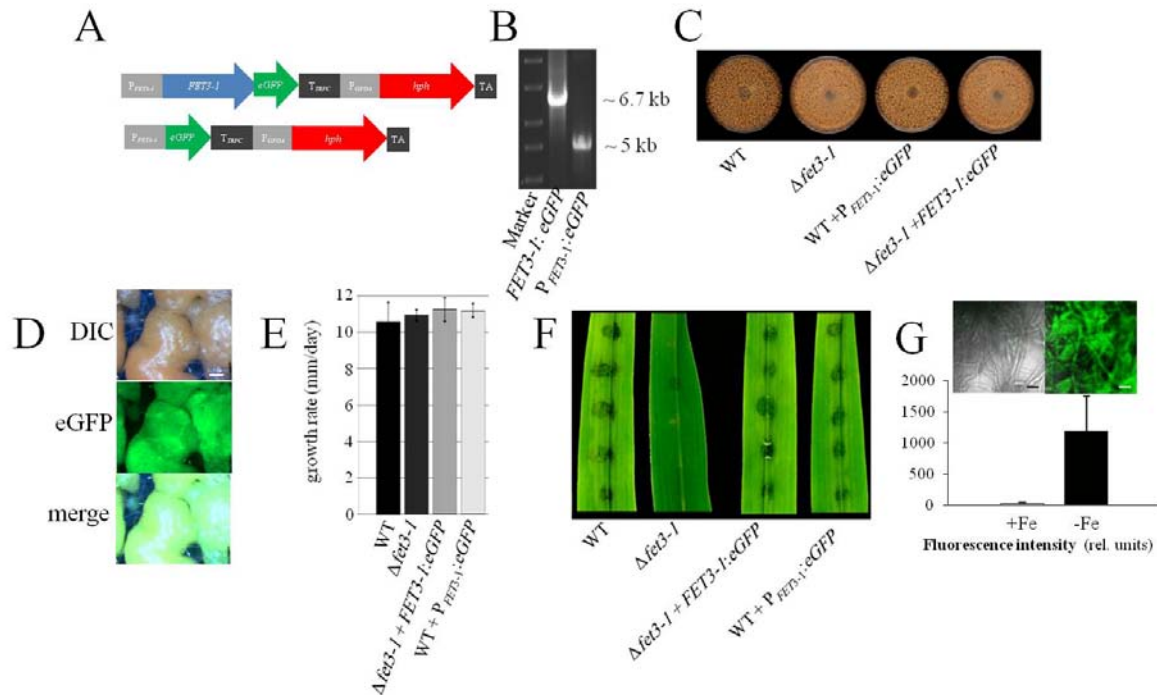
Supplementary Fig. 5: Strains of *C. graminicola* harboring an ectopic copy of P$_{FET3-1}$ or a *FET3-1*:*eGFP* replacement construct are not affected in growth, sporulation, or virulence on maize leaves.

A: Structure of the *eGFP* constructs. P$_{FET3-1}$, *FET3-1* promoter; *FET3-1*, *FET3-1* gene; *eGFP*, enhanced *GFP* gene; T$_{trpC}$, *trpC* terminator from *A. nidulans*; *Hyg*R, hygromycin resistance cassette with the *gpdA* promoter from *A. nidulans*, and the hygromycin phosphotransferase gene from *E. coli*.

B: PCR amplification of the WT and Δ*fet3-1* strains harboring an ectopic copy of either the P$_{FET3-1}$ or the *FET3-1*:*eGFP* replacement construct, using primers FET3-1-eGFP-nest-Fw.1 and FET3-1-eGFP-nest-Rv.1, respectively.

C: The WT strain, the WT strain transformed with the P$_{FET3-1}$:*eGFP* construct, the Δ*fet3-1* strain and the Δ*fet3-1* strain harboring the *FET3-1*:*eGFP* fusion under the control of P$_{FET3-1}$ show comparable colony phenotype and formation of conidia in acervuli.

D: Macrograph show that eGFP fluorescence is highly expressed in matured acervuli developed on oat meal agar (OMA) plates. Bar: 1000 µM, DIC: differential interference contrast.

E: Growth rates of WT and the WT strain transformed with the P$_{FET3-1}$:*eGFP* construct, the Δ*fet3-1* deletion strain and the Δ*fet3-1* strain harboring the *FET3-1*:*eGFP* fusion under the control of P$_{FET3-1}$.

F: Anthracnose disease symptoms on maize leaves inoculated with the WT strain, a WT strain transformed with the P$_{FET3-1}$:*eGFP* construct, the Δ*fet3-1* deletion strain and the Δ*fet3-1* strain harboring the *FET3-1*:*eGFP* fusion under the control of P$_{FET3-1}$. Photographs were taken 4 DPI.

G: Control of *FET3-1* expression by the availability of iron, as measured by the eGFP-fluorescence of the WT strain harboring the P$_{FET3-1}$:*eGFP* fusion. Iron sufficiency (+ Fe) was established by addition of 100 µM FeSO$_4$, and iron limitation (- Fe) was induced by adding the iron scavenger BPS to a concentration of 100 µM. Fluorescence intensity is given in relative units. Bar: 20 µM
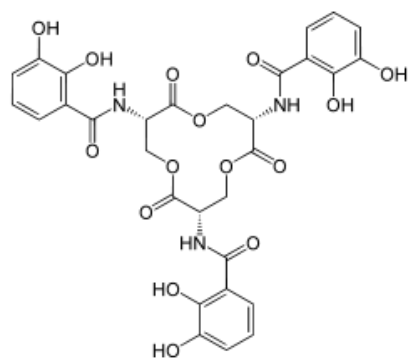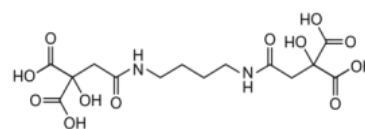
Enterobactin   Rhizoferrin
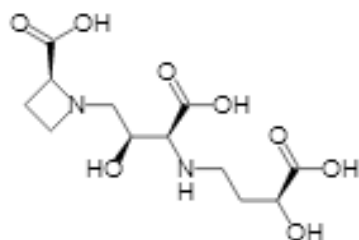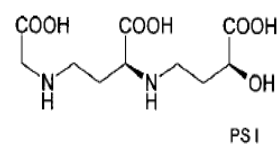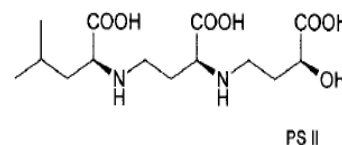
Mugeneic acid   Phytosiderorophores
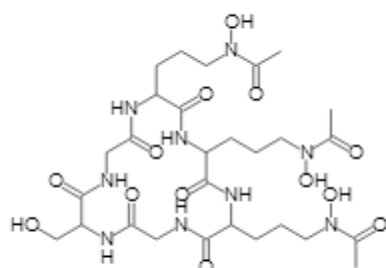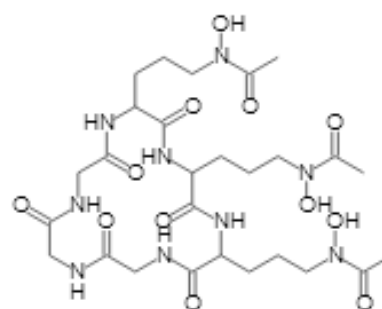
Ferricrocin   Ferrichrome

Supplementary Fig. 6: Molecular structures of the used siderophores in this study.
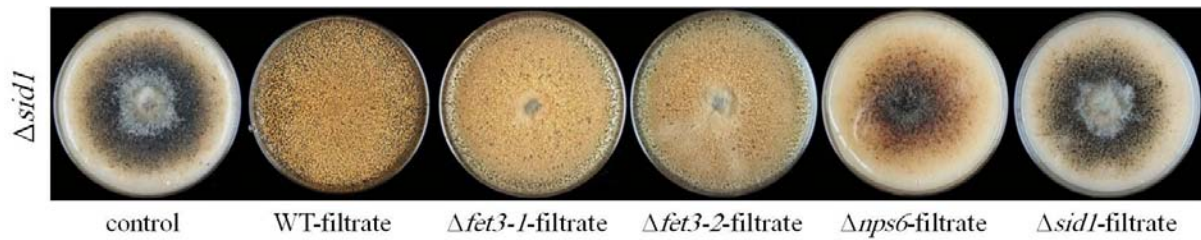
Supplementary Fig. 7: Conidiation of the Δ*sid1* strain by the addition of culture filtrate from different strains. Culture filtrates of *C. graminicola* WT, Δ*fet3-1* and Δ*fet3-2*, but not Δ*nps6* and Δ*sid1*, restored the conidiation ability of Δ*sid1* strain on OMA plates.
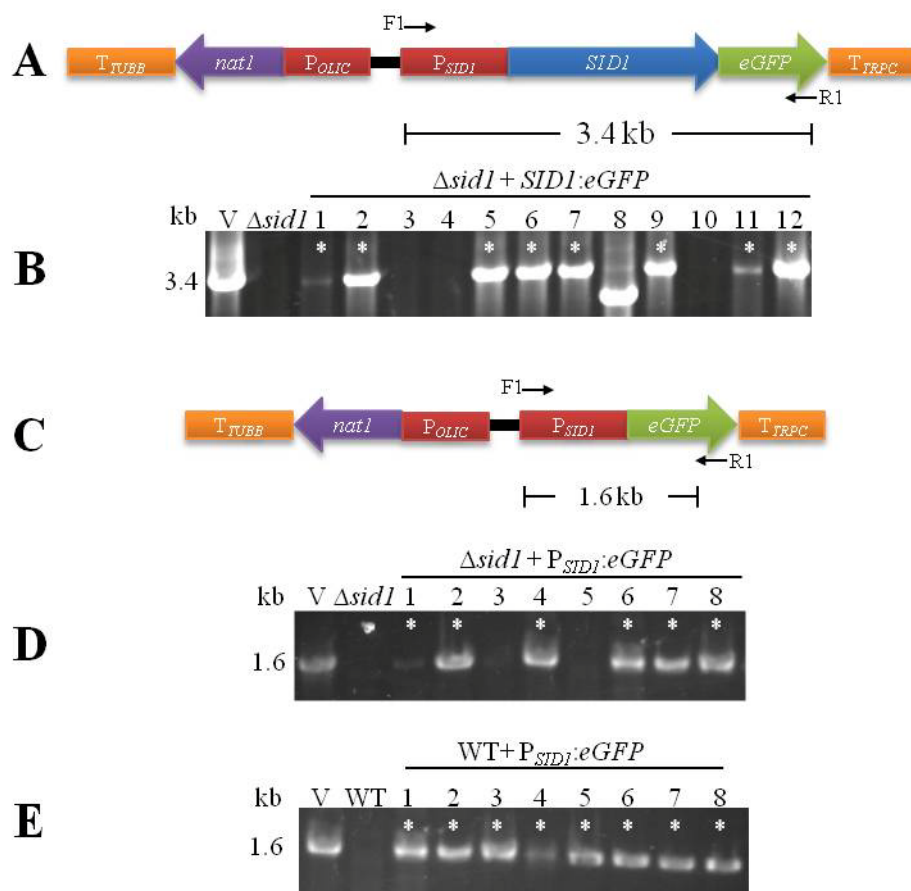
Supplementary Fig. 8: The construction of *SID1*:*eGFP* (A) and *P~SID1~*:*eGFP* (C) fusion constructs and the confirmation of positive transformants by PCR. The full length eGFP-reporter construct was confirmed by PCR using SID1-KO-nest.Fw.1 (F1) and EGFP-Rv.3 (R2) primers and DNA isolated from either the Δ*sid1* transformant (B and D), or the WT transformants (E).
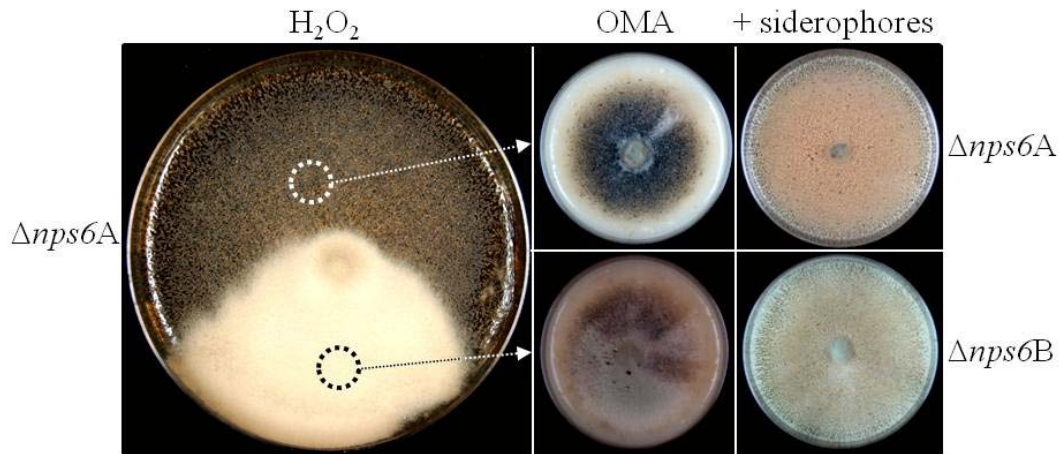
Supplementary Fig. 9: Sectorial growth of the Δ*nps6* strain: The exposure of Δ*nps6* strain to H$_2$O$_2$ leads to sectorial growth and shift from phenotype Δ*nps6*A to phenotype Δ*nps6*B.
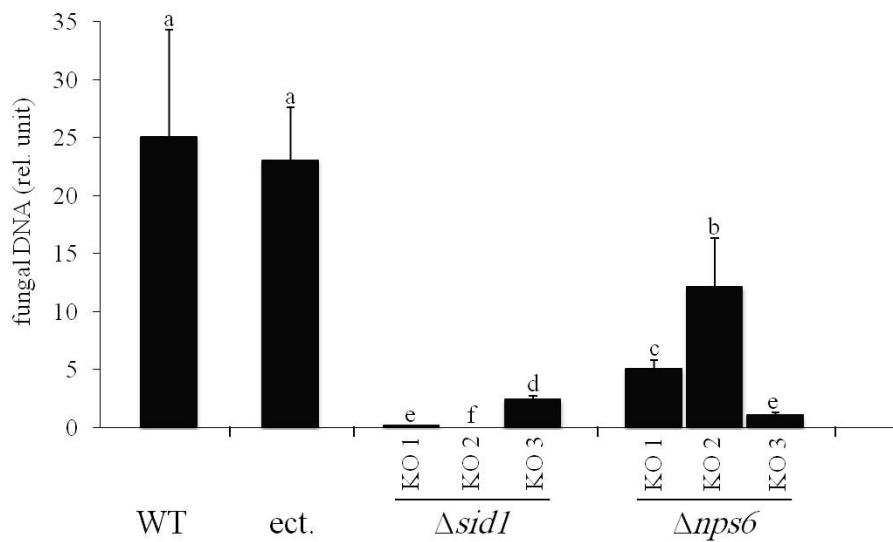
Supplementary Fig. 10: Virulence assay of Δ*sid1* and Δ*nps6* strains. qPCR-based quantification of genomic DNA of *C. graminicola* in non-wounded maize leaves inoculated with the WT, ect., Δ*sid1* and Δ *nps6* strains. Three individual KO mutants of Δ*sid1* and Δ*nps6* strains showed significant virulence reduction in comparison to the WT and the ect. strains. Notice the significant difference between the individual mutants of each strain. Different letters represent significance groups at p ≤ 0.001. Bars = + SD; n = 3.
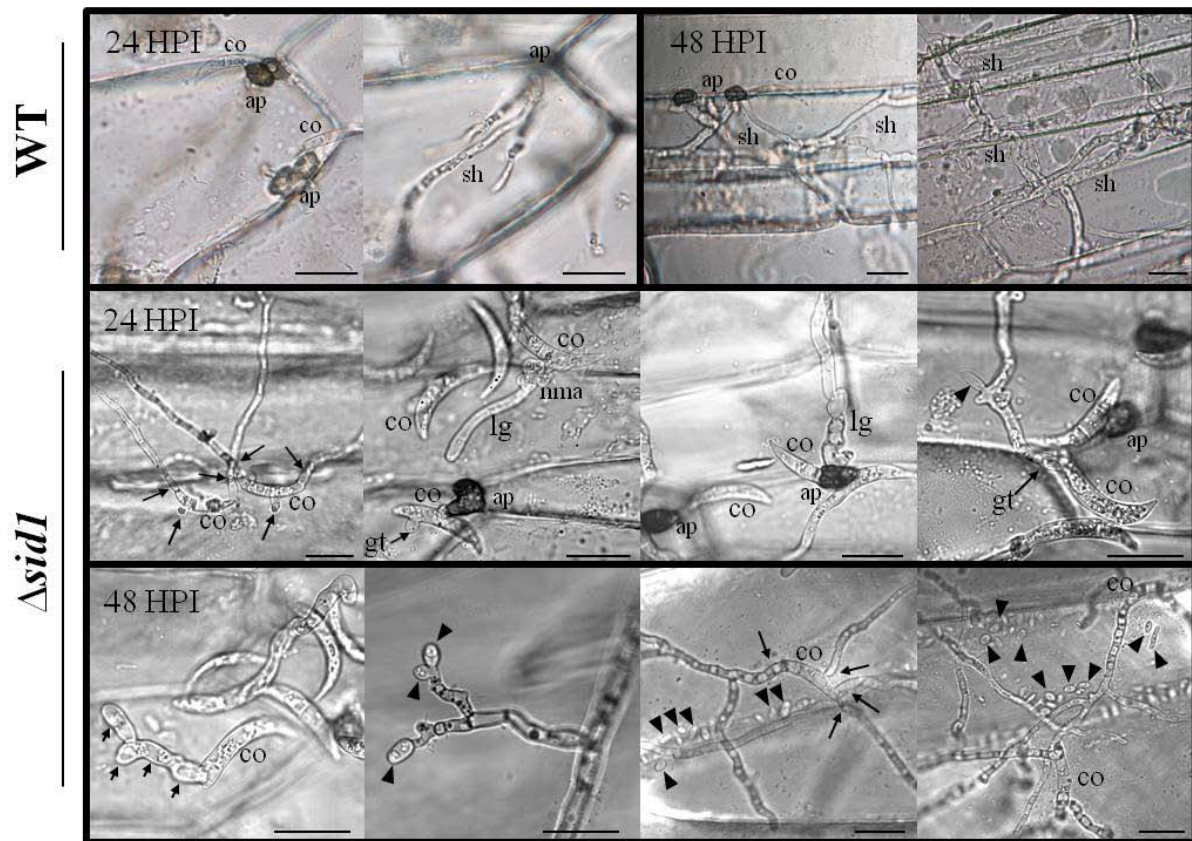
Supplementary Fig. 11: Microscopical analysis of the WT and Δ*sid1* strains on onion epidermis. Germination and *on planta*-developed structures were in analogy to the ones formed on maize leaves. Apparently, the WT forms appressoria (ap) and penetrates the onion epidermis and immediately form secondary-like hyphae (sh) without making the biotrophic hyphae after 24 HPI. After 48 HPI, the WT fully colonized the epidermis. The Δ*sid1* conidia form at 24 HPI several gem tubes (long arrows), non-melanized appressoria (nma) or even fully melanized appressoria are unable to penetrate the onion epidermis and form lateral germ tubes (lg). At 48 HPI, oval conidia production (arrowhead) and pseudo hyphae (short arrows) were also observed in the Δ*sid1* strain.
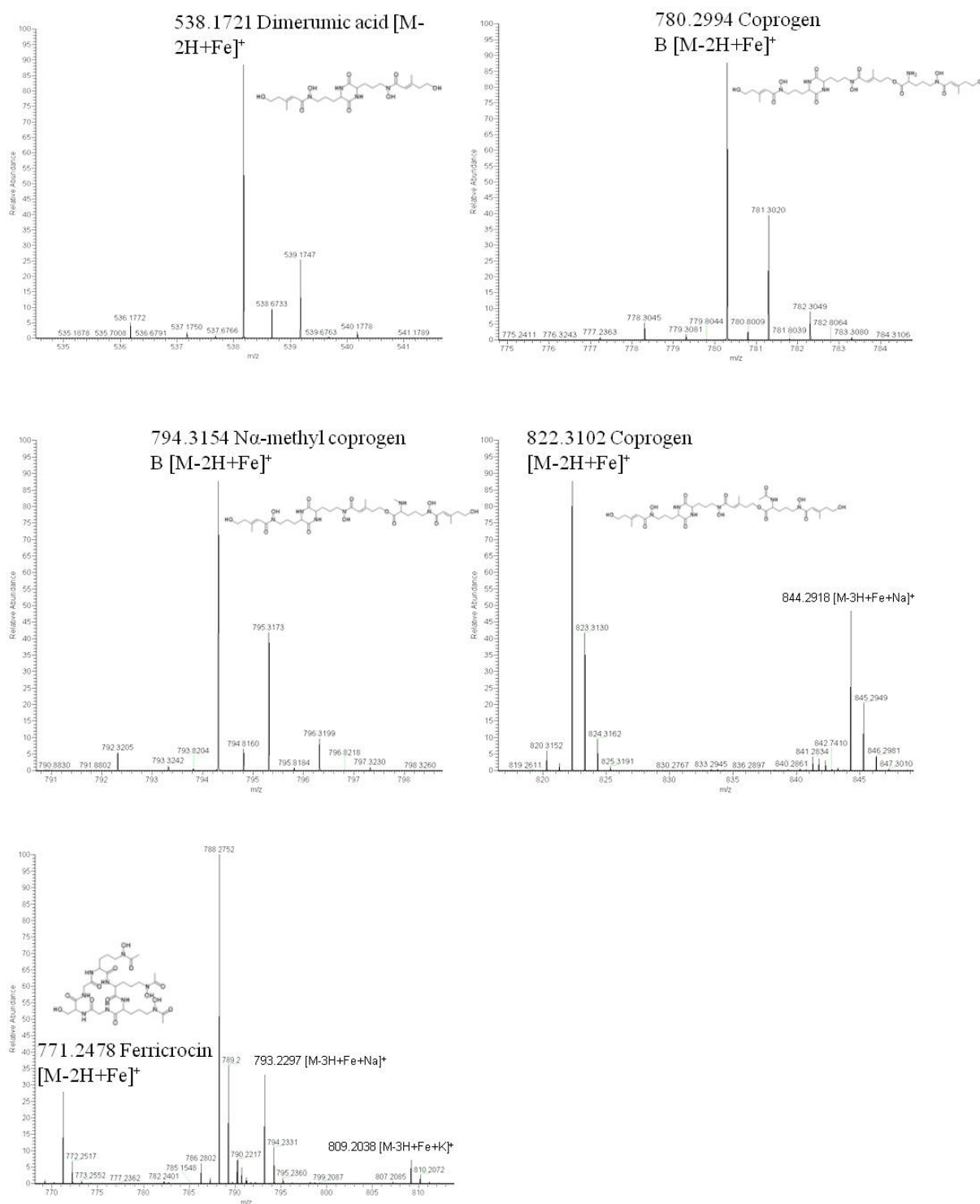
Supplementary Fig. 12: MS analysis of siderophores of *C. graminicola*.
Four different extracellular siderophores (dimerumic acid, coprogen, coprogen B and N$^\alpha$-methylcoprogen B), and ferricrocin as an intracellular siderophore were confirmed by MS analyses.
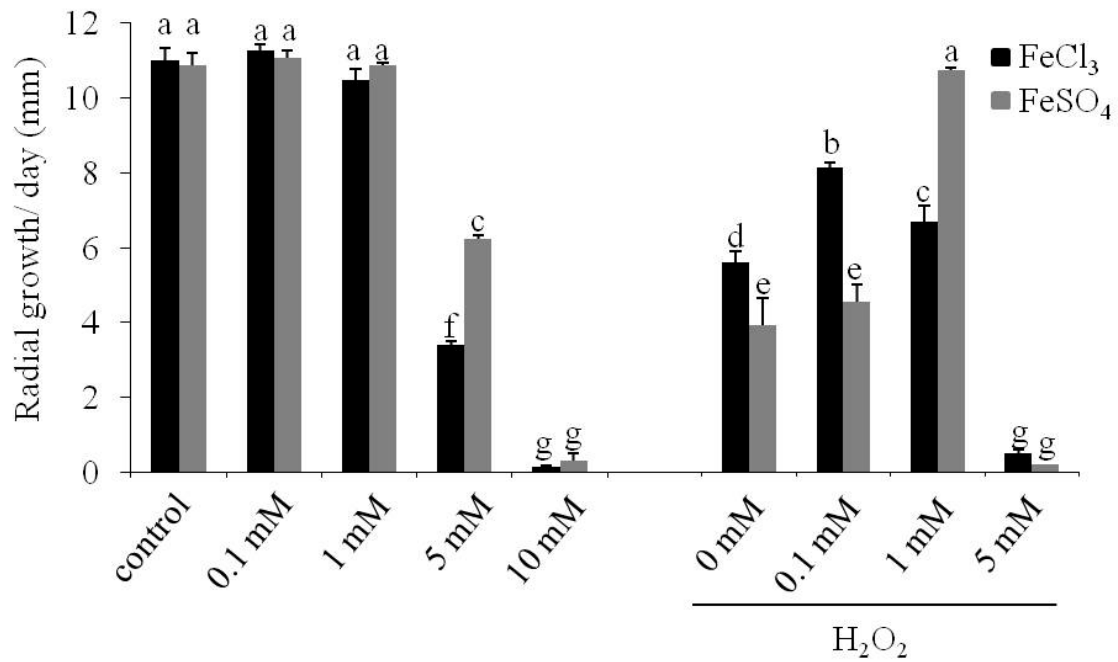
Supplementary Fig. 13: The effect of additive iron on tolerance and hypersensitivity to H_2O_2 of *C. graminicola* wild type strain. Increased iron concentration ($FeCl_3$ or $FeSO_4$) to a concentration higher than 5 mM reduced the growth of *C. graminicola* significantly. The addition of $FeCl_3$ or $FeSO_4$ increased the tolerance of *C. graminicola* toward H_2O_2 until it reached its normal growth at 1 mM of $FeSO_4$. Whereas, the increased iron concentration (5 mM) increase the sensitivity to H_2O_2. Notice the growth at 5 mM of iron plus H_2O_2 approximately equal to the one at 10 mM without H_2O_2. That gives a clear indication of a synergic effect of H_2O_2 under high concentration of iron.
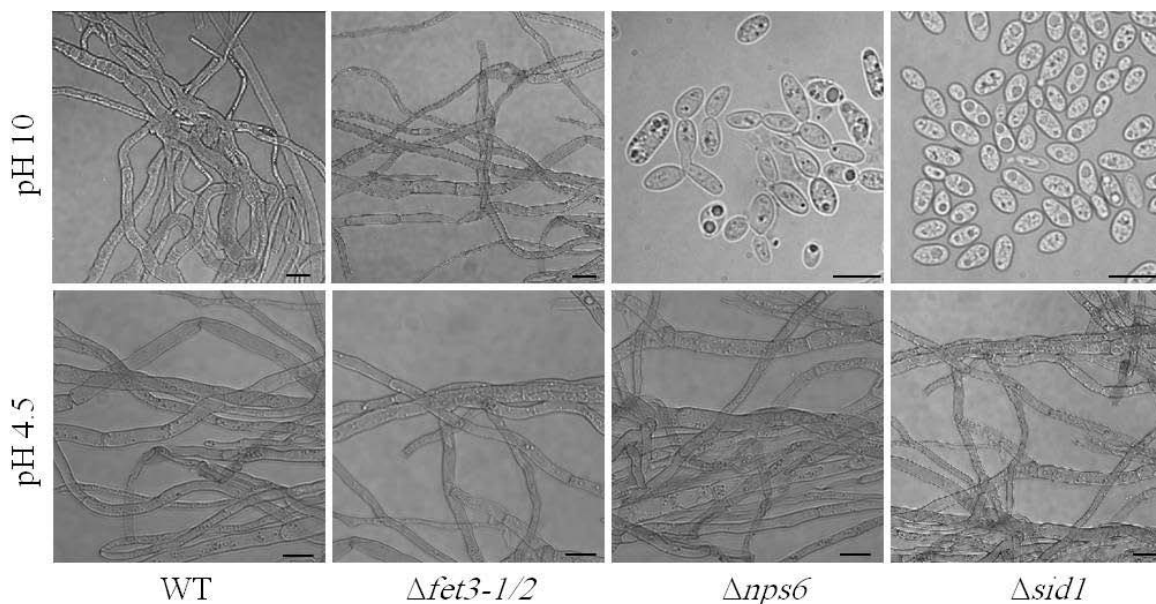
Supplementary Fig. 14: The effect of pH value of growth medium on the phenotype of *C. graminicola* strains. Both Δ*nps6* and Δ*sid1* strains form pseudo-hyphae and yeast-like growth at pH 10, whereas the WT and ferroxidase strains (Δ*fet3-1/2*) form hyphal growth at this condition. Transferring Δ*nps6* and Δ*sid1* strains to normal PD medium restored its hyphal growth form (pH 4.5). bar = 10 μm.
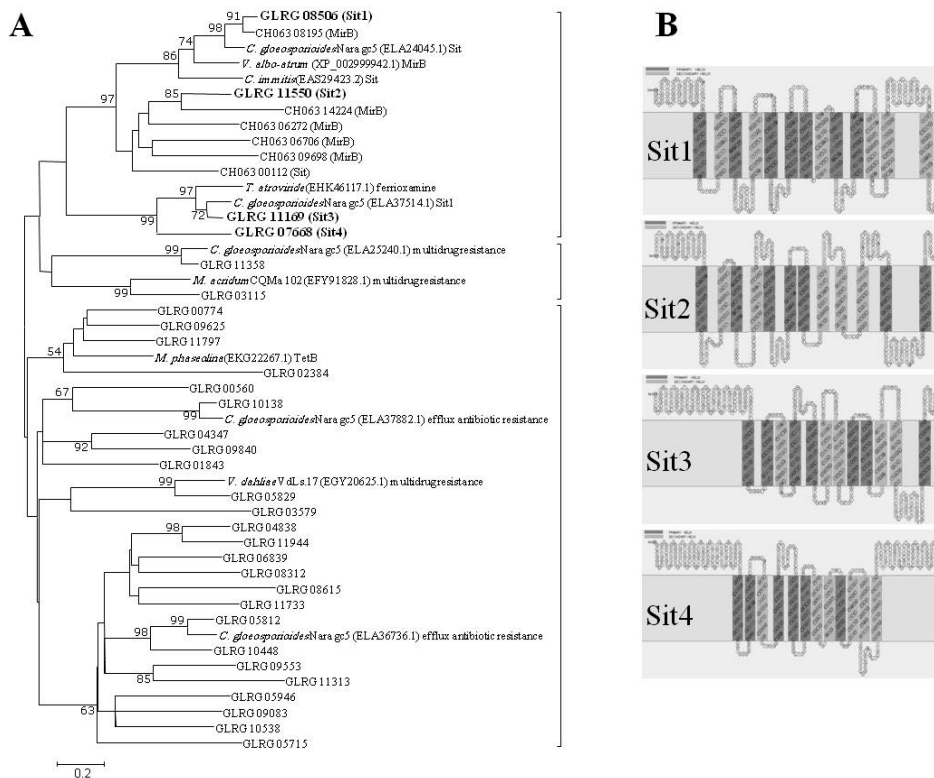
Supplementary Fig. 15: Phylogenic tree and the topology of the putative siderophore transporters of *C. graminicola*.
A: Phylogenic tree depicts putative MFSs of different fungi. The putative siderophore transporters of *C. graminicola* show high similarity with those characterized siderophore transporters of other filamentous ascomycetes. For accession numbers, see VIII.5.2.
B: Topology of the four putative siderophore transporters revealed from the phylogeny. Thirteen (Sit1), and twelve (Sit2, Sit3, and Sit4) transmembrane domain were inferred by SOSUI software.
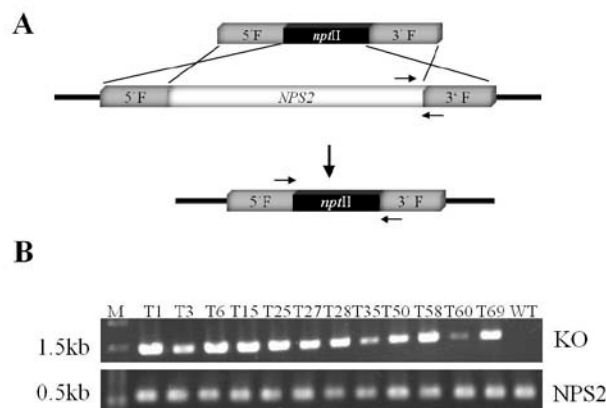
Supplementary Fig. 16: Targeted disruption of *C. graminicola NPS2* genes.
A: Scheme of the disruption strategy of *NPS2* by homologous recombination. The full open reading frame (ORF) of the *NPS2* gene was replaced by a 1231-pb fragment carrying *npt*II gene. Arrows represent the used PCR primers for confirming the ORF deletion.
B: Confirmation of the targeted deletion of the *NPS2* gene using primers specific for the KO and *NPS2* gene respectively. Notice all the proved transformations harboring the KO ectopically. More than 80 transformants have been tested.

VIII.5 Accession numbers

VIII.5.1 Fungal ferroxidases used to construct the phylogenic tree

Fusarium fujikuroi (CCE 73644, CCE 73641, CCE 73646), *F. graminearum* (XP 382318.1, XP 385335.1)*, Nectria haematococca* (EEU 41991.1, EEU 46319.1), *Verticilium dahliae* (EGY 19585, EGY 16062)*, Claviceps purpurea* (CAD 21518.1, CCE 33020), *Neurospora crassa* (XP 955835.1)*, Botryotinia fuckeliana* (XP 001558807)*, Microsporum canis* (EEQ 27170.1)*, Pyrenophora tritici-repentis* (XP 001940701.1)*, Magnaporthe oryzae* (XP 3708928.1)*, Mycosphaerella graminicola* (XP 003854921.1), *Aspergillus clavatus* (XP 001276149.1)*, A. fumigatus* (XP 747965.2)*, A. oryzae* (XP 001823720, XP 001822739)*, Neosartorya fischeri* (XP 001266156.1), XP 716842, XP 711265.1, XP 711288, XP 711286, (XP 711264, XP 711287),XP 446246.1, XP 448770.1), NP 013774, NP 116612)XP 756252)

VIII.5.2 Fungal MFSs used to construct the phylogenic tree

Coccidioides immitis (EAS29423.2), *C. graminicola* (GLRG_00560, GLRG_00774, GLRG_01843, GLRG_02384, GLRG_03115, GLRG_03579, GLRG_04347, GLRG_04838, GLRG_05715, GLRG_05812, GLRG_05829, GLRG_05946, GLRG_06839, GLRG_07668, GLRG_08312, GLRG_08506, GLRG_08615, GLRG_09083, GLRG_09553, GLRG_09625, GLRG_09840, GLRG_10138, GLRG_10448, GLRG_10538, GLRG_11169, GLRG_11313, GLRG_11358, GLRG_11550, GLRG_11733, GLRG_11797 and GLRG_11944), *C. higinseanum* (CH063_00112, CH063_06272, CH063_06706, CH063_08195, CH063_09698, and CH063_14224), *C. gloeosporioides* (ELA24045.1, ELA25240.1, ELA36736.1, ELA37514.1, and ELA37882.1), *Metarhizium acridum* (EFY91828.1), *Macrophomina phaseolina* (EKG22267.1), *Trichoderma atroviride* (EHK46117.1), *Verticillium albo-atrum* (XP_002999942.1), and *V. dahliae* (EGY20625.1).

VIII.5.3 Maize (*Zea mays*) defense genes analyzed in this study.

Pathogenesis-related protein 1 (PR1) (ACG29538.1), chitinase I (ACJ62153.1), PRX346 (AFW78948.1), PRX365 (AFW81877.1), PRX648 (ACG24777.1), and PRX731 (AFW80851.1).

Acknowledgements

Emad Albarouki

Curriculum vitae

Personal data

Name: Emad ALBAROUKI

Date of Birth: October the 5th, 1977.

Place of Birth: Sweida, Syria

Citizenship: Syrian

Address:

Voßstr.9, 06110 Halle (Saale), Germany

Education and qualification

1995 – 2000: Bachelor in Agronomy. Damascus University, Syria.

2000 – 2001: Postgraduate Diploma of Horticulture, Damascus University, Syria.

2001 – 2003: Research assistance at the General Commission for Scientific Agricultural Research (GCSAR), Sweida, Syria

2003 - 2004: Professional workshop of biotechnology, (InWent fellowship), Martin-Luther University, Halle-Wittenberg, Germany.

2004 – 2006: Masters Degree (MSc), Master in plant biotechnology (TEMPUS fellowship). Damascus University and Phytopathology Institute, Martin-Luther University, Halle-Wittenberg, Germany.

2007 – 2011: DAAD Scholarship, PhD in Fungal genetic (Phytopathology Institute), Martin-Luther-University, Halle-Wittenberg, Germany.

2011 – Now: Employee at the Interdisciplinary Center for Crop Plant Research (IZN), Martin-Luther University, Halle-Wittenberg, Germany.

List of scientific publications and attended conferences

Publication

Albarouki, E., and Deising, H. (2013). Infection Structure-Specific Reductive Iron Assimilation is Required for Cell Wall Integrity and Full Virulence of the Maize Pathogen *Colletotrichum graminicola*. Molecular Plant-Microbe Interaction **26 (6): 695–708**.

Albarouki, E., Fanghua, Y., von Wirièn, N., Schafferer, L., Haas, H. and Deising, H. Biotrophy-specific down-regulation of siderophore biosynthesis in Colletotrichum graminicola is required to modulate immune responses of maize. Molecular Microbiology (MMI-2013-13717, peer review).

Ye, F.; Albarouki, E.; Lingam, B.; Deising, H. B.; von Wirèn, N. An adequate Fe nutritional status of maize suppresses infection and biotrophic growth of *Colletotrichum graminicola* (submitted to Physiologia Plantarum - PPL-2013-00506).

Conferences and attempted meeting

Albarouki, E., Ye, F., von Wirén, N., and H.B. Deising 2012: Iron as a determinant of virulence and resistance in *Colletotrichum graminicola*-maize interaction. Interdisciplinary-Center of Crop Plant Research (IZN), Annual Report **TP 10**, **57-68**.

Ye, F., Albarouki, E., von Wirén, N., and H.B. Deising 2011: Iron as a determinant of virulence and resistance in *Colletotrichum graminicola*-maize interaction. Interdisciplinary-Center of Crop Plant Research (IZN), Progress Meeting, **15-16**.

Albarouki, E. and H.B. Deising 2010: The siderophore-mediated, but not the ferroxidase dependent, uptake system plays the major role of iron uptake and storage in *Colletotrichum graminicola*. Journal of Plant Diseases and Protection, **117 (3): pp. 138.**

Albarouki, E. and H.B. Deising 2008: Cloning and Characterization of iron transporters of the Maize pathogen *Colletotrichum graminicola*. In 56th Deutsche Pflanzenschutztagung, Mitteilung Julius Kühn-Institut, **417, pp. 318.**

Eidesstattliche Erklärung / *Declaration under Oath*

Ich erkläre an Eides statt, dass ich die Arbeit selbstständig und ohne fremde Hilfe verfasst, keine anderen als die von mir angegebenen Quellen und Hilfsmittel benutzt und die den benutzten Werken wörtlich oder inhaltlich entnommenen Stellen als solche kenntlich gemacht habe.

I declare under penalty of perjury that this thesis is my own work entirely and has been written without any help from other people. I used only the sources mentioned and included all the citations correctly both in word or content.

_____   _____

Datum / Date   Unterschrift des Antragstellers / *Signature of the applicant*